

Biodegradable Polyol-Based Polymers

A polymer platform for biomedical applications

**Biodegradeerbare Polyol-Gebaseerde Polymeren:
een platform voor biomedische applicaties**

Joost P. Bruggeman

Financial support: J.F.S. Esser Stichting, Nederlandse Vereniging voor Plastische Chirurgie
en Erasmus Universiteit Rotterdam

Cover design: J.P. Bruggeman

Lay out: Legatron Electronic Publishing, Rotterdam, The Netherlands

Printed by Ipskamp Drukkers, Enschede, The Netherlands

ISBN: 978-90-XXXXX-XX-X

© Copyright 2010: J.P. Bruggeman

All rights reserved. No part of this thesis may be reproduced, stored in a retrieval system, or transmitted in any form or means without the prior permission in writing from the author. Articles are reprinted with permission from the respective journals.

Biodegradable Polyol-Based Polymers

A polymer platform for biomedical applications

**Biodegradeerbare Polyol-Gebaseerde Polymeren:
een platform voor biomedische applicaties**

Proefschrift

ter verkrijging van de graad van doctor aan
de Erasmus Universiteit Rotterdam
op gezag van de Rector Magnificus
Prof.dr. H.G. Schmidt
en volgens het besluit van het College voor Promoties.

De openbare verdediging zal plaatsvinden
op vrijdag 22 oktober om 11:30 uur

door

Joost Pieter Bruggeman

geboren te Amsterdam



Promotiecommissie

Promotoren: Prof.dr. S.E.R. Hovius
Prof. R.S. Langer

Overige leden: Dr. G. van Osch
Prof.dr. H. Weinans
Prof.dr. J. Feijen

Paranymfen: Dr. K.P. Mahon
Dr. G.J.D. Van Acker

Aan mijn ouders

Table of Contents

Chapter 1:	Introduction and thesis outline	9
Chapter 2:	Biodegradable xylitol-based polymers	29
Chapter 3:	Biodegradable poly(polyol sebacate) polymers	43
Chapter 4:	Synthesis and characterization of photocurable elastomers from poly(glycerol sebacate)	65
Chapter 5:	Biodegradable xylitol-based elastomers: in vivo behavior and biocompatibility	81
Chapter 6:	In vivo behavior of photocured elastomers from poly(glycerol sebacate): implications for peripheral nerve conduits	105
Chapter 7:	Biodegradable poly(xylitol sebacate) elastomers for peripheral nerve reconstruction	125
Chapter 8:	Biodegradable nanotopographic poly(xylitol sebacate) elastomers for peripheral nerve regeneration	145
Chapter 9:	Fabrication of scaffolds composed of biodegradable poly(polyol sebacate) elastomers for tissue engineering purposes	161
Chapter 10:	General discussion, conclusions	177
Chapter 11:	Dutch Summary/ Nederlandse samenvatting	195
Appendix 1:	Gratitude	203
Appendix 2:	Curriculum vitae	209
Appendix 3:	Scientific publications	211

Chapter 1

Introduction and thesis outline

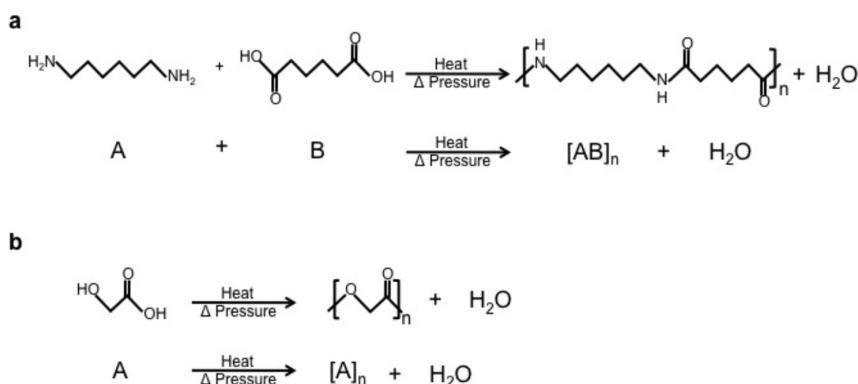
Joost P. Bruggeman, Steven E. R. Hovius, Robert Langer

1. Polymers as biomaterials in surgery

- *A biomaterial is a nonviable material used in a medical device, intended to interact with biological systems.* (Williams, 1987) [1]
- *A biomaterial is any substance, synthetic or natural in origin which treats, augments or replaces any tissue, organ or function of the body.* (Greco, 1994) [2]

Polymers and surgery are inseparable entities: if it is not a polymeric suture to close the wound, it is definitely the crosslinking of fibrin molecules during coagulation that enables an organism to survive and sustain (surgical) wounds. In fact, one can hypothesize that the organism is entirely dependent on polymers in the first place, considering that DNA and collagen (the major component of mammalian connective tissue) are polymers also. Polymers are important molecules. Even before we understood the character and importance of these large molecules, surgeons had been implanting polymeric materials for centuries. Perhaps the first report of a polymeric biomaterial for use in surgical procedures was by the Indian surgeon Sushruta (AD c450-c380), who described sutures made from flax, hemp and hair to close incisions in the skin [3]. Although Sushruta's sutures got out of fashion at some point, the Greek Galen of Pergamon (AD c200-c120) described catgut (collagen) and silk as suture materials [4], materials still used in the operating theatre today, although their use is declining. Polymers (Greek: polu = many, meros = parts) are large molecules composed of small repeating units, the monomers, which are connected by chemical bonds [5]. Man-made polymers have only been around for less than two centuries (one of the first being Leo Beakeland's phenol-formaldehyde resins known as Bakelite) [5]. At that time, the polymer industry had already been established as a multi-billion dollar industry with naturally occurring polymers that had revolutionized daily life, e.g. rubber for tires. But by 1920, most chemists still believed that these materials consisted of physically associated aggregates of small molecules. Hermann Staudinger introduced the concept that these materials were actually composed of very large molecules, which he coined 'macromolecules' [5]. Based on this concept of macromolecules, Wallace Carothers at DuPont worked on the invention of Nylon in the 1930s [6], a commercially successful, rationally designed, synthetic polymer. His invention was based on simple chemical reactions between di-functional molecules, diacids with diamines or diols, thereby extracting a small molecule (e.g. water or methanol). He named these macromolecules 'condensation polymers' (**Scheme 1a**). In 1940, Nylon was patented for its use as suture material [7], and in that same year it was embraced in surgical practice [4].

From the beginning of material sciences, startled by this whole “new” group of organic materials (polymers), research and development had mainly focused on highly stable materials that are virtually indestructible in biological systems, e.g. Nylon. When implanted *in vivo*, Nylon will remain *in situ*, unless it is surgically removed. The development of unstable or degradable biomaterials is a relatively new area of research. Synthetic biodegradable polymers such as poly(glycolic acid), or PGA (**Scheme 1b**) are developed since at least 1954, when Norton Higgins of DuPont patented making it from glycolic acid by carefully manipulating temperature and pressure [8]. Nowadays, PGA is obtained through a (ring-opening, chain growth polymerization) different process [9]. In late 1960s, Edward Schmitt and Rocco Polistina of American Cyanamid Company filed a patent for the formation of sutures from PGA [10,11].



Scheme 1. (a) Wallace Carothers’ condensation polymers are produced by step growth polymerization of difunctional monomers (‘A’ and ‘B’) with the extraction of a small molecule, e.g. water or methanol. In the case of Nylon 6.6, hexamethylene diamine is reacted with adipic acid to form the Nylon polymer and water. **(b)** In the case of PGA described by Higgins in 1954 [8], a similar step growth polymerization of alcohol-acid monomers (‘A’) (glycolic acid) is performed. Nowadays, chain growth polymerization using a catalyst such as $\text{Sn}(\text{Oct})_2$ is the common reaction by which PGA is obtained.

When the PGA sutures (Dexon, Davis and Geck, USA) reached the market a few years later, they were rapidly adopted as a strong, reliable, and workable replacement for the traditional collagen-based (catgut) absorbable sutures. Today, PGA, poly(lactic acid) (PLA), and their co-polymers (poly(lactic-co-glycolic acid) or PLGA) are the most widely used synthetic degradable polymers in medicine and enjoy the largest literature base despite certain drawbacks associated with these molecules, which are discussed below. Soon

after the successful introduction of PGA as the first synthetic biodegradable polymer in medicine, other polymers as well as other applications followed rapidly, ranging from surgical dressings [12], hemostatic felts [13], controlled drug delivery systems [14], nerve conduits [15] and other applications related to tissue engineering [16,17]. From this point on polymer scientists applied their knowledge in collaborations with physicians, and biomaterial research became a mature branch in the field of polymer research.

Of all potential biomedical applications for polymers, tissue engineering and nerve reconstruction are areas of interest in this thesis and briefly discussed below. The last part of this chapter describes several biodegradable polymers.

2. Tissue engineering

It remains unclear when the field was actually conceptualized for the first time. In 1938, Charles Lindbergh, a well-known aviation hero, published a book co-authored by Alexis Carrel, named “The culture of organs” [18]. Nevertheless, the field lay dormant for many decades. This is no surprise, as advances in supportive devices such as the artificial kidney by Dr. Willem Kolff [19] in the 1940s, as well as successful solid organ transplantation since 1953 [20] had revolutionized medicine. However, five decades later, in the late 1980s, scientists, engineers and clinicians began to work culturing *de novo* tissue. This effort was fuelled by the immunologic barriers and tragic shortages associated with organ transplantation [21]. Another important drive towards *de novo* tissue engineering is the goal to individualize treatment to meet the distinctive needs of patients that are confronted with loss or failure of tissue. In the 1980s, Boston (MIT and Harvard University) was the site where human artificial skin was developed [22-24]. Their efforts resulted in current commercially viable tissue engineered products that treat patients with skin defects today [25]. Apart from the exact beginnings, there also remains confusion about what the term *tissue engineering* truly encompasses. Broadly described, tissue engineering is a cross-disciplinary field that includes studies in areas as diverse as synthesis of new polymers, studies of signal transduction and gene regulation in cultured cells as well as organogenesis, and transplantation related immunology [26]. However, as defined in the seminal paper in *Science* by Robert Langer and Joseph Vacanti in 1993 [27], *tissue engineering* is referred to as:

“The use of a natural or synthetic biodegradable material, which has been seeded with living cells when necessary, to regenerate the form and/or function of a damaged or diseased tissue or organ in a human patient.” (Figure 1).

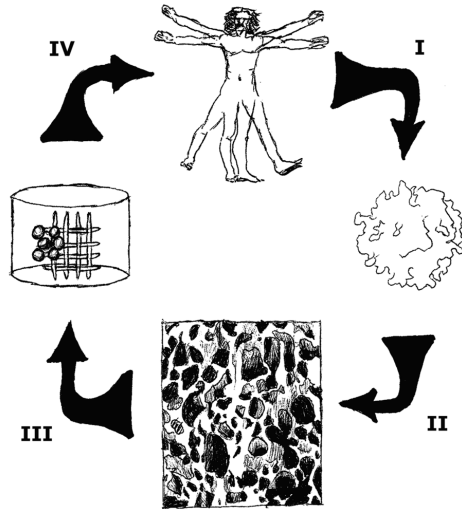


Figure 1. The core principle of tissue engineering. In the first step (I), cells are harvested from the patient that is confronted with tissue or organ loss. Many sources (e.g. skin, fat, bone marrow) and cell types (e.g. stem cells, differentiated cells) have been described. Then, after in vitro expansion and/ or differentiation of cells, the second step (II) is combining these cells with a biodegradable polymeric scaffold. Typically, this is done in a bioreactor (**step III**) of which many types have been described. This allows the in vitro tissue to organize and mature before the cell–polymer matrix is ready for implantation in vivo. The last step (IV) is implanting the engineered tissue into the patient for further maturation and integration, ultimately replacing the lost tissues.

One can see from the definition above as well as **Figure 1** that cells, biodegradable materials and bioreactors are three main pillars in tissue engineering. Searching ideal sources of stem cells [24], reprogramming differentiated cells into pluripotent cells [28], increasing yields upon harvest of cells [25,29], finding ideal growth factor cocktails to differentiate cells into the desired phenotype, genetically modifying (stem)cells, optimizing culture conditions such as mechanical forces, and bioactive coatings [30] as well as engineered cell sheets as implantable tissue engineered devices [31] have been met with varying degrees of success. Matrices, or scaffolds, composed of biodegradable polymers, provide crucial structural support and may induce cell differentiation, cell migration, cell proliferation and/ or act as immunoisolation barriers [30,32,33]. In tissue engineering, the cultured cell population

within the scaffold should ideally replace the polymer with extra-cellular matrix specific for that tissue, preferably at the same rate the polymer degrades. However, cell survival, vascularization and integration of the engineered tissue in vivo is still a challenging task that lays ahead for tissue engineers: hematoma, inflammation, angiogenesis, fibrosis and other wound healing responses upon implantation are complex and tissue-specific processes – and most importantly, not yet fully understood.

3. Peripheral nerve reconstruction and artificial nerve guides

In the United States alone, about 200,000 people per year require surgical treatment for peripheral nerve injuries [34]. The standard technique is end-to-end suture of the severed nerve, or the interposition of an autologous nerve graft when tensionless coaptation cannot be performed. However, nerve conduits can be used for smaller nerve defects and have several advantages over nerve grafting. Nerve grafting requires the sacrifice of a healthy nerve that often displays a donor-acceptor diameter mismatch and unfortunately, does not guarantee optimal functional outcome. Nerve conduits can be sutured between the nerve stumps, allowing for tensionless repair (**Figure 2**). In addition, conduits give directional guidance to migrating Schwann cells and elongating axons, offer a controllable regenerative environment as well as protection from potentially impeding scar tissue formation [36]. Other important advantages of conduits are the prevention of donor-site morbidity (loss of sensation, neuroma formation, infection), reduction of operation time, and the ability to repair nerve lesions in anatomic locations that are difficult to reach.

Around the 1970s, research in peripheral nerve reconstruction focused on silicone tubes as nerve conduits [37]. Silicones, a family of poly(siloxanes), are inert and resistant to enzymatic or acid-base catalyzed hydrolytic cleavage of the Si-O bonds. The inert silicone elastomer tube proved to be an ideal biomaterial to study the nerve regeneration processes in detail [38-40], but was not used in clinical practice as clinicians soon found that the non-degradable silicone elastomers caused a chronic inflammatory (foreign body) response, damaging the regenerated nerve, eventually leading to disappointing clinical outcomes [41]. This is unfortunate, as one year post-operative results demonstrated in a prospective, randomized clinical study by Lundborg *et al.* in 1997 showed promising results for silicone tubular repair [42]. Their study data demonstrated no significant differences between the tubular repair group and the conventional reconstructive procedures for median and ulnar nerve lesions in a total of 18 human forearms. In 2001, Lundborg and co-workers showed

long term results of the silicone tubes implanted in the 11 cases described in their 1997 study. Seven patients were re-explored because of local discomfort from the tube 12-44 (median 22) months after the initial procedure, and found in only two cases a mild foreign body reaction [43]. Degradable nerve conduits were pursued subsequently. Nerve reconstruction and regeneration are inseparable topics from tissue engineering nowadays, but it was empirical clinical evidence at first that pushed (clinical) researchers towards biodegradable polymer solutions. For these reasons, development of nerve conduit materials gained popularity over the last decades. In summary, polymers developed for this application should ideally adhere to important design criteria [15,44-48]: they are summarized in **Table 1**, comparing these for three commercially available biodegradable nerve conduits, used in clinical practice today. Meek and Coert have previously reviewed these clinical available nerve conduits and concluded that there are no adequate prospective studies comparing these conduits in humans [49]. Although there are clear differences between the products to influence a clinician's decision (see **Table 1**), Meek and Coert advised to use the tube with the most available clinical data and best price, which is currently the PGA Neurotube[®] nerve guide in The Netherlands. In addition, in 2000, Weber *et al.* published a randomized prospective study on the use of PGA conduits for digital nerve repair. They observed that tubular nerve repair using PGA tubes, compared to conventional end-to-end repair and nerve grafting, demonstrated improved sensation as determined by two-point discrimination studies up to 1 year postoperatively [50]. However, similar to the surgeon's choosing of suturing materials nowadays, the reconstructive surgeon confronted with a nerve gap should have an armamentarium of conduits to his/ her display, with several degradation rates to correct for the age of the patient, as well as size and location of the nerve defect. The current range of conduits is very limited, and not properly investigated to our knowledge: no randomized controlled trial comparing the current clinically available conduits has been reported to date.

Biodegradable polymers have made a considerable impact in various fields of biomedical engineering, tissue engineering and peripheral nerve reconstruction. The design of synthetic biodegradable polymers for bio-engineering purposes remains challenging however, because of application-specific constraints on the physical properties including mechanical compliance and degradation rates, and the need for biocompatibility and low cytotoxicity.

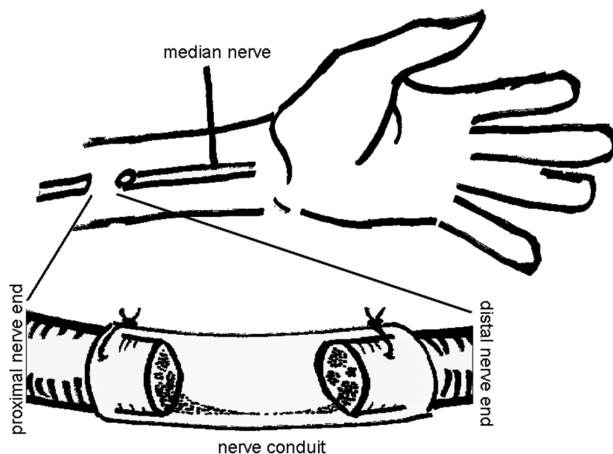


Figure 2. Peripheral nerve reconstruction with a conduit. A nerve itself consists of numerous axons, which conduct action potentials. Axons are either myelinated by Schwann cells (SCs), or non-myelinated. These cells insulate the axons by forming a myelin sheath, enhancing conduction velocities. Following injury of peripheral nerves, Wallerian degeneration is triggered, indicating that axons distal to the lesion degenerate and are phagocytosed. Reestablishment of continuity of the severed nerve stumps occurs by dissociation of SCs with their axons, proliferation and migration of SCs, bridging the gap between the severed nerve endings and guiding elongation of the axons proximal to the lesion towards the distal target organ [35]. Some functional recovery is possible when axons are guided to the target organ by surgical reconstruction of the anatomical continuity. However, when tensionless end-to-end coaptation of the nerve stumps cannot be performed, an autologous nerve graft is used to bridge the existing gap. Nerve grafting is associated with several drawbacks however, and to bypass these, many nerve conduits for reconstruction have been developed with varying success [34]. Conduits can be of natural materials with a tubular structure (veins, inside-out veins, arteries, etc), as well as artificial polymeric materials (silicone, PGA, collagen, etc).

4. Biodegradable polymers

Natural polymers

At the time Nylon was introduced in the operating theatre and for three decades thereafter, natural polymers were the *only* materials that were absorbed by the surrounding tissues after implantation. Still, since 2000 for instance, approximately 84% of all polymers that were approved by the FDA for medical devices were natural biodegradable polymers [51]. Thus, natural polymers are preferred in novel biomedical applications today, despite several drawbacks of natural polymers. The main reason for this is that these polymers have a long, established history of use in humans.

Criteria for peripheral nerve conduits [15,42,44,49]	PGA	PDLLC	Collagen
1 Non-toxic	☹	☹	☺
2 Non-immunogenic	☺	☺	☹
3 Biodegradable	☺	☺	☺
4 Maintain form stability and structural integrity upon hydration and degradation	☹	☹	☺
5 Readily tunable in vivo degradation rate	☺	☺	☺
6 Mechanically match nerve and soft tissue surroundings	☹	☹	☺
7 Soft enough for micro-sutures, strong enough to hold sutures	☹	☹	☺
8 Allow for nerve growth stimulating factors such as			
a. micropatterned walls	☹	☹	☺
b. (micro)porous walls	☺	☹	☺
c. controlled release of growth-stimulating factors	☹	☹	☹
9 Allow for direct SC attachment, migration and proliferation	☺	☹	☺

Table 1. Important design criteria compared for commercially available peripheral nerve conduits and PXS conduits. PGA (Neurotube®), poly((D,L)-lactide-co-e-caprolactone) (PDLLC, Neurolac®) and collagen (NeuraGen® or NeuroMatrix®) are currently the biodegradable polymers of choice for peripheral nerve conduits in clinical practice.

a. Collagen

Collagen is the major component of connective tissue, accounting for 30% of all protein in mammalian organisms. It is found in every major tissue that requires strength and flexibility (e.g. skin, bone). Of all 14 different types, collagen type 1 is the most abundant type found in tissues. The structure, function and synthesis of type 1 collagen has been investigated extensively [25]. Collagen proteins are produced in connective tissues, are characterized by a triple helix structure by definition and contain integrin binding sites (e.g. RGD amino acid sequences) facilitating cell attachment. Thus, it is attractive to use materials that already function in vivo as scaffolds for mammalian organisms. Also, natural polymers that are utilized in the biomedical field are popular because they are usually intrinsically biodegradable and the degradation products can be resorbed and metabolized similar to the natural components of its hosting tissue.

After the extraction of collagen from biological systems, collagen crosslinking can be enhanced through a number of well-described physical or chemical techniques [25]. Increasing crosslink density, biodegradation time is increased, the capacity of collagen to be hydrated decreased and tensile strength of the scaffold is increased, offering a

method to tailor collagen materials for different applications. However, the synthesis of natural polymers is a biological process, and therefore the process is subject to biological variation. This results in difficulty to achieve uniformity and precise control of mechanical properties as well as degradation rates when these polymers are processed for specific applications [52,53]. Also, polymers such as collagen display a limited versatility in mechanical properties. In addition, natural polymers are proteins or can contain proteins or inflammatory molecules such as lipopolysaccharide (LPS) when produced by bacterial fermentation [54]. Despite collagen's phylogenetically well-conserved primary sequence, it is immunoreactive, albeit mild in most cases [55]. Local erythema is the most found and benign clinical response of the immunological response to collagen but there are case reports involving a more dramatic delayed hypersensitivity reactions as well [26,55-57]. Another problem with polymers derived from biological tissues is that they can potentially carry pathogens such as viruses and prions (e.g. transmitting Jacob-Creutzfeldt Disease). Extra and costly purification steps are necessary to obtain clinically safe natural materials [51,58].

b. Other natural polymers

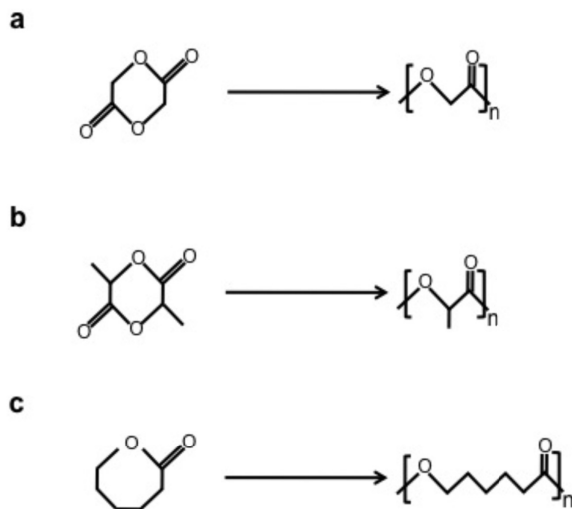
Glycosaminoglycans (e.g. hyaluronic acid), chitosan, silk and poly(hydroxyalkanoate) [58] polymers amongst many others, are other naturally occurring polymers that receive great attention for their potential in tissue engineering as well as other biomedical applications. Another interesting group of novel biomaterials are synthetic biomolecules. These materials are composed of proteins that are engineered in bacterial systems that were genetically modified to produce these rationally designed molecules. This results in polymers with unique amino-acid sequences with homologies to existing natural polymers to mimic specific properties of polymers such as collagen, elastin and silk. This combination of molecular and fermentation biology, creating novel protein-based biomaterials seems very promising, as biological cues can potentially be incorporated within the material [59]. These biological cues can aid in e.g. cell adhesion or stem cell differentiation [60], but can potentially also accidentally contain immunogenic epitopes [26]. In addition, as is the case for collagen, polymers that are extracted from biological systems or produced by bacterial fermentation, require extensive purification, display batch-to-batch differences and have a limited accessible range of mechanical properties and degradation rates when compared to synthetic polymers [58]. Oftentimes these natural polymers are combined with synthetic materials in hybrid systems to achieve the optimal material properties.

Synthetic polymers

The desire of precise control of polymer properties, in addition to the potential adverse events associated with natural polymers such as collagen fueled a quest for synthetic biodegradable materials that could readily be produced and scaled in a reaction vessel. The most well-known and characterized polymers are polymers based on the naturally occurring α -hydroxy acids, such as glycolic –, lactic – and ϵ -caproic acids, as well as numerous co-polymers based on these monomers [25,26].

a. Poly(α -hydroxy acids) (Scheme 2)

PGA, PLA and their co-polymer PLGA are the most widely used synthetic degradable polymers in medicine. The ester bonds between the hydroxy acid monomers are generally cleaved by hydrolysis during degradation, which results in a decrease in polymer molecular weight (but not mass) by exposure to aqueous environments such as the human body, or the atmosphere. The random scission of ester bonds throughout a polymer construct in aqueous environments is a degradation profile often referred to as ‘bulk degradation’ (**Figure 3**) [61-63]. This degradation can be tuned, e.g. by initial molecular weight, by altering the polymer morphology (introducing more or less crystalline segments), or by chemical composition (by introducing more hydrophobic or hydrophilic monomers) [25, 26]. However, although tunable, this random cleavage of the esters within the polymer backbone can result in suboptimal structural integrity and form stability upon degradation. Acidic by-products (oligo-, tri-, di-, and monomers) generated during the degradation of poly(α -hydroxy acids), apart from being toxic, have a cumulative negative effect on degradation: these by-products further catalyze hydrolysis of the polymer by lowering the local pH [62]. Once this process is started, a different concentration in by-products on the outside and on the inside of the implant will exist, as by-products will more readily diffuse into the surrounding tissues on the outside of the polymer implant. This decrease in concentration of acidic products on the outside slows down the rate of hydrolysis on the surface of the implant, as compared to the inside. This different rate in hydrolysis may result in a shell of polymer with a higher molecular weight, trapping even more acidic by-products on the inside of the implant, accelerating the hydrolysis rate on the inside further. When this occurs, the outside shell of the implant will eventually not be able to withstand pressure of surrounding tissues at some point during degradation, deforming the implant. This shell can eventually rupture, causing a burst release of acidic products, leading to deleterious inflammatory responses [62], a well-known complication of these polymers.



Scheme 2. Common biodegradable polyesters based on hydroxy acids. **(A)** Glycolic acid (glycolide) into PGA, **(B)** lactic acid (lactide) into PLA, and **(C)** ϵ -caprolactone into PCL.

b. Synthetic biodegradable elastomers

PGA, PLA and PLGA are stiff and brittle materials. Poor compatibility between artificial materials and the dynamic internal environment of the human body can lead to dysfunctional interactions and subsequent poor outcomes of polymeric implants. The body is a mechanically dynamic environment and implants therefore have to endure constant mechanical stresses and should readily recover from deformations without mechanical failure. Ideally, they should do this without significant friction to the surrounding tissues and implants should therefore resemble their implantation site in terms of mechanical properties. Thus, tissue engineering of soft tissues requires soft, elastomeric synthetic biodegradable polymers with tunable degradation rates. Poly(ϵ -caprolactone) (PCL) is another poly(hydroxy acid) that exhibits a unique low glass transition temperature (-62°C) [66], indicating it is in a rubbery state at room – and physiological temperatures. Compared to PGA and PLA, the degradation process of PCL is very similar to PGA, PLA or PLGA, albeit significantly slower [63,66]. This makes PCL suitable for the design of long-term implantable systems (at least one year). Another monomer that has successfully been employed to obtain promising synthetic biodegradable elastomers is 1,3-trimethylene carbonate. Poly(1,3-trimethylene carbonate) (PTMC) exhibits a low glass transition temperature as well (-15°C) [67] and in vivo degradation of PTMC seems much faster than PCL: high molecular weight PTMC is completely degraded after 3 weeks in vivo [67]. Interestingly, high molecular weight PTMC,

as well as certain crosslinked PCL-based networks [61, 63, 66] reveal a different degradation profile. These elastomers seem to degrade by an enzyme-mediated surface erosion, which leads to a gradual thinning of the implant [61, 63, 67]. Compared to the aforementioned bulk degradation, surface erosion does not impede structural integrity and form stability, which can be an important advantage in biomedical applications (**Figure 3**) [62,63]. However, tuning degradation rates and mechanical properties of these biodegradable elastomers is not straightforward. Many co-polymers have been formulated using ϵ -caprolactone, 1,3-trimethylene carbonate, lactic and/or glycolic acid. The degree of crystallinity of the resulting polymer network (and thus mechanical properties) versus degradation rate as well as degradation mode has frequently resulted in bulk degrading elastomers with suboptimal degradation rates [49]. Other synthetic biodegradable elastomers include poly(urethanes) [68,69], poly(phosphazenes) [70] and poly(ether esters) [71] amongst others. Although promising materials for tissue engineering applications, the production of these polymers usually encompass multi-step procedures, and costly and toxic reagents.

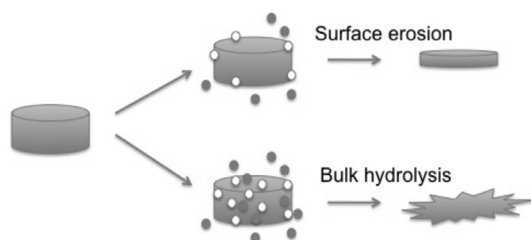


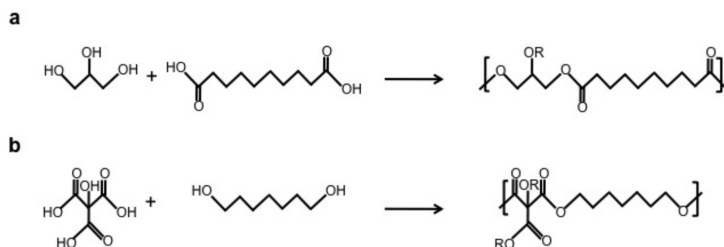
Figure 3. Schematic of bulk hydrolysis versus surface erosion of polymer implants. Surface erosion is characterized by a gradual thinning of the polymer implant by cleavage of the bonds on the outside of the polymer construct. Enzymes may play an important role in surface erosion, as they are sterically shielded from the monomer bonds on the inside of the construct and can therefore only attack the polymer from the outside [63, 64]. Collagen degrades by surface erosion, as well as some synthetic polymers [25, 65]. Bulk hydrolysis is characterized by random cleavage of the monomer bonds throughout the polymer implant. This eventually leads to a loss of structural integrity of the implant, as well as a potential burst release of monomers from the inside of the implant. Clinically applied polymers based on α -hydroxy acids are known to degrade by bulk hydrolysis.

Crosslinked (thermoset) elastomers

Within the class of polyester scaffolds, many examples of both elastomeric thermoplastics and thermosets have been synthesized, incorporating a wide range of monomers. With the requisite of biocompatibility, some polymers have been based on monomers that

are endogenous to the human metabolism. In 2002, Wang *et al.* described a tough biodegradable elastomer, based on the polycondensation reaction of glycerol and sebacic acid into a gelled, crosslinked network, designated poly(glycerol sebacate) (PGS) (**Scheme 3A**) [65,72,73]. The combination of monomers for this polymer was reported before: in 1999 Nagata *et al.* [74] had described a rigid, totally crosslinked polymer composed of glycerol and sebacic acid. Interestingly, Wang's PGS seemed to be tougher and more flexible than most biodegradable elastomers at that time. The low degree of crosslinking and intra-network hydrogen bonding were thought to contribute to the superior elastomeric mechanical properties of PGS. Importantly, PGS proved to have a superior biocompatibility in vitro and in vivo when compared to PLGA, as well as demonstrated a surface degradation profile with subsequent superior structural integrity and form stability. The degradation rate of PGS is not tunable by altering polymerization conditions [75] and PGS is completely degraded within 60 days as determined by subcutaneous implantation in rats [65,75]. A similar elastomer was invented by Ameer *et al.* in 2004 [76-78], using citric acid as the central monomer combined with different aliphatic diols, yielding poly(diols citrate) (PDC) elastomers (**Scheme 3B**) that demonstrated in vitro hydrolysis. Despite a reported superior biocompatibility compared to PLA [76,77], a detailed in vivo degradation profile was never reported for PDC elastomers. However, in vitro degradation is more rapid for PDC than PGS [65,77], perhaps due to citric acid acting as a catalyst of the hydrolysis process. This may result in form instability during degradation, or perhaps even faster degradation rates in vivo of PDC than for PGS. An advantage of PDC over PGS is the increased toughness (perhaps due to increased hydrogen bonding within the polymer by citric acid) and the wider range in mechanical properties tailored by using diols with different chain lengths [65,76,77]. Either way, an increasing number of applications of PGS or PDC elastomers in cardiovascular tissue engineering [79-81], peripheral nerve reconstruction [82], cartilage tissue engineering [83], and retinal tissue engineering [84] amongst others, clearly demonstrates potential of these elastomers.

Major advantages of PGS over other materials (including PDC), is that it is composed of monomers that can be metabolized by the host organisms during in vivo degradation. In addition, PGS displays a negligible degradation in vitro, as it is not susceptible to bulk hydrolysis, an important determinant of shelf-life duration of potential medical devices composed of this material. Lastly, the production process of PGS is very straightforward and low in cost.



Scheme 3. (A) Thermoset elastomers produced by a polycondensation reaction of sebacic acid with glycerol as the trifunctional monomer in PGS elastomers, or (B) 1,8-octanediol with citric acid as the trifunctional monomer in PDC elastomers. R can be a hydrogen or another polymer chain.

5. Aim and outline of this thesis

The aim of this thesis is to develop straightforward synthesis schemes resulting in tunable synthetic biodegradable polymer platforms. We hypothesize that classes of biodegradable polymers can be synthesized that:

1. are composed of monomers endogenous to mammalian metabolism?
2. are elastomeric in nature?
3. can be water soluble or insoluble?
4. can be polymerized under physiological conditions?
5. display a wide range of tunable crosslink densities?
6. display a wide range of tunable mechanical properties?
7. offer a wide range of tunable degradation rates?
8. degrade through surface erosion?
9. can be useful for in vivo biomedical engineering applications, such as peripheral nerve conduits? Are these materials better than current commercially available conduit materials?
10. can be readily developed in scaffolding materials for tissue engineering purposes?

We have set out to develop and diversify a family of polymers, designated ‘polyol-based polymers’ (PBPs). In the first part of this thesis, polymer synthesis schemes of PBPs are described and characterized: **Chapter 2** describes a versatile polymer platform with xylitol as the central monomer, yielding biodegradable elastomers with tunable mechanical properties and degradation rates, as well as photocrosslinkable hydrogels. The polymer platform presented in **Chapter 3** demonstrates the effect of different polyols in the same

synthesis scheme. By virtue of the polyol, as well as stoichiometry of the reacting sebacic acid, mechanical properties can be tuned from mechanical properties that are similar to small-diameter blood vessels, up to those of trabecular bone tissue. Then in **Chapter 4**, a crosslinking method of PGS under mild conditions is described, whilst preserving a wide range of physical properties. This synthesis scheme describes in essence the photocrosslinking of PBPs. In the second part of this thesis, the in vivo behavior of some of the polymers that were described in the first part is investigated in more detail. In **Chapter 5**, the in vivo behavior and biocompatibility of poly(xylitol sebacate) (PXS) elastomers are presented, and the PXS elastomers are compared to the prevalent PLGA polymer. In addition, the in vivo behavior and biocompatibility of the photocrosslinkable elastomers from chapter 4 are described in **Chapter 6**. In the third part, PBPs are investigated for potential in vivo tissue engineering purposes: in **Chapter 7** a xylitol-based elastomer is evaluated as nerve conduit material. In **Chapter 8** we demonstrated that replica-molding techniques apply for the use of PXS elastomers in contact guidance. Sub-micron topographical features on PXS elastomers were investigated for contact guidance in peripheral nerve regeneration in vitro, as well as in vivo. In **Chapter 9**, polyol-based elastomers are briefly investigated as tissue engineering materials. Scaffolds were produced by particulate-leaching, as well as electrospinning and evaluated in vitro and in vivo. In conclusion, **Chapter 10** summarizes the results and discusses the issues we met along the way.

References

1. Williams DF. Definitions in biomaterials. Amsterdam: Elsevier, 1987.
2. Greco R. Implantation biology: The host response and biomedical devices. Boca Raton, FL: CRC Press, 1994.
3. Bhishagratna KK. English translation of Sushruta Samhita (ca 600 B.C.). Calcutta: Bose, 1916.
4. Scott M. 32,000 years of sutures. NATNEWS 1983;20(5):15-17.
5. Young RJ, Lovell PA. Introduction to Polymers. 2nd ed. London: Chapman & Hall, 1991.
6. Carothers WH, inventor. Linear Condensation Polymers. US Patent 2071250, 1937.
7. DeWitt Graves G, inventor. Synthetic Polymers and Shaped Articles Therefrom. US Patent 2212772, 1940.
8. Higgins NA, inventor; DuPont, assignee. Condensation polymers of hydroxyacetic acid. United States, 1954.
9. Dechy-Cabaret O, Martin-Vaca B, Bourissou D. Controlled ring-opening polymerization of lactide and glycolide. Chem Rev 2004;104(12):6147–6176.
10. Schmitt EE, Polistina RA, inventors. Surgical Sutures. US Patent 3297033, 1967.
11. Schmitt EE, Polistina RA, inventors. Process of Polymerizing a Glycolide. US Patent 3468853, 1969.

12. Schmitt EE, Polistina RA, inventors. Surgical Dressings of Absorbable Polymers. US Patent 3875937, 1975.
13. Roth RW, inventor. Compacted Surgical Hemostatic Felt. US Patent 3937223, 1976.
14. Schmitt EE, Polistina RA, inventors. Controlled Release of Medicaments Using Polymers from Glycolic Acid. US Patent 3991766, 1976.
15. Mackinnon SE, Dellon AL. Clinical Nerve Reconstruction with a Bioabsorbable Poly(glycolic acid) Tube. *Plast Reconstr Surg* 1990;85:419-424.
16. Schmidt RA, Tanagho EA, inventors. Growing of Long-term Biological Tissue Correction Structures In Vivo. US Patent 4520821, 1985.
17. Delany HM, Ivatury RR, Blau SA, Gleeson M, Simon R, Stahl WM. Use of biodegradable (PGA) fabric for repair of solid organ injury: a combined institution experience. *Injury* 1993;24(9):585-589.
18. Carrel A, Lindbergh CA. The culture of organs. New York: Paul B. Hoeber Inc., 1938.
19. Broers H. Inventor for Life, The Story of W. J. Kolff, Father of Artificial Organs. Apeldoorn: B&Vmedia Publishers, 2007.
20. Murray JE, Merrill JP, Harrison JH. Renal homotransplantation in identical twins. *Surg Forum* 1955;6:432-436.
21. Vacanti JP. Beyond transplantation: Third annual Samuel Jason Mixter lecture. *Arch Surg* 1988;123(5):545-549.
22. Yannas IV, Burke JF, Orgill DP, Skrabut EM. Wound tissue can utilize a polymeric template to synthesize a functional extension of skin. *Science* 1982;215(4529):174-176.
23. Bell E, Ehrlich HP, Buttle DJ, Nakatsuji T. Living tissue formed in vitro and accepted as skin-equivalent tissue of full thickness. *Science* 1981;211(4486):1052-1054.
24. Gallico GG, O'Connor NE, Compton CC, Kehinde O, Green H. Permanent coverage of large burn wounds with autologous cultured human epithelium. *N Engl J Med* 1984;311(7):448-451.
25. Lanza R, Langer R, Vacanti JP. Principles of Tissue Engineering. 3rd ed. Burlington, MA: Elsevier, 2007.
26. Atala A, Mooney DJ, Vacanti JP, Langer R. Synthetic Biodegradable Polymer Scaffolds. Boston, MA: Birkhauser, 1997.
27. Langer R, Vacanti JP. Tissue engineering. *Science* 1993;260(5110): 920-926.
28. Amabile G, Meissner A. Induced pluripotent stem cells: current progress and potential for regenerative medicine. *Trends Mol Med* 2009;15(2):59-68.
29. Rakhorst HA. Cultured mucosal substitutes; from lab bench to bedside? Rotterdam: Erasmus University Rotterdam; 2008.
30. Discher DE, Mooney DJ, Zandstra PW. Growth factors, matrices, and forces combine and control stem cells. *Science* 2009;324(5935):1673-1677.
31. Nagase K, Kobayashi J, Okano T. Temperature-responsive intelligent interfaces for biomolecular separation and cell sheet engineering. *J R Soc Interface* 2009;6(Suppl 3):S293-309.
32. Levenberg S, Huang NF, Lavik E, Rogers AB, Itskovitz-Eldor J, Langer R. Differentiation of human embryonic stem cells on three-dimensional polymer scaffolds. *Proc Natl Acad Sci USA* 2003;100(22):12741-12746.
33. Yang F, Mei Y, Langer R, Anderson DG. High throughput optimization of stem cell microenvironments. *Comb Chem High Throughput Screen* 2009;12(6):554-561.
34. Madison RM, Archibald SJ, Krarup C. Peripheral nerve injury. Philadelphia: W. B. Saunders, 1992.
35. Bungner OV. Über die Degenerations- und Regenerationsvorgänge am Nerven nach Verletzungen. *Beitr Pathol Anat* 1981;10:321-387.

36. Chamberlain LJ, Yannas IV, Hsu H-P, Strichartz G, Spector M. Collagen-GAG Substrate Enhances the Quality of Nerve Regeneration through Collagen Tubes up to Level of Autograft. *Exp Neurol* 1998;154:315–329.
37. Dahlin LB, Lundborg G. Use of tubes in peripheral nerve repair. *Neurosurg Clin N Am* 2001;12(2):341-352.
38. Aebischer P, Guenard V, Brace S. Peripheral-nerve regeneration through blind-ended semipermeable guidance channels - effect of the molecular-weight cutoff. *J Neurosci* 1989;9:3590-3595.
39. Aebischer P, Guenard V, Winn SR, Valentini RF, Galletti PM. Blind-ended semipermeable guidance channels support peripheral- nerve regeneration in the absence of a distal nerve stump. *Brain Res* 1988;454:179-187.
40. Longo FM, Skaper SD, Manthorpe M, Williams LR, Lundborg G, Varon S. Temporal changes of neuronotrophic activities accumulating in vivo within nerve regeneration chambers. *Exp Neurol* 1983 81(3):756-769.
41. Merle M, Dellon AL, Campbell JN, Chang PS. Complications from silicon-polymer intubulation of nerves. *Microsurgery* 1989;10(2):130-133.
42. Lundborg G, Rosén B, Dahlin L, Danielsen N, Holmberg J. Tubular versus conventional repair of median and ulnar nerves in the human forearm: early results from a prospective, randomized, clinical study. *J Hand Surg Am* 1997;22(1):99-106.
43. Dahlin LB, Anagnostaki L, Lundborg G. Tissue response to silicone tubes used to repair human median and ulnar nerves. *Scand J Plast Reconstr Surg Hand Surg* 2001;35(1):29-34.
44. Dahlin LB, Lundborg G. Use of tubes in peripheral nerve repair. *Neurosurg Clin N Am* 2001;12(2):341-352.
45. Den Dunnen WFA, Stokroos I, Schakernraad JM, Zondervan GJ, Pennings AJ, Van der Lei B, *et al.* A New PLLA/PCL Copolymer for Nerve Regeneration. *J Mater Sci Mater Med* 1993;4:521-525.
46. Harley BA, Spilker MH, Wu JW, Asano K, Hsu HP, Spector M, *et al.* Optimal degradation rate for collagen chambers used for regeneration of peripheral nerves over long gaps. *Cells Tissues Organs* 2004;176(1-3):153-165.
47. Hoppen HJ, Leenslag JW, Pennings AJ, Van der Lei B, Robinson PH. Two-ply biodegradable nerve guide: basic aspects of design, construction and biological performance. *Biomaterials* 1990;1990(11):286-290.
48. Pêgo AP, Poot AA, Grijpma DW, Feijen J. Copolymers of trimethylene carbonate and ϵ caprolactone for porous nerve guides: Synthesis and properties. *J Biomater Sci Polymer Edn* 2001;12(1):35-53.
49. Meek MF, Coert JH. US Food and Drug Administration/Conformit Europe-Approved Absorbable Nerve Conduits for Clinical Repair of Peripheral and Cranial Nerves. *Ann Plast Surg* 2008;60:110–116.
50. Weber RA, Breidenbach WC, Brown RE, Jabaley ME, Mass DP. A randomized prospective study of polyglycolic acid conduits for digital nerve reconstruction in humans. *Plast Reconstr Surg* 2000;106(5):1036-1048.
51. <http://www.accessdata.fda.gov>. 2009
52. Gonen-Wadmany M, Oss-Ronen L, Seliktar D. Protein-polymer conjugates for forming photopolymerizable biomimetic hydrogels for tissue engineering. *Biomaterials* 2007;28(26):3876-3886.
53. Ma L, Gao C, Mao Z, Zhou J, Shen J. Enhanced biological stability of collagen porous scaffolds by using amino acids as novel cross-linking bridges. *Biomaterials* 2004;25(15):2997-3004.
54. Friedman PM, Mafong EA, Kauvar AN, Geronemus RG. Safety data of injectable nonanimal stabilized hyaluronic acid gel for soft tissue augmentation. *Dermatol Surg* 2002 Jun;28(6):491-494.

55. Ellingsworth LR, DeLustro F, Brennan JE, Sawamura S, McPherson J. The human immune response to reconstituted bovine collagen. *J Immunol* 1986;136(3):877-882.
56. Stothers L, Goldenberg SL. Delayed hypersensitivity and systemic arthralgia following transurethral collagen injection for stress urinary incontinence. *J Urol* 1998;159(5):1507-1509.
57. Heit M. Prolonged urinary retention after collagen periurethral injections: a sequela of humoral immunity. *Obstet Gynecol* 1997;90(4 Pt 2):693-695.
58. Williams SF, Martin DP, Horowitz DM, Peoples OP. PHA applications: addressing the price performance issue. I. Tissue engineering. *Int J Biol Macromol* 1999;25:111-121.
59. McGrath KP, Fournier MJ, Mason TL, Tirrell DA. Genetically directed synthesis of new polymeric materials. Expression of artificial genes encoding proteins with repeating (AlaGly)₃ProGluGly-elements. *J Am Chem Soc* 1992;114:727-733.
60. Silva GA, Czeisler C, Niece KL, Benias E, Harrington DA, Kessler JA, *et al.* Selective differentiation of neural progenitor cells by high-epitope density nanofibers. *Science* 2004;3003(5662):1352-1355.
61. Amsden BG, Tse MY, Turner ND, Knight DK, Pang SC. In Vivo Degradation Behavior of Photo-Cross-Linked *star*-Poly(epsilon-caprolactone-co-D,L-lactide) Elastomers. *Biomacromolecules* 2006;7:365-372.
62. Middleton JC, Tipton AJ. Synthetic biodegradable polymers as orthopedic devices. *Biomaterials* 2000;21:2335-2346.
63. Pitt GG, Hendren RW, Schindler A. The enzymatic surface erosion of aliphatic polyesters. *J Control Release* 1984;1(1):3-14.
64. Bettinger CJ, Bruggeman JP, Borenstein JT, Langer R. In vitro and in vivo degradation of poly(1,3-diamino-2-hydroxypropane-co-polyol sebacate) elastomers. *J Biomed Mater Res A* 2009;91(14):1077-1088.
65. Wang Y, Kim YM, Langer R. In vivo degradation characteristics of poly(glycerol sebacate). *Journal of biomedical materials research* 2003 Jul 1;66(1):192-197.
66. Pitt CG, Gratzl MM, Kimmel GL, Surles J, Sohindler A. Aliphatic polyesters II. The degradation of poly (DL-lactide), poly (epsilon-caprolactone), and their copolymers in vivo. *Biomaterials* 1981;2(4):215-220.
67. Pêgo AP. Biodegradable Polymers Based On Trimethylene Carbonate For Tissue Engineering Applications. Enschede: University of Twente; 2002.
68. De Groot JH, Nijenhuis AJ, Bruin P, Pennings AJ, Veth RPH, Klompmaker J, *et al.* Use of porous biodegradable implants in meniscus reconstruction. 1) Preparation of porous biodegradable polyurethanes for the reconstruction of meniscus lesions. *Colloid Polym Sci* 1990;268:1073-1081.
69. Bogdanov B, Toncheva V, Schacht E. Synthesis and characterization of poly(ester-urethanes). *Macromol Symp* 2000;152:117-126.
70. Crommen J, Vanderpore J, Schacht E. Degradable polyphosphazenes for biomedical applications. *J Control Release* 1993;24:167-180.
71. Deschamps AA, Van Apeldoorn AA, Hayen H, De Bruin JD, Karst U, Grijpma DW, *et al.* In vivo and in vitro degradation of poly(ether ester) block copolymers based on poly(ethylene glycol) and poly(butylene terephthalate). *Biomaterials* 2004;25(2):247-258.
72. Wang Y, Ameer GA, Langer R, inventors. Biodegradable polymer, 2003.
73. Wang Y, Ameer GA, Sheppard BJ, Langer R. A tough biodegradable elastomer. *Nat Biotechnol* 2002;20(6):602-606.
74. Nagata M, Machida T, Sakai W, Tsutsumi N. Synthesis, characterization, and enzymatic degradation of network aliphatic copolyesters. *J Polym Sci Part A: Polym Chem* 1999;37(13):2005-2011.
75. Pomerantseva I, Krebs N, Hart A, Neville CM, Huang AY, Sundback CA. Degradation behavior of poly(glycerol sebacate). *J Biomed Mater Res A* 2009;91(4):1038-1047.

76. Yang F, Webb AR, Ameer GA. Novel Citric Acid-Based Biodegradable Elastomers for Tissue Engineering. *Advanced Materials* 2004;16(6): 511-516.
77. Yang J, Webb AR, Pickerill SJ, Hageman G, Ameer GA. Synthesis and evaluation of poly(diols citrate) biodegradable elastomers. *Biomaterials* 2006;27(9):1889-1898.
78. Ameer GA, Yang J, Webb AR, inventors. Novel biodegradable elastomeric scaffold for tissue engineering and light scattering fingerprinting methods for testing the same. United States, 2005.
79. Engelmayr GCJ, Cheng M, Bettinger CJ, Borenstein JT, Langer R, Freed LE. Accordion-like honeycombs for tissue engineering of cardiac anisotropy. *Nat Mater* 2008;7(12):1003-1010.
80. Fidkowski C, Kaazempur-Mofrad MR, Borenstein JT, Vacanti JP, Langer R, Wang Y. Endothelialized microvasculature based on a biodegradable elastomer. *Tissue Eng* 2005;11(1-2):302-309.
81. Motlagh D, Yang J, Lui KY, Webb AR, Ameer GA. Hemocompatibility evaluation of poly(glycerol sebacate) in vitro for vascular tissue engineering. *Biomaterials* 2006;27(24):4315-4324.
82. Sundback CA, Shyu JY, Wang Y, Faquin WC, Langer RS, Vacanti JP, *et al.* Biocompatibility analysis of poly(glycerol sebacate) as a nerve guide material. *Biomaterials* 2005 Sep;26(27):5454-5464.
83. Kang Y, Yang J, Khan S, Anissian L, Ameer GA. A new biodegradable polyester elastomer for cartilage tissue engineering. *J Biomed Mater Res A* 2006;77(2):331-339.
84. Redenti S, Neeley WL, Rompani S, Saigal S, Yang J, Klassen H, *et al.* Engineering retinal progenitor cell and scrollable poly(glycerol sebacate) composites for expansion and subretinal transplantation. *Biomaterials* 2009;30(20):3405-3414.
85. Sun ZJ, Wu L, Huang W, Chen C, Chen Y, Lu XL, *et al.* Glycolic acid modulates the mechanical property and degradation of poly(glycerol sebacate, glycolic acid). *J Biomed Mater Res A* 2010;92(1):332-339.

Chapter 2

Biodegradable xylitol-based polymers

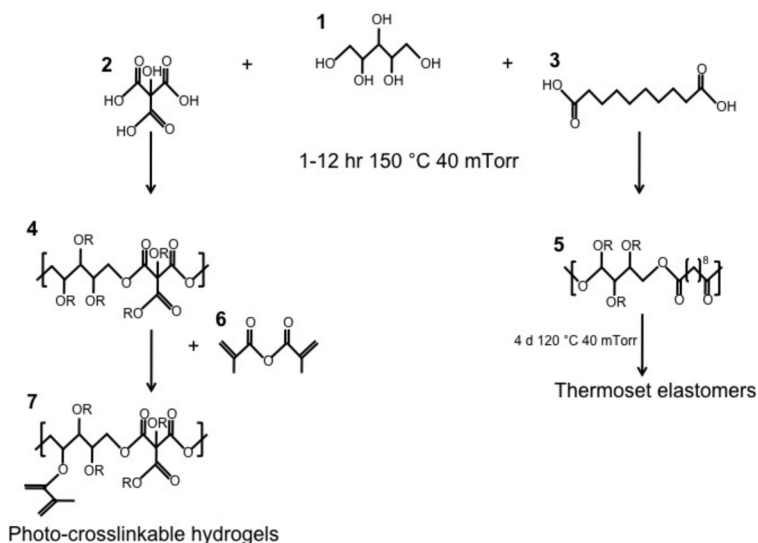
Joost P. Bruggeman, Christiaan L.E. Nijst, Christopher J Bettinger, Daniel S. Kohane, Robert Langer

Adv Mater 2008;20(10):1922-7

Synthetic biodegradable polymers have made a considerable impact in various fields of biomedical engineering, such as drug delivery and tissue engineering. The design of synthetic biodegradable polymers for bioengineering purposes is challenging because of the application-specific constraints on the physical properties, including mechanical compliance and degradation rates, and the need for biocompatibility and low cytotoxicity [1]. The monomer selection frequently limits the range of required material properties. Our goal was to design a class of synthetic biopolymers based on a monomer that possesses a wide range of properties that are biologically relevant. This monomer ideally should be: (1) multifunctional to allow the formation of randomly crosslinked networks and a wide range of crosslinking densities; (2) nontoxic; (3) endogenous to the human metabolic system; (4) FDA approved; and (5) preferably inexpensive. We chose xylitol as it meets these criteria. We hypothesized that biodegradable polyesters could be obtained through copolymerization reactions with polycarboxylic acids; the hydration of such biodegradable polymers could be controlled by tuning the different compositions and stoichiometry of the reacting monomer.

Here, we describe xylitol-based polymers that realize this design. Polycondensation of xylitol with water soluble citric acid yielded biodegradable, water soluble polymers. Acrylation of this polymer resulted in an elastomeric photocrosslinkable hydrogel. Polycondensation of xylitol with the water insoluble sebacic acid monomer produced tough, biodegradable elastomers with tunable mechanical and degradation properties. These xylitol-based polymers exhibited excellent in vitro and in vivo biocompatibility compared to the well-characterized poly(L-lactic-co-glycolic acid) (PLGA), and are promising biomaterials. Sebacic acid (a metabolite in the oxidation of fatty acids) and citric acid (a metabolite in the Krebs cycle) were chosen as the reacting monomers for their proven biocompatibility [2,3]; they are also FDA-approved compounds. Polycondensation of xylitol with sebacic acid produced water insoluble waxy pre-polymers (termed PXS pre-polymers). PXS pre-polymers with a monomer ratio of xylitol: sebacic acid of 1:1 and 1:2 were synthesized and had a weight-average molecular weight (M_w) of 2,443 g/mol ($M_n = 1,268$ g/mol, polydispersity index (PDI) 1.9) and 6,202 g/mol ($M_n = 2,255$ g/mol, PDI 2.7), respectively. The PXS prepolymers were melted into the desired form and cured by polycondensation (120°C, 40 mTorr for 4 days, [1 Torr = 133.3 Pa]) to yield low-modulus (PXS 1:1) and high-modulus (PXS 1:2) elastomers. PXS pre-polymers are soluble in ethanol, dimethyl sulfoxide, tetrahydrofuran and acetone, which allows processing into more complex geometries. Polycondensation of xylitol with citric acid resulted in a water soluble pre-polymer (designated PXC pre-polymer), of which the M_w was 298,066 g/mol and the M_n was 22,305 g/mol (PDI 13.4),

compared to linear poly(ethylene glycol) (PEG) standards. To crosslink the water soluble PXC pre-polymer in an aqueous environment, we functionalized the hydroxyl groups of PXC with vinyl groups (designated PXCma) using methacrylic anhydride, as previously described for photocrosslinkable hyaluronic acid [4,5]. During this reaction, the M_w and M_n of the polymer did not change appreciably. The PXCma pre-polymer was photopolymerized in a 10% (w/v) aqueous solution using a photoinitiator. This is referred to as the PXCma hydrogel. The synthetic route for these polymers is summarized in **Scheme 1**. Fourier-transform infrared (FT-IR) spectroscopy confirmed ester bond formation in all polymers (**Figure 1A**), with a peak at $1,740\text{ cm}^{-1}$, which corresponds to ester linkages. A broad stretch was also observed at approximately $3,448\text{ cm}^{-1}$, which was attributed to hydrogen-bonded hydroxyl groups. Compared to the FT-IR spectrum of PXC, the spectrum of PXCma illustrated an additional stretch at $1,630\text{ cm}^{-1}$, which was associated with the vibration of the vinyl groups. $^1\text{H-NMR}$ spectroscopy revealed a polymer composition of 1.10:1 xylitol to sebacic acid for PXS 1:1, 1.08:2 xylitol to sebacic acid for PXS 1:2, and 1.02:1 xylitol to citric acid for PXC. The degree of substitution of xylitol monomers with a methacrylate group was found to be 44% for the PXCma pre-polymer (average percentage of xylitol monomers modified with a methacrylate group). Ideally, the mechanical properties of an implantable biodegradable device should match its implantation site to minimize mechanical irritation to surrounding tissues and should permit large deformations [2], inherent to the dynamic in vivo environment. All xylitol-based polymers revealed elastic properties (**Figure 1B and C**). The PXS 1:1 elastomer had an average Young's modulus of $0.82 \pm 0.15\text{ MPa}$ with an average elongation at failure of $205.2 \pm 55.8\%$ and an ultimate tensile stress of $0.61 \pm 0.19\text{ MPa}$. Increasing the crosslink density by doubling the feed ratio of the sebacic acid monomer resulted in a stiffer elastomer. The PXS 1:2 elastomer had a Young's modulus of $5.33 \pm 0.40\text{ MPa}$, an average elongation-at-failure of $33.1 \pm 4.9\%$ and an ultimate tensile stress of $1.43 \pm 0.15\text{ MPa}$. The stress versus strain curves of PXS 1:1 and PXS 1:2 were typical for low- and high-modulus elastomers (**Figure 1B**) [2]. DSC showed a glass-transition temperature of 7.3 and 22.9°C for PXS 1:1 and 1:2, respectively, indicating that these elastomers are in a rubbery state at room and physiological temperature. The mechanical properties of the PXS 1:1 elastomer were similar to those of a previously developed elastomer, composed of glycerol and sebacic acid [2]. Altering monomer-feed ratios of sebacic acid in PXS elastomers resulted in a wide range of crosslink densities, whilst maintaining elastomeric properties. The molecular weight between crosslinks (M_c) of the PXS polymers varied by about one order of magnitude (from $10,517.4 \pm 102\text{ g/mol}$ for PXS 1:1 to $1,585.1 \pm 43\text{ g/mol}$ for PXS 1:2, **Table 1**) and decreased as more crosslinking entities



Scheme 1. Schematic representation of the general synthesis scheme of xylitol-based polymers. Xylitol (**1**), was polymerized with citric acid (**2**) or sebacic acid (**3**) into poly(xylitol-co-citrate) (PXC) (**4**), and poly(xylitol-co-sebacate) (PXS) (**5**). Further polycondensation of PXS yielded elastomers. Photocrosslinkable hydrogels were obtained by acrylation of PXC in ddH₂O using methacrylic anhydride (**6**) to yield PXC-methacrylate (PXCma) (**7**). PXCma was polymerized into a hydrogel by free radical polymerization using a photoinitiator. A simplified representation of the polymers is shown. R can be H, OCH₂(CH(OR))₃CH₂OR (xylitol), CO(CH₂)₆COOR (sebacic acid), CO(CH₂)ROC(COOR)(CH₂)COOR (citric acid), or –C(CH₃)=CH₂ (methacrylate group).

were introduced. Such an appreciable difference cannot be obtained by changing the condensation parameters of PXS 1:1. The increased crosslink density in PXS 1:2 also resulted in significantly less equilibrium hydration as determined by mass differential of PXS 1:2 in ddH₂O (24 h at 37 °C), when compared to PXS 1:1, $4.1 \pm 0.3\%$ and $12.6 \pm 0.4\%$, respectively; PXS 1:2 also showed a lower sol content (i.e. the fraction of free macromolecules not covalently bound to the PXS network, **Table 1**). The addition of more sebacic acid molecules to the polymer affects the water-in-air contact angle (PXS 1:1 $26.58 \pm 3.68^\circ$, PXS 1:2 $52.78 \pm 5.78^\circ$, after 5 min), as more aliphatic monomers are being introduced; this observation is in agreement with the findings above. The equilibrium hydration of PXCma hydrogels determined by mass differential was $23.9 \pm 6.2\%$ after 24 h at 37 °C. Volumetric-swelling analysis revealed that the polymer volume fraction in the relaxed state (v_r) was $6.9 \pm 0.1\%$ and the polymer volume fraction in the swollen state (v_s) was $5.8 \pm 0.2\%$, whereby

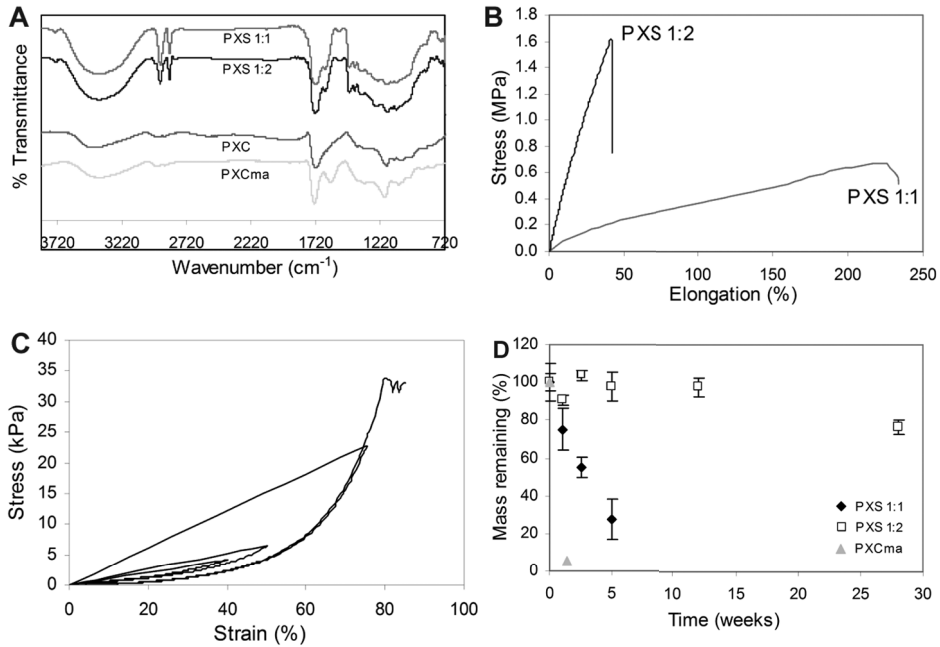


Figure 1. (A) FT-IR analysis of xylitol-based polymers. (B) Typical tensile stress versus strain curve of the PXS elastomers. (C) Typical compression stress versus strain plot of the 10% (w/v) PXCma hydrogel with cyclic compression at 40%, 50%, and 75%, to failure (at ~80%). (D) In vivo mass-loss over time.

v_r was measured immediately after crosslinking, but before equilibrium swelling and v_s was determined at equilibrium swelling. Cyclic compression up to 75% strain of the PXCma hydrogel was possible without permanent deformation and only limited hysteresis was observed during cyclic conditioning, revealing the elastic properties over a wide range of strain conditions. The PXCma hydrogel failed at a compressive strain of $79.9 \pm 5.6\%$ and showed a compressive modulus of 5.84 ± 1.15 kPa (**Figure 1C**). The mechanical properties of the PXCma hydrogel discs were similar to those of the previously reported photocured hyaluronic acid hydrogels (50 kDa, 2-5% (w/v)) [4], although the PXCma hydrogel showed a lower compression modulus for a similar ultimate-compression stress. The physical properties of the elastomers and the hydrogel are summarized in **Table 1**. Xylitol-based biopolymers degrade in vivo. After subcutaneous implantation, approximately 5% of the mass of the hydrogel was found to remain after 10 days. The degradation rate of PXS elastomers varied according to the stoichiometric ratios. PXS 1:1 had fully degraded after 7 weeks. However, $76.7 \pm 3.7\%$ of the PXS 1:2 elastomer still remained after 28 weeks (**Figure**

Polymer	Young's/ compression modulus (kPa)	Elongation/ compression at break (%)	Equilibrium hydration by mass (%)	Sol content (%)	Contact angle (°)	Polymer density (g/cm ³)	Crosslink density (mol/m ³)	M _c (gmol)
PXS 1:1	820±150	205.2±55.8	12.6±0.4	11.0±2.7	26.5±3.6	1.18±0.02	112.2±30.5	10517.4±102.1
PXS 1:2	5330±400	33.1±4.9	4.1±0.3	1.2±0.8	52.7±5.7	1.16±0.02	729.3±57.3	1585.1±43.7
PXCma	5.8±1.2	79.9±5.6	23.9±6.2	31.7±10.6	n/a	1.51±0.05	136.4±27.9	11071.1±115.6

Table 1. Physical properties of xylitol-based polymers (PXS 1:1 and 1:2 are elastomers, PXCma is a photocured hydrogel). M_c is the molecular weight between crosslinks, which was calculated from Equation 1 for the PXS elastomers and from Equations 2 and 3 for the PXCma hydrogel (see Experimental for details).

1D). This demonstrates that the in vivo degradation kinetics of xylitol-based elastomers can be tuned in addition to the crosslink density, surface energy, and equilibrium hydration. Thus, this polymer platform describes a range of physical properties that allow a tuneable in vivo degradation rate. The PXS 1:2 elastomers were optically transparent during the first 15 weeks in vivo and turned opaque upon degradation (in week 28). Compared to the prevalently used synthetic polymer PLGA (65/35 LA/GA, high M_w), xylitol-based polymers show competitive biocompatibility properties, both in vitro and in vivo. Regardless of the eventual in vivo application of these xylitol-based polymers, a normal wound-healing process, which is orchestrated by residential fibroblasts, is mandatory upon implantation; we therefore chose primary human foreskin fibroblasts (HFFs) to test the in vitro biocompatibility. All xylitol-based elastomers and hydrogels were transparent polymers, which facilitated characterization of cell-biomaterial interactions. HFFs readily attached to PXS elastomers and proliferated into a confluent monolayer in 6 days. HFFs cultured on PXS elastomers showed a similar cell morphology and proliferation rate compared to HFFs grown on PLGA (**Figure 2A and B**). There was no cell attachment on PXCma hydrogels. It is known that cells in general do not attach to hydrogels, unless attachment-promoting entities are incorporated [6]. We therefore examined the cytotoxicity of soluble PXCma pre-polymers in culture media. HFFs exposed for 4 or 24 h to PXCma pre-polymer fractions in the growth media (0.01-1% (w/v)) were not compromised in their mitochondrial metabolism, as confirmed with a (1-(4,5- dimethylthiazol-2-yl)-3,5- diphenyltetrazolium bromide) (MTT) assay, compared to HFFs with no PXCma in the growth media (**Figure 2C**). Clinical and histologic assessments showed that none of the animals exhibited an abnormal post-operative healing process after subcutaneous implantation. The PXS 1:1 and 1:2 discs were encased in a translucent tissue capsule after one week, which did not become more substantial throughout the rest of the study. Histological sections confirmed that the polymer/tissue interface was characterized by a mild fibrous-capsule formation (**Figure 2Dii and iii**). No abundant inflammation was seen in the surrounding tissues and the sections showed a quiet polymer/tissue interface, which was characteristic for the PXS elastomers after the first week in vivo. Furthermore, no perivascular infiltration was noted in the surrounding tissues of the PXS discs. This quiescent tissue response was evident when compared to the tissues in contact with the PLGA implants (**Figure 2Di**). A more substantial vascularized fibrous capsule with minor perivascular infiltration (arrow) was seen surrounding the PLGA implants. A comparable thickness of fibrouscapsule formation was noted for the 10% PXCma hydrogel at day 10 (**Figure 2Div**). No PXCma hydrogel was found at day 14 after repetitive sectioning of the explanted tissue. Long-term histological sections of PXS 1:1 and 1:2 at week 5 and 12 demonstrated that even upon degradation

the fibrous capsule remained quiescent: at week 5 the PXS 1:1 elastomer had degraded by approximately 73%, whereas the PXS 1:2 polymer showed no degradation at all at week 12. Thus, xylitol-based polymers exhibited excellent biocompatibility compared to PLGA.

Our goal was to develop a polymer synthesis scheme that required very simple adjustments in chemical composition to achieve a wide range of material properties. We have described a process for the synthesis of xylitol-based polymers. Xylitol is well studied in terms of biocompatibility and pharmacokinetics in humans [7,8]. It is a metabolic intermediate in the mammalian carbohydrate metabolism with a daily endogenous production of 5-15 g in adult humans [9]. The entry into metabolic pathways is slow and independent of insulin, and does not cause rapid fluctuations of blood glucose levels [10]. As a monomer, xylitol is an important compound in the food industry, where it has an established history as a sweetener with proven anti-cariogenic activity [11]. Moreover, it has an antimicrobial effect on upper-airway infections caused by Gram-positive streptococci [12–15]. Although xylitol has been studied in polymer synthesis, others have typically utilized it as an initiator [16] or altered xylitol to yield linear polymers by protecting three of the five functional groups [17]. They were produced in sub-kilogram quantities without the use of organic solvents or cytotoxic additives. Xylitol-based polymers are endotoxin-free and do not impose a potential immunological threat like biological polymers extracted from tissues or produced by bacterial fermentation, such as collagen and hyaluronic acid [18,19]. In addition, the mechanical properties of xylitol-based elastomers correspond to biologically relevant values that fall close to or are equal to those of various tissues, such as acellular peripheral nerves [20], small diameter arteries [21], cornea [22] and intervertebral discs [23]. In this report, we have shown only three examples of possible polymers based on this monomer. Potential combinations for the chemical composition of xylitol-based polymers are numerous and therefore it provides a platform to tune mechanical properties, degradation profiles and cell attachment.

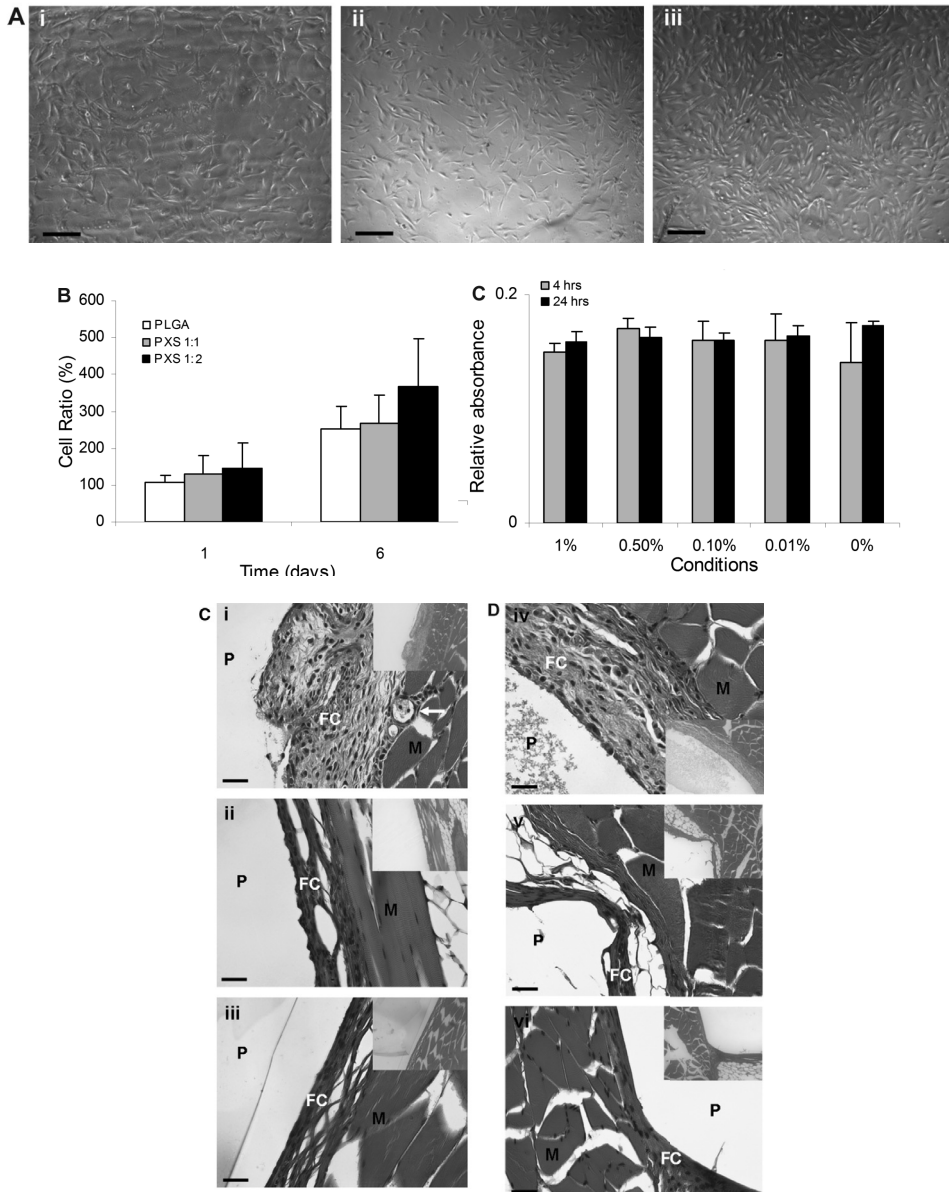


Figure 2. (A) Phase-contrast images (10x) of human primary fibroblasts after 5 days of in vitro culture, seeded on PLGA (i), PXS 1:1 (ii) and PXS 1:2 (iii). Bars represent 250 μ m. (B) Growth rates of fibroblasts on PLGA, PXS 1:1 and PXS 1:2, expressed as cell differential. (C) MTT assay of fibroblasts exposed to different PXCma prepolymer fractions in their growth medium. (D) Representative images of H&E-stained sections of subcutaneous implantation sites of (i) PLGA discs, (ii) PXS 1:1 discs, (iii) PXS 1:2 discs, (iv) 10% (w/v) PXCma hydrogel discs, 1 week after implantation. (v) Shows the PXS 1:1 implantation site at week 5 (~73% had degraded) and (vi) shows PXS 1:2 at week 12 (no degradation). The arrow (i) points to a vessel of the fibrous capsule surrounding the PLGA implant, where some perivascular infiltration is observed. P = polymer, FC = fibrous capsule, M = muscle. Inserts are 5x overviews, full images are magnified 25x. Bars represent 100 μ m.

Experimental

Synthesis and Characterization of the Polymers: All chemicals were purchased from Sigma-Aldrich unless stated otherwise. Appropriate molar amounts of the polyol and reacting acid monomer were melted in a round bottomed flask at 150°C under a blanket of inert gas and stirred for 2 h. A vacuum (~50 mTorr) was applied to yield the pre-polymers PXS 1:1 (12 h), PXS 1:2 (6 h) and PXC (1 h). The PXC polymer was dissolved in ddH₂O and lyophilized. Methacrylated PXC pre-polymer (PXCma) was synthesized by the addition of methacrylic anhydride in a ~20-fold molar excess, as previously described for the methacrylation of hyaluronic acid [5], dialyzed in double-distilled water (ddH₂O, M_w cutoff: 1 kDa) and lyophilized. PXCma hydrogels were fabricated by dissolving 10% (w/v) PXCma in a phosphate-buffered saline (PBS) solution containing 0.05% (w/v) 2-methyl-1-(4-(hydroxyethoxy) phenyl)-2-methyl-1-propanone (Irgacure 2959, I2959) as the photoinitiator under exposure of ~4 mW/cm² ultraviolet light (lamp model 100AP, Black-Ray). All PXS 1:1 and 1:2 elastomers were produced by further polycondensation (120°C, 140 mTorr for 4 days). The pre-polymers were characterized using gel permeation chromatography using THF or filtered ddH₂O as eluentia and Styragel columns (series of HR-4, HR-3, HR-2, and HR-1, Waters, Milford, MA, USA). FT-IR analysis was carried out on a Nicolet Magna-IR 550 spectrometer. ¹H-NMR spectroscopy was performed on a Varian Unity-300 NMR spectrometer; ¹H-NMR spectra of the PXS pre-polymers were determined in C₂D₆O and spectra of the PXCma pre-polymers were obtained in D₂O. The chemical composition of the pre-polymers was determined by calculating the signal integrals of xylitol and compared to the signal integrals of sebacic acid or citric acid. The signal intensities showed peaks of (–OCH₂(CH(OR))₃CH₂O–) at 3.5–5.5 ppm from xylitol, (–CH₂–) at 2.3–3.3 ppm from citric acid, and peaks of (–COCH₂CH₂CH₂–) at 1.3, 1.6 and 2.3 ppm from sebacic acid. The final degree of substitution after acrylation of the PXC pre-polymer was calculated by the signal integral of the protons associated with (–C(CH₃)–CH₂) at 1.9, 5.7 and 6.1 ppm from the methacrylate groups. Tensile tests were performed on hydrated (ddH₂O at 37 °C > 24 h) dog bone-shaped polymer strips and conducted on an Instron 5542 (according to the American Society for Testing and Materials (ASTM) standard D412-98a). Compression analysis of the photocrosslinked PXCma hydrogels was performed as described previously [5]. Differential scanning calorimetry (DSC) was performed as reported previously [24]. The mass density was measured using a pycnometer (Humboldt, MFG. CO). The crosslink density (n) and M_c were calculated from the following equations for an ideal elastomer [25]:

$$n = \frac{E_0}{3RT} = \frac{\rho}{M_c} \quad (1)$$

where E_0 is the Young's modulus, R the universal gas constant, T temperature and ρ is the mass density. According to Peppas *et al.* [26], this rubber-elasticity theory can also be utilized to calculate the effective M_c for hydrogels that show elastic behavior and were prepared in the presence of a solvent:

$$\tau = \frac{\rho RT}{M_c} \left[1 - \frac{2M_c}{M_n} \right] \left(a - \frac{1}{a^2} \right) \left(\frac{v_s}{v_r} \right)^{1/3} \quad (2)$$

where τ is the compression modulus of the hydrogel, v_s (0.058 ± 0.002) is the polymer volume fraction in the swollen state, and v_r (0.069 ± 0.001) is the polymer volume fraction in the relaxed state. For an isotropically swollen hydrogel, the elongation ratio (a) is related to the swollen polymer-volume fraction:

$$a = v_s^{1/3} \quad (3)$$

The water-in-air contact-angle measurements were carried out as published previously [2]. Degradation of the explanted polymers was determined by mass differential, calculated from the polymer's dry weight at $t = t$ days, and compared to the dry weight at the start of the study ($t = 0$). All data were obtained from at least four replicate samples and were expressed as means \pm standard deviation.

In Vitro and In Vivo Biocompatibility: Primary human foreskin fibroblasts (ATCC, Manassas, VA, USA) were cultured in growth media, as described previously [24]. Glass Petri dishes (60 mm diameter) contained 3 g of cured elastomers (120°C , 140 mTorr for 4 days). Petri dishes prepared with a 2% (w/v) PLGA solution (65/35, high M_w , Lakeshore Biomedical, Birmingham, AL, USA) in dichloromethane at $100 \mu\text{L}/\text{cm}^2$ and subsequent solvent evaporation served as control. Washes with sterile PBS were done before the polymer-loaded dishes were sterilized by UV radiation. Cells were seeded (at $2,000 \text{ cells}/\text{cm}^2$) in the biomaterial-laden dishes without prior incubation of the polymers with growth media. Cells were allowed to grow to confluency and imaged at 4 h, and 1, 3, 5, and 6 days after initial seeding. Phase micrographs of cells were taken at 10x magnification using Axiovision software (Zeiss, Germany). For cell proliferation measurements, randomly picked areas were imaged and cells were counted. That cell number was expressed as the percentage increase of cells compared to the initial seeding, designated cell differential. To assess cytotoxicity of the PXCma macromers, cells were seeded in tissue culture-treated polystyrene dishes at 10,000

cells/cm² and allowed to settle for 4 h. After a gentle wash with sterile PBS, 1%, 0.5%, 0.1%, and 0.01% (w/v) of PXCma in growth media was added for 4 or 24 h. Cell viability via the mitochondrial metabolism was measured using the methylthiazoletetrazolium (MTT) assay as previously reported [2]. The statistical significance between two sets of data was calculated using a two-tailed Student's t-test. For the in vivo biocompatibility and degradation study, elastomeric discs (d = 10 mm, h = 1 mm) were implanted. PLGA pellets were melt-pressed (0.3 g, 172°C, 5,000 MPa) into a mold (d = 10 mm, h = 1mm) using a Carver Hydraulic Unit Model #3912-ASTM (Carver, Inc. Wabash, IN). Female Lewis rats (Charles River Laboratories, Wilmington, MA) weighing 200–250 g were housed in groups of two and had access to water and food *ad libitum*. Animals were cared for according to the protocols of the Committee on Animal Care of MIT in conformity with the National Institute of Health (NIH) guidelines (NIH publication #85–23, revised 1985). The animals were anaesthetized using continuous 2% isoflurane/ O₂ inhalation. The implants were introduced by two, small, midline dorsal incisions and two polymer formulations (each on one side) were placed in subcutaneous pockets created by lateral blunt dissection. The skin was closed with staples. Per time data point, three rats were sacrificed, from which four implants were analyzed for the degradation study, and two implants were resected *en bloc* with the surrounding tissue and fixed in formalin-free fixative (Accustain). These specimens were embedded in paraffin after a series of dehydration steps in ethanol and xylene. Sequential sections (8–15 mm) were stained with hematoxylin and eosine (H&E) and were evaluated by two medical doctors (JPB, DSK). Throughout the study, all rats remained in good general health as assessed by their weight gain.

References

1. Langer R, Vacanti JP. Tissue engineering. *Science* 1993;260(5110):920-6.
2. Wang Y, Ameer GA, Sheppard BJ, Langer R. A tough biodegradable elastomer. *Nat Biotechnol* 2002;20(6):602-606.
3. Yang J, Webb AR, Ameer GA. Novel citric acid-based biodegradable elastomers for tissue engineering. *Adv Mater* 2004;16(6):511-616.
4. Burdick JA, Chung C, Jia X, Randolph MA, Langer R. Controlled degradation and mechanical behavior of photopolymerized hyaluronic acid networks. *Biomacromolecules* 2005;6:386-391.
5. Smeds KA, Pfister-Serres A, Miki D, Dastgheib K, Inoue M, Hatchell DL, Grinstaff MW. Photocrosslinkable polysaccharides for in situ hydrogel formation. *J Biomed Mater Res* 2001;54(1):115-121.
6. Hern DL, Hubbell JA. Incorporation of adhesion peptides into nonadhesive hydrogels useful for tissue resurfacing. *J Biomed Mater Res* 1998;39:266-276.

7. Sestoft L. An evaluation of biochemical aspects of intravenous fructose, sorbitol and xylitol administration in man. *Acta Anaesthesiol Scand Suppl* 1985;82:19-29.
8. Talke H, Maier KP. [Glucose, fructose, sorbitol and xylitol metabolism in man] *Infusionstherapie* 1973;1(10):49-56.
9. Winkelhausen E, Kuzmanova S. Microbial conversion of D-xylose to xylitol. *J Ferment Bioeng* 1998;86(1):1-14.
10. Natah SS, Hussien KR, Tuominen JA, Koivisto VA. Metabolic response to lactitol and xylitol in healthy men. *Am J Clin Nutr* 1997;65(4):947-950.
11. Honkala E, Honkala S, Shyama M, Al-Mutawa SA. Field trial on caries prevention with xylitol candies among disabled school students. *Caries Res.* 2006;40(6):508-513.
12. Uhari M, Kontiokari T, Koskela M, Niemela M. Xylitol chewing gum in prevention of acute otitis media: double blind randomized trial. *BMJ* 1996;313(7066):1180-1184.
13. Uhari M, Tapiainen T, Kontiokari T. Xylitol in preventing acute otitis media. *Vaccine* 2000; 19(Suppl 1):S144-147.
14. Durairaj L, Launspach J, Watt JL, Mohamad Z, Kline J, Zabner J. Safety assessment of inhaled xylitol in subjects with cystic fibrosis. *J Cyst Fibros* 2007;6(1):31-34.
15. Zabner J, Seiler MP, Launspach JL, Karp PH, Kearney WR, Look DC, Smith JJ, Welsh MJ. The osmolyte xylitol reduces the salt concentration of airway surface liquid and may enhance bacterial killing. *Proc Natl Acad Sci USA* 2000;97(21):1161-1169.
16. Hao Q, Li F, Li Q, Li Y, Jia L, Yang J, Fang Q, Cao A. Preparation and crystallization kinetics of new structurally well-defined star-shaped biodegradable poly(L-lactide)s initiated with diverse natural sugar alcohols. *Biomacromolecules* 2005;6(4):2236-2247.
17. Gracia Garca-Martin M, Benito Hernandez E, Ruiz Perez R, Alla A, Munoz-Guerra S, Galbis JA. Synthesis and characterization of linear polyamides derived from L-arabinitol and xylitol. *Macromolecules* 2004;37:5550-5556.
18. Ellingsworth LR, DeLustro F, Brennan JE, Sawamura S, McPherson J. The human immune response to reconstituted bovine collagen. *J Immunol* 1986;136(3):877-882.
19. Lupton JR, Alster TS. Cutaneous hypersensitivity reaction to injectable hyaluronic acid gel. *Dermatol Surg* 2000;26(2):135-137.
20. Borschel GH, Kia KF, Kuzon WM Jr, Dennis RD. Mechanical properties of acellular peripheral nerve. *J Surg Res* 2003;114:133-139.
21. Clerin V, Nichol JW, Petko M, Myung RJ, Gaynor W, Gooch KJ. Tissue engineering of arteries by directed remodeling of intact arterial segments. *Tissue Eng* 2003;9(3):461-472.
22. Hjortdal JO. Regional elastic performance of the human cornea. *J Biomech* 1996;29(7):931-942.
23. Skrzypiec DM, Pollintine P, Przybyla A, Dolan P, Adams MA. The internal mechanical properties of cervical intervertebral discs as revealed by stress profilometry. *Eur Spine J* 2007;16(10):1701-1709.
24. Nijst CLE, Bruggeman JP, Karp JM, Ferreira L, Zumbuehl A, Bettinger CJ, Langer R. Synthesis and characterization of photocurable elastomers from poly(glycerol sebacate). *Biomacromolecules* 2007;8(10):3067-3073.
25. Flory PJ. *Principles of Polymer Chemistry*, Cornell University Press, Ithaca, New York 1953.
26. Peppas NA, Hilt JZ, Khademhosseini A, Langer R. Hydrogels in biology and medicine: from molecular principles to bionanotechnology. *Adv Mater* 2006;18:1345-1360.

Chapter 3

Biodegradable poly(polyol sebacate) polymers

Joost P. Bruggeman, Berend-Jan de Bruin, Christopher J Bettinger, Robert Langer

Biomaterials 2008;29(36):4726-4735

Abstract

We have developed a family of synthetic biodegradable polymers that are composed of structural units endogenous to the human metabolism, designated poly(polyol sebacate) (PPS) polymers. Material properties of PPS polymers can be tuned by altering the polyol monomer and reacting stoichiometric ratio of sebacic acid. These thermoset networks exhibited tensile Young's moduli ranging from 0.37 ± 0.08 to 378 ± 33 MPa with maximum elongations at break from $10.90 \pm 1.37\%$ to $205.16 \pm 55.76\%$, and glass transition temperatures ranging from ~ 7 – 46 °C. In vitro degradation under physiological conditions was slower than in vivo degradation rates observed for some PPS polymers. PPS polymers demonstrated similar in vitro and in vivo biocompatibility compared to poly(L-lactic-co-glycolic acid) (PLGA).

1. Introduction

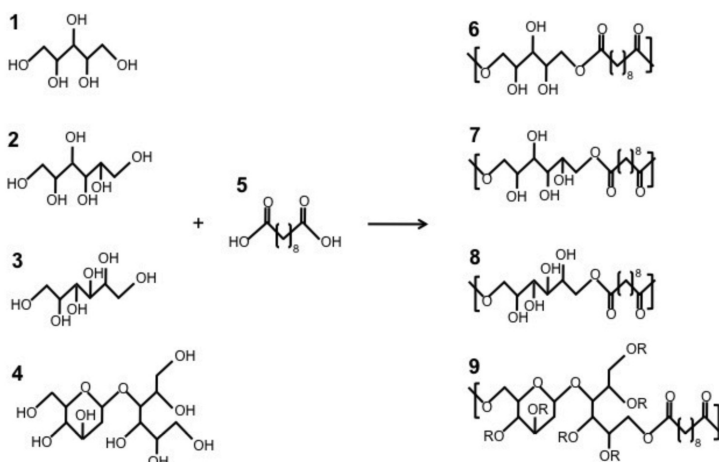
Biodegradable elastomers have been developed to overcome problems associated with biodegradable thermoplastic materials, such as rigid mechanical properties, bulk degradation and acidic degradation products in some cases [1-3]. Thermoset elastomers such as poly(glycerol sebacate) (PGS) have shown to primarily degrade by surface erosion [5], retaining their structural integrity and form stability during degradation in vivo. Therefore, biomaterials based on these elastomers hold great promise in soft tissue applications that require small features, such as gecko-inspired surgical adhesives [6], microfabricated scaffolds [7,8], cardiovascular tissue engineering applications [9,10] and small diameter nerve grafts [11]. However, current PGS elastomers cover a modest range in mechanical properties and degradation rates, limiting them to relatively short-term soft tissue applications. Recently, a versatile polymer platform composed of metabolites endogenous to the mammalian organism was described using xylitol as the central monomer, yielding hydrogels and elastomers with tunable mechanical properties and in vivo degradation rates [12].

In this study, polyols were reacted with sebacic acid, yielding a family of thermoset poly(polyol sebacate) (PPS) polymers. Three general criteria led to the selection of polyols as monomers in this design: they are (1) non-toxic, (2) multifunctional to allow the formation of randomly crosslinked networks as well as a wide range of crosslink densities, and (3) allow formation of hydrolysable esters in polycondensation polymerizations. The monomers of PPS polymers have the potential to be metabolized in vivo, as sebacic acid is a metabolite in fatty acid oxidation and polyols are intermediates in mammalian carbohydrate metabolism. Polyols such as xylitol, sorbitol, mannitol and maltitol are metabolized in an insulin-independent manner [13-15]. The functionality and physical properties of the different polyols influenced polymer properties. Stoichiometry further allowed for tuning chemical, physical and mechanical properties, as well as in vitro and in vivo degradation rates. The potential use of PPS polymers in a wide variety of biomedical applications was assessed through in vitro and in vivo biocompatibility tests, and compared to PLGA.

2. Materials and Methods

2.1 Synthesis and characterization of PPS polymers

All chemicals were purchased from Sigma-Aldrich (St. Louis, MO, USA) unless stated otherwise. Appropriate molar amounts of the polyol and sebacic acid monomer were melted in a 250 mL round bottomed flask at 150°C under a blanket of inert gas, and stirred for 2 h. Vacuum (~50 mTorr) was applied for 2-12 h, yielding the pre-polymers poly(xylitol sebacate) (PXS) 1:1 and PXS 1:2, poly(sorbitol sebacate) (PSS) 1:1 and PSS 1:2, poly(mannitol sebacate) (PMS) 1:1 and PMS 1:2, and poly(maltitol sebacate) (PMtS) 1:4 (**Scheme 1**, **Table 1**). The pre-polymers were characterized using linear polymer standards for gel permeation chromatography (GPC) using tetrahydrofuran (THF) on Styragel columns (series of HR-4, HR-3, HR-2, and HR-1, Waters, Milford, MA, USA). ^1H -NMR spectra were obtained of all pre-polymers in $(\text{CD}_3)_2\text{NCOD}$, on a Varian Unity-300 NMR spectrometer.



Scheme 1. General synthetic scheme of polyol-based polymers. Xylitol (**1**), sorbitol (**2**), mannitol (**3**) and maltitol (**4**) were polymerized with sebacic acid (**5**) in different stoichiometries, yielding PXS (**6**), PSS (**7**), PMS (**8**) and PMtS (**9**). Simplified representations of the polymers are shown.

Pre-polymer	Composition by ¹ H-NMR (°C)	T _m	M _w (g/ mol)	M _n (g/ mol)	PDI
PXS 1:1	1.10 : 1.00	~80	2443	1268	1.9
PXS 1:2	1.08 : 2.00	~100	6202	2255	2.7
PSS 1:1	0.91 : 1.00	~80	6093	3987	1.5
PSS 1:2	0.89 : 2.00	~100	23013	8990	2.6
PMS 1:1	0.99 : 1.00	~100	3182	2038	1.6
PMS 1:2	1.06 : 2.00	~120	10097	4379	2.3
PMtS 1:4	1.18 : 4.00	~130	13265	2992	4.4

Table 1. Polycondensation conditions, composition, melting temperatures and molecular weight distributions of PPS pre-polymers T_m was the observed temperature below which a transition from opaque waxy polymers to viscous clear liquid polymers was observed. M_n: number average molecular weight. M_w: weight average molecular weight. PDI: polydispersity index (M_w/M_n).

The chemical composition of the pre-polymers was determined by comparing the signal integrals of the polyol, and compared to the signal integrals of sebacic acid. The signal intensities showed peaks of $-\text{OCH}_2(\text{CH}(\text{OR}))_n\text{CH}_2\text{O}-$ at 3.5-5.5 ppm from the polyol, and peaks of $-\text{COCH}_2\text{CH}_2\text{CH}_2-$ at 1.3, 1.6 and 2.3 ppm from sebacic acid. The PPS polymers were produced by another polycondensation step using 120-150°C under vacuum (~2 Pa) for 4 d (see **Table 2** for specific curing conditions). Attenuated total reflectance-Fourier transform infrared spectroscopy (ATR-FTIR) analysis was performed on these polymer networks using a Nicolet Magna-IR 500 spectrophotometer. The wettability of PPS polymers was determined by contact-angle measurements, and the hydration of these polymers, determined by mass differential after 24 h in ddH₂O at 37 °C. The water-in-air contact angle of polymer films was measured using the sessile-drop method and VCA2000 image analysis software ($n = 10$). Tensile tests were performed on hydrated (ddH₂O at 37 °C >24 h) dog-bone shaped polymer strips ($n = 4$) and conducted on an Instron 5542 (according to ASTM standard D412-98a) using a 50 or a 500 N load cell equipped with Merlin software. Glass transition temperatures (T_g) and other potential phase transitions were measured within the temperature range of -90°C and 250°C with a heating/cooling rate of 10°C/min using a Q1000 DSC equipped with Advantage Software v2.5 (TA Instruments, Newcastle, DE USA) and analyzed with Universal Analysis Software v4.3A (TA Instruments). The mass densities were measured using a pycnometer (Humboldt, MFG. CO), and crosslink density (n) as well as the relative molecular mass between crosslinks (M_c) were calculated from the following equations for an ideal elastomer [16], where E_0 is the Young's modulus, R is the universal gas constant, T is the temperature and ρ is the mass density:

$$n = \frac{E_0}{3RT} = \frac{\rho}{M_c} \quad (1)$$

2.2 In vitro degradation of PPS polymers

Degradation rates via hydrolysis were observed of sol-free PPS samples ($n = 4$) continuously agitated at 37 °C in 20 mL PBS containing sodium azide (0.05 % w/v), or in 20 mL of 0.1 M NaOH at 37 °C as previously reported [17]. At designated time points, samples were removed, washed in ddH₂O, incubated in ethanol overnight, dried at 90°C for 1 d and weighed again to determine mass loss. The mass loss was calculated from dry weight at t (M_t) and compared to the dry weight at the start of the study (M_o) using the following equation:

$$M_{Loss} = \frac{M_o - M_t}{M_o} \times 100\% \quad (2)$$

2.3 In vitro biocompatibility of PPS polymers

Glass Petri dishes (60 mm diameter, Fisher Scientific) contained 3 g of cured elastomers (120°C, 140 mTorr for 4 d). Petri dishes prepared with a 1.5% w/v PLGA (65/35, high M_w , Lakeshore Biomedical, Birmingham, AL, USA) solution in dichloromethane at 60 $\mu\text{L}/\text{cm}^2$ and subsequent solvent evaporation served as control. Washes with sterile PBS were done and before the polymer loaded dishes were autoclaved. Primary human foreskin fibroblasts (HFFs) (ATCC, Manassas, VA, USA) were cultured in high glucose Dulbecco's Minimal Essential Medium (DMEM) supplemented with 10% (v/v) fetal bovine serum (Invitrogen), 100 $\mu\text{g}/\text{mL}$ streptomycin (Invitrogen), and 100 U/mL penicillin (Invitrogen). Cells between passage three and six were harvested using trypsin 0.025%/ EDTA 0.01% and quenched with an equal volume of medium to resuspend the cells. Additional cell systems were chosen from tissues with mechanical properties that match, or fall close to the mechanical properties of specific PPS polymers tested. A human bone cell line derived from an osteosarcoma (OS) (CRL-1545, ATCC, Manassas, VA, USA) was cultured in PMTs 1:4 coated dishes. A human muscle cell line derived from a rhabdomyosarcoma (RMS) (CCL-136, ATCC,

Polymer (curing condition)	Young's modulus (MPa)	Ultimate tensile stress (MPa)	Ultimate elongation (%)	Contact angle (°)	T_g (°C)	Hydration by mass (%)	ρ (g/cm ³)	n (mol/m ³)	M_c (g/mol)
PXS 1:1 (120°C, 2 Pa, 4 d)	0.82 ± 0.15	0.61 ± 0.19	205.16 ± 55.76	26.5 ± 3.6	7.3	5.10 ± 0.12	1.18 ± 0.02	112.2 ± 30.5	10517.4 ± 102.1
PXS 1:2 (120°C, 2 Pa, 4 d)	5.33 ± 0.40	1.43 ± 0.15	33.12 ± 4.85	52.7 ± 5.7	22.9	1.74 ± 0.1	1.16 ± 0.02	729.32 ± 57.3	1585.1 ± 43.7
PSS 1:1 (120°C, 2 Pa, 5 d)	0.37 ± 0.08	0.57 ± 0.15	192.24 ± 60.12	9.6 ± 3.0	18.1	6.28 ± 0.27	1.13± 0.04	50.6 ± 10.3	22320.1 ± 85.3
PSS 1:2 (120°C, 2 Pa, 4 d)	2.67 ± 0.12	1.16 ± 0.33	65.94 ± 24.87	36.6 ± 3.1	26.9	1.80 ± 0.09	1.16± 0.02	365.3 ± 21.5	3175.2 ± 132.1
PMS 1:1 (140°C, 2 Pa, 5 d)	2.21 ± 0.21	0.79 ± 0.10	50.54 ± 9.01	32.2 ± 9.0	16.5	4.45 ± 0.14	1.18± 0.02	302.4 ± 60.2	3902.2 ± 109.1
PMS 1:2 (140°C, 2 Pa, 5 d)	12.82 ± 2.90	3.32 ± 0.76	44.99 ± 11.81	40.4 ± 9.3	32.2	1.82 ± 0.15	1.16± 0.03	1754.2 ± 242.4	661.3 ± 219.2
PMIS 1:4 (150°C, 2 Pa, 5 d)	378.0 ± 33.0	17.64 ± 1.30	10.90 ± 1.37	26.3 ± 8.4	45.6	1.40 ± 0.03	1.18 ± 0.01	n/a	n/a

Table 2. Curing conditions, physical and mechanical properties of PPS polymers. M_c : the molecular weight between crosslinks, and n : crosslink density, both calculated with Eq. (1) (Section 2).

Manassas, VA, USA) was cultured in PSS 1:1 coated dishes. Bovine articular chondrocytes (BAC) were harvested from femoropatellar grooves of 2-4 week-old bovine calves, as previously described [18] and cultured in PMS 1:2 coated dishes. Human umbilical vein endothelial cells (HUVECs) (Cambrex, Walkersville, MD) were cultured on PXS 1:1 laden dishes, in EGM-2 media supplemented with SingleQuot Kits (Cambrex). HUVECs were used by passage five and in accordance with the manufacturer's instructions. The fibroblasts and tissue specific cells were seeded (at 7500 cells/cm²) in PLGA- or PPS-laden dishes and were allowed to grow to a confluent cell monolayer at 37 °C and 5% CO₂, whilst imaged after 4 h and every subsequent day after initial seeding. Phase micrographs of cells were taken at 10x magnification using Axiovision software (Zeiss). For cell proliferation measurements, randomly picked areas were imaged and cells were counted and averaged. The area and circularity [19] of cell populations were calculated manually using perimeter and area measurements by using Axiovision software (Zeiss). The circularity C was calculated using the following formula:

$$C = \frac{4\pi A}{P^2} \quad (3)$$

where A is the projected area of the cell and P is the perimeter of the cell. Circularity was used as an index of cell spreading. Three distinct cell populations ($n = \sim 80$ total) were measured to find cell population means.

2.4 In vivo biocompatibility of PPS polymers

PPS discs $d = 10$ mm, $h = 1$ mm were implanted. Comparable PLGA pellets were melt-pressed (0.3 g, 172°C, 5000 MPa) into a mold ($d = 10$ mm, $h = 1$ mm) using a Carver Hydraulic Unit Model #3912ASTM (Carver, Inc. Wabash, IN). Two female Lewis rats (Charles River Laboratories, Wilmington, MA) weighing 200-250 grams had access to water and food *ad libitum*. Animals were cared for according to the protocols of the Committee on Animal Care of MIT in conformity with the NIH guidelines (NIH publication #85-23, revised 1985). The animals were anaesthetized using continuous 2% isoflurane/O₂ inhalation. The implants were introduced by three small midline dorsal incisions, and five polymer formulations were placed in subcutaneous pockets created by blunt lateral dissection. The skin was closed with staples. Rats were sacrificed, the implants were resected *en bloc* with surrounding tissue and fixed in formalin-free fixative (Accustain). These specimens were embedded in paraffin after a series of dehydration steps in ethanol and xylene. Sequential sections (8-

15 μm) were stained with hematoxylin and eosine (H&E) and histology was evaluated by a medical doctor (JPB). Throughout the study, all rats remained in good general health as assessed by their weight gain.

2.5 Statistical analysis

Two-tailed student's t-tests with unequal variances were performed to determine statistical significance (Microsoft Excel, Redmond, WA USA). Two-way ANOVA tests were performed where appropriate (GraphPad Prism 4.02, GraphPad Software, San Diego, CA USA). Bonferroni multiple comparison post-tests were used to determine significance between specific treatments. All tabulated and graphical data is reported as mean \pm S.D. Significance levels were set at $p < 0.05$ (indicated with *).

3. Results

3.1 Pre-polymer synthesis and characterization

All pre-polymers were prepared through bulk polycondensation reactions of the polyol and sebacic acid monomers (**Scheme 1**). The following stoichiometric ratios were prepared: PXS 1:1 and 1:2, PSS 1:1 and 1:2, PMS 1:1 and 1:2, and PMtS 1:4. **Figure 1A** shows a typical ^1H NMR spectrum of a PPS pre-polymer. The chemical composition of the pre-polymers was determined by calculating the ratios of the signal integrals of the polyol to sebacic acid. ^1H NMR revealed polymer compositions that are summarized in **Table 1**. In addition, weight average molecular weight (M_w), number average molecular weight (M_n) and polydispersity index (PDI) for all PPS pre-polymers were determined by GPC, and are shown in **Table 1**. No distinct, broad peaks associated with a melting temperature (T_m) could be detected with DSC for the pre-polymers, most likely due to the polydispersity of the pre-polymers. However, different temperatures were used to melt process these pre-polymers, and are listed in **Table 1** as well. All polymers are clear, viscous liquids at 130°C , and waxy, opaque materials at room temperature. The pre-polymers are soluble in common solvents such as ethanol, acetone, dimethyl sulfoxide, tetrahydrofuran, and dimethylformamide.

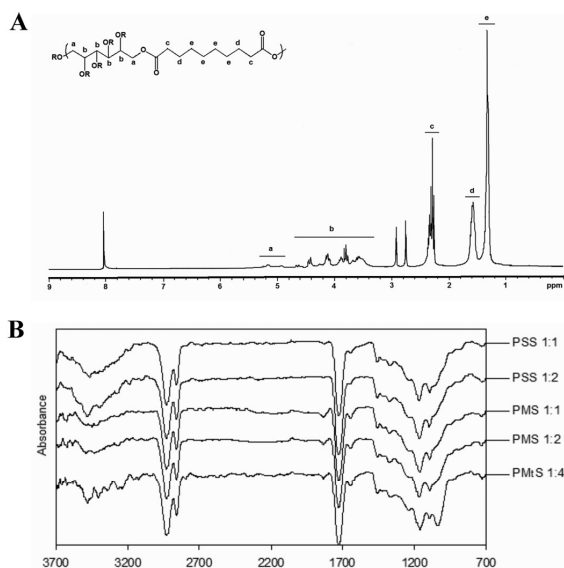


Figure 1. (A) A representative ^1H NMR spectrum of PPS polymers, PMS 1:1 in this case. Signal intensities of the polyols at 3.5–5.5 ppm, and of sebacic acid in the polymer were identified at 1.2, 1.5, 2.2 ppm by hydrogens on the carbons labeled 'a'–'b', and 'c'–'e' respectively. (B) FTIR analysis of PPS polymers.

3.2 Characterization and physical properties of PPS polymers

The pre-polymers were thermally cured into thermoset networks under different curing conditions, as summarized in **Table 2**. FT-IR of the cured polymers confirmed ester bond formation in all polymers, with a peak at 1740 cm^{-1} which corresponds to the ester linkages. A broad stretch was also observed at approximately 3448 cm^{-1} which corresponds to hydrogen bonded hydroxyl groups. The FT-IR spectrum of PMtS 1:4 illustrated an additional stretch at 1050 cm^{-1} compared to the spectra of the other PPS polymers, which is associated with the vibration of the ether bond within the maltitol monomer (**Figure 1B**). The thermal properties of the PPS polymers were revealed by DSC: PXS 1:1, PSS 1:1 and PMS 1:1 had glass transition temperatures below room temperature. PXS 1:2, PSS 1:2 and PMS 1:2 had glass transition temperatures higher than the 1:1 stoichiometries, but still remained below 37°C , indicating that these PPSs are rubbery at physiological temperatures. PMtS 1:4 showed the highest glass transition temperature at 45°C , demonstrating that this polymer is glassy at 37°C (**Table 2**). Increasing the sebacic acid monomer feed ratio resulted in a higher crosslink density and in lesser wettability of the polymers, as demonstrated by weight differential at equilibrium hydration, as well as contact angle measurements, as summarized in **Table 2**.

3.3 Mechanical properties of PPS polymers

All hydrated PPS polymers, with the exception of PMtS 1:4, showed stress versus strain plots that are typical of hydrated high- and low-modulus PPS elastomers above their glass transition temperatures. **Figure 2A** and **B** show representative stress versus strain plots for the PPS polymers studied here. The average tensile Young's modulus, ultimate tensile strength (UTS) and elongation at break for the PPS polymers are summarized in Table 2. PMtS 1:4 was observed to be the stiffest material and revealed a tensile Young's modulus of 378 ± 33.0 MPa, UTS of 17.6 ± 1.30 MPa, and average elongation at break of $10.90 \pm 1.37\%$ (**Table 2**, **Figure 2A**). PSS 1:1 was observed to be the softest material with a tensile Young's modulus of 0.37 ± 0.08 MPa, UTS of 0.57 ± 0.15 MPa and elongation at break of $192.24 \pm 60.12\%$. In addition, limited hysteresis was seen after 1000 cyclic compression cycles up to 50 N for the PXS 1:1 elastomer as shown in **Figure 2C**. Also, PPS pre-polymers are miscible and allowed for formation of co-polymers. As an example, three PXS 1:1 and PMtS 1:4 co-polymers were produced. Representative stress versus strain plots for different PXS 1:1/PMtS 1:4 w/w ratios are shown in **Figure 2D**: the average tensile Young's moduli of these PXS 1:1/PMtS 1:4 copolymers were 7.25 ± 0.47 MPa, 3.94 ± 0.32 MPa and 1.61 ± 0.22 MPa for the 25/75, 50/50 and 75/25 PXS 1:1/PMtS 1:4 w/w ratios, respectively.

3.4 In vitro degradation of PPS polymers

Biodegradable polyesters can degrade through hydrolysis. Therefore, the in vitro degradation under physiological conditions was investigated. Mass loss was detected for all PPS polymers (**Figure 3A**). After 105 d, PXS 1:1 and 1:2 revealed a mass loss of $1.78 \pm 0.30\%$ and $1.88 \pm 0.22\%$, respectively. PXS 1:1 did not reveal a similar mass loss profile as PSS 1:1 ($15.66 \pm 1.75\%$) and PMS 1:1 ($21.90 \pm 6.99\%$). PSS 1:1 and PMS 1:1 had degraded more than their corresponding 1:2 stoichiometries: PSS 1:2 had degraded $5.57 \pm 1.00\%$ of their original mass, and PMS 1:2 degraded $9.00 \pm 0.54\%$ at this time. PMtS 1:4 showed the least mass loss of $0.76 \pm 0.30\%$ (**Figure 3A**). Although degradation under physiological conditions was observed for all PPS polymers, an additional in vitro degradation study at high pH (0.1 N NaOH) was performed as previously described [17]. Again, all polymers revealed a mass loss over a course of 50 h, and showed resemblance to what was found in the previous degradation study: at 50 h, PMtS 1:4 revealed a mass loss of $4.07 \pm 2.80\%$, and PXS 1:1 and 1:2 a mass loss of $4.40 \pm 0.33\%$ and $4.24 \pm 0.52\%$, respectively. PSS 1:1 and PMS 1:1 had fully degraded within 20 h. Also, in concert with their degradation in PBS, PSS 1:2 and PMS 1:2 degraded at a lower rate than the 1:1 stoichiometric ratios. After 50 h, $74.10 \pm 0.41\%$ of the original mass of PSS 1:2, and $13 \pm 7.45\%$ of PMS 1:2 remained (**Figure 3B**).

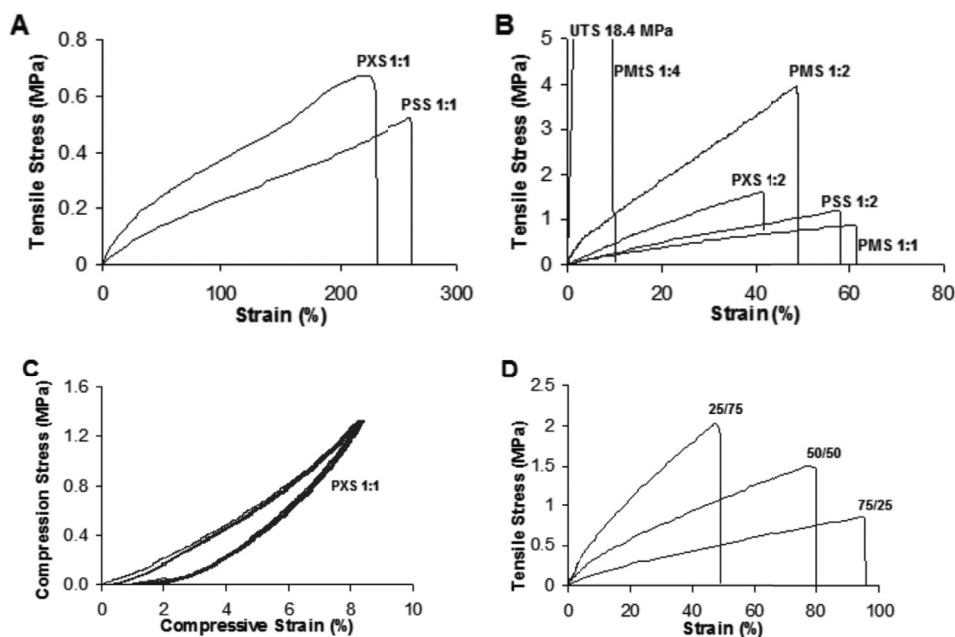


Figure 2. (A) Typical tensile stress versus strain curves of low Young's modulus PPS elastomers (PXS 1:1 and PSS 1:1). (B) Typical tensile stress versus strain curves of PPS elastomers with higher Young's moduli. (C) The first and last 10 compression cycles of 1000, from 0 to 50 N on PXS 1:1. (D) Co-polymers composed of low- and high-modulus PPS polymers, PXS 1:1 and PMtS 1:4 respectively, with 25/75, 50/50 and 75/25 PXS/PMtS w/w ratios.

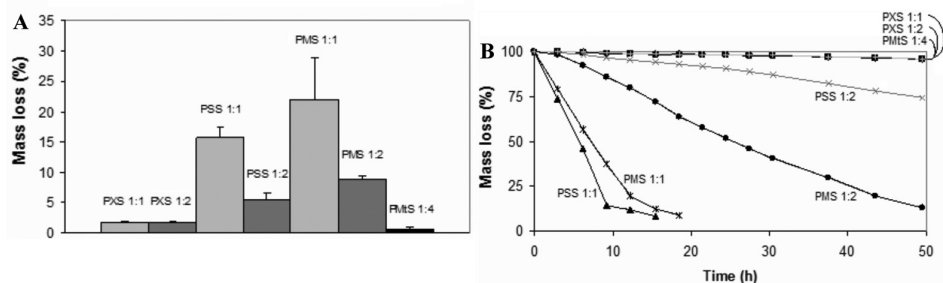


Figure 3. (A) Degradation of PPS polymers in PBS at 37°C for 105 d. (B) Degradation of PPS polymer in 0.1 N NaOH.

3.5 In vitro biocompatibility

The biocompatibility of PXS 1:1 and PXS 1:2 elastomers has been reported elsewhere [12,20]. We therefore conducted an initial in vitro biocompatibility of the other PPS polymers with primary HFFs. Fibroblasts are important regulators of the wound healing process in vivo. The initial attachment and subsequent proliferation into a confluent cell monolayer was compared to PLGA (**Figure 4**). HFFs readily attached on all but PSS 1:1 and PMS 1:1 polymers. A confluent cell layer was achieved after 5 d for all substrates, except PSS 1:2 (achieved at 7 d, data not shown). Sporadic attachment was seen on PSS 1:1 and PMS 1:1 substrates (**Figure 4A, B, D**).

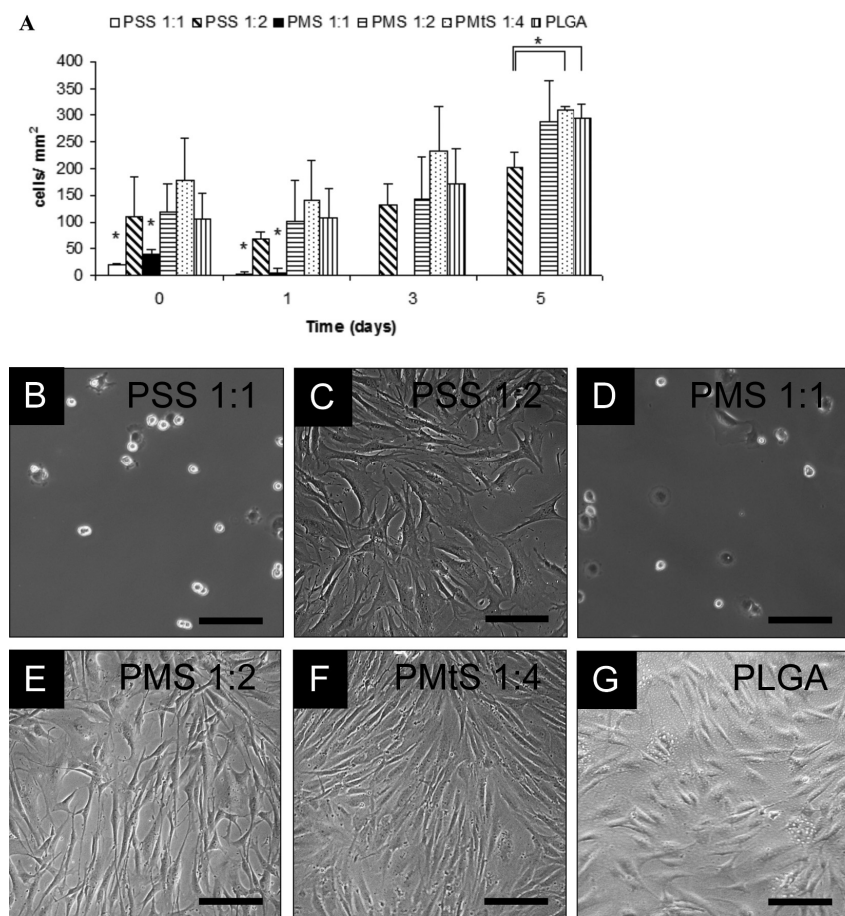


Figure 4. (A) Attachment and proliferation of HFFs on PPS polymers. The (*) indicates significant difference ($p < 0.05$) to the other PPS polymers for that time point. Representative phase contrast micrographic images of HFFs on PSS 1:1 (B), PSS 1:2 (C), PMS 1:1 (D), PMS 1:2 (E), PMtS 1:4 (F), and PLGA (G). Images are of 10 x magnification. Bars represent 150 μm .

3.6 In vivo biocompatibility and degradation

The in vivo biocompatibility of PPS polymers was evaluated via subcutaneous implantation in rats. After 10 d in vivo, the acute inflammatory response was mild for all implanted polymers. The surrounding tissues did not show necrosis, or an abundant perivascular infiltration of mononuclear cells. In addition, the fibrous capsules surrounding the PPS polymers were thin (**Figure 5A-E**). The assessment of the chronic inflammatory response at 12 weeks of implantation revealed thicker fibrous capsules in comparison to the acute inflammatory response at 10 d (**Figure 6**). The fibrous capsule formation surrounding PPS polymers however, seemed similar, or less to the prevalently used PLGA at 12 weeks (**Figure 6E**). At this point, the foreign body response was still mild, as suggested by the thicknesses of these capsules and the presence of few visible vessels within the capsules (**Figure 6A-D**). The PSS 1:1 elastomer appeared to have fully degraded at this time, without detectable trace despite repetitive sectioning of the implantation area.

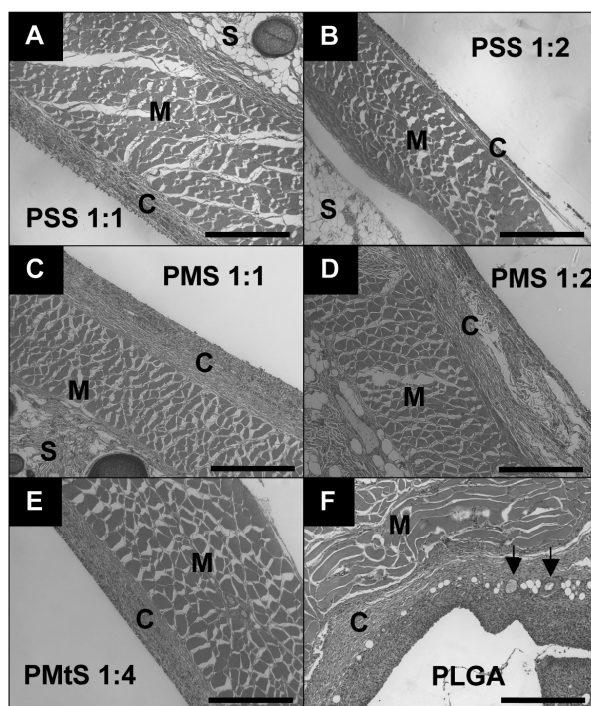


Figure 5. Representative images of H&E stained sections demonstrating the acute inflammatory response to subcutaneous implanted PPS polymers. After 10 d, (A) PSS 1:1, (B) PSS 1:2, (C) PMS 1:1, (D) PMS 1:2, (E) PMtS 1:4 revealed mild inflammatory responses as compared to (F) PLGA. Images are 10 x and bars represent 200 μ m. C = fibrous capsule, S = skin and M = muscle.

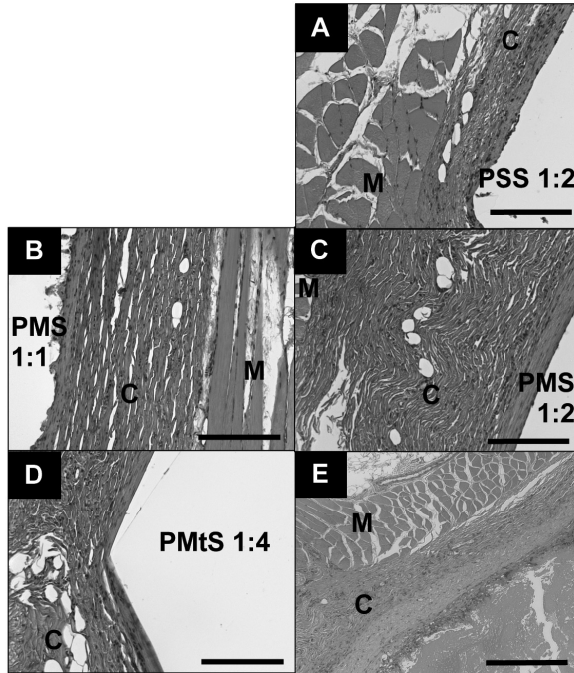


Figure 6. Representative images of H&E stained sections demonstrating the chronic inflammatory response to subcutaneous implanted PPS polymers, 12 weeks after implantation. The PSS 1:1 elastomer had completely degraded at this time. (A) PSS 1:2, (B) PMS 1:1, (C) PMS 1:2, (D) PMtS 1:4 and (E) PLGA. Images A–D are 20 x and bars represent 100 μ m. Image E is 10 x and bar represents 200 μ m. C = fibrous capsule and M = muscle.

3.7 Initial in vitro biocompatibility analysis of PPS for tissue specific applications

In vitro attachment and subsequent proliferation into a confluent cell monolayer of tissue specific cell lines and primary cells were assessed by light microscopy (**Figure 7**). PMtS 1:4 revealed similar attachment and growth rate of a human osteosarcoma (OS) cell line (derived from bone) compared to PLGA. In addition, cell morphology, as assessed by circularity and cell area, was not significantly different for OS cells that were cultured on PLGA (**Figure 7Ai-v**). A difference in cell morphology was found however, for a rhabdomyosarcoma (RMS) cell line (human muscle origin) that was cultured on PSS 1:2 substrates, and compared to PLGA (**Figure 7Bi**). RMS cells revealed more spindle-like morphology before a confluent cell layer was achieved, as shown in **Figure 7Bii-v**: cell circularity was significantly less for cells cultured on PSS 1:2 ($p < 0.05$). In addition, RMS cells spread more, resulting in a larger cell area ($p < 0.05$) (**Figure 7Biii**). However, initial cellular attachment and subsequent

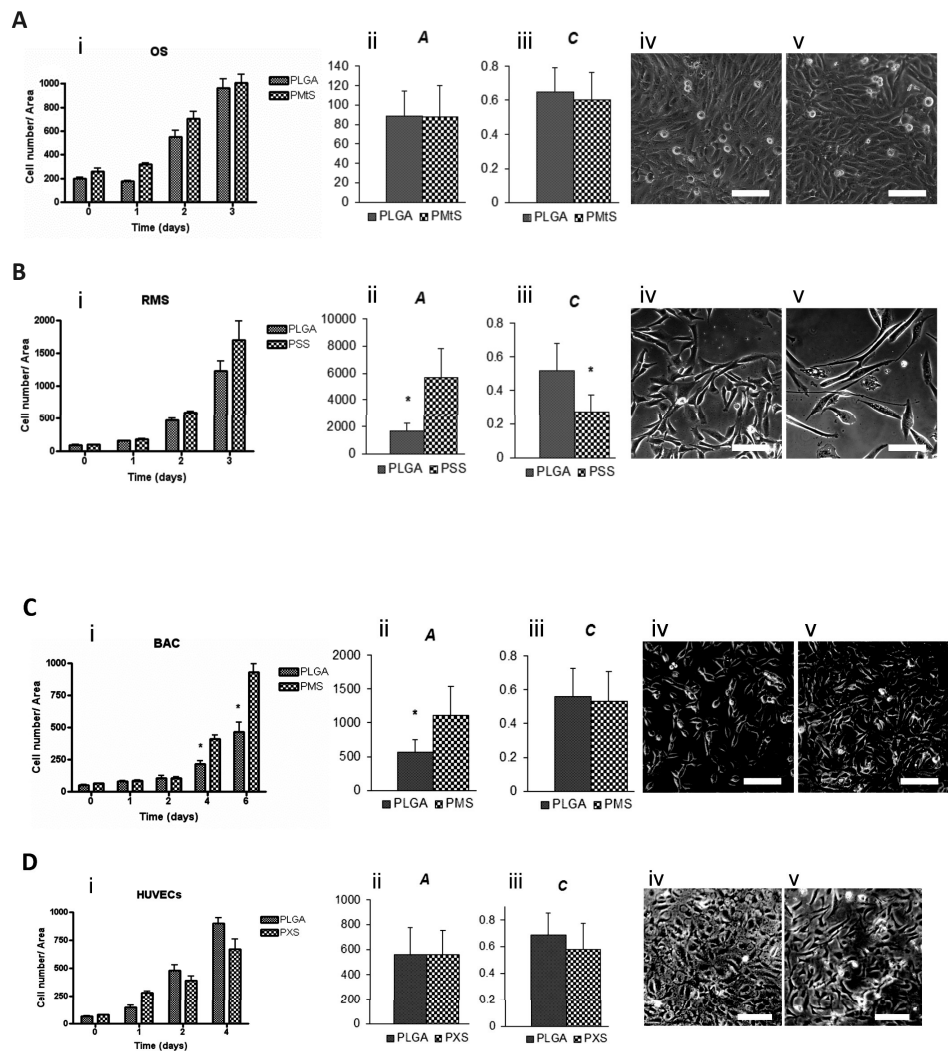


Figure 7. Initial in vitro analysis of PPS polymers for musculoskeletal tissues. **(A)** Attachment and subsequent proliferation of an OS cell line derived from human bone on PMtS 1:4, compared to PLGA (i). OS cell morphology was quantified by cell area (A in mm^2) (ii) and circularity (C) (iii). In addition, representative phase contrast images of OS cells on PLGA (iv) and on PMtS 1:4 (v) are shown. **(B)** Attachment and proliferation of RMS cells derived from human muscle on PSS 1:2 and compared to PLGA (i), as well as A (ii) and C (iii) (* $p < 0.05$). Representative images of RMS on PLGA (iv) and PSS 1:2 (v) also revealed a difference in morphology. **(C)** Seeding of primary BACs on PMS 1:2 and PLGA revealed a similar attachment but different cell numbers after 4 and 6 d (i) (* $p < 0.05$). A (ii), but not C (iii) showed a difference between the polymers (* $p < 0.05$). Representative images of BACs on PLGA (iv) and PMS 1:2 (v) revealed cell number difference at 6 d. **(D)** HUVECs attached and proliferated on PXS 1:1 elastomers similar to PLGA (i), and revealed a comparable cell shape (ii) (iii), also demonstrated by phase contrast images of HUVECs on PLGA (iv) and PXS 1:1 (v). All phase contrast images are 10 x, bars represent 50 μm .

cell numbers during proliferation were not different from PLGA. Cell numbers however, did reveal significant difference for primary BACs after 4 and 6 d culture on PMS 1:2 as compared to PLGA (**Figure 7Ci**). A difference in chondrocyte morphology was also noted. Although cell area was greater for BACs cultured on PMS 1:2 ($p < 0.05$), cell circularity was not significantly different ($p > 0.05$) (**Figure 7Cii–v**). HUVECs cultured on PXS 1:1 exhibited attachment, growth rates and cell morphology that were comparable to PLGA substrates (**Figure 7Di–v**).

4. Discussion

The synthesis of PPS polymers is straightforward and does not require the use of organic solvents or cytotoxic additives. PPS polymers were produced in sub-kilogram quantities and are inexpensive. The first polycondensation step yields PPS pre-polymers that allowed processing into various scaffold geometries, after which the second polycondensation step cures the pre-polymers into a set crosslinked polymer network of desired shape. Curing conditions can be adjusted to modify crosslink densities within a modest range [12,21]. However, adjusting stoichiometry allowed for a much wider range of crosslink densities and subsequent polymer properties (**Table 2**). The reacting stoichiometry of sebacic acid to polyol was chosen such that the number of hydroxyl functionalities of the polyol was always greater than the number of carboxylic functionalities by 1 or 2, to ensure step-growth polymerization whilst exposing free hydroxyl groups in the polymer backbone. These free hydroxyl groups may contribute in intranetwork hydrogen bond formation and may be available for functionalization chemistries, as previously shown [1,12].

Of the PPS polymers, PXS and PSS elastomers revealed comparable physical and mechanical properties, most likely because their polyol monomers have T_m s close to each other (95 and 97°C, respectively) and have similar water solubility (**Table 2**). Using mannitol as a monomer, polymers were produced exhibiting higher tensile Young's moduli and T_g s than PSS elastomers (**Figure 2**), as well as higher contact angles (**Table 2**) although mannitol is a stereoisomer of sorbitol. Mannitol has a higher T_m (165°C) and a lower water solubility, which may explain the differences observed between PSS and PMS elastomers. Maltitol-based polymers (PMtS 1:4) on the other hand, showed similar contact angles to PXS 1:2 and PSS 1:2 stoichiometries, which can be rationalized if PMtS 1:4 is essentially viewed as a glucose:sorbitol:sebacate 1:1:4 polymer. However maltitol, exposing nine hydroxyl groups, allowed for a higher sebacic acid monomer feed ratio. This resulted in a higher degree of

crosslinking, and therefore in a glassy polymer with a T_g above ambient and physiological temperatures, as well as resulting in a limited water-uptake (**Figure 2, Table 2**). The tensile Young's moduli of PMtS 1:4 polymers are comparable to trabecular bone (50-100 MPa) and may potentially be developed for bone tissue engineering or osteosynthesis applications [22]. In addition, copolymers of PPS polymers can be produced as shown in **Figure 2D**. Thus, additional to the choice of polyol as well as monomer stoichiometry, co-polymerization allowed for tuning mechanical properties of PPS polymers.

The in vivo degradation mechanism of PXS elastomers is dominated by surface erosion and is reported elsewhere [12,20]. In vitro degradation rates of PXS however, did not clearly correspond to in vivo degradation rates. In addition, in vitro degradation of PXS elastomers was significantly slower than PSS and PMS elastomers, and comparable to the PMtS 1:4 polymer under similar conditions (**Figure 3A**). This hydrolysis profile was confirmed for hydrolysis in a high pH environment (**Figure 3B**). Interestingly, during the in vivo biocompatibility study presented here, we observed that the PSS 1:1 polymer appeared to completely degrade within 12 weeks, but had only lost $15.66 \pm 1.75\%$ of its original mass after 105 d in vitro. This in vivo mass loss of PSS 1:1 is similar to the previously observed degradation of PXS 1:1, which had an in vivo half life of 3-4 weeks. It is postulated that a higher crosslink density as well as the introduction of more hydrophobic entities (sebacic acid) are responsible for tuning the degradation rate. In vitro hydrolysis under physiological conditions occurred for all PPS polymers and revealed similar differences between the 1:1 and 1:2 stoichiometries, as was observed in vivo for PXS elastomers.

PPS polymers support cellular attachment with the exception of PSS 1:1 and PMS 1:1 elastomers (**Figure 4**). The in vitro cell attachment and proliferation studies were performed without pre-treating or coating the polymers with adhesion proteins such as fibronectin and collagen. If cellular attachment is not warranted, which can be important in some applications such as contact guidance [8,23], PSS 1:1 and PMS 1:1 can be applied. Alternatively, PSS 1:1 and PMS 1:1 elastomers could be modified with adhesion-promoting proteins and peptides by grafting them onto the exposed hydroxyl groups. The fibrous capsules during the acute inflammatory response to PPS foreign materials seemed consistent with fibrous capsule thicknesses of previously reported values for soft thermoset elastomers (**Figure 5**) [2,12,17,20,21]. However, the fibrous capsules of the chronic inflammatory response surrounding the higher modulus materials (PMS 1:2 and PMtS 1:4), seemed more pronounced than observed for PSS 1:2 and PMS 1:1, but was still lesser than the reported values for PLA and PLGA polymers, which are frequently reported to be around 400-600 microns thick (**Figure 6**) [2,5,24]. PPS polymers are composed of structural units that are

endogenous to the mammalian metabolism, but have advantages associated with synthetic polymers. PPS polymers revealed mechanical properties that can be useful for a variety of implantable medical devices. As an example, human ulnar metacarpophalangeal thumb joint ligament has a UTS and a Young's modulus of 11.4 ± 1.2 MPa and 37.3 ± 5.1 MPa, respectively [25], and several human cervical spinal components such as intervertebral discs, as well as their associated ligaments, have mechanical properties [26] that fall within the limits of the PPS polymer platform shown here. This is also true for softer tissues such as nerves [27] and blood vessels [28]. Therefore, PPS polymers potentially offer a material platform for surgical procedures and tissue engineering applications.

5. Conclusions

PPS polymers are synthetic in nature but have the advantage of being composed of structural units endogenous to the human metabolism. We have presented seven polymers in this report. Chemical, physical, and mechanical properties as well as degradation rates of these polymers can be tuned by altering the polyol and stoichiometry of the reacting sebacic acid. Potentially, many copolymers and composite materials are possible, resulting in a considerable number of polymers accessible through the synthetic scheme presented here. PPS polymers exhibited comparable biocompatibility to materials approved for human use, such as PLGA.

6. Acknowledgements

JPB acknowledges financial support from the J.F.S. Esser Stichting and the Stichting Prof. Michaël-Van Vloten Fonds. CJB was funded by a Charles Stark Draper Laboratory Fellowship. This work was funded by NIH grant HL060435 and through a gift from Richard and Gail Siegal.

7. References

1. Nijst CLE, Bruggeman JP, Karp JM, Ferreira L, Zumbuehl A, Bettinger CJ, *et al.* Synthesis and characterization of photocurable elastomers from poly(glycerol sebacate). *Biomacromolecules* 2007;8(10):3067-3073.
2. Wang Y, Ameer GA, Sheppard BJ, Langer R. A tough biodegradable elastomer. *Nat Biotechnol* 2002;20(6):602-6.
3. Den Dunnen WFA, Meek MF, Grijpma DW, Robinson PH, Schakenraad JM. In vivo and in vitro degradation of poly[50/50(85/15 L/D)LA/3-CL], and the implications for the use in nerve reconstruction. *J Biomed Mater Res A* 2000;51:575-85.
4. Wang Y, Kim YM, Langer R. In vivo degradation characteristics of poly(glycerol sebacate). *J Biomed Mater Res A* 2003 Jul 1;66(1):192-7.
5. Mahdavi A, Ferreira L, Sundback C, Nichol JW, Chan EP, Carter DJ, *et al.* A biodegradable and biocompatible gecko-inspired tissue adhesive. *Proc Natl Acad Sci U S A* 2008;105(7):2307-12.
6. Bettinger CJ, Weinberg EJ, Kulig KM, Vacanti JP, Wang Y, Borenstein JT, *et al.* Three-dimensional microfluidic tissue-engineering scaffolds using a flexible biodegradable polymer. *Adv Mater* 2006;18(2):165-9.
7. Bettinger CJ, Orrick B, Misra A, Langer R, Borenstein JT. Microfabrication of poly(glycerolsebacate) for contact guidance applications. *Biomaterials* 2006;27:2558-65.
8. Motlagh D, Yang J, Lui KY, Webb AR, Ameer GA. Hemocompatibility evaluation of poly(glycerol sebacate) in vitro for vascular tissue engineering. *Biomaterials* 2006;27(24):4315-24.
9. Chen QZ, Bismarck A, Hansen U, Junaid S, Tran MQ, Harding SE, *et al.* Characterisation of a soft elastomer poly(glycerol sebacate) designed to match the mechanical properties of myocardial tissue. *Biomaterials* 2008;29(1):47-57.
10. Sundback CA, Shyu JY, Wang Y, Faquin WC, Langer RS, Vacanti JP, *et al.* Biocompatibility analysis of poly(glycerol sebacate) as a nerve guide material. *Biomaterials* 2005;26(27):5454-64.
11. Bruggeman JP, Bettinger CJ, Nijst CLE, Kohane DS, Langer R. Biodegradable xylitol-based polymers. *Adv Mater* 2008;20(10):1922-7.
12. Elwood KC. Methods available to estimate the energy values of sugar alcohols. *Am J Clin Nutr* 1995;62(Suppl):1169-74.
13. Natah SS, Hussien KR, Tuominen JA, Koivisto VA. Metabolic response to lactitol and xylitol in healthy men. *Am J Clin Nutr* 1997;65(4):947-50.
14. Sestoft L. An evaluation of biochemical aspects of intravenous fructose, sorbitol and xylitol administration in man. *Acta Anaesthesiol Scand Suppl* 1985;82:19-29.
15. Flory PJ. Principles of polymer chemistry. Ithaca, New York: Cornell University Press; 1953.
16. Yang J, Webb AR, Pickerill SJ, Hageman G, Ameer GA. Synthesis and evaluation of poly(diols citrate) biodegradable elastomers. *Biomaterials* 2006;27(9):1889-98.
17. Tognana E, Chen F, Padera RF, Leddy HA, Christensen SE, Guilak F, *et al.* Adjacent tissues (cartilage, bone) affect the functional integration of engineered calf cartilage in vitro. *Osteoarthritis Cartil* 2005;13(2):129-38.
18. Thurston G, Jaggi B, Palcic B. Measurement of cell motility and morphology with an automated microscope system. *Cytometry* 1988;9(5):411-7.
19. Bruggeman JP, Bettinger CJ, Langer R. Biodegradable xylitol-based elastomers: in vivo behavior and biocompatibility. *J Biomed Mater Res A* 2010;95(1):92-104.

20. Bettinger CJ, Bruggeman JP, Borenstein JT, Langer RS. Amino alcohol-based degradable poly(ester amide) elastomers. *Biomaterials* 2008;29(15):2315–25.
21. Anseth KS, Shastri VR, Langer R. Photopolymerizable degradable polyanhydrides with osteocompatibility. *Nat Biotechnol* 1999;17:156–9.
22. Schmalenberg KE, Uhrich KE. Micropatterned polymer substrates control alignment of proliferating Schwann cells to direct neuronal regeneration. *Biomaterials* 2005;26(12):1423–30.
23. Mainil-Varlet P, Gogolewski S, Nieuwenhuis P. Long-term soft tissue reaction to various polylactides and their in vivo degradation. *J Biomed Mater Res A* 1996;7(12):6713–21.
24. Firoozbakhsh K, Yi IS, Moneim MS, Umada Y. A study of ulnar collateral ligament of the thumb metacarpophalangeal joint. *Clin Orthop Relat Res* 2002;403:240–7.
25. Ha SK. Finite element modeling of multi-level cervical spinal segments (C3–C6) and biomechanical analysis of an elastomer-type prosthetic disc. *Med Eng Phys* 2006 Jul;28(6):534–41.
26. Rydevik BL, Kwan MK, Myers RR, Brown RA, Triggs KJ, Woo SL, *et al.* An in vitro mechanical and histological study of acute stretching on rabbit tibial nerve. *J Orthop Res* 1990;8(5):694–701.
27. Clerin V, Nichol JW, Petko M, Myung RJ, Gaynor W, Gooch KJ. Tissue engineering of arteries by directed remodeling of intact arterial segments. *Tissue Eng* 2003;9(3):461–72.

Chapter 4

Synthesis and characterization of photocurable elastomers from poly(glycerol sebacate)

Christiaan L.E. Nijst, Joost P. Bruggeman, Jeffrey M. Karp, Lino Ferreira,
Andreas Zumbuehl, Christopher J. Bettinger, Robert Langer

Biomacromolecules 2007;8(10):3067-3073

Abstract

Elastomeric networks are increasingly being investigated for a variety of biomedical applications including drug delivery and tissue engineering. However, in some cases, their preparation requires the use of harsh processing conditions (e.g., high temperature), which limits their biomedical application. Herein, we demonstrate the ability to form elastomeric networks from poly(glycerol sebacate) acrylate (PGSA) under mild conditions while preserving a wide range of physical properties. These networks presented a Young's modulus between 0.05 and 1.38 MPa, an ultimate strength from 0.05 to 0.50 MPa, and elongation at break between 42% and 189% strain, by varying the degree of acrylation (DA) of PGSA. The in vitro enzymatic and hydrolytic degradation of the polymer networks was dependent on the DA. The copolymerization of poly(ethylene glycol) diacrylate with PGSA allowed for an additional control of mechanical properties and swelling ratios in an aqueous environment, as well as enzymatic and hydrolytic degradation. Photocured PGSA networks demonstrated in vitro biocompatibility as judged by sufficient human primary cell adherence and subsequent proliferation into a confluent monolayer. These photocurable degradable elastomers could have potential application for the encapsulation of temperature sensitive factors and cells for tissue engineering.

1. Introduction

The development of biodegradable elastomers has increasingly become important in biomedical applications. Elastomers have gained popularity because they can provide stability and structural integrity within a mechanically dynamic environment without irritation to the hosting tissues [1,2] while they exhibit mechanical properties similar to those of soft tissues [2-5]. Biodegradable elastomers can be important materials for a wide variety of medical applications including drug delivery and tissue regeneration, where (cell-seeded) constructs are designed to aid or replace damaged or diseased tissue [2-4]. Examples of applications for elastomeric biodegradable biomaterials are small diameter vascular grafts [6,7] and nerve conduits [8-10]. Current biodegradable elastomers include poly(glycerol sebacate) [2], poly(diols citrate) [4], star poly(ϵ -caprolactone-*co*-(D,L)lactide) [5,11], poly(trimethylene carbonate-*co*- ϵ -caprolactone) [12] and poly(trimethylene carbonate-*co*-(D,L)lactide) [13]. We recently created a tough biodegradable elastomer, poly(glycerol sebacate) (PGS), which features robust mechanical properties and in vitro and in vivo biocompatibility [2,14]. However, harsh conditions ($>80^{\circ}\text{C}$, $<5\text{ Pa}$) and long reaction times (typically $>24\text{ h}$) are required for its curing and thus limit its ability to polymerize directly in a tissue or to incorporate cells or temperature-sensitive molecules. As such, there is an unmet need to develop alternative processing strategies to overcome the limitations of thermally processing PGS. One convenient strategy is the implementation of photopolymerization. This technique has been utilized for several decades in biomedical research and has become an integral method for in situ delivery of resins in the practice of dentistry [15-17]. Recently, there has been great interest in using photopolymerization techniques to prepare polymeric networks for tissue engineering applications as well as for minimally invasive medical procedures [18,19]. To this end, acrylate groups have been included in polymers for participation in chemical cross-linking between polymer chains by photo-induced free radical polymerization [11,20-22].

In this paper, we describe the synthesis and characterization of a photocurable polymer based on the chemical modification of PGS with acrylate moieties (designated poly(glycerol sebacate)-acrylate, or PGSA). PGSA can be cured rapidly (within minutes) at ambient temperatures to form polymeric networks with a wide range of mechanical properties and in vitro enzymatic degradation and hydrolysis profiles. Incorporation of poly(ethylene glycol) (PEG) diacrylate (PEG-DA) allowed for additional control of mechanical properties and swelling ratios in an aqueous environment. Initial experiments with photocured

PGSA networks demonstrated *in vitro* biocompatibility by sufficient cell adherence and subsequent proliferation into a confluent cell monolayer.

2. Experimental Section

2.1 Synthesis of PGSA

All chemicals were purchased from Sigma-Aldrich (Milwaukee, WI), unless stated otherwise. PGS was synthesized according to previously published methods [2]. Briefly, the PGS pre-polymer was synthesized by polycondensation of equimolar glycerol and sebacic acid (Fluka, Buchs, Switzerland) at 120°C under argon for 24 h before reduction of the pressure from 1 Torr to 40 mTorr over 5 h. The polycondensation was continued for another 24 h. This material was used without any further purification. The PGS pre-polymer was acrylated in the following manner: a flame-dried round bottomed flask was charged with PGS pre-polymer (20 g, with 78 mmol of hydroxyl groups), 200 mL of anhydrous dichloromethane, and 4-dimethylaminopyridine (DMAP) (20 mg, 0.18 mmol). The reaction flask was cooled to 0°C under a positive pressure of N₂. Acryloyl chloride (0.25-0.80 mol/mol of hydroxyl groups on the PGS pre-polymer) was slowly added parallel to an equimolar amount of triethylamine. The reaction was allowed to reach room temperature and was stirred for an additional 24 h. The resulting mixture was dissolved in ethyl acetate, filtered, and dried at 45°C and 5 Pa.

2.2 Polymer Characterization

¹H nuclear magnetic resonance (¹H-NMR) spectra of the PGS pre-polymer and PGSA were recorded (Varian Unity-300 NMR spectrometer). Chemical shifts were referenced relative to the peak for CDCl₃ at 7.27 ppm. The chemical composition was determined by calculating the signal integrals of –COCH₂CH₂CH₂– at 1.2, 1.5, and 2.2 ppm for sebacic acid, –CH₂CH– at 3.7, 4.2, and 5.2 ppm for glycerol, and –CH=CH₂ at 5.9, 6.1, and 6.5 ppm for the protons on the acrylate groups. The signal intensity of the methylene groups of sebacic acid (1.2 ppm) and the acrylate groups (average signal intensities of 5.9, 6.1, and 6.5 ppm) were used to calculate the degree of acrylation (DA). The molecular weights of the PGS pre-polymer and PGSA were determined by gel permeation chromatography (GPC) using THF on Styragel columns (series of HR-4, HR-3, HR-2, and HR-1, Waters, Milford, MA).

2.3 Preparation and Characterization of Photocured PGSA

PGSA networks were formed by mixing PGSA with 0.1% (w/w) photoinitiator (2,2-dimethoxy-2-phenylacetophenone), and the polymerization reaction was initiated by exposure to ultraviolet light (ca. 4 mW/cm², model 100AP, Black-Ray) for 10 min. Attenuated total reflectance Fourier transform infrared (ATR-FTIR) spectroscopy analysis was performed on a Nicolet Magna-IR 500 spectrophotometer to confirm the cross-link reaction. For that purpose, thermally cured PGS and photocured PGSA slabs, PGS pre-polymer, and PGSA dissolved in chloroform were placed on top of a ZnSe crystal. The thermal properties of disks from thermally cured PGS, photocured PGSA (DA of 0.31 and 0.54), and photocured PGSA-PEG (PGSA DA = 0.34 containing 5% PEG diacrylate) were characterized using differential scanning calorimetry (DSC; DSC Q 1000), for two cycles, within the temperature range from -90 to 250 °C using a heating/cooling rate of 10°C/min. Tensile tests were conducted using an Instron 5542 (according to ASTM standard D412-98a) on dog-bone shaped polymer strips (115 x 25 x 1.2 mm) cut from photocured PGSA sheets. The photocured networks were first soaked in 100% ethanol for 24 h and subsequently soaked in PBS for 24 h prior to mechanical testing. The strain rate was 50 mm/min, and all samples were elongated to failure. The sol content was measured by the mass differential after incubation of the PGSA samples in 100% ethanol for 24 h. Swelling by hydration was measured by the mass differential after incubation of the PGSA samples in PBS for 24 h. The mass density was measured with a pycnometer (Humboldt Manufacturing Co.). The density and Young's modulus of the samples were used to calculate the cross-linking density and relative molecular mass between cross-links (M_c) as described previously [2].

2.4 Co-polymerization of PEG-diacrylate and PGSA

Networks of PGSA-PEG diacrylate were prepared by mixing 10%, 50%, and 90% (w/w) PGSA (DA = 0.34) with PEG diacrylate (M_w = 700 Da) including 0.1% (w/w) photoinitiator, followed by photopolymerization under UV light for 10 min. Poly(ethylene glycol) polymers were prepared from PEG diacrylate (liquid) containing 0.1% (w/w) photoinitiator, followed by photopolymerization. The swelling ratio in PBS was determined by the mass differential.

2.5 In Vitro Degradation

Degradation rates via hydrolysis were measured by incubating sol-free samples ($n = 4$) of PGS, photocured PGSA (DA of 0.31 and 0.54), and photocured PGSA containing 5% PEG diacrylate in 20 mL of 0.1 mM NaOH at 37 °C. The samples were removed, washed in ddH₂O, dried at 90 °C for 7 d, and weighed again to determine the mass loss. In the enzyme

degradation study, these samples ($n = 4$) were degraded in vitro in PBS in the presence of bovine pancreatic cholesterol esterase (40 units/mL) and incubated at 37°C. The samples were removed, washed in ddH₂O, dried at 90°C for 7 d, and weighed again to determine the mass loss.

2.6 In Vitro Cell Attachment and Proliferation

Primary human foreskin fibroblasts (HFFs; ATCC, Manassas, VA) were cultured in high-glucose Dulbecco's minimal essential medium (DMEM) supplemented with 10% (v/v) fetal bovine serum (Invitrogen), 100 µg/mL streptomycin (Invitrogen), and 100 U/mL penicillin (Invitrogen) (further denoted as growth medium) at 37°C and 5% CO₂. Cells between passages four and six were harvested by using trypsin (0.025%)/EDTA (0.01%) and quenched with an equal volume of growth medium to resuspend the cells. Photocured PGSA (DA = 0.34) covered glass slides (diameter 18 x 1 mm, $n = 3$) were prepared by spin-coating 20% (w/v) PGSA in dimethyl sulfoxide (DMSO) at 3400 rpm for 5 min followed by a 10 min UV polymerization. The photocured spin-coated PGSA disks were incubated with growth medium in a 12-well plate for 4 h to remove photoinitiator, residual DMSO, and any unreacted monomers prior to seeding. Each disk was seeded with 5000 cells/cm² using 2 mL of growth medium. The cell attachment was evaluated after the cell-seeded constructs were lightly washed with PBS after 4 h, and the cell density was assessed and compared to that of cell attachment on tissue-cultured polystyrene (TCPS). Subsequently, at predetermined times, these cell cultures were washed with PBS and fixed with 4% formaldehyde solution for 10 min, and the cell density was determined by counting the cells from randomly picked equally sized areas (0.005 cm², $n = 9$). Phase micrographs of the cells were taken at 10x magnification, and the cell perimeter (P) and cell area (A) were calculated using Axiovision software (Zeiss, Germany). For the cell morphology measurements, each data set consists of measurements of at least 100 cells across several images from randomly picked areas. Scanning electron microscopy (SEM) images were taken after culture substrates were washed three times in PBS and fixed with 4% (v/v) paraformaldehyde in PBS. After being rinsed with PBS buffer three times, the dishes were dehydrated in graded alcohols (50%, 70%, 80%, 90%, 95%, and 100%) and then air-dried in HMDS. The samples were then sputter-coated with platinum and examined on a JEOL JSM5910 scanning electron microscope.

3. Results and Discussion

3.1 Polymer Characterization

PGSA was prepared by the acrylation of PGS pre-polymer (**Figure 1A, B**). The PGS pre-polymer had a weight-average molecular weight (M_w) of 23,000 g/mol, a number-average molecular weight (M_n) of 6,500 g/mol as determined by GPC, and a polydispersity index (*PDI*) of 3.5. The molar composition of the PGS pre-polymer was approximately 1:1 glycerol/sebacic acid as confirmed by ^1H NMR analyses (**Figure 2A**). The incorporation of acrylate groups was confirmed by ^1H NMR by the appearance of the peaks at δ 5.9, 6.1, and 6.4 ppm (**Figure 2B**). This was also confirmed by ATR-FTIR by the appearance of an absorption band at 1375 cm^{-1} , corresponding to the $-\text{CH}$ stretching of the secondary alkyl group related to the acrylate groups [23] and known not to be present in poly(acryloyl chloride) [24] (**Figure 2C**). Typically, 66% of the acryloyl chloride added in the experiment was incorporated in the pre-polymer as calculated from signal intensities of ^1H -NMR (**Figure 1C**). PGSA with a DA between 0.17 and 0.54 was obtained. The ^1H -NMR data show that acryloyl chloride reacts preferentially with the hydroxyl groups of glycerol compared to the carboxylate groups of sebacic acid. This was confirmed by the increase of the signal integral at δ 5.2 ppm, corresponding to the resonance of protons from the tri-substituted glycerol, and the decrease of the signal integral at ca. δ 3.7 ppm, corresponding to the resonance of protons from monosubstituted glycerol (**Figure 2A, B**), with the increment of the DA. As determined by GPC analysis, the M_w of the PGSA remained unchanged after acrylation (data not shown). The PGSA pre-polymer is not soluble in aqueous solutions but is soluble in most organic solvents such as ethanol, dimethyl sulfoxide, benzene, tetrahydrofuran, acetyl acetate, dichloromethane, and dimethylformamide.

3.2 Characterization of Photocured PGSA

The polymerization of PGSA using UV light in the presence of the photoinitiator 2-dimethoxy-2-phenylacetophenone yields elastomeric networks. ATR-FTIR analysis of all photocured PGSA elastomers (**Figure 2C, D**) showed typical absorption bands of hydroxyl ($3500\text{--}3200\text{ cm}^{-1}$) and ester ($1800\text{--}1600\text{ cm}^{-1}$) groups in the polymer backbone, as was observed for thermally cured PGS. The broad peak at 3475 cm^{-1} is assigned to hydrogen-bonded hydroxyl groups, likely from free hydroxyl groups that are not modified by acryloyl chloride. The formation of a polymer network after photocuring of PGSA was confirmed by the increase of the band at 2930 cm^{-1} , corresponding to the vibration of alkyl groups, and the elimination of the band at 1375 cm^{-1} , known to be associated with acrylate groups [23].

The T_g values of thermally cured PGS, photocured PGSA (DA = 0.31, 0.54), and photocured PGSA-PEG ranged from -28.1 to -31.4 °C. These results indicate that all polymers and copolymers are in a rubbery state at 37 °C. Currently, the mechanical properties of thermally cured PGS and other similar polymers can be controlled by altering the processing conditions or by changing the molecular weight of the di-functional precursors [2,4]. The introduction of acrylate groups into the pre-polymer facilitated an additional level of control. Specifically, Young's modulus and the ultimate tensile strength of the photocured PGSA were linearly proportional to the DA (**Figure 3A, B**), and no permanent deformations were observed after mechanical testing. The mechanical properties of the photocured PGSA spanned from soft to relatively stiff as determined by the tensile Young modulus of the polymer, which varied from 0.05 MPa (DA = 0.17) to 1.38 MPa (DA = 0.54). This demonstrates the potential to achieve the mechanical compliance of, for instance, the peripheral nerve, which has a Young modulus of approximately 0.45 MPa [25]. The ultimate tensile strength ranged from 0.05 to 0.50 MPa (**Figure 3B**), whereas the strain to failure of photocured PGSA ranged from 170% to 47.4% with increasing DA (**Figure 3A**). The degree of swelling of the elastomeric networks in ethanol and water ranged from 50% to 70% and from 8% to 12% , respectively, and did not change appreciably as a function of the DA (**Figure 3C**). The high degree of swelling in ethanol facilitates removal of monomers and macromers not attached to the polymer network (sol content) or potential incorporation of specific factors. The low degree of swelling in water may help to maintain the mechanical properties once implanted. The sol content of the polymer decreased from 40% to $<10\%$ by increasing the DA from 0.20 to 0.54 (**Figure 3C**). This is likely due to the increasing number of new crosslinks between the polymer chains. The high sol content, which was achieved with a lower DA, may be unfavorable for in situ polymerization where unreacted acrylated macromers would diffuse into the surrounding tissue. The mechanical properties, however, are linearly proportional to the DA and are correlated to the formation of new cross-links within the polymer network and not to the unreacted macromers in the network. The density of the photocured elastomers decreased slightly with increasing DA (**Table 1**), which is similar to other thermally cured elastomers in which the density is inversely proportional to the curing time [26]. The cross-linking density and relative molecular mass between crosslinks (M_c) were calculated using the density and Young modulus of the samples (**Table 1**) as previously described [2]. By increasing the DA in photocured PGSA from 0.17 to 0.54 , the cross-linking density increased from 6.4 to 185 mol/m³ and the relative molecular mass between cross-links decreased from $18\,000$ to 600 g/mol.

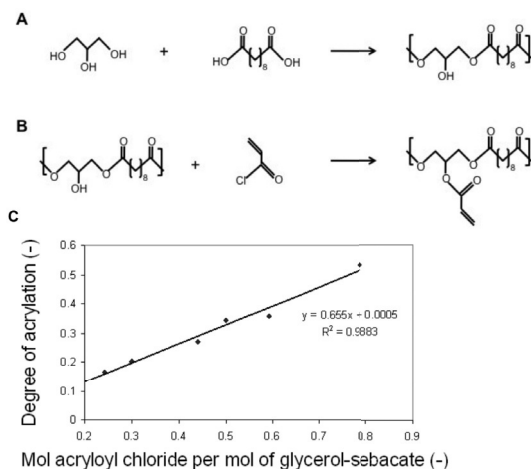


Figure 1. (A) Polycondensation of glycerol and sebacic acid, yielding the PGS prepolymer. R represents H or the polymer chain. (B) Acrylation of the prepolymer (not all binding possibilities are shown). To simplify the scheme, 100% conversion is shown. (C) Increasing the molar equivalent of acryloyl chloride increases the degree of acrylation linearly.

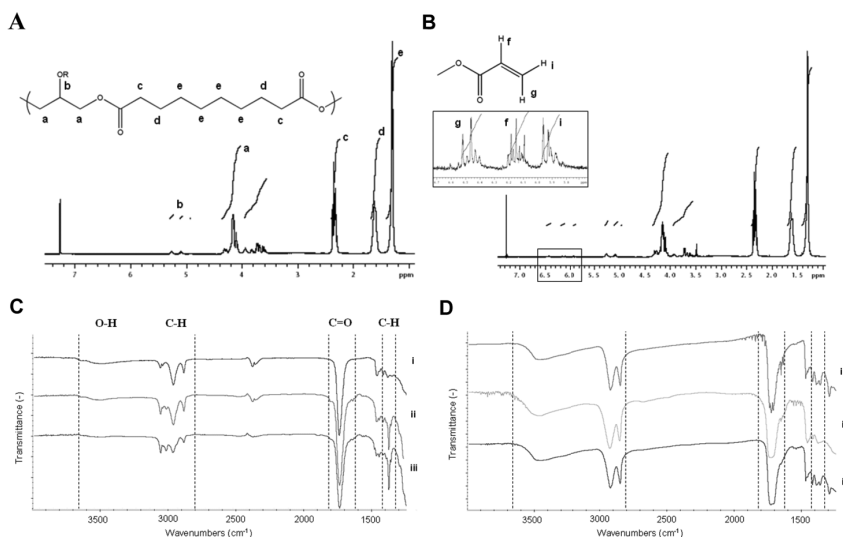


Figure 2. ¹H NMR spectrum of (A) PGS pre-polymer and (B) PGSA. The sebacic acid and glycerol in the polymer matrix were identified at 1.2, 1.5, and 2.2 ppm and 3.7, 4.2, and 5.2 ppm by hydrogens located on the carbons labeled “a”-“e”. Vinyl groups located on the PGSA were identified at 5.9, 6.1, and 6.4 ppm labeled “f”-“i”. (C) ATR-FTIR spectra of PGS pre-polymer (C,i); PGSA with DA = 0.20 (C,ii); PGSA with DA = 0.54 (C,iii); thermally cured PGS (D,i); photocured PGSA (DA = 0.20) (D,ii); and photocured PGSA (DA = 0.54) (D,iii). The absorption band at 1375 cm⁻¹ associated with acrylate groups (spectra in (C,ii) and (C,iii)) disappeared after the photopolymerization reaction (spectra in (D,ii) and (D,iii)).

Degree of acrylation	ρ (g/cm ³)	Young's modulus (MPa)	Ultimate elongation (%)	Ultimate strength (MPa)	n (mol/m ³)	M_c (g/mol)
0.17	1.21±0.02	0.048±0.005	170±17.2	0.054±0.005	6.6±0.07	18906±232
0.20	1.19±0.02	0.148±0.004	101±26.5	0.109±0.011	19.8±0.6	6013±253
0.31	1.16±0.02	0.383±0.028	54.7±14.1	0.163±0.034	51.5±3.9	2262±185
0.34	1.15±0.02	0.568±0.222	60.0±5.73	0.270±0.032	76.4±3.0	1514±73.3
0.41	1.15±0.02	0.895±0.052	51.1±7.41	0.364±0.034	120.4±7.0	953.9±69.1
0.54	1.15±0.01	1.375±0.084	47.4±11.3	0.498±0.079	185±11.3	620.1±42.4

Table 1. Physical and mechanical properties of PGSA networks. Values are reported as the mean followed by the standard deviation in braces. M_c : the molecular weight between crosslinks, and n : crosslink density.

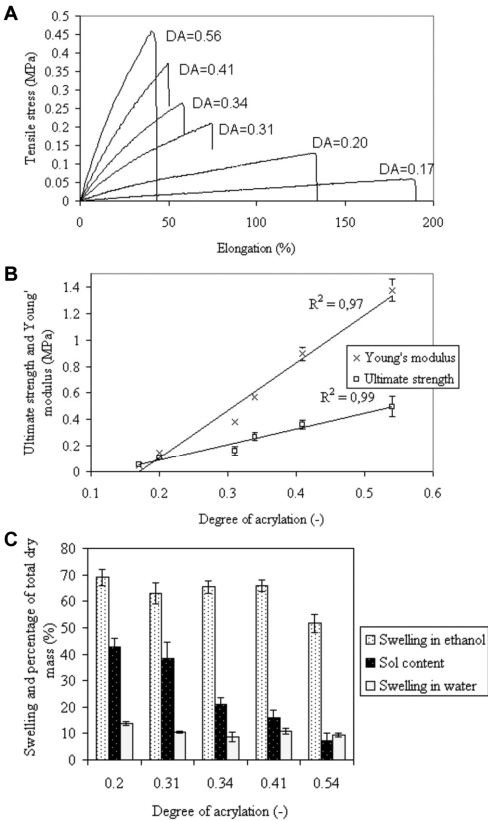


Figure 3. (A) Stress-strain curves of photocured PGSA elastomer from a representative experiment ($n = 4$). (B) Through increasing the degree of acrylation, the ultimate tensile strength and Young modulus increased linearly. (C) Degree of swelling in ethanol and water and sol content as a function of the degree of acrylation.

3.3 Co-polymerization of PGSA with PEG Diacrylate

Another advantage of photocurable PGSA is that it can be easily combined with other acrylated precursors to achieve a wider range of material properties. As an example, we chose to co-polymerize PGSA with PEG diacrylate (0.7 kDa), a hydrophilic non-degradable polymer. The effect on the physical properties (Young's modulus, ultimate strength, elongation, and swelling ratio in water) was studied of elastomers formed by changing the weight percentage of PEG diacrylate with PGSA (DA = 0.34) (**Figure 4**). Specifically, by increasing the concentration of PEG diacrylate, the elongation ranged from 60% to 4%, Young's modulus from 0.6 to 20 MPa, and the ultimate strength from 0.270 to 0.890 MPa. The elastomer formed by the copolymerization of PEG diacrylate with PGSA (DA = 0.34) mixed with equal masses, 50:50 PGSA-PEG, showed a 10-fold higher Young's modulus and ultimate strength than the 95:05 PGSA-PEG elastomer, while its elongation was maintained. Furthermore, the swelling behavior of these networks could be tuned from 45% to 10% by changing the concentration of PEG diacrylate from 90% to 0%.

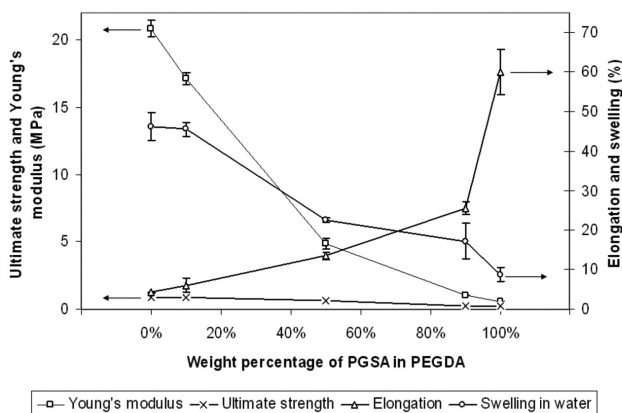


Figure 4. Co-polymerization of PGSA (DA = 0.34) and PEG diacrylate (M_w 700 Da) where PEG chains become incorporated as cross-links within the PGSA network. Increasing the concentration of PGSA decreases the Young modulus, ultimate strength, and swelling in water, whereas the elongation increases.

3.4 In Vitro Degradation of Photocured PGSA

Previous studies have shown that the degradation of PGS in vitro is difficult to correlate with the in vivo degradation [2,14]. PGS degrades 15% in 10 weeks in PBS as determined by mass loss, whereas full degradation is observed after 6 weeks in vivo. Similar to PGS, PGSA (DA = 0.31) degraded only 10% after 10 weeks in PBS (data not shown). Given this

discrepancy between in vitro degradation and in vivo degradation results, we performed in vitro hydrolysis and enzymatic degradation studies to examine the relative differences in mass loss over time between the different polymer networks. The polymer networks that were examined in these degradation studies were thermally cured PGS, photocured PGSA with 2 degrees of acrylation (low degree of acrylation, PGSA-LA (DA = 0.31), and high degree of acrylation, PGSA-HA (DA = 0.54)), and PGSA-PEG (PGSA-LA co-polymerized with 5% PEG-diacrylate). In the enzyme degradation study, these polymers were degraded in vitro in PBS in the presence of bovine pancreatic cholesterol esterase (40 units/mL). Pancreatic cholesterol esterase has been shown to be identical to the esterases associated with macrophages that are known to degrade polyesters [27-29]. PGS and PGSA-LA showed mass loss over time, whereas PGSA-HA and PGSA-PEG did not. PGS degraded by 60% over 48 h, while PGSA-LA, which has a lower cross-linking density, only degraded by 40% (**Figure 5A**). These results suggest that the alkyl cross-links formed in PGSA networks by the acrylate groups may be less susceptible to cholesterol esterase than the polymer networks with only ester cross-links, as formed in PGS networks. The hydrolysis study was performed in a sodium hydroxide (0.1 mM) solution as described previously [4,26]. The mass loss profile via hydrolysis of photocured PGSA-LA and PGSA-HA was similar to that of PGS (**Figure 5B**). However, the absolute mass loss of PGSA-LA was significantly ($p < 0.01$) higher compared to those of PGS and PGSA-HA at all time points. Interestingly, the rate of mass loss of PGSA-PEG was significantly ($p < 0.01$) lower compared to those of PGS and PGSA-HA, and the mass loss revealed a more linear profile. Hence, co-polymerization of PGSA-LA with 5% PEG diacrylate resulted in elastomers with mechanical properties (**Figure 4**) similar to those of PGSA-HA, but showed a much slower degradation rate via hydrolysis when compared to photocured PGSA and PGS (**Figure 5B**). These results show that the in vitro hydrolytic degradation rate of photocured PGSA can be decreased, independent of the initial mechanical strength.

3.5 In Vitro Cell Adhesion and Proliferation on Photocured PGSA

Our initial in vitro biocompatibility study showed that the photocured elastomers support cell adhesion and proliferation: $59 \pm 12\%$ of the primary human foreskin fibroblasts seeded on photocured PGSA attached after 4 h, as compared to the attachment on TCPS, which we set at 100%. The cells were viable, assessed by trypan blue staining, as only $1.4\% \pm 0.5\%$ of the cells were positive. The attached cells showed a relatively normal morphology, as displayed in **Figure 6A-C**. **Figure 6B** shows a detailed SEM image of cell spreading (F = fibroblast). Morphometric data revealed a similar cell surface area (A) as compared to that of the fibroblasts seeded on TCPS (**Figure 6E**, $p > 0.05$). However, the circularity index (C)

was less for the fibroblasts cultured on the PGSA as compared to TCPS (**Figure 6F**, $p < 0.05$). There was more variety in the morphometric data of the fibroblasts cultured on the PGSA, leading to larger standard deviations than for the fibroblasts cultured on TCPS. The difference of cell attachment on PGSA and TCPS might be related to several factors including surface topography and protein adsorption on the material's surface. The attached cells on the PGSA however proliferated in a linear fashion, forming a confluent cell monolayer at day 12 (**Figure 6D**). This shows that the *in vitro* biocompatibility of photocured PGSA allows for cellular attachment and subsequent proliferation into a confluent cell monolayer of primary human fibroblasts.

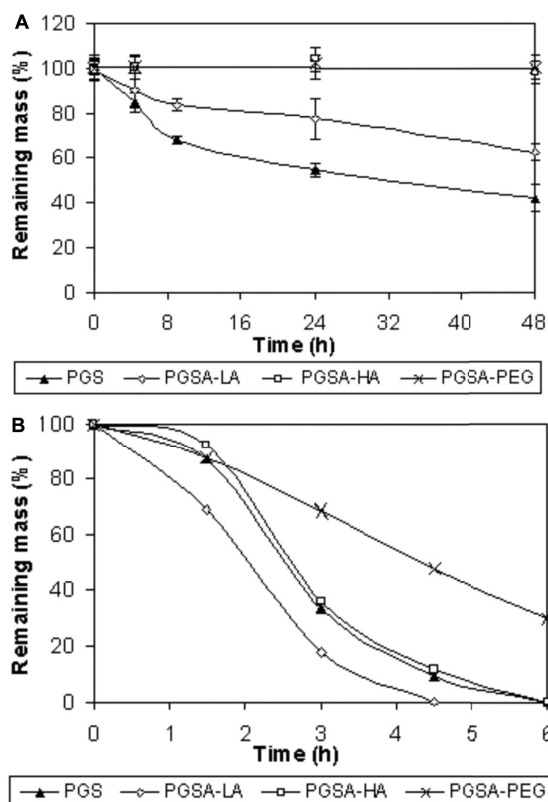


Figure 5. (A) *In vitro* enzymatic degradation of PGS, photocured PGSA (DA = 0.31, 0.54), and PGSA-PEG (DA = 0.34 + 5% PEG diacrylate) in bovine cholesterol esterase (pH 7.2, 37°C, $n = 3$) for 4, 8, 24, and 48 h. (B) *In vitro* hydrolytic degradation of PGS, photocured PGSA (DA = 0.31, 0.54), and PGSA-PEG in NaOH (0.1 mM) ($n = 3$) for 0, 1.5, 3, 4.5, and 6 h at 37°C.

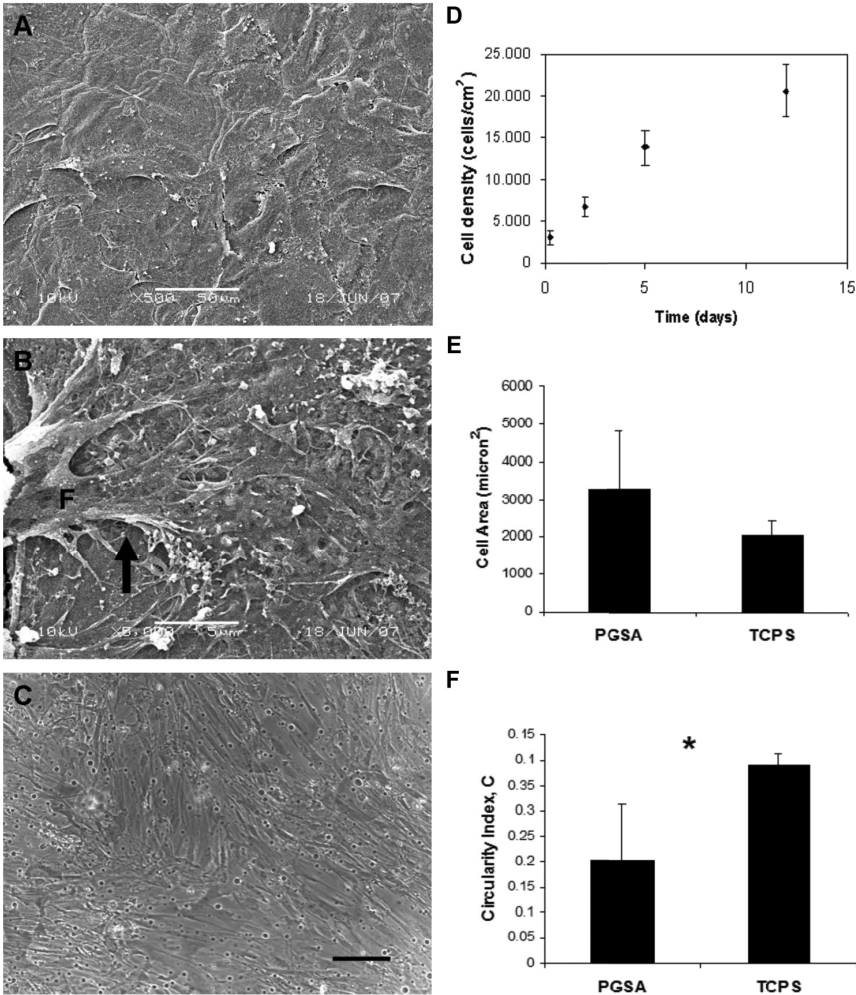


Figure 6. (A) Representative SEM image of the confluent cell monolayer after 12 days of culture on photocured PGSA (DA = 0.34). The white bar represents 50 μm . (B) Representative SEM image of a single fibroblast (F = fibroblast) spreading (arrow) after 24 h of culture on PGSA (DA = 0.34). The white bar represents 5 μm . (C) Representative phase-contrast image of the confluent cell monolayer after 12 days of culture on photocured PGSA (DA = 0.34) (the black bar represents 100 μm). (D) Cell attachment and subsequent proliferation of primary human fibroblasts in vitro on photocured PGSA (DA = 0.34). (E) Cell area, A, in micrometers squared after 24 h of culture on PGSA or TCPS. Error bars represent the standard deviation of the mean ($p > 0.05$). (F) The circularity, C, of non-confluent cells was calculated with the equation $C = 4(\pi)A/P^2$, where P is the perimeter of the cell in micrometers and A is the area of the cell in micrometers squared. Error bars represent the standard deviation of the mean. (* $p < 0.05$).

4. Conclusions

We synthesized novel biocompatible, elastomeric biomaterials that are rapidly polymerized at room temperature using UV photopolymerization. These elastomers contain functional hydroxyl groups and exhibit tunable mechanical properties. The liquid acrylated polymer precursor can be combined with other acrylated molecules to further control the physical properties. The development of these novel elastomers could therefore lead to new materials for a variety of potential biomedical applications.

5. Acknowledgments

C.L.E.N. acknowledges the financial support of Dr. Saal van Zwanenberg Stichting, Vreede Stichting, Shell, and KIVI. J.P.B. acknowledges the J.F.S. Esser Stichting and Stichting Michaël-Van Vloten Fonds for financial support. L.F. acknowledges the financial support of Fundacao para a Ciencia e a Tecnologia (Grant SFRH/BPD/14502/2003). A.Z. acknowledges financial support from the Swiss National Science Foundation. This work was funded by NIH Grant R01 DE13023, NIH Grant HL060435, and NSF Grant NIRT 0609182.

6. References

1. Langer R, Vacanti JP. Tissue engineering. *Science* 1993;260(5110):920-926.
2. Wang Y, Ameer GA, Sheppard BJ, Langer R. A tough biodegradable elastomer. *Nat Biotechnol.* 2002;20(6):602-606.
3. Pego AP, Poot AA, Grijpma DW, Feijen J. Biodegradable elastomeric scaffolds for soft tissue engineering. *J Contr Release* 2003;87:69-79.
4. Yang J, Webb AR, Ameer GA. Novel Citric Acid-Based Biodegradable Elastomers for Tissue Engineering. *Adv Mater* 2004;16(6):511-516.
5. Gu F, Younes HM, El-Kadi AO, Neufeld RJ, Amsden BG. Sustained interferon-gamma delivery from a photocrosslinked biodegradable elastomer. *J Contr Release* 2005;102(3):607- 617.
6. Nasser BA, Pomerantseva I, Kaazempur-Mofrad MR, Sutherland FW, Perry T, Ochoa E, Thompson CA, Mayer JE Jr, Oesterle SN, Vacanti JP. Dynamic rotational seeding and cell culture system for vascular tube formation. *Tissue Eng.* 2003;9(2):291-299.
7. Nugent HM, Edelman ER. Tissue engineering therapy for cardiovascular disease. *Circ Res* 2003;92(10):1068-1078.
8. Belkas JS, Shoichet MS, Midha, R. Peripheral nerve regeneration through guidance tubes. *Neurol Res* 2004;26(2):151-160.
9. Lundborg, G. Alternatives to autologous nerve grafts. *Handchir Mikrochir Plast Chir* 2004;36(1):1-7.
10. Sundback CA, Shyu JY, Wang Y, Faquin WC, Langer RS, Vacanti JP, Hadlock TA. Biocompatibility analysis of poly(glycerol sebacate) as a nerve guide material. *Biomaterials* 2005;26:5454-5464.

11. Amsden BG, Tse MY, Turner ND, Knight DK, Pang SC. In vivo degradation behavior of photo-cross-linked star-poly-(epsilon-caprolactone-co-D,L-lactide) elastomers. *Biomacromolecules* 2006;7(1):365-372.
12. Pego AP, Poot AA, Grijpma DW, Feijen J. Copolymers of trimethylene carbonate and epsilon-caprolactone for porous nerve guides: synthesis and properties. *J Biomater Sci, Polym Ed* 2001;12(1):35-53.
13. Pego AP, Siebum B, Van Luyn MJ, Gallego Y, Van Seijen XJ, Poot AA, Grijpma DW, Feijen J. Preparation of degradable porous structures based on 1,3-trimethylene carbonate and D,L-lactide (co)polymers for heart tissue engineering. *Tissue Eng* 2003;9(5):981-994.
14. Wang Y, Kim YM, Langer R. In vivo degradation characteristics of poly(glycerol sebacate). *J Biomed Mater Res A* 2003;66(1):192-197.
15. Young KC, Main C, Gillespie FC, Stephen KW. Ultraviolet absorption by two ultra-violet activated sealants. *J Oral Rehabil* 1978;5(3):207-13.
16. Venhoven BA, de Gee AJ, Davidson CL. Light initiation of dental resins: dynamics of the polymerization. *Biomaterials* 1996;17(24):2313-2318.
17. Leonard DL, Charlton DG, Roberts HW, Cohen MW. Polymerization efficiency of LED curing lights. *J Esthet Restor Dent* 2002;14(5):286-295.
18. West JL, Hubbell JA. Comparison of covalently and physically cross-linked polyethylene glycol-based hydrogels for the prevention of postoperative adhesions in a rat model. *Biomaterials* 1995;16(15):1153-1156.
19. Elisseeff J, McIntosh W, Anseth K, Riley S, Ragan P, Langer R. Photoencapsulation of chondrocytes in poly(ethylene oxide)-based semi-interpenetrating networks. *J Biomed Mater Res A* 2000;51(2):164-171.
20. Cruise GM, Scharp DS, Hubbell JA. Characterization of permeability and network structure of interfacially photopolymerized poly(ethylene glycol) diacrylate hydrogels. *Biomaterials* 1998;19(14):1287-1294.
21. Anseth KS, Burdick JA. New directions in photopolymerizable biomaterials. *MRS Bull* 2002;27(2):130-136.
22. Ferreira L, Gil MH, Cabrita AM, Dordick JS. Biocatalytic synthesis of highly ordered degradable dextran-based hydrogels. *Biomaterials* 2005;26(23):4707-4716.
23. Tsujimoto K, Uyama, H, Kobayashi S. Enzymatic Synthesis and Curing of Biodegradable Crosslinkable Polyesters. *Macromol Biosci* 2002;2(7):329-335.
24. Yang YS, Qi GR, Qian JW, Yang SL. Acryloyl chloride polymer. *J Appl Polym Sci* 1998;68:665-670.
25. Rydevik BL, Kwan MK, Myers RR, Brown RA, Triggs KJ, Woo SL, Garfin SR. An in vitro mechanical and histological study of acute stretching on rabbit tibial nerve. *J Orthop Res* 1990;8(5):694-701.
26. Yang J, Webb AR, Pickerill SJ, Hageman G, Ameer GA. Synthesis and evaluation of poly(diols citrate) biodegradable elastomers. *Biomaterials* 2006;27(9):889-1898.
27. Woo GL, Mittelman MW, Santerre JP. Synthesis and characterization of a novel biodegradable antimicrobial polymer. *Biomaterials* 2000;21(12):1235-1246.
28. Tang YW, Labow RS, Santerre JP. Enzyme induced biodegradation of polycarbonatepolyurethanes: dose dependence effect of cholesterol esterase. *Biomaterials* 2003;24(12):2003-2011.
29. Santerre JP, Woodhouse K, Laroched G, Labow RS. Understanding the biodegradation of polyurethanes: from classical implants to tissue engineering materials. *Biomaterials* 2005;26(35):7457-7470.

Chapter 5

Biodegradable xylitol-based elastomers: in vivo behavior and biocompatibility

Joost P. Bruggeman, Christopher J. Bettinger, Robert Langer

J Biomed Mater Res A 2010;95(1):92-104

Abstract

Biodegradable elastomers based on polycondensation reactions of xylitol with sebacic acid, referred to as poly(xylitol sebacate) (PXS) elastomers have recently been developed. Herein, we describe the in vivo behavior of PXS elastomers. Four PXS elastomers were synthesized, characterized and compared to poly(L-lactic-co-glycolic acid) (PLGA). PXS elastomers displayed a high level of structural integrity and form stability during degradation. The in vivo half-life ranged from approximately 3 to 52 weeks. PXS exhibited increased biocompatibility compared to PLGA implants.

1. Introduction

Synthetic biodegradable polyesters have become important materials in medicine and bio-engineering [1,2]. Initial biodegradable polymers were based on short hydroxy acids such as glycolic and lactic acid. Degradation rates for co-polymers based on these monomers can be tuned by altering their stoichiometry and molecular weights [3]. Despite the widespread and immediate use of these polymers in surgery, tissue engineering and drug delivery [4], other monomers were introduced to realize more elastomeric materials, tailoring them for soft tissue applications [5,6]. However, these thermoplastic polymers exhibit several drawbacks including bulk degradation and acidic byproducts [3,6,7]. This also results in non-linear loss of mechanical properties versus mass loss, as well as loss of form stability and considerable construct swelling during degradation [3,6,8].

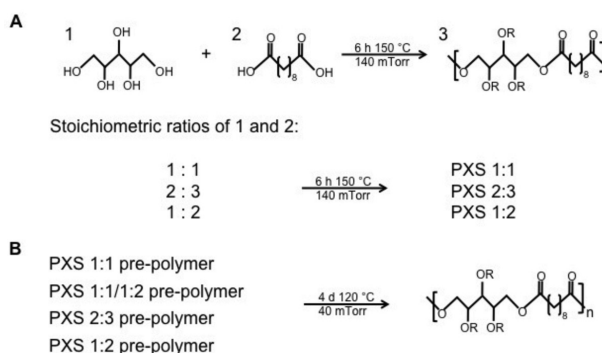
We have recently developed a versatile platform of biodegradable elastomers, based on polycondensation reactions of xylitol with sebacic acid, referred to as poly(xylitol sebacate) (PXS) elastomers [9]. PXS elastomers are composed of monomers natural to the mammalian organism, but exhibit advantages of synthetic biomaterials. These advantages include rapid scalable synthesis as well as avoiding potential immune responses related to natural polymers such as collagen [10,11]. We hypothesized that the degradation rate of PXS elastomers could be altered by simple adjustments in chemical composition. In this report, we describe the synthesis and *in vivo* behavior of four PXS elastomers: three PXS elastomer formulations were synthesized by altering the stoichiometric ratios of xylitol to sebacic acid. An additional polymer was produced through a co-polymerization strategy of two polymers with different stoichiometric ratios. Throughout degradation, PXS elastomers displayed structural integrity and form stability. *In vivo* half-lives of these elastomers ranged from approximately 3 to 52 weeks. Based on morphological evaluation of PXS implants, we propose a surface eroding mechanism for PXS elastomers. In addition, PXS elastomers exhibited enhanced biocompatibility compared to PLGA.

2. Materials and Methods

2.1 Synthesis and characterization of PXS pre-polymers

All chemicals were purchased from Sigma-Aldrich (St. Louis, MO, USA) unless otherwise stated. Polymers with xylitol: sebacic acid ratios of 1:1, 2:3 and 1:2 were prepared, referred to as PXS 1:1, PXS 2:3 and PXS 1:2 respectively. Appropriate molar amounts of the polyol

and reacting acid monomer were melted in a round bottomed flask at 150 °C under a blanket of inert gas, and stirred for 2 h. Vacuum (~50 mTorr) was then applied yielding the pre-polymers PXS 1:1 (12 h), PXS 2: 3 (6 h) and PXS 1:2 (6 h) (**Scheme 1A**). The molecular weights of the pre-polymers were measured and compared to linear standards using gel permeation chromatography (GPC) using tetrahydrofuran on Styragel columns (series of HR-4, HR-3, HR-2, and HR-1, Waters, Milford, MA, USA). FT-IR analysis was carried out on a Nicolet Magna-IR 550 spectrometer. ^1H -NMR spectra were obtained of the PXS pre-polymers in $\text{C}_2\text{D}_6\text{O}$, on a Varian Unity-300 NMR spectrometer. The chemical composition of the pre-polymers was determined by calculating the signal integrals of xylitol, and compared to the signal integrals of sebacic acid. The signal intensities showed peaks of $-\text{OCH}_2(\text{CH}(\text{OR}))_3\text{CH}_2\text{O}-$ at 3.5-5.5 ppm from xylitol, and peaks of $-\text{COCH}_2\text{CH}_2\text{CH}_2-$ at 1.3, 1.6 and 2.3 ppm from sebacic acid.



Scheme 1. General synthetic scheme for PXS elastomers. **(A)** Xylitol (1) was polymerized with sebacic acid (2) in different stoichiometries, yielding PXS pre-polymers (3). **(B)** Pre-polymers of different stoichiometric ratios (PXS 1:1, PXS 2:3 and PXS 1:2) as well as a 50/50 w/w mixture of PXS 1:1/PXS 1:2 pre-polymers were further polymerized into elastomeric networks. A simplified representation of the pre-polymers is shown. R can be hydrogen, xylitol or sebacic acid.

2.2 Synthesis and characterization of PXS elastomers

All PXS pre-polymers were further cured by polycondensation, yielding the PXS 1:1, PXS 2:3 and PXS 1:2 elastomers. An additional elastomer was made from a 50/50 w/w mixture of PXS 1:1 and PXS 1:2 pre-polymers, yielding a PXS 1:1/1:2 co-polymer. The polycondensation was done at 120°C and 140 mTorr for 4 days. Tensile tests were performed on dog-bone shaped polymer strips that were hydrated for at least 24 h in ddH_2O at 37 °C on an Instron 5542 (according to ASTM standard D412-98a). Differential scanning calorimetry (DSC) was

performed as previously reported [9]. Briefly, glass transition temperature (T_g) and other potential phase transitions were measured between -90°C and 250°C with a heating/cooling rate of $10^{\circ}\text{Cmin}^{-1}$, using a Q1000 DSC equipped with Advantage Software v2.5 (TA Instruments, Newcastle, DE USA) and analyzed with Universal Analysis Software v4.3A (TA Instruments). The T_g measurements were performed on sol-free, dry elastomers, and therefore only resemble the thermal properties of the ‘naked’ degrading polymer network, without water and other molecules (sol). The change of T_g over time (ΔT_g) was calculated by subtracting the T_g at the start of the experiment ($T_{g, t=0}$) with the T_g at time point t ($T_{g, t=0}$):

$$\Delta T_g = T_{g, t=0} - T_{g, t} \quad (1)$$

The mass density was measured using a pycnometer (Humboldt, MFG. CO), and crosslink density (n) as well as the relative molecular mass between crosslinks (M_c) were calculated from the following equations for an ideal elastomer, where E_0 is the Young’s modulus, R is the universal gas constant, T is the temperature and ρ is the mass density:

$$n = \frac{E_0}{3RT} = \frac{\rho}{M_c} \quad (2)$$

The water-in-air contact angle measurements were carried out as previously mentioned [12].

2.3 In vivo implantation of PXS elastomers

Female Lewis rats (Charles River Laboratories, Wilmington, MA) weighing 200-250 g were housed in groups of 2 and had access to water and food *ad libitum*. Animals were cared for according to the approved protocols of the Committee on Animal Care of the Massachusetts Institute of Technology in conformity with the NIH guidelines for the care and use of laboratory animals (NIH publication #85-23, revised 1985). The animals were anaesthetized using continuous 2% isoflurane/ O_2 inhalation. Two or three small midline incisions on the dorsum of the rat were performed and the implants were introduced in lateral subcutaneous pockets created by blunt dissection. The skin was closed using staples. Each rat carried either PXS 1:1, PXS 1:2 and PLGA, or PXS 2:3 and 50/50 PXS 1:1/1:2 PLGA implants. The animals were inspected daily until post-operative day 10 for any wound healing problems. Throughout the study, all rats stayed in good general health as assessed by their weight gain.

2.3 In vivo degradation and biocompatibility of PXS elastomers

For the degradation study, PXS elastomeric discs (diameter 10×1.6 mm) ($n = 4$) were implanted subcutaneously in rats. Before implantation, polymer discs were weighed (M_0) and their thickness (H_0) was measured between two glass cover slides using calipers. To investigate in vivo degradation, implants were harvested at pre-determined time points and collected in sterile saline. Directly upon surgical removal, the explants were dabbed dry, weighed (M_{wet}), and their thickness (H_t) was measured again. The explants were then dried at 90°C for 3 days and weighed (M_{dry}) again. Water content (hydration) by mass and implant dimensions at time point t were calculated as follows:

$$\frac{M_{wet} - M_{dry}}{M_{dry}} \times 100\% \quad (3)$$

for water content, and

$$\frac{H_t - H_0}{H_0} \times 100\% \quad (4)$$

for implant size. The in vivo mass loss over time was calculated using equation 5:

$$\frac{M_0 - M_{dry}}{M_0} \times 100\% \quad (5)$$

Compression tests were performed on the wet explants with a 50N load cell at a compression rate of 5 mm/min using an Instron 5542, according to ASTM standard D575-91. All samples were compressed to 50 N and the compression modulus was calculated from the initial slope (0-10%) of the stress-strain curve. The compression modulus was determined before implantation, and the ratio of the initial modulus was calculated to the modulus at the pre-determined time point (E_t) as follows:

$$\frac{E_t}{E_0} \times 100\% \quad (6)$$

Explants dedicated for scanning electron microscopy (SEM) were sputter-coated with platinum/palladium ($\approx 250\text{\AA}$), mounted on aluminum stubs with carbon tape, and examined on a JEOL JSM-5910. Explants dedicated to determine sol content were weighed (M_{dry}), placed in 100% ethanol for 3 days on a orbital shaker, dried at 90°C for 3 days and weighed ($M_{solfree}$) again. The sol content of the explants was calculated, using the following equation:

$$\frac{M_{dry} - M_{solfree}}{M_{solfree}} \times 100\% \quad (7)$$

For biocompatibility analysis, explants and surrounding tissues were harvested, and fixed in Accustain for 24 h, dehydrated in graded ethanol (70-100%), embedded in paraffin, sectioned using a microtome ($4\text{ }\mu\text{m}$). Sequential sections ($8\text{--}15\text{ }\mu\text{m}$) were stained with hematoxylin and eosin (H&E). The H&E stains were used to analyze for the presence of fibroblasts and neutrophils in the tissues surrounding the material, and for the presence of multinucleated giant cells, ingrowth of cells into the material as well as phagocytosis of the material. Tissue macrophages were identified by staining sections with primary rabbit anti-rat CD68 [13] (1:200, Abcam, England UK), followed by goat anti-mouse secondary antibody (Vector Burlingame, CA USA). Samples were incubated with streptavidin horseradish peroxidase (1:100, Dako, Denmark) and developed with DAB substrate chromogen (Dako). Histology images were recorded with a Zeiss CCD Camera equipped with Axiovision software (Zeiss, Germany).

2.4 Statistical analysis

At least four fibrous capsule thickness measurements were made across at least ten randomly selected images per time point per sample, and the number of CD68+ macrophages were similarly based on at least ten randomly selected images per time point per sample. Non-parametric two-way ANOVA tests were performed where appropriate (GraphPad Prism 4.02, GraphPad Software, San Diego, CA USA). Dunn's multiple comparison post-tests were used to determine significance between specific treatments. All graphical data is reported as mean \pm S.D. Significance levels were set at * $p < 0.05$.

3. Results

3.1 Pre-polymer synthesis and characterization

PXS pre-polymers (**Scheme 1A**) and their chemical compositions were confirmed by $^1\text{H-NMR}$ spectra, as shown in **Table 1**. Molecular weight distributions are summarized in **Table 1** as well. PXS pre-polymers have accessible melting temperatures (T_m s), allowing for processing and mixing pre-polymers. The temperatures used for processing are listed in **Table 1**. A blend of PXS 1:1 and PXS 1:2 at 50/50 w/w was prepared additionally and, similar to the PXS 1:1, PXS 2:3 and PXS 1:2 pre-polymers, further cured into elastomeric networks (**Scheme 1B**).

Pre-polymer	Composition by $^1\text{H-NMR}$	T_m (°C)	M_w (g/mol)	M_n (g/mol)	PDI
PXS 1:1	1.0:0.91	80	2443	1268	1.9
PXS 1:1/1:2	1.0:1.56	90	4690	1689	2.8
PXS 2:3	1.0:1.63	100	3156	1117	2.7
PXS 1:2	1.0:1.85	100	6202	2255	2.7

Table 1. PXS pre-polymers. T_m s are temperatures where the polymer revealed a transition from a white, opaque wax to a clear flowing liquid.

3.2 Characterization of PXS elastomers

PXS 1:1, PXS 2:3 and PXS 1:2 elastomers as well as the PXS 1:1/1:2 co-polymer revealed stress strain curves as shown in **Supplementary Figure 1**. Tensile Young's moduli ranged from 0.82 ± 0.15 to 5.33 ± 0.40 MPa as previously reported for PXS 1:1 and PXS 1:2 elastomers [9]. The PXS 1:1/1:2 co-polymer and PXS 2:3 elastomer revealed Young's moduli of 2.32 ± 0.27 and 3.42 ± 0.13 MPa respectively, and fall within the limits defined by the PXS 1:1 and 1:2 elastomers. The mechanical properties of PXS elastomers are summarized in **Table 2**. T_g s ranged from a lower limit of PXS 1:1 (7.3°C) to an upper limit value of PXS 1:2 (22.9°C) and in between these limits were the values of the PXS 1:1/1:2 (18.7°C) and PXS 2:3 (20.2°C) elastomers. The molecular weight between crosslinks revealed a similar trend: PXS 1:2 had the lowest molecular weight between crosslinks (M_c , 1585.1 ± 43.7 mol/m³), PXS 1:1 the highest (10517.4 ± 102.1 mol/m³) and in between were the values for PXS 1:1/1:2 (3685.7 ± 90.5 mol/m³) and PXS 2:3 (2521.6 ± 100.5 mol/m³). The contact angle measurements and in vitro hydration (determined by mass differential), showed a similar trend: PXS 1:1 films exhibited the lowest contact angle and highest hydration by mass ($26.5 \pm 3.6^\circ$ and

Polymer	Curing process	Young's modulus (MPa)	Compression modulus (MPa)	T _g (°C)	Contact angle (°)	Hydration by mass (%)	ρ (g/cm ³)	n (mol/m ³)	M _c (g/mol)
PXS 1:1	120 °C; 2 Pa; 4 d	0.82 ± 0.15	1.67 ± 0.20	7.3	26.5 ± 3.6	12.6 ± 0.4	1.18 ± 0.02	112.2 ± 30.5	10517.4 ± 102.1
PXS 1:1/1:2	120 °C; 2 Pa; 4 d	2.32 ± 0.27	2.67 ± 0.59	18.7	31.6 ± 4.3	8.3 ± 1.6	1.17 ± 0.03	317.4 ± 21.0	3685.7 ± 90.5
PXS 2:3	120 °C; 2 Pa; 4 d	3.42 ± 0.13	3.71 ± 0.20	20.2	43.8 ± 2.2	3.7 ± 0.9	1.18 ± 0.01	468.0 ± 29.2	2521.6 ± 100.5
PXS 1:2	120 °C; 2 Pa; 4 d	5.33 ± 0.40	5.68 ± 0.56	22.9	52.7 ± 5.7	4.1 ± 0.3	1.16 ± 0.02	729.3 ± 57.3	1585.1 ± 43.7

Table 2. Physical and mechanical properties of PXS elastomers. M_c: the molecular weight between crosslinks, and n: crosslink density, both calculated from Eqn. 1 (Materials and Methods).

12.6 \pm 0.4%), PXS 1:2 films the highest contact angle with the lowest hydration (52.7 \pm 5.7° and 4.1 \pm 0.3%) and PXS 1:1/1:2 and PXS 2:3 (31.6 \pm 4.3°, 8.3 \pm 1.6% and 43.8 \pm 2.2°, 3.7 \pm 0.9% respectively), again, in between the values of PXS 1:1 and PXS 1:2. The physical properties of PXS elastomers are summarized in **Table 2**.

3.3 In vivo degradation of PXS elastomers

Similarly, the in vivo mass loss, hydration by mass, construct sol content, loss of mechanical properties, and implant thickness, were also confined by limits set by the PXS 1:1 and PXS 1:2 elastomers, with values of PXS 1:1/1:2 and PXS 2:3 elastomers within these limits. The in vivo half life of PXS 1:1 implants was approximately 3 to 4 weeks, and revealed a roughly linear decrease in mass over time (**Figure 1A**). PXS 1:2 implants degraded much slower, with 76.7 \pm 3.7% of its original dry weight remaining after 28 weeks in vivo. PXS 1:1/1:2 implants appeared to have a mass loss profile that was a combination of the separate PXS 1:1 and PXS 1:2 elastomers: it had an in vivo half life of approximately 15 weeks and had almost completely degraded at 27 weeks (**Figure 1A**). PXS 2:3 implants had a projected half life of approximately 30 weeks, and similar to the PXS 1:2 elastomers, showed an initial lag time where no mass loss was observed, after which a linear loss in mass was observed (**Figure 1A**).

PXS implant thickness during degradation gradually decreased over time, meaning that these polymers do not extensively swell in vivo (**Figure 1B**). Hydration of PXS elastomers was relatively mild and never exceeded 40% of their dry mass (**Figure 1C**). PXS 1:1 implants showed the highest hydration during their degradation. The PXS 1:1/1:2 co-polymer, as well as the PXS 2:3 and PXS 1:2 elastomers demonstrated similar hydration profiles (**Figure 1C**).

Thermoset polymer networks contain a fraction of loose, entangled macromers that are not covalently attached to the polymer network, referred to as the sol fraction. Upon degradation of polyesters, scission of esters bonds occurs. This random scission of esters can potentially change a network's sol fraction [14]. This behavior was observed for all PXS elastomers in vivo: sol fractions were observed to increase over time, being at their highest values near complete degradation, but never exceeded 30% of their dry mass (**Figure 1D**).

Observation of the mechanical properties of PXS elastomers revealed a decrease in compression moduli over time, with the exception of PXS 1:2 (**Figure 1E**). At 23.3 \pm 3.7% mass loss of PXS 1:2 implants, no deterioration in compression modulus was observed. When PXS 1:1 elastomers had degraded 24.7 \pm 11.0% however, a decrease of 35.2 \pm 4.7% of their original compression modulus was observed. The relationship between mass loss and mechanical properties for all four PXS elastomers is shown in **Supplementary Figure 2**, and

demonstrated a different trend for the PXS 1:2 elastomers in comparison to the other PXS elastomers. Unlike PXS 1:2, the PXS 1:1, PXS 1:1/1:2 and PXS 2:3 implants revealed a roughly linear decrease of mechanical properties, as the material degraded.

ΔT_g s of PXS elastomers over time were initially negative, and then increased with time as degradation occurred, displayed by PXS 1:1/1:2, PXS 2:3 and PXS 1:2 (**Figure 1F**). An initial negative ΔT_g however, was not observed for PXS 1:1 elastomers.

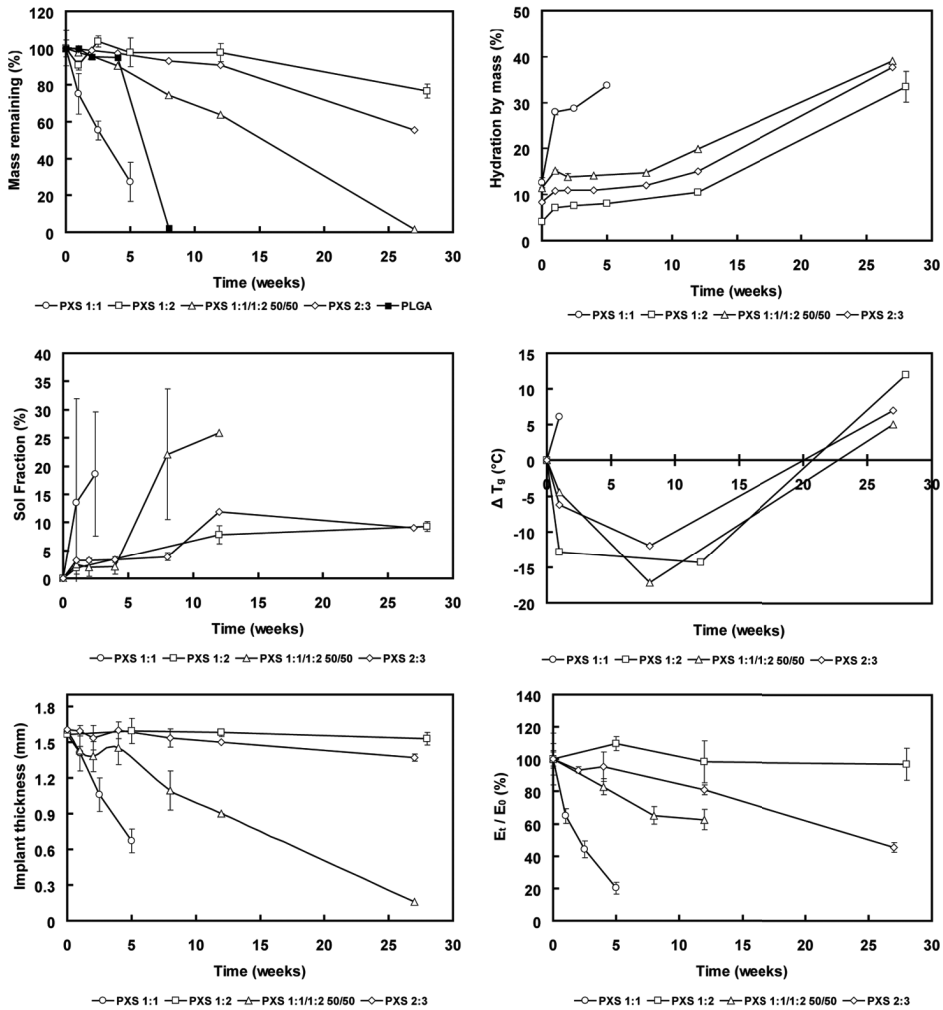


Figure 1. *In vivo* behavior of PXS elastomers over time. Mass loss (A), implant thickness (B), hydration by mass (C), sol fraction (D), mechanical properties (E) and ΔT_g (F).

3.4 Morphological assessment of PXS and PLGA implants

PXS elastomers appeared smooth-surfaced and optically clear at early time points upon visual inspection. Surfaces appeared progressively rough, and implants became more opaque as degradation progressed. Observation of gross morphology revealed that PXS elastomers maintain a high level of structural integrity and form stability compared to PLGA implants during degradation (**Figure 2A-J**).

Surface analysis through SEM revealed a degradation front that progressed inward from the surface (PXS 1:1 and PXS 1:2 elastomers are shown) (**Figure 3A-D**). After 1 week, surfaces of PXS 1:1 elastomers showed excavates and the interior of the implant seemed intact (**Figure 3A**). When PXS 1:1 implants had lost more than $76.7 \pm 3.7\%$ of their initial mass, a more porous surface was observed, covered with excavates (**Figure 3B**). At 5 weeks in vivo, when PXS 1:2 implants had not shown mass loss, no changes on the surface were observed, nor on the interior of the implant (**Figure 3C**). When PXS 1:2 implants degraded however, a rough surface was observed, but the pores appeared smaller as compared to the degrading PXS 1:1 surfaces (**Figure 3D**). The general resulting morphology of PXS implants contrasted that of PLGA implants significantly. PLGA implants showed signs of bulk degradation and the absence of surface erosion (**Figure 3E, F**).

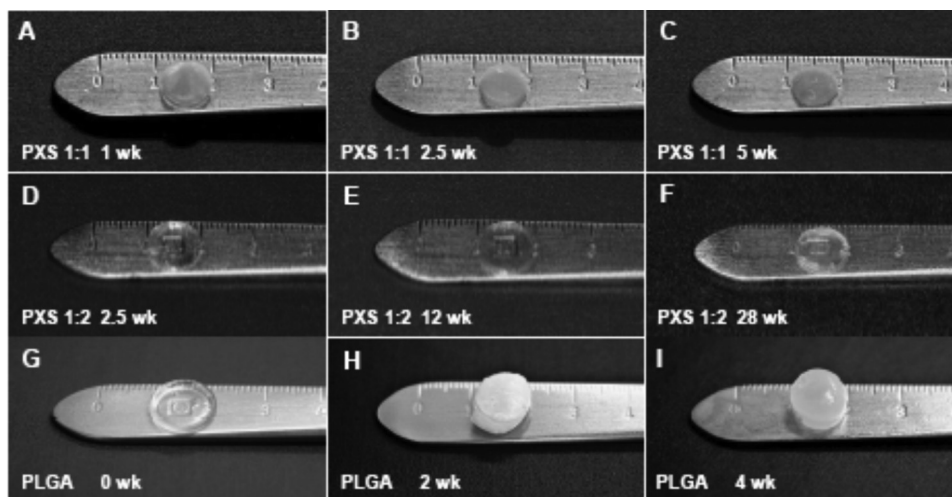


Figure 2. Macroscopic morphology of implants: PXS 1:1 became opaque after 1 week (**A**) but did not swell during degradation, at 2.5 (**B**), and 5 (**C**) weeks. PXS 1:2 implants remained optically transparent after 2.5 (**D**) and 12 (**E**) weeks, and became slightly opaque after 28 (**F**) weeks of implantation. PLGA implants (**G**) became swollen and opaque at 2 (**H**) and 4 (**I**) weeks.

3.5 *In vivo* biocompatibility of PXS 1:1 and 1:2

An initial biocompatibility study of PXS 1:1 and PXS 1:2 elastomers was reported previously, and demonstrated *in vivo* biocompatibility compared to PLGA implants [9]. Here, we studied the biocompatibility in more detail. Following implantation, none of the animals showed post-operative abnormalities in their wound healing process. At all time points during the *in vivo* experiment, PXS implants were encased by a very thin, translucent fibrous capsule, which appeared thicker macroscopically for PLGA implants. On autopsy, occasional vascularization of the capsule was observed for PXS implants, but this seemed more prominent for PLGA implants. Clinically, the surrounding tissues of both PXS and PLGA implants appeared normal. Microscopic evaluation of the histological specimens revealed a thin fibrous capsule surrounding PXS 1:1 elastomers after 1 week *in vivo* (**Figure 4A**). When this was examined in more detail (insert of **Figure 4A** shown in **Figure 4B**), this capsule seemed to consist mainly of lymphocytes, macrophages and fibroblasts. The degradation

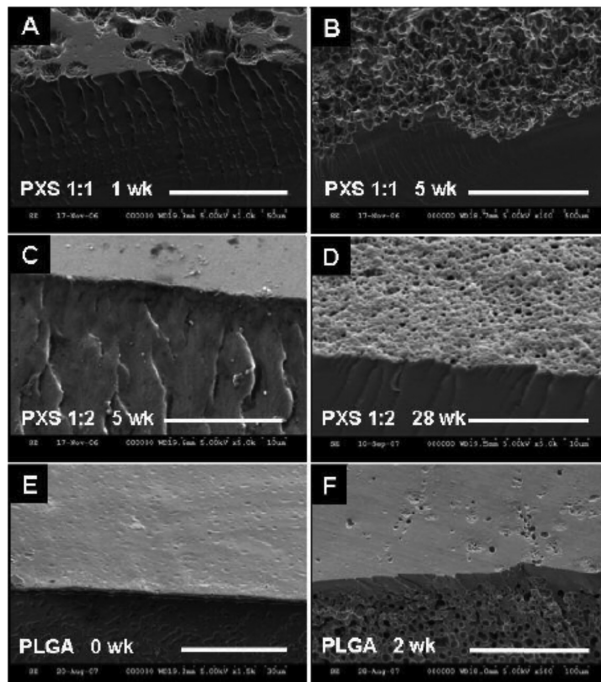


Figure 3. SEM micrographs of PXS and PLGA implants. Representative images of PXS 1:1 at 1 week (**A**) (bar represents 50 µm) and at 5 weeks *in vivo* (**B**) (bar represents 500 µm), PXS 1:2 at 5 weeks (**C**) (bar represents 10 µm) and at 28 weeks *in vivo* (**D**) (bar represents 10 µm), and PLGA at 0 weeks (**E**) (bar represents 30 µm) and at 2 weeks *in vivo* (**F**) (bar represents 100 µm) are shown.

products did not seem to influence fibrous capsule thickness at time points where significant mass loss for PXS 1:1 elastomers was observed (5 weeks, **Figure 4C**). However, the fibrous capsule did show signs of chronic inflammation with fewer lymphocytes, macrophages and giant cells at the polymer surface, as shown at 20x (**Figure 4D**). This thin fibrous capsule was predominantly composed of fibroblasts and vascularization of this capsule was not obvious. A very similar tissue response was observed for fibrous capsules surrounding the PXS 1:2 elastomers, despite their slower degradation rate (**Figure 5A**). Lymphocytes, macrophages and fibroblasts were visible in this capsule, demonstrating the similar wound healing response as PXS 1:1 implants. Also, PXS 1:2 did not trigger noticeable infiltration in the surrounding tissues (**Figure 5B**). After 28 weeks of implantation time, PXS 1:2 elastomers were still encased by a thin fibrous capsule (**Figure 5C**). At the corners of the implants, where most friction with surrounding tissues is expected, fibrous capsules of less

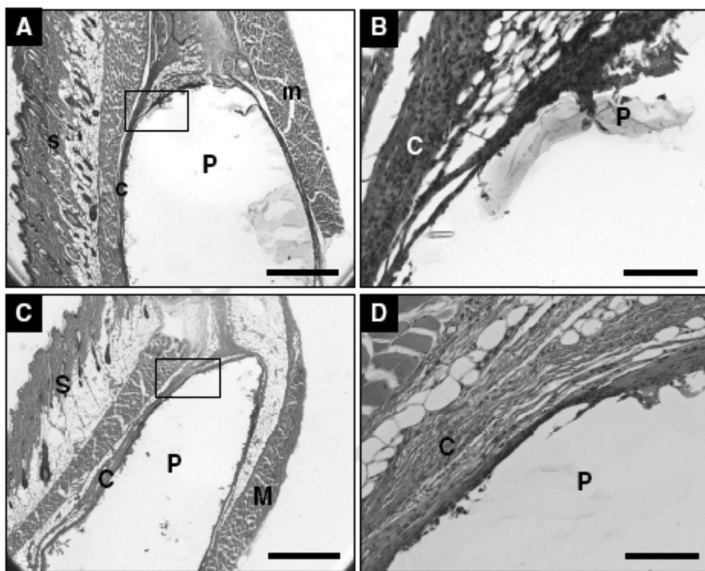


Figure 4. Representative images of H&E stained sections of subcutaneous implantation sites of PXS 1:1 elastomers. An overview of the acute inflammatory response surrounding PXS 1:1 implants at week 1 is shown at 2.5x (**A**) (bar represents 500 μm), and in more detail at 20x (**B**) (bar represents 75 μm). An overview of the chronic foreign body response surrounding degrading PXS 1:1 implants is shown at 2.5x (**C**) (bar represents 500 μm), and in more detail at 20x (**D**) (bar represents 75 μm). The areas of the detailed images are represented in A and C by the black rectangular. P = polymer, C = fibrous capsule, S = skin and M = muscle.

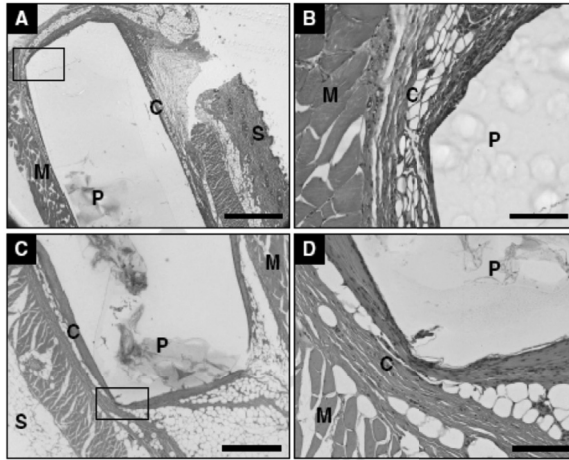


Figure 5. Representative images of H&E stained sections of subcutaneous implantation sites of PXS 1:2 elastomers. An overview of the acute inflammatory response surrounding PXS 1:2 implants at week 1 is shown at 2.5x (A) (bar represents 500 μ m), and in more detail at 10x (B) (bar represents 150 μ m). An overview of the chronic foreign body response surrounding degrading PXS 1:2 implants at 28 weeks is shown at 5x (C) (bar represents 250 μ m), and in more detail at 20x (D) (bar represents 75 μ m). The areas of the detailed images are represented in A and C by the black rectangular. P = polymer, C = fibrous capsule, S = skin and M = muscle.

than 20 cell layers thick were observed (Figure 5D). The fibrous capsules were also mostly composed of fibroblasts with a few scattered macrophages and giant cells at the polymer – tissue interface. PLGA implants however, showed fibrous capsules that were evidently vascularized after 1 week in vivo (Figure 6). In addition, tissues not in direct contact with the implants demonstrated infiltration with mononuclear cells (Figure 6A, B). This response was nearly absent for PXS elastomers. Upon degradation of PLGA implants at 12 weeks in vivo, a different tissue response was observed also, compared to PXS elastomers. Fibrous capsules were thicker (Figure 6C) and contained higher numbers of macrophages and giant cells compared to PXS elastomers. In addition, evident phagocytosis of polymer was observed during polymer degradation, which was not the case for PXS elastomers (Figure 6D). When quantified, an objective difference in biocompatibility was noted between PXS elastomers and the PLGA polymer as well. Figure 7 demonstrates differences in fibrous capsule thicknesses. At week 1, PXS 1:1 and 1:2 were surrounded by significantly thinner capsules than PLGA (* $p < 0.05$), as measured by non-parametric two-way ANOVA. No significant difference in fibrous capsule thickness at week 2 was observed between the PLGA and PXS implants ($p > 0.05$). Also, there was no difference in capsule thickness between the PXS elastomers at week 5 ($p > 0.05$). At week 12, as well as week 27 for PXS 1:2, fibrous

capsules surrounding the PXS elastomers were significantly thinner than capsules around PLGA implants (** $p < 0.05$).

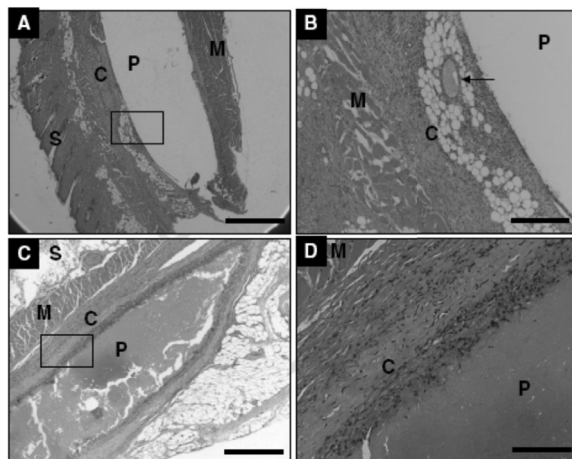


Figure 6. Representative images of H&E stained sections of subcutaneous implantation sites of PLGA implants. An overview of the acute inflammatory response surrounding PLGA implants at week 1 is shown at 2.5x (A) (bar represents 500 μm), and in more detail at 10x (B) (bar represents 150 μm). An overview of the chronic foreign body response surrounding degrading PLGA implants at 12 weeks is shown at 5x (C) (bar represents 250 μm), and in more detail at 20x (D) (bar represents 75 μm). The areas of the detailed images are represented in A and C by the black rectangular. P = polymer, C = fibrous capsule, S = skin and M = muscle. The arrow points to a large vessel of the fibrous capsule surrounding the PLGA implant.

When histological specimen were stained for the presence of CD68 (a marker for activated macrophages), a qualitative difference was observed for PXS elastomers and PLGA polymers (Figure 8A-I), as expected on the previous H&E observations. When quantified, significantly less macrophages were recruited by PXS 1:1 and PXS 1:2 than PLGA at week 1 (* $p < 0.05$ for PXS 1:1, ** $p < 0.001$ for PXS 1:2), but not at week 2 between PXS 1:1 and PLGA implants ($p > 0.05$), as determined by two-way ANOVA. Interestingly, the fraction of CD68+ cells surrounding PXS 1:2 was lower than PXS 1:1 at week 1 ($p < 0.05$) and PLGA implants at week 2 (§ $p < 0.05$). When degradation advanced however, PXS 1:1 (at week 5) revealed significant less CD68+ cells compared to degrading PLGA implants at week 12 ($p < 0.05$). The number of CD68+ cells surrounding the PXS 1:2 was also significantly less than the number of activated macrophages surrounding PLGA implants at week 12 (***) ($p < 0.001$) (Figure 9).

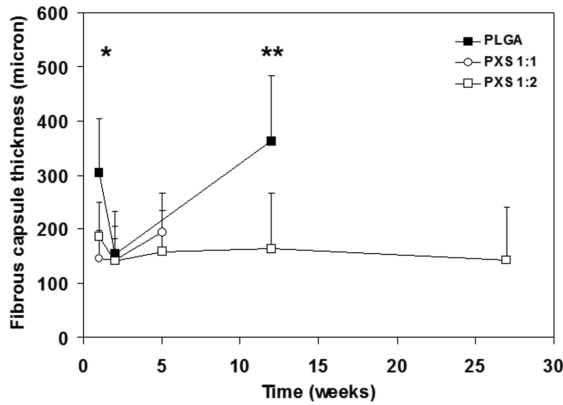


Figure 7. Quantitative analysis of *in vivo* biocompatibility. Fibrous capsule thicknesses were measured and compared for PXS 1:1, 1:2 and PLGA implants. * indicates $p < 0.01$ between PXS 1:1 or PXS 1:2 and PLGA, as well as $p < 0.05$ between PXS 1:1 and PXS 1:2 at week 1. At week 12, ** indicates $p < 0.05$ between PXS 1:2 and PLGA (by non-parametric two-way ANOVA).

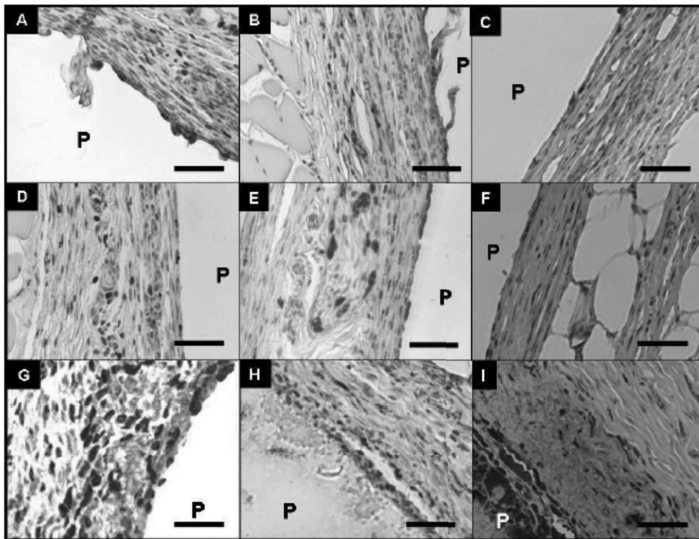


Figure 8. Representative images of CD68 stained sections of subcutaneous implantation sites of PXS and PLGA implants. Recruited and activated macrophages are CD68+ [13]. All images are magnified at 20x (bars represent 25 μ m). Fibrous capsules surrounding PXS 1:1 at 1 week (A), 2 weeks (B) and 5 weeks (C) showed CD68+ cells, similar to the PXS 1:2 at 1 week (D), 2 weeks (E) and 12 weeks (F). Fibrous capsules surrounding the PLGA implants seemed to have more CD68+ cells at 1 week (G), 2 weeks (H) and 12 weeks (I).

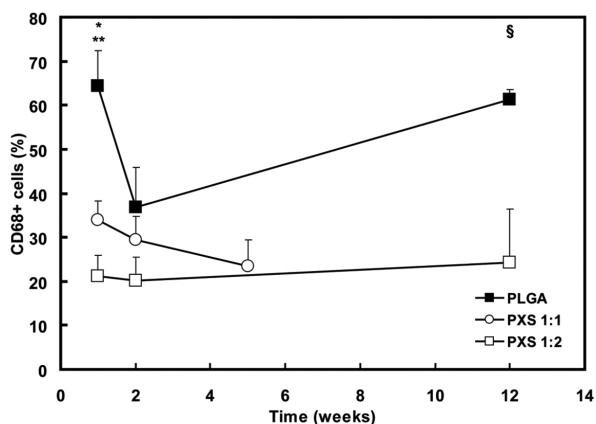


Figure 9. Quantitative analysis of in vivo biocompatibility. Fraction of activated macrophages (CD68+) surrounding the implants. Significance levels were determined by non-parametric two-way ANOVA (* $p < 0.05$ for PXS 1:1 and PLGA at week 1, ** $p < 0.001$ for PXS 1:2 and PLGA at week 1, § $p < 0.05$ for PXS 1:2 and PLGA at week 2, and *** $p < 0.001$ for PXS 1:2 compared to PLGA at week 12).

4. Discussion

Tuning the in vivo behavior of biodegradable polymers is important to meet application-specific demands [9,15]. This proved to be straightforward for PXS elastomers and was demonstrated by adjusting monomer feed ratios as well as by co-polymerization of pre-polymers with different stoichiometries. Taking step-growth polymer kinetics into account, and using the hydroxyl groups as the dominant functionality by 1, the PXS 1:2 stoichiometry shown here represented an upper limit of accessible crosslinking densities for PXS elastomers. As the ratio of aliphatic monomers (sebacic acid) in the polymerization reaction was increased to alter crosslink density, changes in glass transition, tensile Young's – and compression modulus, as well as contact angles, and therefore changes in degradation rates were observed [16]. Similar to reported degradation rates for FDA approved medical devices composed of thermoplastic polymers such as PLGA [3] and poly(⁵⁰/50 (⁸⁵/15 D/L)-lactic-co-ε-caprolactone) [8], subcutaneous degradation rates of PXS elastomers could be tuned from 7 weeks (PXS 1:1), up to a projected in vivo life time of approximately 2 years (PXS 1:2) (Figure 1A).

Bulk degrading materials such as PLGA can reveal a non-linear deterioration in mechanical properties after an initial lag time, before significant mass loss has been

achieved [3,8,17]. PXS elastomers never exhibited this *in vivo* behavior. Mass loss and loss of mechanical properties were roughly linear, whereas PXS 1:2 implants retained their mechanical properties throughout the initial $23.3 \pm 3.7\%$ mass loss (**Supplementary Figure 2**). Furthermore, the presented degradation rates were accessible for PXS elastomers without consequences in construct swelling (**Figure 1C**) or form stability during degradation (**Figure 2 and 3**). This is an important advantage for small-feature medical devices such as flexible drug eluting chips and biosensors [18], peripheral nerve conduits [19] and small vascular grafts [20]. In addition, through co-polymerization of pre-polymers, we have demonstrated PXS elastomers with relatively similar mechanical properties (PXS 1:1/1:2 and PXS 2:3) and different degradation rates (**Table 2, Figure 1, Supplementary Figure 1**). To this date, tuning degradation rate as well as decoupling degradation rate with mechanical properties as demonstrated here has not been shown for comparable thermoset elastomers, *e.g.* PGS. Therefore, PXS elastomers offer a platform of elastomers of which the *in vivo* properties can be tuned to meet a broad variety in application-specific demands.

Although the T_g of some PXS elastomers rose close to 37°C during degradation, PXS implants were observed to remain in a rubbery state at room temperature, most likely due to ΔT_g suppression from the presence of plasticizers including water and molecules that compose the sol fraction [15]. The value of ΔT_g of PXS elastomers was observed to be initially negative, but eventually trended positive during *in vivo* degradation. This implies that there are multiple events which lead to counteracting trends in ΔT_g . Decreases in ΔT_g ($\Delta T_g < 0$) are thought to arise from the following modifications to the polymer network: (1) reduction in crosslink density through cleavage of crosslinked chains; (2) increase in free volume through dissociation and subsequent removal of polymer sol. Increases in T_g ($\Delta T_g > 0$) could arise to other types of network modifications upon degradation: (1) reduction of freely rotating polymer chains due to the cleavage of exposed polymer segments [21]; (2) increased hydrogen bonding due to increased formation of hydroxyl and carboxylic acid groups upon ester cleavage [22,23]. Thus, the observed kinetics of T_g s of most PXS elastomers suggest that degradation mechanisms initially reduce the T_g , but that degradation mechanisms increasing T_g eventually dominated. The PXS 1:1 elastomer however never demonstrated this initial decrease in T_g .

The overall trend in T_g can be explained by considering two types of degradation events: hydrolysis of ester bonds and enzymatic scission via esterase activity, acting across two different phases of the polymer construct. Some appreciable volume fraction of the polymer is able to be accessed by enzymes which can then work to degrade the polymer at localized surfaces. Conversely, the volume fraction that is not able to be accessed by

diffusion of enzymatic species throughout the network is degraded primarily through hydrolysis. Enzymatic activity on polyesters is hypothesized to work primarily to increase the T_g by reducing the amount of mobile polymer chains attached to the network [21,24,25]. Hydrolysis is thought to work primarily to decrease the T_g by widespread reduction of crosslink density as random scission occurs throughout the network. Both enzymatic activity and hydrolysis can lead to increasing T_g through the possibility of increased hydrogen bonding. As previously reported [26], PXS 1:1 elastomers revealed a negligible in vitro mass loss after 105 d in PBS at 37 °C. This observed discrepancy with the in vivo mass loss profile for PXS 1:1 elastomers suggests that the degradation mechanisms may be dominated by an enzyme-driven degradation of PXS elastomers [17]. The exact mechanism of degradation will need to be explored further by comparing the effects on T_g of controlled in vitro degradation conditions as well as additional polymers of varied chemical composition with the observed in vivo trends [21].

Subcutaneously placed PXS elastomers revealed improved biocompatibility when compared to PLGA implants, as PXS implants recruited less activated macrophages and were encased by thinner fibrous capsules (**Figure 5 – 9**). Histology however revealed tissue reactions typical of a foreign body response to implants. In general, it is thought that materials with higher moduli result in harsher tissue reactions [12]. This is also demonstrated by the differences in fibrous capsule thickness between PLGA and PXS implants. Interestingly, the in vivo biocompatibility profiles of PXS 1:1 and 1:2 elastomers were not completely comparable: PXS 1:2 elastomers revealed significant lower CD68+ cell numbers surrounding the implants, compared to PXS 1:1 at all time points (**Figure 9**). This indicates that the more slowly degrading PXS elastomers are better tolerated by the host tissue, despite the higher Young's modulus of PXS 1:2 elastomers compared to PXS 1:1. The different numbers of activated macrophages found in this study may be due to a difference in quantity (PXS 1:1 vs PXS 1:2) as well as chemical composition (PLGA vs PXS) of the degradation products.

5. Conclusions

Biodegradable PXS elastomers revealed precise control of material properties by adjusting the stoichiometric ratios as well as through co-polymerization of different stoichiometries. A wide range of in vivo degradation rates and mechanical properties were achieved. We

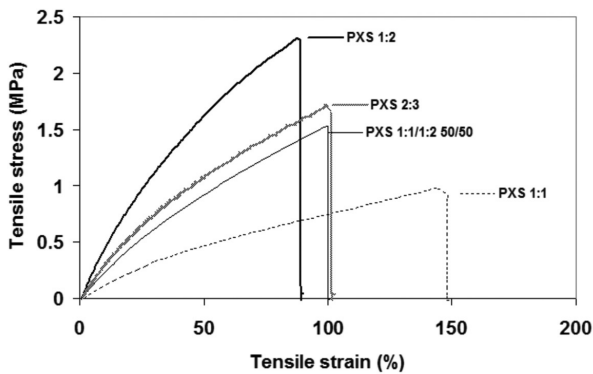
hypothesize that *in vivo* degradation of PXS elastomers occurred predominantly through an enzyme-driven degradation mechanism. PXS elastomers retained structural integrity and form stability during degradation. In addition, PXS elastomers revealed biocompatibility, demonstrated by thinner fibrous capsules as well as lower numbers of activated macrophages surrounding the implants, compared to PLGA. These results suggest that the reduced fibrous wall thickness and macrophage recruitment *in vivo* are enabling properties of PXS elastomers, which makes them potentially suitable for biodegradable medical devices that require structural integrity and form stability for use in short, as well as long-term implantation applications.

6. References

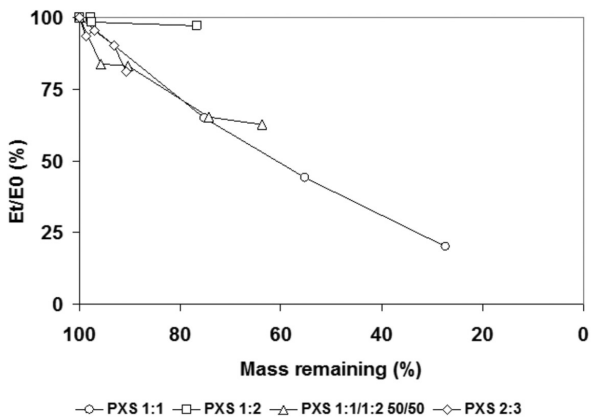
1. Langer R, Vacanti JP. Tissue engineering. *Science* 1993;260(5110):920-6.
2. Scott M. 32,000 years of sutures. *NATNEWS* 1983;20(5):15-17.
3. Middleton JC, Tipton AJ. Synthetic biodegradable polymers as orthopedic devices. *Biomaterials* 2000;21:2335-2346.
4. Langer R. Drug delivery and targeting. *Nature* 1998;392(6679 Suppl):5-10.
5. Den Dunnen WF, Van der Lei B, Schakenraad JM, Blaauw EH, Stokroos I, Pennings AJ, Robinson PH. Long-term evaluation of nerve regeneration in a biodegradable nerve guide. *Microsurgery* 1993;14(8):508-515.
6. Pêgo AP. Biodegradable polymers based on trimethylene carbonate for tissue engineering applications. Enschede: University of Twente; 2002.
7. Wang Y, Kim YM, Langer R. *In vivo* degradation characteristics of poly(glycerol sebacate). *J Biomed Mater Res A* 2003;66(1):192-7.
8. Den Dunnen WFA, Meek MF, Grijpma DW, Robinson PH, Schakernraad JM. *In Vivo* and *in vitro* degradation of poly[50/50(85/15 L/D)LA/ε-CL], and the implications for the use in nerve reconstruction. *J Biomed Mater Res A* 2000;51:575-585.
9. Bruggeman JP, Bettinger CJ, Nijst CLE, Kohane DS, Langer R. Biodegradable xylitol-based polymers. *Adv Mater* 2008;20(10):1922–1927.
10. Badylak SF. The extracellular matrix as a biologic scaffold material. *Biomaterials* 2007;28(25):3587-3593.
11. Ellingsworth LR, DeLustro F, Brennan JE, Sawamura S, McPherson J. The human immune response to reconstituted bovine collagen. *J Immunol* 1986;136(3):877-882.
12. Wang Y, Ameer GA, Sheppard BJ, Langer R. A tough biodegradable elastomer. *Nat Biotechnol* 2002;20(6):602-606.
13. Greaves DR, Gordon S. Macrophage-specific gene expression: current paradigms and future challenges. *Int J Hematol*. 2002;76(1):6-15.
14. Amsden B. Curable, biodegradable elastomers: emerging biomaterials for drug delivery and tissue engineering. *Soft Matter* 2007;3:1335-1348.
15. Bettinger CJ, Bruggeman JP, Borenstein JT, Langer R. Amino alcohol-based degradable poly(ester amide) elastomers. *Biomaterials* 2008;29(15):2315-2325.

16. LaVan DA, McGuire T, Langer R. Small-scale systems for in vivo drug delivery. *Nat Biotechnol* 2003;21:1184-1191.
17. Meek MF, Coert JH. US Food and Drug Administration/Conformit Europe-approved absorbable nerve conduits for clinical repair of peripheral and cranial nerves. *Ann Plast Surg* 2008;60:110–116.
18. Yang J, Webb AR, Pickerill SJ, Hageman G, Ameer GA. Synthesis and evaluation of poly(diols citrate) biodegradable elastomers. *Biomaterials* 2006;27(9):1889-98.
19. Bettinger CJ, Bruggeman JP, Borenstein JT, Langer R. Tunable In vitro and in vivo degradation of poly(1,3-diamino-2-hydroxypropane-co-polyol sebacate) elastomers. *J Biomed Mater Res A* 2009;91(14):1077-1088.
20. Bruggeman JP, De Bruin BJ, Bettinger CJ, Langer R. Biodegradable poly(polyol sebacate) polymers. *Biomaterials* 2008;29(36):4726-4735.
21. Amsden BG, Tse MY, Turner ND, Knight DK, Pang SC. In vivo degradation behavior of photo-cross-linked star-poly(epsilon-caprolactone-co-D,L-lactide) elastomers. *Biomacromolecules* 2006;7(1):365-372.

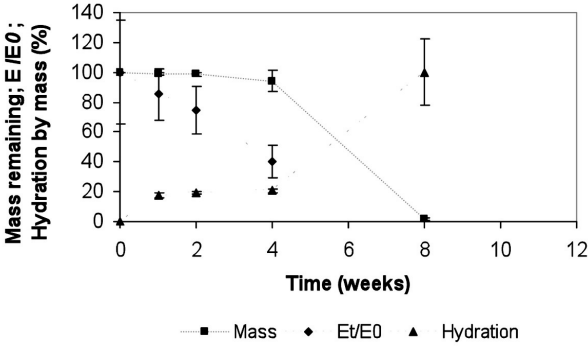
7. Supplementary Figures



Supplementary Figure 1. Representative tensile stress versus strain plots of the PXS elastomers studied here.



Supplementary Figure 2. Loss of mechanical properties (E_t/E_0 in %) versus mass loss (M_t/M_0 in %) for PXS elastomers.



Supplementary Figure 3. *In vivo* mass loss, loss of mechanical properties (E_t/E_0) and hydration by mass (in %) over time for PLGA implants studied here.

Chapter 6

**In vivo behavior of photocured elastomers
from poly(glycerol sebacate): implications for
peripheral nerve conduits**

Joost P. Bruggeman, Christiaan L.E. Nijst, Jeffrey M. Karp, Christopher J. Bettinger,
Michael Moore, Daniel S. Kohane, Robert Langer

Abstract

Recently, we have described the synthesis and characterization of a photocurable elastomer, designated poly(glycerol-co-sebacate)-acrylate (PGSA). The degree of acrylation (DA) of PGSA allowed for controlling the physical properties as well as in vitro degradation rates. Here, we describe the performance of PGSA elastomers in vivo. Mass loss, implant dimensions, hydration, sol content and mechanical strength are described of PGSA implants over time, and were in fact dependent on DA. SEM evaluation of the PGSA constructs revealed a migrating degradation front with a seemingly intact inside of the construct. We hypothesize that PGSA elastomers mainly degrade through a surface eroding mechanism, and most likely through enzymatic degradation. All PGSA elastomers revealed a similar, excellent biocompatibility as compared to thermally cured poly(glycerol-co-sebacate) (PGS). These photopolymerized elastomers comply with important design criteria for nerve conduit biomaterials.

1. Introduction

Over the last decades, biodegradable polymers have made an important contribution in many biomedical technologies such as drug delivery and tissue engineering [1]. One concentrated area of research is the development of biodegradable elastomers because conventional polyesters based on alpha-hydroxy acids, such as poly(glycolic-co-lactic acid) (PLGA), demonstrate rigid mechanical properties and questionable biocompatibility in some cases [2-7]. Biodegradable elastomers have shown to provide form stability and structural integrity within the mechanically challenging in vivo environment [1,6,8-10]. In addition, because elastomers adapt to repetitive mechanical stresses, they are thought to cause less mechanical friction to the surrounding tissues, potentially resulting in less fibrosis [1,6,7,11-13].

In the United States alone, about 200,000 people per year require surgical treatment for peripheral nerve injury [14]. To avoid obvious disadvantages accompanying autologous nerve grafting, much research has gone into the development of artificial nerve conduits. Six important criteria for the design of nerve conduit biomaterials can be drawn from a growing body of literature [15-21]: the polymer should (1) be non-toxic and non-immunogenic; (2) be biodegradable; (3) maintain form stability and structural integrity upon degradation and hydration in vivo; (4) mechanically comply with the nerve and its surroundings; (5) have a tunable in vivo half-life, to be able to correct for the age of the patient, location of the lesion and the extent of the nerve gap; and (6) ideally allow for the incorporation of nerve growth stimulating features such as controlled porosity, patterned surfaces and neurotrophic drug delivery.

We have recently developed a tough biodegradable elastomer, poly(glycerol-co-sebacate) (PGS), to meet this need for tough, biodegradable elastomers [6,12]. In addition, PGS demonstrated promise as nerve conduit biomaterial [22]. However, PGS degraded rapidly upon implantation, with an in vivo half-life of approximately 3.5 weeks. This degradation rate may be unfavorable for in vivo applications such as the peripheral nerve conduit, requiring slower in vivo degradation rates [5]. In addition, harsh curing conditions (high temperatures, vacuum) and long reaction times are required for the synthesis of PGS. We therefore altered PGS and developed a photocurable form of PGS, designated poly(glycerol-co-sebacate)-acrylate (PGSA) [8]. We equipped PGS pre-polymers with acrylate moieties which can be polymerized rapidly at ambient temperatures by free-radical polymerization induced by a photoinitiator exposed to UV-light. The incorporation of acrylate groups and subsequent free-radical induced polymerization of PGSA allowed to control mechanical

properties, as well as in vitro enzymatic degradation rates, simply by altering the degree of acrylation (DA). Photocured PGSA networks demonstrated to allow for the encapsulation of stem cells [23] and for complex polymer substrates with nanotopography, resulting in a promising tissue adhesive inspired on the nanotopography of Gecko feet [24]. Ifkovits *et al.* investigated the photocurable PGSA elastomer as an electrospun scaffold for tissue engineering purposes and confirmed the additional control of material properties by the DA, in addition to other processing conditions such as molecular weight of the acrylated PGS pre-polymer [25].

Here, we report biocompatibility and degradation profiles of PGSA elastomers in vivo. The mechanical properties, hydration, sol content and mass loss over time were studied for thermally PGS networks, PGSA networks with a low- (PGSA-LA) and a high (PGSA-HA) DA, as well as a co-polymer of PGSA-LA and poly(ethylene glycol)-diacrylate (PEG-da). In addition, a photocured PGSA tube was implanted subcutaneously to evaluate its potential as a peripheral nerve conduit.

2. Materials and Methods

2.1 Polymer synthesis

All chemicals were purchased from Sigma-Aldrich (Milwaukee, WI, USA), unless stated otherwise. Both PGS and PGSA were synthesized as previously described [6,8]. The PGS pre-polymer was synthesized by polycondensation of equimolar amounts of glycerol and sebacic acid (Fluka, Buchs, Switzerland) at 120°C under a blanket of argon for 24 h before reducing the pressure from 1 Torr to 40 mTorr over 5 h. The polycondensation was continued for another 24 h, yielding the PGS pre-polymer. The PGS pre-polymer was used without further purification for the PGSA synthesis. A flame-dried round bottomed flask was charged with PGS pre-polymer (20 g, with 78 mmol hydroxyl groups), 200 mL anhydrous dichloromethane, and 4-(dimethylamino)-pyridine (DMAP) (0.18 mmol). The reaction flask was cooled to 0°C under a positive pressure of N₂. Acryloyl chloride was slowly added parallel to an equimolar amount of triethylamine. The reaction was allowed to reach room temperature and was stirred for an additional 24 h. The resulting mixture was dissolved in ethyl acetate, filtered and dried at 45°C and 5 Pa. ¹H Nuclear Magnetic Resonance (¹H-NMR) spectra of the PGS pre-polymer and PGSA were recorded (Varian Unity-300 NMR Spectrometer). Chemical shifts were referenced relative to CDCl₃ at 7.27 ppm. The chemical composition was determined by calculating the signal integrals of –COCH₂CH₂– at 1.2, 1.5, 2.2 ppm for the sebacic

acid, $-\text{CH}_2-\text{CH}-$ at 3.7, 4.2 and 5.2 ppm for glycerol and $-\text{CH}=\text{CH}_2$ at 5.9 ppm, 6.1 ppm and 6.5 ppm for the protons on the acrylate groups. The signal intensity of the methylene groups of the sebacic acid (1.2 ppm) and the acrylate groups (average signal intensity of 5.9, 6.1 and 6.5 ppm) were used to calculate the degree of acrylation (DA). In this study, PGSA with a low DA (DA = 0.31), designated PGSA-LA, and a high DA (DA = 0.41), designated PGSA-HA, were investigated, in addition to PGSA-LA containing PEG-DA. Photocured PGSA-LA and PGSA-HA sheets were formed by mixing PGSA with 0.1% (w/w) photoinitiator (2,2-dimethoxy-2-phenylacetophenone). The polymerization reaction was initiated by exposure to ultraviolet light (ca. 4 mW/cm^2 , model 100AP, Black-Ray) for 10 minutes between two glass slides with a 1.0 mm spacer. Photocured PGSA-PEG was prepared similarly by mixing PGSA-LA with 5% (w/w) PEG-DA ($M_w = 700 \text{ Da}$). PGS polymer sheets were prepared by melting the PGS pre-polymer into a 1.6 mm thick sheet and subsequent thermally curing at 120°C and 40 mTorr for 16 h. All polymer sheets were washed in 100% ethanol for 24 h to remove macromers or photoinitiator and subsequently washed in 70, 50, 30 % (v/v) ethanol/ddH₂O and dried in the oven at 60°C for 24 h. Prior to in vivo implantation, polymer discs were punched out of the polymer sheets, hydrated in sterile saline and UV irradiated for 40 min. Photocured PGSA elastomers can be photopolymerized in a glass mold of appropriate dimensions to produce peripheral nerve conduits. We prepared tubes of 1.2 cm length with an inner diameter of 1 mm and a 250 μm tube wall thickness, similar to the synthesis of aforementioned PGSA sheets.

2.2 In vivo implantation

Female Lewis rats (Charles River Laboratories, Wilmington, MA) weighing 200-250 g were housed in groups of 2 and had access to water and food ad libitum. Animals were cared for according to the approved protocols of the Committee on Animal Care of the Massachusetts Institute of Technology in conformity with the NIH guidelines for the care and use of laboratory animals (NIH publication #85-23, revised 1985). The animals were anaesthetized using continuous 2% isoflurane/O₂ inhalation. Two rats per group per time point received four implants. Two small midline incisions on the dorsum of the rat and the implants were introduced in lateral subcutaneous pockets created by blunt dissection. The skin was closed using staples. The most cranially placed implants were used for histology and were resected en bloc with surrounding tissue. The caudally placed implants were harvested for the assessment of degradation and mechanical testing. Each side of the rat carried either PGS, PGSA-LA, PGSA-HA or PGSA-PEG implants. The animals were inspected daily until post-operative day 10 for any wound healing problems. Throughout the study, all rats stayed in good general health as assessed by their weight gain.

2.3 In Vivo Degradation and Biocompatibility

For the degradation study, discs of photocured PGS, PGSA-LA, PGSA-HA and PGSA-PEG (diameter 10×1.6 mm) ($n = 4$) were implanted subcutaneously in rats. Before implantation, polymer discs were weighed (M_o) and their thickness (H_o) was measured between two glass cover slides using calipers. To investigate in vivo degradation, implants were harvested at pre-determined time points and were collected in sterile saline. Directly upon surgical removal, the explants were dabbed dry, weighed (M_{wet}), and their thickness (H_t) was measured again. The explants were then dried at 90°C for 3 days and weighed (M_{dry}) again. Water content (swelling) by mass and implant dimensions over time were calculated as follows:

$$\frac{M_{wet} - M_{dry}}{M_{dry}} \times 100\% \quad (1)$$

for water content, and

$$\frac{H_t - H_o}{H_o} \times 100\% \quad (2)$$

for implant size.

The mass loss over time was calculated using equation 3.

$$\frac{M_o - M_{dry}}{M_o} \times 100\% \quad (3)$$

Compression tests were performed on the wet explants with a 50N load cell at a compression rate of 5 mm/min using an Instron 5542, according to ASTM standard D575- 91. All samples were compressed to 40% and the compression modulus was calculated from the initial slope (0-10 %) of the stress-strain curve. The compression modulus was determined before implantation, and the ratio of the initial modulus was calculated to the modulus at the pre-determined time point (E_t) as follows:

$$\frac{E_t}{E_o} \times 100\% \quad (4)$$

The explants were cut in half with a razorblade. One half of all the explants was prepared for scanning electron microscope (SEM), sputter-coated with platinum/palladium ($\approx 250\text{\AA}$), mounted on aluminum stubs with carbon tape and examined on a JEOL JSM-5910. The other half of the explants was used to assess the sol content of the material. For this purpose, the dry explants were weighed (M_{dry}), placed in 100% ethanol for 3 days on a orbital shaker, dried at 90°C for 3 days and weighed ($M_{solfree}$) again. The sol content of the explants was calculated, using the following equation:

$$\frac{M_{dry} - M_{solfree}}{M_{solfree}} \times 100\% \quad (5)$$

For biocompatibility analysis, explants and surrounding tissues were harvested, and fixed in Accustain for 24 h, dehydrated in graded ethanol (70-100%), embedded in paraffin, sectioned using a microtome ($4\text{ }\mu\text{m}$). Sequential sections ($8\text{--}15\text{ }\mu\text{m}$) were stained with hematoxylin and eosin (H&E). The H&E stained sections were analyzed by a medical doctor experienced in pathology who was blinded for the chemical composition of the polymer implants. The H&E stains were used to analyze for the presence of fibroblasts and neutrophils in the tissues surrounding the material, and for the presence of multinucleated giant cells, ingrowth of cells into the material as well as phagocytosis of the material.

2.4 Statistical analysis

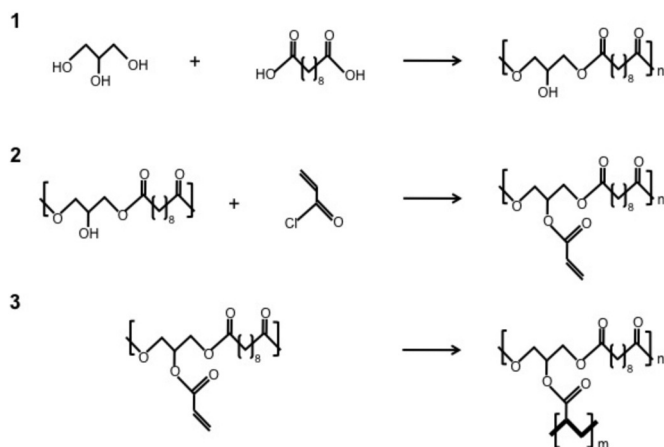
Statistical analysis was performed using a two-tailed Student's t-test with a minimum confidence level of $p < 0.05$ for statistical significance. All values are reported as the mean \pm standard deviation.

3. Results

3.1 Polymer synthesis

The PGSA pre-polymer was prepared by acrylating the PGS pre-polymer (**Scheme 1, step 1 and 2**), which had a weight average molecular weight (M_w) of 23 kDa, a number average molecular weight (M_n) of 6.5 kDa and a polydispersity index (PDI) of 3.5 as determined by GPC. Acrylation had no appreciable effect on the size distribution of the PGS pre-polymer, as previously described [8]. The DA was confirmed by $^1\text{H-NMR}$ as previously reported [8]. The photopolymerization step (**Scheme 1, step 3**) was performed at room temperature by

mixing PGSA with 0.1% (w/w) photo initiator (2,2dimethoxy-2-phenyl-acetophenone). The polymerization reaction was executed by exposure to ultraviolet light. The physical properties of photocrosslinked PGSA polymers and the thermally cured PGS polymer are summarized in **Table 1**.



Scheme 1. Synthetic Scheme of PGSA elastomers. (1) Polycondensation of glycerol and sebacic acid, yielding the PGS pre-polymer. (2) Acrylation of the PGS pre-polymer, yielding the PGSA pre-polymer (not all binding possibilities are shown). (3) Upon free-radical induced polymerization of the PGSA pre-polymer, PGSA elastomers are formed. This additional polymerization leads to alkyl chains of unknown lengths.

Polymer	Degree of acrylation (DA)	T_g (°C)	Young's modulus (MPa)	Ultimate elongation (%)	Crosslink density (mol/m ³)
PGS	-	-28	0.76 ± 0.02	80 ± 32.2	102 ± 2.1
PGSA-LA	0.31	-32	0.38 ± 0.03	55 ± 14.1	52 ± 3.9
PGSA-HA	0.41	-31	0.89 ± 0.05	51 ± 7.4	120 ± 7.0
PGSA-PEG	0.31	-32	0.80 ± 0.03	45 ± 9.7	108 ± 2.8

Table 1. Composition and physical properties of the elastomers studied. Values are reported as the mean ± standard deviation.

3.2 In vivo degradation

Figure 1A demonstrates mass loss of implanted PGS discs, which decreased linearly over time, with an in vivo half-life of two to three weeks. The acrylate groups in the PGS backbone and subsequent photocrosslinking increased the in vivo half-life up to $\sim 4\frac{1}{2}$ weeks for PGSA-LA and ~ 10 weeks for PGSA-HA. Non-degradable PEG-DA entities within the PGSA-LA network dramatically decreased the degradation rate, with a mass loss of $19 \pm 9\%$ after 12 weeks (**Figure 1A**). The dimensions of PGS and PGSA-LA implants decreased almost linearly over time in vivo (**Figure 1B**). PGSA-HA implants however, showed an increase in polymer thickness up to 110% of the original value at 5 weeks in vivo, after which a continuous linear decrease was seen. PGSA-PEG underwent a constant, gradual increase in thickness over the course studied, up to $117 \pm 12\%$ after 9 weeks in vivo. Except for the PGS implants (**Figure 2A**), all acrylated polymers showed an equilibrium swelling in vivo as high as $39 \pm 2\%$ of the dry polymer weight at week 3 for PGSA-LA (**Figure 2B**), $35 \pm 12\%$ at week 5 for PGSAHA (**Figure 2C**), and $34 \pm 9\%$ at week 9 for PGSA-PEG (**Figure 2D**). PGS implants never reached a water content of higher than 20% throughout their entire residence in vivo, which is in accordance with previously published results [12]. Upon degradation, PGSA-LA implants showed the highest sol content, being $41 \pm 11\%$ of the dry polymer weight at week 3, subsequently decreasing to $15 \pm 1\%$ and $28 \pm 2\%$ in the weeks thereafter (**Figure 2B**). The sol content of the PGSA-HA (**Figure 2C**) and PGSA-PEG (**Figure 2D**) implants averaged both $< 20\%$ throughout the course of the study, which was similar to the results obtained for PGS, which averaged at around $9 \pm 3\%$. This finding is consistent with previous reported findings for PGS [12]. All polymer implants showed a non-linear decrease in mechanical strength over time, expressed as a percentage of the initial compression modulus at the time of implantation. PGS implants showed loss in mechanical strength over time, similar to what was previously reported by Wang *et al.* [12], PGSA-LA and PGSA-HA implants revealed a similar pattern, but maintained their mechanical strength over a longer period of time, as shown in **Figure 2A-C**. The PGSA-PEG implants maintained their mechanical strength over a much longer period of time: the implants retained $55.52 \pm 14.84\%$ of their original strength at the end of the study (12 weeks) (**Figure 2D**). At that time, the PGSA-PEG implants had degraded $19 \pm 9\%$.

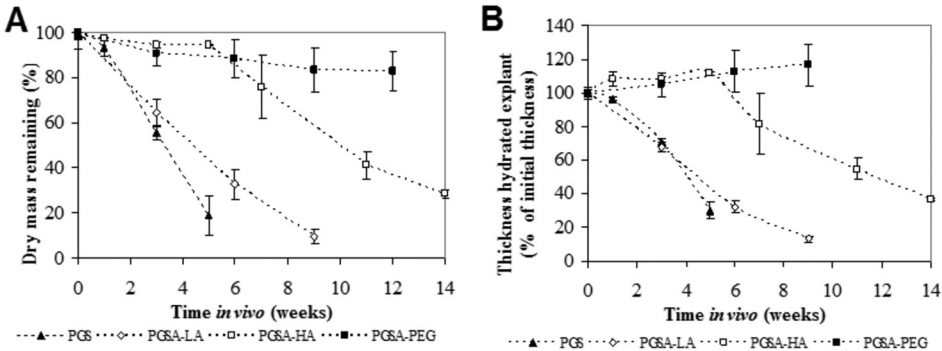


Figure 1. (A) Dry mass loss and (B) implant thickness over time for PGS, PGSA and PGSA-PEG elastomers in vivo.

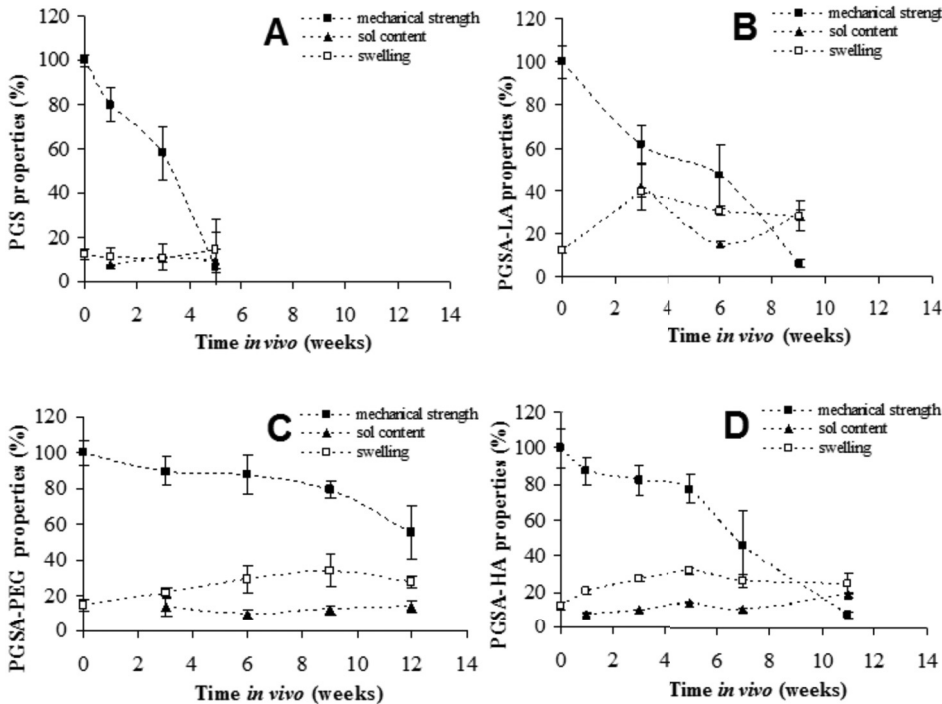


Figure 2. Mechanical strength, sol content and degree of swelling (by mass) over time for (A) PGS, (B) PGSA-LA, (C) PGSA-HA and (D) PGSA-PEG elastomers.

Figure 3 shows the loss of mechanical strength as function of mass loss, and PGSA-PEG implants revealed a clear drop in mechanical strength, before significant degradation had taken place. This appeared to be different for PGS, PGSA-LA and PGSA-HA of which the loss in mechanical strength related to mass loss may be roughly viewed as linear.

At all time points during the *in vivo* experiment, polymer discs were easily separated from their thin capsules for further *ex vivo* characterization of the degradation kinetics. Upon visual inspection, they appeared smooth-surfaced and optically clear at early time points, but became progressively rougher and more opaque over time as degradation occurred. During degradation, PGS, PGSA-LA and PGSAHA polymers showed a degradation front that migrated inwards, as revealed by SEM. Thinning of the constructs occurred, and no obvious erosion was observed in the center of the construct (**Figure 4AC**). This was not the case for PGSA-PEG implants, which showed degradation on the inside of the construct as well (**Figure 4D**). **Figure 4E-H** shows SEM images of the surface of the implants, demonstrating roughly a similar morphology between the implants, which in general terms was characterized by the formation of deep cracks and resulting pillars of polymer.

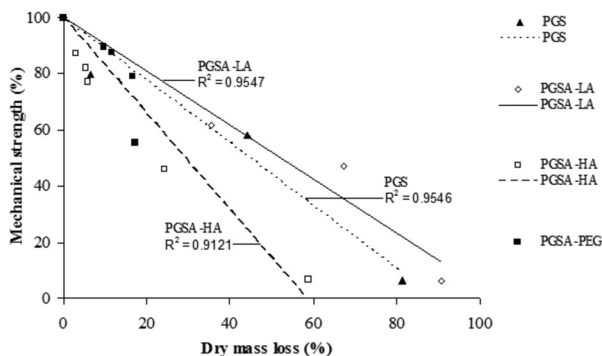


Figure 3. Loss of mechanical strength ($E_v/E_0 \times 100\%$) as a function of mass loss for all elastomers. A trend-line for PGSA-PEG elastomer is not shown, as $R^2 = 0.6659$, and can not be seen as a linear correlation.

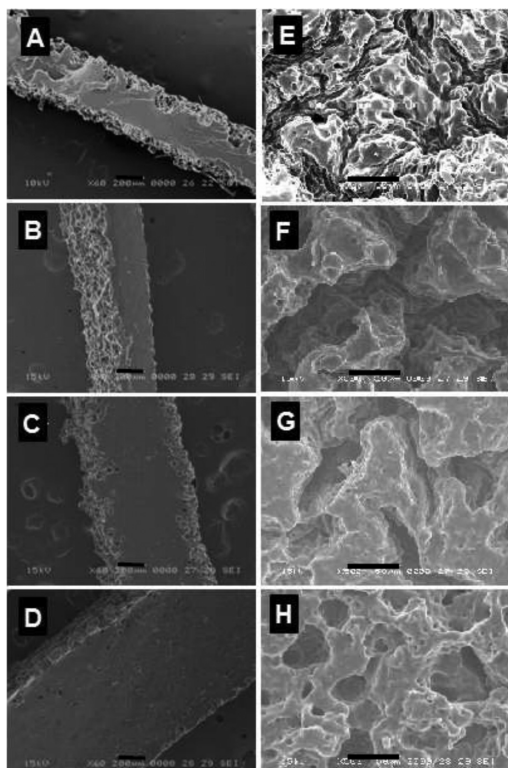


Figure 4. Representative SEM images of degraded elastomeric constructs composed of (A) PGS at 5 weeks, (B) PGSA-LA at 6 weeks, (C) PGSA-HA at 11 weeks and (D) PGSA-PEG at 12 weeks in vivo, as well as their close up images of surfaces of PGS (E), PGSA-LA (F), PGSA-HA (G) and PGSA-PEG (H). Bars in A-D represent 200 μm , and in E-F 50 μm .

3.3 In vivo biocompatibility

Following implantation, none of the animals showed post-operative abnormalities in their wound healing process. On autopsy, the implanted polymer discs were encased in a translucent tissue capsule, which became more substantial over time. Vascularization of the capsule was observed for most implants, and the surrounding tissues all appeared to be normal macroscopically. Upon microscopy, the foreign body reaction seemed very mild, and was similar to what was previously described for PGS implants [6,12]. The thicknesses of the fibrous capsule at all time points never exceeded 180 μm (Figure 5A). Representative images of the initial inflammatory response are shown only for PGS and PGSA-HA at week 1 (Figure 5B-E) and of the chronic inflammatory response at week 3 for PGSA-LA (Figure 5F, G) as well as at 12 weeks for PGSA-PEG (Figure 5H, I). Inflammation surrounding PGS

and PGSA-LA in the first week was mostly characterized by a mononuclear cellular infiltrate (**Figure 5A-E**) in the surrounding tissues in contact with the implant, up to a maximum distance of $112 \pm 20 \mu\text{m}$ from PGS implants, or $69 \pm 23 \mu\text{m}$ for PGSA-LA implants ($p < 0.05$). After 3 weeks, during the chronic inflammatory phase, PGS, PGSA-LA, PGSA-HA and PGS-PEG implants demonstrated fibrous capsules with thicknesses of $67 \pm 29 \mu\text{m}$, $70 \pm 23 \mu\text{m}$, $62 \pm 25 \mu\text{m}$ and $53 \pm 36 \mu\text{m}$ respectively ($p > 0.05$, **Figure 5A, F-I**). The fibrous capsule consisted primarily of collagen, fibroblasts and macrophages. No cell ingrowth into the polymer discs was observed for all time points and polymer compositions.

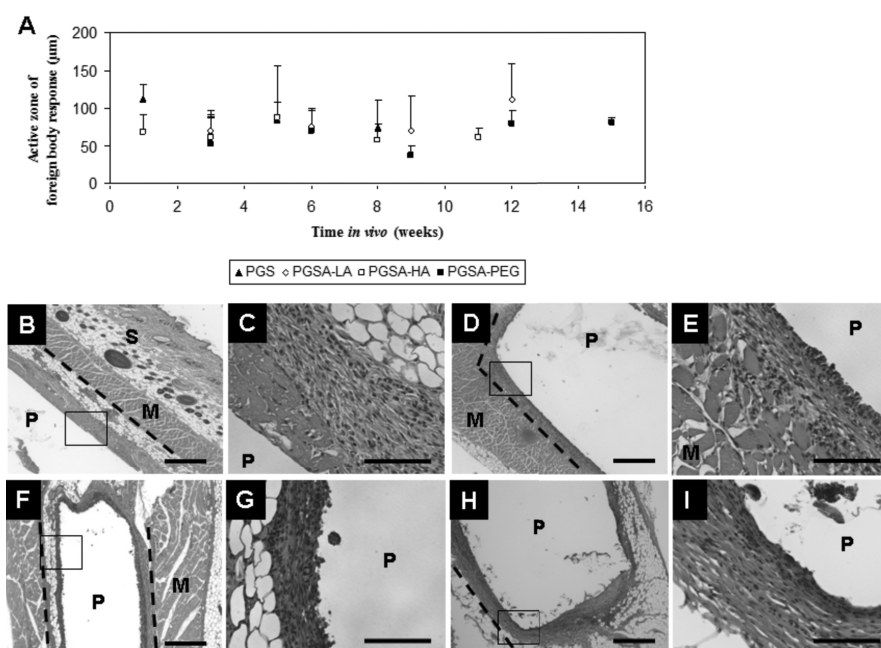


Figure 5. (A) The extent of active foreign body response, meaning the area of infiltration, measured from the edge of the polymer (P) to an imaginary line (dashed black line in B and D) within the surrounding muscle (M) or skin (S) where the tissue does not show any inflammation, or to the edge of the fibrous capsule (dashed black line in F and H). The black squares in B, D, F and H resemble the areas of magnification as shown in C, E, G and I. Representative H&E images of the acute inflammation: at 1 week in vivo at 5x for PGS implants (**B**) and at 40x (**C**). PGSA-LA implants showed a similar wound healing response around the implant at week 1, shown at 5x (**D**) and at 40x (**E**) as well. Evident fibrous capsule formation and chronic inflammation is seen after this acute inflammatory response: PGSA-HA implants at 3 weeks, shown at 5x (**F**) and at 40x (**G**). At 12 weeks in vivo, PGSA-PEG implants shown at 5x (**H**) and at 40x (**I**) showed more collagen within the fibrous capsule. Bars represent 250 μm in B, D, F and H, and 50 μm in C, E, G and I.

3.4 Subcutaneous implantation of PGSA-HA tubes

Photocured PGSA elastomers can be polymerized in a glass mold of appropriate dimensions to produce peripheral nerve conduits. We prepared PGSA-HA tubes of 1.2 cm length with an inner diameter of 1 mm and a 250 μm tube wall thickness (**Figure 6A**). At 1 and 3 months, PGSA-HA tubes did not collapse and allowed for fibrous tissue ingrowth within the tube (**Figure 6D**), which was also macroscopically visible. Fibrin seemed to be the tube content at the earlier time point (**Figure 6B**). The PGSA tube had degraded on the outside more than the inside. The rate at which it degraded seemed slower than solid PGSA-HA polymer discs, as shown by SEM (**Figure 6C**). However, this difference was not quantified.

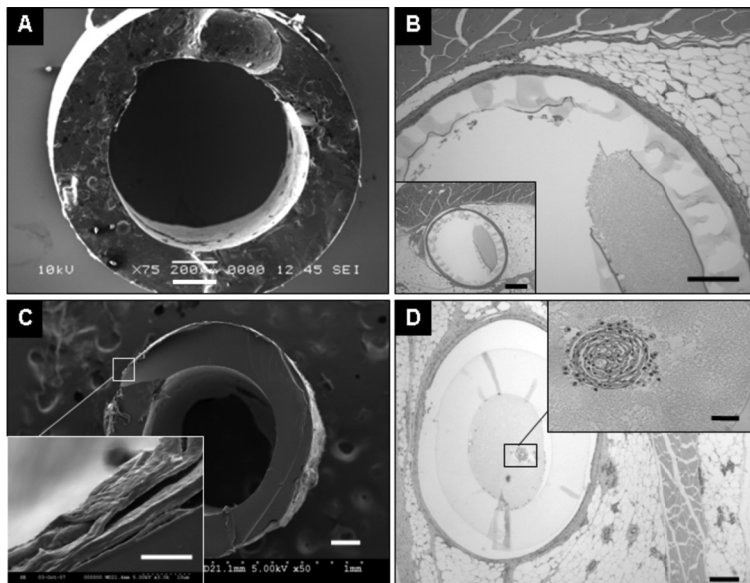


Figure 6. (A) SEM image of a PGSA-HA tube. Bar represents 200 μm . (B) A representative H&E image of a PGSA-HA tube placed subcutaneously after 1 month. Bar represents 200 μm . A cable of fibrous tissue has formed within the tube (See insert. Bar represents 30 μm). (C) SEM image of a PGSA-HA tube after 3 months in vivo. Bar represents 200 μm . Degradation was noted only on the outside of the conduit (See insert. Bar represents 10 μm). (D) Representative H&E image of a subcutaneously placed PGSA-HA tube, confirming fibrous tissue ingrowth within the tube after 3 months in vivo. Bar represents 150 μm . The insert is an overview of the tissue at 2.5 x.

4. Discussion

Biodegradable elastomeric polyesters are hypothesized to degrade through surface erosion and/ or bulk degrading mechanisms [10,26]. As previously shown in vitro for the same PGS, PGSA and PGSA-PEG elastomers studied here, the presence and concentration of acrylate groups, and not crosslink density, seemed to determine the susceptibility and rate of enzymatic degradation. However, when in vitro hydrolysis was investigated, crosslink density as well as the concentration of acrylate groups determined the degradation rate for PGS and PGSA elastomers [8]. As demonstrated by **Figure 1**, chain growth polymerization through acrylate groups within the PGSA polymer backbone, and not crosslink density per se negatively influenced in vivo mass loss: PGSA-LA was observed to degrade slower than PGS, although its crosslink density of PGSA-LA is half of the crosslink density of PGS (**Table 1**). We therefore hypothesized that enzymes seemed to play an important role in the degradation process of PGS and PGSA elastomers. Introducing non-degrading PEG-DA entities within the PGSA-LA polymer dramatically slowed down the rate of degradation, increased swelling and dimensions of the construct. Mixing PGSA-LA and PEGda pre-polymers may have caused a separation of pre-polymers, resulting in domains of PEGda networks and PGSA-LA networks throughout the PGSA-PEG construct. The PEGda networks are not susceptible to degradation while PGSA-LA networks are degraded by enzymatic species and disappeared from the PGSA-PEG construct, resulting in an increase in free volume within the PGSA-PEG construct, resulting in a sponge-like material. This is demonstrated by the mechanical properties, which were maintained over a longer period compared to the other elastomers. However, PGSA-PEG constructs demonstrated a drop in mechanical properties before a significant mass loss was achieved (**Figure 3**). This is most likely explained by an increase of free volume within the polymer bulk as demonstrated by **Figure 4D**, as well as bulk hydrolysis of the PGSA domains within the PGSA-PEG construct. However, to further confirm this possibility of degradation mechanism for PGSA-PEG, thermal properties should have been included in the design of this study. Long-term in vivo applications of PGSA-PEG elastomers seem appropriate, although we cannot state from these results that PGSA-PEG polymers are completely biodegradable. SEM images of PGS and PGSA constructs revealed a clear degradation front that moved towards the center of the construct, with a seemingly intact bulk (**Figure 4**), however, PGS and PGSA elastomers showed a continuous decrease in mechanical strength over time (**Figure 2A-C**). One explanation for this is that PGSA and PGS elastomers degrade through both bulk degradation as well as surface erosion. Bulk hydrolysis can be considered the main reason of mechanical deterioration, despite the lack

of visible changes by SEM. However, we hypothesize that the mechanical deterioration may also be a reflection of an enzyme-driven surface erosion on the surfaces of PGS and PGSA elastomers. The degradation of PGS and PGSA elastomers proceeds through the formation of micron-scale cracks and pores at the surfaces of the construct. This layer of cracks and pores progressively make up a part of the total construct dimensions (the degradation front indicated by dashed lines in **Figure 7**). The part of the construct where degradation occurs, has different mechanical properties than the inner, intact construct due to its porous nature, and therefore affects the average modulus of the entire construct. Thus, the construct can be considered to be a layered composite material. This porous, degrading part of the construct increases proportionally over time, as the construct thins, and the width of the degradation front most likely does not.

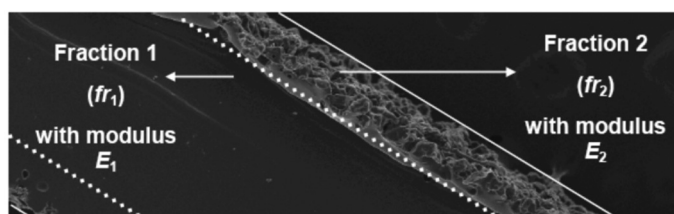


Figure 7. A representative image of a degrading PGSA-HA elastomeric construct at 5 weeks. The construct appears to be composed of an inner untouched part (fraction 1, fr_1) and degrading parts (fraction 2, fr_2) on both sides of fr_1 . When considered a layered composite material, the modulus of the whole construct, E_t , will deteriorate as fraction 2, and its modulus E_2 , will proportionally increase as erosion progresses, with a negative effect on the modulus of the entire construct.

PGSA elastomers are biocompatible. A favorable foreign body response was observed for all polymers, as photocured PGSA showed a similar extent of foreign body response, when compared to PGS (**Figure 5**). The excellent biocompatibility of PGS, as well as PGSA, may be due to the elastic nature of the material, as well as the chemical composition of the polymer and degradation profile. PLGA is composed of short aliphatic acids which, upon bulk degradation, may accumulate within the polymer construct. These acidic products may be subsequently released all at once in the surrounding tissues, leading to a questionable biocompatibility for this polymer [4]. PGSA elastomers however do not primarily degrade through bulk hydrolysis and are composed of less, non-water soluble, acid monomers.

The limiting factors to apply PGS in experimental nerve reconstruction procedures were overcome by the development of PGSA, which revealed a controllable *in vivo*

degradation rate. Subcutaneously implanted PGSA-HA tubes revealed mechanical stability and allowed for tissue growth within the conduit for up to three months (**Figure 6B, D**). This means that PGSA tubes do not collapse or swell to an extent that a tissue bridge is allowed to form. Furthermore, degradation was more prominent on the outside of the conduit. This discrepancy might be due to the fact that there is less exposure to enzymes within the tubes. However, as the rate of degradation of PGSA-HA tubes seemed lower than we would expect based on the data obtained from implanted discs (**Figure 6C**), more studies should be performed to evaluate the degradation kinetics of PGSA tubes before they can be tested in an in vivo experimental model for peripheral nerve repair.

5. Conclusions

Similar and in addition the effect of DA on mechanical properties of PGSA elastomers, in vivo degradation rates and profiles could be controlled. PGSA elastomers are mainly degraded through an enzyme-driven surface eroding mechanism in vivo. The biocompatibility of PGSA elastomers is comparable to that of thermally cured PGS. These photopolymerized elastomers comply with design criteria for peripheral nerve conduits. PGSA elastomers were non-toxic, biocompatible, biodegradable and importantly, maintained form stability and structural integrity upon degradation in vivo.

6. Acknowledgements

JPB acknowledges financial support from the J.F.S. Esser Stichting and the Stichting Prof. Michaël-Van Vloten Fonds. C.L.E.N. acknowledges the financial support of Dr. Saal van Zwabenberg Stichting. CJB acknowledges the Draper Laboratory for direct funding. This work was funded by NIH grant HL060435 and through a gift from Richard and Gail Siegal.

7. References

1. Langer R, Vacanti JP. Tissue engineering. *Science* 1993;260(5110):920-6.
2. Den Dunnen WFA, Meek MF, Grijpma DW, Robinson PH, Schakernraad JM. In Vivo and in vitro degradation of poly[50/50(85/15 L/D)LA/ ϵ -CL], and the implications for the use in nerve reconstruction. *J Biomed Mater Res A* 2000;51:575-585.

3. Evans GRD, Brandt K, Widmer MS, Lu L, Meszlenyi RK, Gupta PK, Mikos AG, Hodges J, Williams J, Gurlek A and others. In Vivo Evaluation of Poly(L-lactic acid) Porous Conduits for Peripheral Nerve Regeneration. *Biomaterials* 1999;20:1109-1115.
4. Middleton JC, Tipton AJ. Synthetic biodegradable polymers as orthopedic devices. *Biomaterials* 2000;21:2335-2346.
5. Pêgo AP. Biodegradable Polymers Based On Trimethylene Carbonate For Tissue Engineering Applications. Enschede: University of Twente; 2002.
6. Wang Y, Ameer GA, Sheppard BJ, Langer R. A tough biodegradable elastomer. *Nat Biotechnol* 2002;20(6):602-6.
7. Yang J, Webb AR, Ameer GA. Novel Citric Acid-Based Biodegradable Elastomers for Tissue Engineering. *Advanced Materials* 2004;16(6):511-516.
8. Nijst CLE, Bruggeman JP, Karp JM, Ferreira L, Zumbuehl A, Bettinger CJ, Langer R. Synthesis and Characterization of Photocurable Elastomers from Poly(glycerol-co-sebacate). *Biomacromolecules* 2007;8(10):3067-3073.
9. Pêgo AP, Poot AA, Grijpma DW, Feijen J. Biodegradable elastomeric scaffolds for soft tissue engineering. *J Control Release* 2003;87:69-79.
10. Amsden BG, Tse MY, Turner ND, Knight DK, Pang SC. In Vivo Degradation Behavior of Photo-Cross-Linked *star*-Poly(epsilon-caprolactone-co-D,L-lactide) Elastomers. *Biomacromolecules* 2006;7:365-372.
11. Bruggeman JP, Bettinger CJ, Nijst CLE, Kohane DS, Langer R. Biodegradable Xylitol-Based Polymers. *Adv Mater* 2008;20(10):1922-7.
12. Wang Y, Kim YM, Langer R. In vivo degradation characteristics of poly(glycerol sebacate). *J Biomed Mater Res A* 2003;66(1):192-7.
13. Yang J, Webb AR, Pickerill SJ, Hageman G, Ameer GA. Synthesis and evaluation of poly(diols citrate) biodegradable elastomers. *Biomaterials* 2006;27(9):1889-98.
14. Madison RM, Archibald SJ, Krarup C. Peripheral nerve injury. Philadelphia: W. B. Saunders; 1992. 450-487 p.
15. Dahlin LB, Lundborg G. Use of tubes in peripheral nerve repair. *Neurosurg Clin N Am*. 2001;12(2):341-52.
16. Den Dunnen WFA, Stokroos I, Schakernraad JM, Zondervan GJ, Pennings AJ, Van der Lei B, Robinson PH. A New PLLA/PCL Copolymer for Nerve Regeneration. *J Mater Sci Mater Med*. 1993;4:521-525.
17. Harley BA, Spilker MH, Wu JW, Asano K, Hsu HP, Spector M, Yannas IV. Optimal degradation rate for collagen chambers used for regeneration of peripheral nerves over long gaps. *Cells Tissues Organs*. 2004;176(1-3):153-165.
18. Hoppen HJ, Leenslag JW, Pennings AJ, Van der Lei B, Robinson PH. Two-ply biodegradable nerve guide: basic aspects of design, construction and biological performance. *Biomaterials* 1990;1990(11):286-290.
19. Mackinnon SE, Dellon AL. Clinical Nerve Reconstruction with a Bioabsorbable Poly(glycolic acid) Tube. *Plast Reconstr Surg* 1990;85:419-424.
20. Pêgo AP, Poot AA, Grijpma DW, Feijen J. Copolymers of trimethylene carbonate and ϵ caprolactone for porous nerve guides: Synthesis and properties. *J. Biomater. Sci. Polymer Edn*. 2001;12(1):35-53.
21. Rosen JM, Padilla JA, Nguyen KD, Siedman J, Pham HN. Artificial nerve graft using glycolide trimethylene carbonate as a nerve conduit filled with collagen compared to sutured autograft in a rat model. *J Rehabil Res Dev* 1992;29:1-12.
22. Sundback CA, Shyu JY, Wang Y, Faquin WC, Langer RS, Vacanti JP, Hadlock TA. Biocompatibility analysis of poly(glycerol sebacate) as a nerve guide material. *Biomaterials* 2005;26(27):5454-64.

23. Gerecht S, Townsend SA, Pressler H, Zhu H, Nijst CLE, Bruggeman JP, Nichol JW, Langer R. A porous photocurable elastomer for cell encapsulation and culture. *Biomaterials* 2007;28(320):4826-4835.
24. Mahdavi A, Ferreira L, Sundback C, Nichol JW, Chan EP, Carter DJ, Bettinger CJ, Patanavanich S, Chignozha L, Ben-Joseph E and others. A biodegradable and biocompatible gecko-inspired tissue adhesive. *Proc Natl Acad Sci U S A*. 2008;105(7):2307-2312.
25. Ifkovits JL, Padera RF, Burdick JA. Biodegradable and radically polymerized elastomers with enhanced processing capabilities. *Biomed Mater* 2008;3(3):034104.
26. Storey RF, Hickey TP. Degradable polyurethane networks based on D,L lactide, glycolide, epsilon-caprolactone, and trimethylene carbonate homopolyester and copolyester triols. *Polymer* 1994;35(4):830-838.

Chapter 7

Biodegradable poly(xylitol sebacate) elastomers for peripheral nerve reconstruction

Joost P. Bruggeman, Berend-Jan de Bruin, Alex Alford, Christopher J. Bettinger,
Paul M. George, Steven E. Hovius, Robert Langer

Abstract

Current clinically available artificial nerve conduits possess unfavorable mechanical properties, conduit swelling, as well as harmful acidic byproducts during degradation. This study examined the biocompatibility and performance of a novel biodegradable elastomer, poly(xylitol sebacate) (PXS) as a peripheral nerve conduit. Composed of monomers endogenous to mammalian metabolism but synthetic in nature, PXS elastomers possess favorable mechanical properties, degradation behavior and biocompatibility comparable to materials composed of α -hydroxy acids. Biodegradable PXS elastomers enabled attachment and subsequent proliferation of primary rat Schwann cells in vitro and demonstrated in vivo biocompatibility with sciatic nerve tissue. Furthermore, PXS conduits allowed for peripheral nerve regeneration over the critical sized nerve gap in an experimental rat model. This initial study demonstrates PXS has potential as peripheral nerve conduit material.

1. Introduction

In the United States alone, about 200,000 people per year require surgical treatment for peripheral nerve injuries [1]. The standard technique is end-to-end suture of severed nerve, or the interposition of an autologous nerve graft when tensionless coaptation cannot be performed. However, nerve conduits are used for smaller nerve defects and have several advantages over nerve grafting. Conduits give directional guidance to migrating Schwann cells and elongating axons, and offer a controllable regenerative environment, as well as protection from potentially impeding scar tissue formation [2]. Other important advantages of conduits are the prevention of donor-site morbidity (loss of sensation, neuroma formation, infection), reduction of operation time, and the ability to repair nerve lesions in anatomic locations that are difficult to reach.

For these reasons, development of nerve conduit materials gained popularity over the last decades. Polymers used for this application ideally adhere to several important design criteria [3-8]: they should ideally (1) be non-cytotoxic and non-immunogenic; (2) be biodegradable; (3) maintain form stability and structural integrity upon degradation and hydration in vivo; (4) have a tunable in vivo half-life to account for the age of the patient, location of the lesion and the extent of the nerve gap, (5) mechanically match the nerve and its surroundings; (6) be soft enough to allow micro-suturing and strong enough to hold the sutures and; (7) potentially allow for the incorporation of nerve growth stimulating features such as (micro)porous walls, patterned surfaces and/or controlled release of neurotrophic agents, as well as (8) Schwann cell (SC) adhesion and subsequent proliferation. Currently, three biodegradable nerve conduits are used in clinical practice [9]: conduits composed of (Type I bovine) collagen, poly(glycolic acid) (PGA), or poly(⁶⁵/35(⁸⁵/15 D/L) lactide-co- ϵ -caprolactone) (PDLLC). Natural polymers such as collagen are prone to biological variation, resulting in batch-to-batch differences in mechanical properties and degradation rates [10]. Collagen is also known to elicit immune responses in some cases and carries a small potential risk of transferring pathogens such as viruses and prions [11]. In addition, human or animal collagen may be problematic for cultural or religious reasons. On the other hand, conduits composed of synthetic polyesters, such as PGA and PDLLC, reveal rigid mechanical properties, are known to swell significantly and decompose into fragments during degradation as well as produce acidic degradation products, potentially harming the regenerating nerve [9,10,12].

Recently, we have described biodegradable poly(xylitol sebacate) (PXS) elastomers [13]. PXS elastomers are composed of non-toxic monomers that are endogenous to the

mammalian metabolism, but are synthetic in nature. PXS elastomers have tunable in vivo half lives, ranging from 1 to 24 months [14]. PXS elastomers degrade primarily through surface erosion, revealing minimal swelling and excellent form stability [14]. This is advantageous for small lumen devices such as conduits, but also for the incorporation of (sub)micron sized features into the conduit, e.g. for multi-lumen conduits, porous walls, or contact guidance. In previous subcutaneous biocompatibility studies, PXS implants were encased by thinner fibrous capsules and recruited less activated macrophages in vivo, as compared to polymers based on α -hydroxy acids [14]. Thus, PXS elastomers can potentially provide advantages of both natural and synthetic conduit materials for use in the clinical setting.

In this study, we investigated PXS as a potential nerve conduit material. In vitro attachment and proliferation of primary SCs was assessed as well as in vivo biocompatibility with rat peripheral nerve. PXS conduits were compared to commercially available PGA, as well as silicone conduits in rats with critical sized sciatic nerve defects.

2. Materials and Methods

2.1 Synthesis of PXS

All chemicals were purchased from Sigma-Aldrich unless otherwise stated. PXS elastomers were synthesized as previously reported [13]. Briefly, equimolar amounts of xylitol and sebacic acid were melted in a round bottomed flask at 150°C under a blanket of inert gas, and stirred for 1 h. Vacuum (~50 mTorr) was applied for 12 h, yielding the PXS 1:1 prepolymer. The PXS elastomer was then manufactured by further polycondensation (120°C, 140 mTorr for 4 days) in an aluminum mold to yield PXS conduits, or processed onto glass slides to yield 1.5 mm thick PXS films for in vivo biocompatibility analysis.

2.2 In vitro biocompatibility analysis

Glass Petri dishes (6 cm diameter, Fisher Scientific) contained 3 g of cured elastomers (120°C, 140 mTorr for 4 days). Petri dishes prepared with a 2% w/v PLGA (65/35, high M_w , Lakeshore Biomedical, Birmingham, AL, USA) solution in dichloromethane at 100 $\mu\text{L}/\text{cm}^2$ and subsequent solvent evaporation served as control. Substrates were washed with sterile PBS prior to sterilization.

Cultures of primary SCs were set up as previously described [15]. Briefly, dissected sciatic nerves from postnatal day 1 Sprague-Dawley rat pups (Charles River Laboratories,

Wilmington, MA) were collected in L-15 Leibovitz (Invitrogen). Nerves were transferred to L-15 containing 0.1% w/v collagenase (Invitrogen), incubated at 37 °C for 30 minutes, and disrupted by repetitive pipetting. The cells were washed once with L-15 containing 10% fetal calf serum (FCS) (Invitrogen), plated onto 10 cm Primaria™ dishes (Fisher Scientific) in Cb-medium [15]: DMEM (high glucose, pyruvate) media (Invitrogen), 10% FCS, 10 ng/ml 7S NGF, 100 µg/mL streptomycin (Invitrogen), and 100 U/mL penicillin (Invitrogen). The cells were incubated overnight at 37 °C and 5% CO₂. The next day, SCs were harvested using the 'cold jet' method [16] and plated onto Primaria™ dishes. SCs were expanded in DMEM containing 3% FCS, 10 µM Forskolin, 5 ng/mL neuregulin-1 and 1% pen/strep, harvested using Trypsin 0.025%/ EDTA 0.01% (Invitrogen), and used between passage three and ten. Cells were seeded (at 2.000 cells/cm²) in the biomaterial-laden or Primaria™ (5 cm diameter) dishes, without prior incubation of the polymers with growth media, and allowed to grow to confluency at 37 °C and 5% CO₂. SCs were imaged at 4 h and every subsequent day after initial seeding. Phase micrographs of cells were taken at 10x magnification using Axiovision software (Zeiss, Germany). For cell proliferation measurements, randomly picked areas were imaged and cells were counted, and averaged. The area and circularity [17] of cell populations were calculated manually using perimeter and area measurements by using Axiovision software (Zeiss, Germany). The circularity *C* was calculated using the following formula:

$$C = \frac{4\pi A}{P^2} \quad (1)$$

where *A* is the projected area of the cell and *P* is the perimeter of the cell. Circularity was used as an index of cell spreading. Three distinct cell populations (*n* = 80 total) were measured to find cell population means.

2.3 In vivo biocompatibility analysis

Two female Lewis rats (Charles River Laboratories, Wilmington, MA), weighing approximately 200 grams, had access to water and food *ad libitum*. Animals were cared for according to the protocols of the Committee on Animal Care of MIT in conformity with the NIH guidelines (NIH publication #85-23, revised 1985). The animals were anaesthetized using continuous 2% isoflurane/O₂ inhalation. Under sterile conditions and external body warming, the sciatic nerve on the left side was approached through a semitendinosus-

biceps femoris muscle splitting approach. The sciatic nerve was exposed and 1.5 x 2.0 x 20 mm PXS bars cut from PXS films were placed on top of the sciatic nerve. The muscle layer was then closed using 4-0 Vicryl sutures, and the skin was closed using staples. After 1 and 12 weeks, the rats were sacrificed and the muscle, nerve and PXS bar were resected en bloc and fixed in formalin-free fixative (Accustain). These specimens were embedded in paraffin after a series of dehydration steps in ethanol and xylene. Sequential sections (8-15 μ m) were stained with hematoxylin and eosine (H&E).

2.4 Peripheral nerve conduits and surgical procedure

PXS conduits with an internal diameter of 1.5 mm, an average outer diameter of 2.5 mm, and a length of 12 mm were retrieved from the aluminum mold and cut to size using a razor blade. Conduits of medical grade silicone (Cole-Palmer) with an internal diameter of 1.6 mm, an outer diameter of 3.6 mm, and a length of 12 mm were cut in a similar manner. PXS and silicone conduits were sterilized by repetitive washes with 70% ethanol and sterile PBS. One animal in a pilot experiment received a PXS conduit and was sacrificed 3 weeks after nerve reconstruction. The explant was cut in half, and prepared for scanning electron microscopy (SEM): it was sputter-coated with platinum/palladium (\approx 250Å), mounted on aluminum stub with carbon tape, and examined on a JEOL 5600LV. Commercially available PGA conduits (Neurotube™, Synovis Life Technologies Inc., Birmingham, AL) were trimmed to size during the nerve reconstruction procedure.

Twenty-four female Lewis rats participated in the experimental nerve reconstruction study. The animals were randomized into three experimental groups: 8 animals received PXS conduits, 8 animals received PGA conduits, and 8 animals received silicone conduits. The contralateral legs were used as unoperated controls. The animals were anaesthetized using continuous 2% isoflurane/O₂ inhalation. The sciatic nerve on the left side was exposed through a semitendinosus-biceps femoris muscle splitting approach and dissected free of surrounding connective tissue using an operating microscope (Nikon SM21000). A 10 mm segment of the nerve was resected, leaving a gap. Conduits were sutured in position using two 9-0 nylon sutures (Ethicon, Somerville, NJ), telescoping both nerve stumps 1 mm into the conduit. The muscle layer was then closed using 4-0 Vicryl sutures (Ethicon, Somerville, NJ), and the skin was closed using staples, which were removed 10 days post-operatively.

2.5 Assessment of peripheral nerve regeneration

Assessment of functional recovery was performed based on three experiments, i.e. electrophysiological recordings, wet muscle weights and histology. The electrophysiological

recordings were performed 12 weeks after surgery, as described previously [18]. Each animal was reanesthetized, and the coaptation site was exposed as described for the nerve reconstruction procedure. Isometric contractile force measurements were made *in situ* by a technique initially described by Zhao *et al.* [19]. In brief, the tibialis anterior muscle was identified, and the distal tendon of this muscle was then divided at its insertion, mobilized, and connected to a force transducer (Lutron, FG-5000A, McMaster Carr). The peak height force transducer signal was recorded. Electrical stimulation was performed at 10 mm proximal to the proximal coaptation site of the sciatic nerve. A stimulator (HP 6614C) was used to generate supramaximal stimuli (square wave impulses with a frequency of 100 Hz and duration of 0.6 msec). Four measurements of maximal isometric contraction force of the tibialis anterior muscle of all animals were measured with the force transducer. Similar measurements were made for the unoperated control side. The ratio of maximal output of experimental to the unoperated control side was recorded. Then, the tibialis anterior muscles were harvested from the experimental and the unoperated side and collected in sterile PBS. Wet muscle weights were measured and recorded as a ratio of the operated to the contralateral, unoperated side. After these measurements, the muscles as well as the nerves and conduits were prepared for histological analysis.

2.6 Histology and morphological analysis

The harvested tissues (muscle, nerves and conduits) were fixed in Accustain for 24 h, dehydrated as described above. Sequential sections of the muscles were stained with hematoxylin and eosin (H&E) to assess muscle fiber size. The area of cross-sectioned muscle fibers were calculated manually, similar to measurements of perimeter and area measurements of individual cells as described above. Masson's trichrome staining was applied to histological sections of the regenerating nerves, as well as Luxol Fast Blue staining [20]. For the latter staining, thinner sections were cut using a microtome (2 μm), and oil immersion microscopy was applied to obtain images. Random images of regenerating nerves under 100x magnification were taken and analyzed. Nerve cross-sectional area, as well as nerve fiber diameter distributions were manually measured from 4 random images per animal that demonstrated nerve regeneration, similar to measurements of perimeter and area measurements of individual cells as described above.

2.7 Statistical analysis

Two-tailed student's t-tests with unequal variances were performed to determine statistical significance (Microsoft Excel, Redmond, WA USA). Two-way ANOVA tests were performed

where appropriate (GraphPad Prism 4.02, GraphPad Software, San Diego, CA USA). Bonferroni multiple comparison post-tests were used to determine significance between specific treatments. All tabulated and graphical data is reported as mean \pm S.D. Significance levels were set at * $p < 0.05$, ** $p < 0.01$ and *** $p < 0.001$.

3. Results

3.1 In vitro Schwann cell attachment and proliferation

Attachment of SCs on PXS substrates was similar to PLGA dishes, as well as Primaria™ dishes (tissue culture treated polystyrene dishes), as shown in **Figure 1A**. After the initial attachment, SCs proliferated more readily on PXS and Primaria™ dishes, as compared to PLGA dishes. After 4 d, SCs on Primaria™ dishes had proliferated into a confluent monolayer. At this time, significantly less SCs per area were present on PLGA coated dishes than on Primaria™ dishes (** $p < 0.01$). Cell numbers on PLGA and PXS dishes however, as well as PXS and Primaria™ dishes, were never statistically significant at all time points. Representative phase contrast images of SCs on the different culture substrates are shown in **Figure 1B**. Cell morphology analysis demonstrated that cell area (**Figure 1C**) and circularity (**Figure 1D**) of SCs on the three different polymer substrates were not statistically significant ($p > 0.05$).

3.2 In vivo PXS implants: degradation and tissue response

Implantation of PXS bars revealed no evident inflammation after 7 d at the site of the sciatic nerve as determined by histology (**Figure 2AB**). There was no infiltration of polymorphonuclear neutrophils, lymphocytes or other inflammatory cells in the surrounding muscle or nerve tissue. A thin tissue capsule seemingly composed of macrophages and fibroblasts of at most 10 cell layers thick surrounded the PXS implant at this time. During degradation of the PXS polymer at 40 d a similar response was observed compared to the 7 d time point (**Figure 2CD**). Although the fibrous capsule was slightly thicker and appeared to contain more macrophages, no infiltration of inflammatory cells in surrounding tissues was observed. After the acute and chronic inflammatory response of the tissues surrounding the PXS implants, there were no notable accumulations of inflammatory cells that would indicate an adverse reaction to PXS. No capillaries and blood vessels were found dispersed through the thin tissue capsules surrounding the PXS implants. Interestingly, the PXS polymer appeared to degrade lower rate than was expected based on previous experiments with subcutaneously PXS polymers [14]. PXS conduits with rectangular prism geometry and

cylindrical lumen were created using an aluminum mold (**Figure 3A**). A PXS implant was evaluated, bridging a 1 cm peripheral nerve gap in the rat sciatic nerve. 9-0 Nylon sutures smoothly cut through the soft elastomer and easily held and telescoped the nerve stumps into the 12 mm long conduit lumen. Upon implantation, the optically transparent conduit degraded and gradually transformed into a rounded, brown-yellowish colored conduit (**Figure 3B**). At 21 d, the implant demonstrated sufficient structural integrity and form stability as a peripheral nerve conduit. A tissue bridge was observed mid-graft of this PXS conduit, as demonstrated by SEM imaging of the conduit lumen (**Figure 3C**). The interior of the lumen did not appear to degrade in a similar fashion compared to the outside of the conduit and seemed to degrade slower.

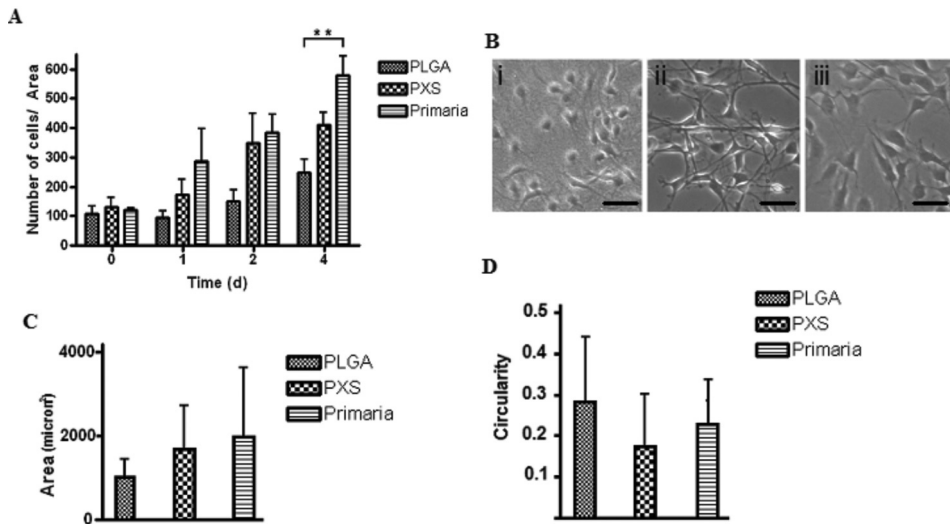


Figure 1. (A) The attachment and subsequent proliferation of primary rat SCs on PLGA, PXS and Primaria™ dishes (* $p < 0.01$) (B) Representative phase contrast images of SCs attached after 2 d culture in (i) PLGA, (ii) PXS and (iii) Primaria™ dishes. Bars represent 100 μm . (C) The cell area (A) of SCs in μm^2 after 24 h of cell culture on PLGA, PXS and Primaria™ dishes (means were not significantly different). (D) Circularity (C) of SCs after 24 h of cell culture on PLGA, PXS and Primaria™ dishes (means were not significantly different).

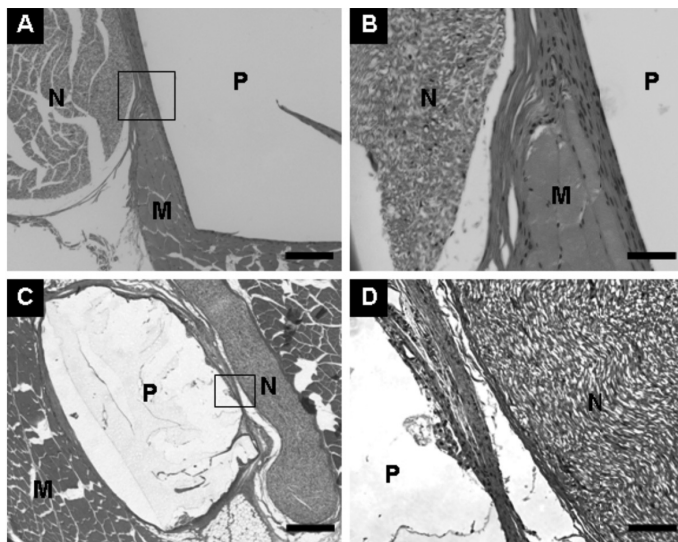


Figure 2. Representative photomicrographs of H&E sections of the in vivo inflammatory response to PXS bars implanted intramuscularly at the site of the right sciatic nerve. (A) 10x magnification of the sciatic nerve and surrounding tissues after 7 d. Bar represents 150 μm . (B) 40x magnification of the outlined area in (A). Bar represents 40 μm . (C) 2.5x magnification of the sciatic nerve and surrounding tissue after 40 d implantation. Bar represents 600 μm . (D) 20x magnification of the outlined area in (C). Bar represents 75 μm . P = PXS polymer, M = muscle, N = nerve.

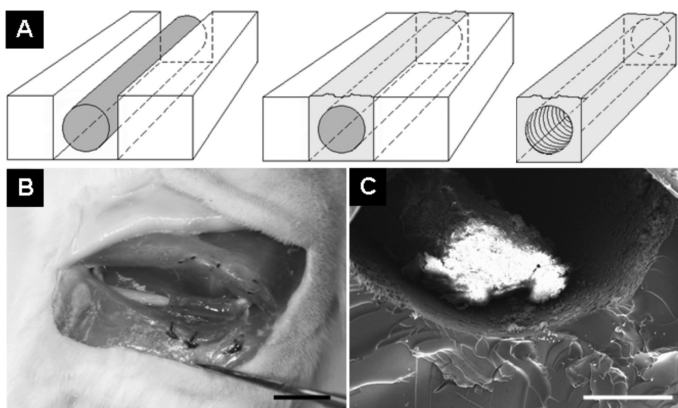


Figure 3. (A) PXS nerve conduits were produced by pouring the PXS pre-polymer (yellow) into the aluminum mold with a stainless steel rod (grey) with 1 mm diameter. The pre-polymer was thermally cured and removed from the mold. (B) A PXS conduit was used to reconstruct a sciatic nerve defect of 1 cm. Image taken after 3 weeks of implantation. Bar represents 1.2 cm. (C) SEM micrograph taken mid-graft of inner lumen of an explanted PXS conduit after 21 d in vivo. Bar represents 250 μm .

3.3 PXS conduits in experimental nerve reconstruction

Microscopic examination after dissection of the reconstructed sciatic nerves at 60 d revealed that most of the sciatic nerves had regenerated, in all three experimental groups (4 rats in the PGA group (50%), 5 in the PXS group (63%), and 8 in the silicone group (100%)). Representative Masson's trichrome stained sections of responsive rats, taken midgraft, are shown in **Figure 4**. The sections revealed infiltration of lymphocytes, fibroblasts and macrophages within the woven walls of the PGA conduits (**Figure 4A**). Upon explantation, PGA conduits were macroscopically still intact, as were the silicone conduits. However, the PGA conduits seemed to have lost mechanical stability after 60 d in vivo. The PGA conduit's diameter had shrunk (2.3 mm upon implantation) and had collapsed onto the regenerating tissue cable. The regenerating tissue in the middle of the conduits in the PGA treatment group displayed the presence of significant numbers of fibroblasts and intrafascicular collagen (**Figure 4B**). The PXS conduits however, seemed to have degraded much faster, as it was difficult to recognize the conduit macroscopically in some rats. Also, the 3 unresponsive rats from the PXS group revealed distal sutures that were disconnected from the conduit. Microscopically, it appeared that the transverse regenerative nerve area in the PXS treated rats were smaller than that of the PGA and silicone groups (**Figure 4C**) although intrafascicular collagen seemed much less compared to PGA and silicone treated rats (**Figure 4D**). Regenerative cables were visible in all silicone tubes, and these were microscopically surrounded by a collagenous fibrous capsule (**Figure 4E, F**). The transverse regenerative nerve area was quantified and plotted in **Figure 5A**. PXS showed the smallest area of regeneration, significantly smaller than PGA and silicone conduit treated rats (** $p < 0.001$ for both PGA and silicone). Regenerative area of PGA conduits was not significantly larger than that of silicone conduits ($p > 0.05$). Although regenerative area of PGA conduits was the largest of the three groups, it demonstrated the least amount of regenerative fibers per area (69.4 ± 35.4) as demonstrated in **Figure 5B**. PXS conduits demonstrated the most fibers per area (160.0 ± 57.8), followed by the silicone treated group (127.8 ± 30.8). PXS and silicone treated groups were not significantly different ($p > 0.05$), but were so compared to the PGA treated group (both groups ** $p < 0.01$ compared to PGA).

To examine these regenerative fibers, light micrographs of mid-graft Luxol Fast Blue stained sections were taken and the corresponding myelin fiber diameter distributions were plotted. Across the PGA, PXS and silicone treated groups (**Figure 6A-C**), the distribution of fiber sizes was statistically similar ($p > 0.05$; **Figure 7**). Rats treated with PXS conduits were the only group with few regenerative fibers in the 6.0-7.0 μm section.

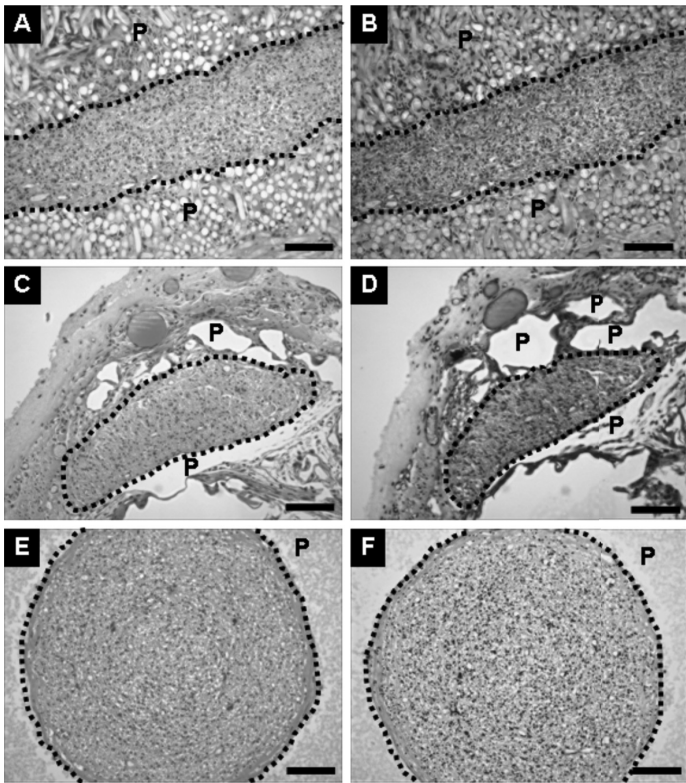


Figure 4. Representative photomicrographs of sections, taken mid-graft after 12 weeks for three peripheral nerve conduits. H&E sections taken from a sciatic nerve reconstructed with PGA conduits (A), PXS conduits (C) and silicone conduits (E). MT sections taken from a sciatic nerve reconstructed with PXS conduits (D), PGA conduits (F) and silicone conduits (F). Images are shown at 20x magnification Bars represent 25 μm . P = polymer. Dashed line indicates the area of regeneration within conduits.

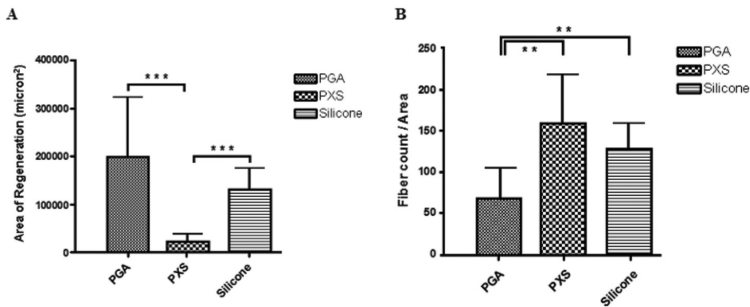


Figure 5. (A) Area of regeneration in μm^2 for PGA, PXS and silicone conduits after 12 weeks. (B) Average regenerative fiber counts per area for PGA, PXA and silicone conduit after 12 weeks. Average \pm SD (** p < 0.01, *** p < 0.001).

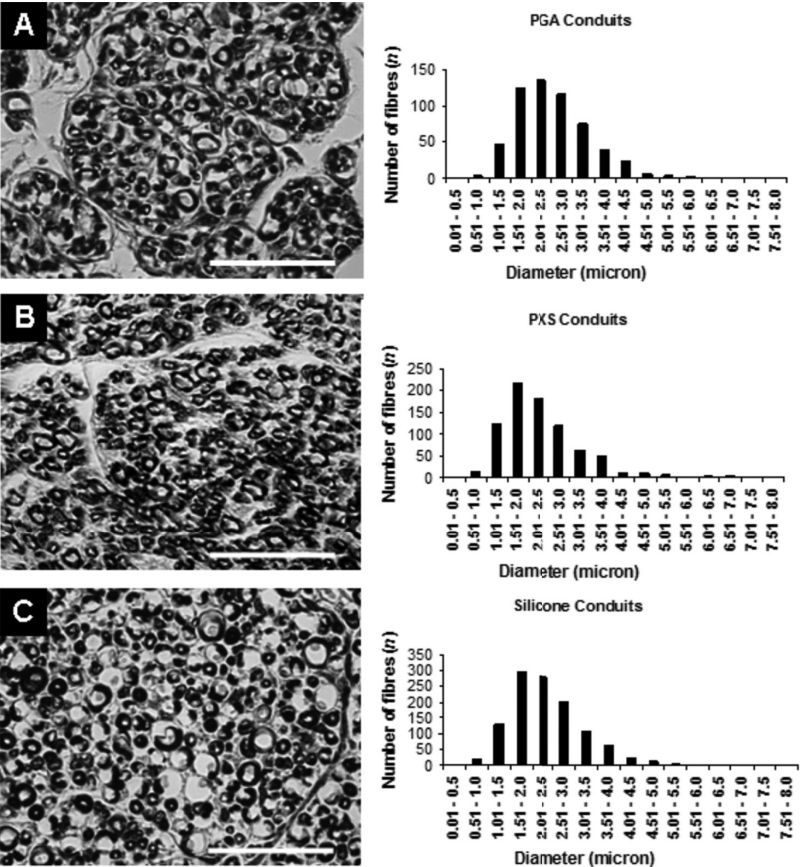


Figure 6. Representative light micrographs of mid-graft Fast Tuxol Blue stained sections and myelin fiber diameter distributions for PGA (A), PXS (B) and silicone conduits (C). Images are shown at 100x magnification. Bars represent 12 μ m.

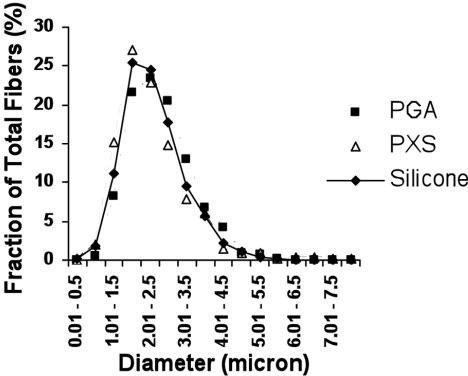


Figure 7. Myelin fiber diameter distribution for three different conduits expressed as fraction of total number of regenerating fibers stained midgraft.

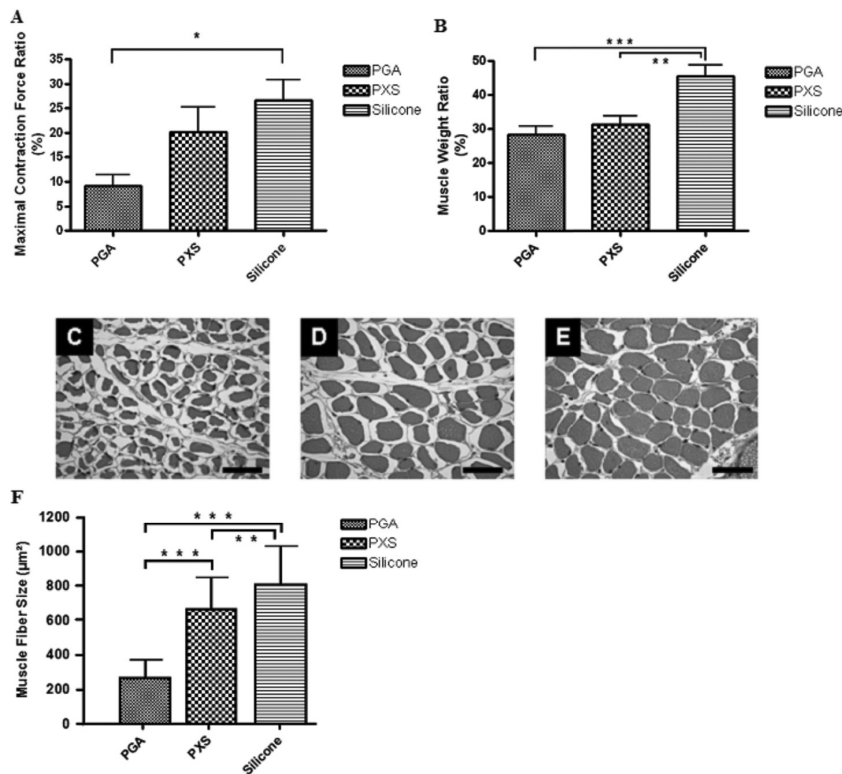


Figure 8. Target anterior tibial muscle characteristics. **(A)** Maximum contraction force, expressed as ratio of the unoperated, healthy side. Average \pm SD. (* $p < 0.05$) **(B)** Wet muscle weight ratios. Average \pm SD. (** $p < 0.01$, *** $p < 0.001$) Representative H&E sections of target anterior tibial muscles of sciatic nerves reconstructed with PGA **(C)**, PXS **(D)**, or silicone conduits **(E)**. Images shown are 40x magnified. Inserts are 20x. Bars represent 40 μ m. **(F)** Muscle fiber size of H&E sections taken mid-muscle, in μ m². Average \pm SD. (* $p < 0.001$, ** $p < 0.01$ *** $p < 0.001$).

Denervation of a target muscle occurs as a consequence of motor nerve injury, and the extent of this denervation process after 60 d can be evaluated by maximal contraction force (**Figure 8A**) and wet muscle weight (**Figure 8B**), both expressed as ratio of the unoperated, healthy side. Rats treated with PGA conduits had the least reinnervation of the anterior tibial muscle, and silicone the highest as measured by in vivo maximum contraction force (* $p < 0.05$). Rats with PXS conduits exhibited comparable contraction forces to PGA or silicone treated rats ($p > 0.05$). Wet muscle weight ratios also revealed that PGA and PXS conduits failed to reinnervate muscle at the level silicone conduits did (*** $p < 0.001$, ** $p < 0.01$ respectively). PXS conduits revealed comparable wet muscle

weight ratios to the PGA conduits ($p > 0.05$) (**Figure 8B**). Representative H&E sections of the anterior tibial muscles (**Figure 8C-E**) however, revealed a trend that was quantified in **Figure 8F**: PGA treated sciatic nerves had significant smaller transverse muscle fiber area, than PXS ($*** p < 0.001$) and silicone ($*** p < 0.001$) treated sciatic nerves. Sciatic nerves reconstructed with silicone conduits revealed transverse muscle fiber areas that were significantly greater than for the PXS conduit treated rats ($** p < 0.01$).

4. Discussion

PXS substrates supported the attachment and rapid proliferation of primary rat SCs. This behavior, as well as cell morphology, was comparable to SCs cultured on Primaria™ coated polystyrene substrates, without pre-coating or grafting cell-adhesion promoting entities to the PXS polymer (**Figure 1**). This is a clinically relevant property of PXS, because it allows the engraftment of viable SCs without loss of proliferation capability [21]. The in vivo biocompatibility was previously demonstrated for PXS elastomers in subcutaneous tissues and compared to PLGA [13,14]. The biocompatibility of PXS implants may depend upon the location of the implant and the surrounding biological environment, as previously shown for other materials [22]. We observed that PXS elastomers elicited a benign in vivo foreign body response when PXS elastomers were placed adjacent to the sciatic nerve. Inflammation of the sciatic nerve and surrounding muscle tissues could not be detected in the acute and chronic inflammatory response to foreign materials. Degradation of PXS did not trigger cellular infiltration in surrounding tissues as well (**Figure 2**). This in vivo behavior implies that PXS polymers are biocompatible with peripheral nerve tissue and the subsequent cellular components.

Furthermore, in this initial study in an experimental model for nerve reconstruction, PXS elastomers showed potential as nerve conduit material, as compared to commercially available PGA conduits. Although the area of the regenerating tissue cable through the conduit was the largest for PGA conduits, and the smallest for PXS conduits (**Figure 5**), this did not negatively influence the morphology of the regenerating nerve fibers (**Figure 6 and 7**), nor the regenerative capacity as indicated by maximal contraction force ratio, wet muscle weight ratio, as well as muscle fiber size (**Figure 8**). This discrepancy may be due to less collagen deposition within the regenerative tissue cable (i.e. less endoneurial scar formation), as shown in representative mid-graft sections (**Figure 4, 5B**). We hypothesize that the increased collagen deposition in the PGA treated group may be an effect of local

acidosis by the degradation products of PGA, as previously reported [12]. Macroscopically, PGA and PXS conduits revealed loss of entubulation after 12 weeks, which is known to have a negative effect on regeneration [10]: degrading PGA conduits had lost all mechanical stability and had collapsed onto the regenerating tissue cable (**Figure 4**). PXS conduits had opened up longitudinally along the thinnest conduit walls, most likely too early in the regeneration process (**Figure 3**). This may explain why silicone conduits showed greater regenerative capacity than the two degradable conduits in this relatively short term study.

Thermoset elastomers comparable to PXS (e.g. PGS [23, 24] and poly(diols citrate)s [25]) have not yet been studied in in vivo applications such as peripheral nerve conduits. By adjusting the stoichiometric ratio of xylitol and sebacic acid in the polycondensation reaction to produce PXS elastomers, degradation rates can be tuned as demonstrated in a subcutaneous setting: PXS 1:1 is the fastest degrading material (in vivo lifetime of 7-8 weeks), and PXS 1:2 the slowest degrading elastomer (in vivo lifetime of > 2 years) [13, 14]. As the degradation rate of intramuscularly placed PXS elastomers seemed slower than subcutaneously placed elastomers, and to have a baseline for tunable PXS elastomers in terms of regeneration over a critical gap length in rats, we chose PXS 1:1 as a starting material for this in vivo nerve reconstruction study. Although the PXS 1:1 formulation was chosen for this study, it was hypothesized that the PXS 1:1 conduits may have degraded too rapidly for the study design presented here.

Historically, the inert silicone elastomer tube proved to be an ideal biomaterial to study the nerve regeneration processes in detail [26-28], but was left in clinical practice as clinicians soon found that the non-degradable silicone elastomers caused a chronic inflammatory (foreign body) response, damaging the regenerated nerve, eventually leading to disappointing clinical outcomes [29]. This is unfortunate, as one year post-operative results demonstrated in a prospective, randomized clinical study by Lundborg *et al.* in 1997 showed promising results for silicone tubular repair [30]. Their study data demonstrated no significant differences between the tubular repair group and the conventional reconstructive procedures for median and ulnar nerve lesions in a total of 18 human forearms. In 2001, Lundborg and co-workers showed long term results of the silicone tubes implanted in the 11 cases described in their 1997 study. Seven patients were re-explored because of local discomfort from the tube 12-44 (median 22) months after the initial procedure, and found in only two cases a mild foreign body reaction [31]. In a recent review by Meek and Coert [9], advantages and shortcomings of conduits used in clinical practice were compared taking literature, material properties, availability of convenient sizes and economical considerations into account, and advised to utilize PGA conduits. In

addition, in 2000, Weber *et al.* published a randomized prospective study on the use of PGA conduits for digital nerve repair. They observed that tubular nerve repair using PGA tubes, compared to conventional end-to-end repair and nerve grafting, demonstrated improved sensation determined by two-point discrimination studies up to 1 year post-operatively [32]. Compared to PGA, PXS conduits, despite our hypothesized suboptimal degradation rate as well as conduit configuration, seemed promising. However, more research is warranted to obtain PXS conduits with clinically relevant improvements over silicone conduits, and eventually, autologous nerve grafting.

5. Conclusions

Biodegradable PXS elastomers enabled the attachment and subsequent proliferation of primary rat SCs, and demonstrated biocompatibility with rat sciatic nerve tissue *in vivo*. Furthermore, PXS conduits allowed for peripheral nerve regeneration over a critical size nerve gap in an experimental rat model. The PXS formulation of the conduits studied herein (PXS 1:1) revealed similar outcomes to PGA nerve conduits, but not silicone conduits. As the PXS 1:1 formulation is the fastest degrading PXS elastomer, room exists to optimize PXS elastomers for this specific application.

6. References

1. Madison RM, Archibald SJ, Krarup C. Peripheral nerve injury. Philadelphia: W. B. Saunders, 1992.
2. Chamberlain LJ, Yannas IV, Hsu H-P, Strichartz G, Spector M. Collagen-GAG Substrate Enhances the Quality of Nerve Regeneration through Collagen Tubes up to Level of Autograft. *Exp Neurol* 1998;154:315–329.
3. Dahlin LB, Lundborg G. Use of tubes in peripheral nerve repair. *Neurosurg Clin N Am* 2001;12(2):341–352.
4. Den Dunnen WFA, Stokroos I, Schakernraad JM, Zondervan GJ, Pennings AJ, Van der Lei B, *et al.* A New PLLA/PCL Copolymer for Nerve Regeneration. *J Mater Sci Mater Med* 1993;4:521–525.
5. Harley BA, Spilker MH, Wu JW, Asano K, Hsu HP, Spector M, *et al.* Optimal degradation rate for collagen chambers used for regeneration of peripheral nerves over long gaps. *Cells Tissues Organs* 2004;176(1-3):153–165.
6. Hoppen HJ, Leenslag JW, Pennings AJ, Van der Lei B, Robinson PH. Two-ply biodegradable nerve guide: basic aspects of design, construction and biological performance. *Biomaterials* 1990;1990(11):286–290.
7. Mackinnon SE, Dellon AL. Clinical Nerve Reconstruction with a Bioabsorbable Poly(glycolic acid) Tube. *Plast Reconstr Surg* 1990;85:419–424.

8. Pêgo AP, Poot AA, Grijpma DW, Feijen J. Copolymers of trimethylene carbonate and ϵ caprolactone for porous nerve guides: Synthesis and properties. *J Biomater Sci Polymer Edn* 2001;12(1):35-53.
9. Meek MF, Coert JH. US Food and Drug Administration/Conformit Europe-Approved Absorbable Nerve Conduits for Clinical Repair of Peripheral and Cranial Nerves. *Ann Plast Surg* 2008;60:110-116.
10. Yannas IV. Tissue and organ regeneration in adults. New York: Springer-Verlag, 2001.
11. Ellingsworth LR, DeLustro F, Brennan JE, Sawamura S, McPherson J. The human immune response to reconstituted bovine collagen. *J Immunol* 1986;136(3):877-882.
12. Gibson KL, Remson L, Smith A, Satterlee N, Strain GM, Daniloff JK. Comparison of nerve regeneration through different types of neural prostheses. *Microsurg* 1991;12:80-85.
13. Bruggeman JP, Bettinger CJ, Nijst CLE, Kohane DS, Langer R. Biodegradable xylitol-based polymers. *Adv Mater* 2008;20(10):1922-7.
14. Bruggeman JP, Bettinger CJ, Langer R. Biodegradable xylitol-based elastomers: in vivo behavior and biocompatibility. *J Biomed Mater Res A* 2010;95(1):92-104.
15. Mandemakers W, Zwart R, Jaegle M, Walbeehm E, Visser P, Grosveld F, *et al.* A distal Schwann cell-specific enhancer mediates axonal regulation of the Oct-6 transcript factor during peripheral nerve development and regeneration. *EMBO* 2000;19(12):2992-3003.
16. Jirsova K, Sodaar P, Mandys V, Bar PR. Cold jet: a method to obtain pure Schwann cell cultures without the need for cytotoxic, apoptosis-inducing drug treatment. *J Neurosci Methods* 1997;78:133-137.
17. Thurston G, Jaggi B, Palcic B. Measurement of cell motility and morphology with an automated microscope system. *Cytometry* 1988;9(5):411-417.
18. Waitayawinyu T, Parisi DM, Miller B, Shai Luria S, Morton HJ, Chin SH, *et al.* A comparison of polyglycolic acid versus type 1 collagen bioabsorbable nerve conduits in a rat model: an alternative to autografting. *J Hand Surg [Am]* 2007;32A:1521-1529.
19. Zhao Q, Dahlin LB, Kanje M, Lundborg G. Specificity of muscle reinnervation following repair of the transected sciatic nerve. A comparative study of different repair techniques in the rat. *J Hand Surg* 1992;17B:257-261.
20. Song C, Zhang F, Zhang J, Mustain WC, B. CM, Chen T, *et al.* Neuroma-in-continuity model in rabbits. *Ann Plast Surg* 2006;57(3):317-322.
21. Guenard V, Kleitman N, Morrissey TK, Bunge RP, Aebischer P. Syngeneic schwann cells derived from adult nerves seeded in semipermeable guidance channels enhance peripheral nerve regeneration. *J Neurosci* 1992;12:3310-3320.
22. Kohane DS, Tse JY, Yeo Y, Padera R, Shubina M, Langer R. Biodegradable polymeric microspheres and nanospheres for drug delivery in the peritoneum. *J Biomed Mater Res Part A* 2006;77:351-361.
23. Sundback CA, Shyu JY, Wang Y, Faquin WC, Langer RS, Vacanti JP, *et al.* Biocompatibility analysis of poly(glycerol sebacate) as a nerve guide material. *Biomaterials* 2005;26(27):5454-5464.
24. Wang Y, Ameer GA, Sheppard BJ, Langer R. A tough biodegradable elastomer. *Nature biotechnology* 2002 Jun;20(6):602-606.
25. Yang J, Webb AR, Pickerill SJ, Hageman G, Ameer GA. Synthesis and evaluation of poly(diols citrate) biodegradable elastomers. *Biomaterials* 2006;27(9):1889-1898.
26. Aebischer P, Guenard V, Brace S. Peripheral-nerve regeneration through blind-ended semipermeable guidance channels - effect of the molecular-weight cutoff. *J Neurosci* 1989;9:3590-3595.
27. Aebischer P, Guenard V, Winn SR, Valentini RF, Galletti PM. Blind-ended semipermeable guidance channels support peripheral- nerve regeneration in the absence of a distal nerve stump. *Brain Res* 1988;454:179-187.

28. Longo FM, Skaper SD, Manthorpe M, Williams LR, Lundborg G, Varon S. Temporal changes of neuronotrophic activities accumulating in vivo within nerve regeneration chambers. *Exp Neurol* 1983 81(3):756-769.
29. Merle M, Dellon AL, Campbell JN, Chang PS. Complications from silicon-polymer intubulation of nerves. *Microsurgery* 1989;10(2):130-133.
30. Lundborg G, Rosén B, Dahlin L, Danielsen N, Holmberg J. Tubular versus conventional repair of median and ulnar nerves in the human forearm: early results from a prospective, randomized, clinical study. *J Hand Surg Am* 1997;22(1):99-106.
31. Dahlin LB, Anagnostaki L, Lundborg G. Tissue response to silicone tubes used to repair human median and ulnar nerves. *Scand J Plast Reconstr Surg Hand Surg* 2001;35(1):29-34.
32. Weber RA, Breidenbach WC, Brown RE, Jabaley ME, Mass DP. A randomized prospective study of polyglycolic acid conduits for digital nerve reconstruction in humans. *Plast Reconstr Surg* 2000;106(5):1036-1048.

Chapter 8

Biodegradable nanotopographic poly(xylitol sebacate) elastomers for peripheral nerve regeneration

Joost P. Bruggeman, Christopher J. Bettinger, Berend-Jan de Bruin, Alex Alford,
Jeffrey T. Borenstein, Robert Langer

Abstract

Conduits containing aligned Schwann cells (SC) have shown to be beneficial to the regeneration process, but aligned SCs are not always readily available. Substrate nanotopography is known to induce highly specific cellular responses in the absence of soluble factors including alignment and elongation in the case of ridge-groove structures. In this study, we developed flexible, biodegradable poly(xylitol sebacate) (PXS) substrates with submicron-scale ridge-groove features for in vitro and in vivo contact guidance applications, such as peripheral nerve reconstruction. We studied the in vitro alignment and migration velocity of primary rat SCs on patterned PXS films, as well as the effect on nerve regeneration in vitro using dorsal root ganglia (DRG). Also, the in vivo contact guidance was investigated, suturing a patterned PXS film into a sciatic nerve defect in a rat. Patterned PXS elastomers showed promising contact guidance properties in vitro as well as in vivo.

1. Introduction

Autologous nerve grafts remain the superior therapeutic option for regeneration over critical sized peripheral nerve defects. Following injury of peripheral nerves, Wallerian degeneration is triggered, indicating that axons distal to the lesion degenerate and are being phagocytosed. Re-establishment of continuity of the severed nerve stumps occurs by dissociation of Schwann cells (SC) with their axons, proliferation and migration of SCs, bridging the gap of the severed nerve. Fibroblasts and SCs form a bridge between the nerve ends, guiding the elongation of the severed axons towards the distal target organ. Although inferior compared to autologous nerve grafting, nerve conduits possess several important advantages: nerve grafting requires the sacrifice of a healthy nerve that oftentimes displays a donor-acceptor diameter mismatch and unfortunately, does not guarantee optimal functional outcome. Other important advantages of conduits are the prevention of donor-site morbidity (loss of sensation, neuroma formation, infection), reduction of operation time, and the ability to repair nerve lesions in anatomic locations that are difficult to reach.

Similar to nerve grafts, conduits give directional guidance to migrating SCs and elongating axons, offer a controllable regenerative environment as well as protection from potentially impeding scar tissue formation. However, the aligned basement membranes and aligned SC populations present in autologous nerve grafts are thought to be valuable advantages over artificial, empty nerve conduits. We know that conduits containing aligned SCs are beneficial to the regeneration process [1], although populations of autologous aligned SCs are typically not available at the time of nerve injury [2].

Substrate topographies on biomaterials induce highly specific cellular responses in the absence of soluble factors [3-5]. Therefore, contact guidance cues within the conduit may induce alignment of migrating SCs during regeneration. This seems a straightforward step towards the improvement of an empty conduit's nerve regeneration stimulating potential, mimicking topographic cues that are present within natural basement membranes of nerve grafts. In addition, enhancing SC motility has also been acknowledged as a prerequisite for increased myelination during regeneration after injury, resulting in superior nerve maturation and less muscle atrophy [6]. Thus, conduits that align, as well as stimulate SCs to migrate faster, may improve nerve regeneration.

Studies published to date that aim to control axon guidance by topographical cues on macro- [7] and micronscale resolution [8-11], have either utilized polymers that were non-biodegradable (polystyrene), or based on α -polyhydroxy acids such as glycolic- and lactic acid. Although biodegradable, the latter group of materials exhibit suboptimal properties for small feature applications within peripheral nerve conduits, such as rigid

mechanical properties, bulk degradation kinetics, and questionable biocompatibility, resulting in increased intra-fascicular scarring in some cases. Poly(xylitol sebacate) (PXS) is a recently synthesized biodegradable elastomer and may be a good candidate material for axon guidance within conduits. PXS 1) is very flexible, 2) is a surface eroding polymer, demonstrating insignificant swelling upon degradation, 3) has tunable in vivo half lives, and 4) exhibits improved biocompatibility and form stability compared to poly(lactic-co-glycolic acid) (PLGA) upon degradation in vivo.

In this study, we developed flexible, biodegradable substrates with submicron-scale features for in vitro and in vivo contact guidance applications. Using replica-molding, we created grooves with periodicity on a micron scale, as previously described [5]. In vitro, patterned PXS elastomers showed that SCs were readily aligned as well as dorsal root ganglia (DRG), and demonstrated increased migration velocity of SCs compared with flat PXS surfaces. In addition, patterned PXS bars were sewn into rat a sciatic nerve defect and displayed contact guidance.

2. Materials and Methods

2.1 Microfabrication of silicon masters

Traditional photolithographic techniques were used to fabricate silicon masters with line-grating geometries with target dimensions of 1200 \pm 200 nm periodicity (600 nm ridges with 600 nm spacing) and 600 \pm 150 nm feature height (MEMS Exchange, Reston, VA). Briefly, 100 mm silicon wafers were coated with Shipley SPR220-3 photoresist, exposed using a GCA AS200 stepper, and post-baked. Wafers were etched using a silicon ICP etch process using SF₆/Argon in a VLR-700. Silicon wafers were then plasma ashed and cleaned for preparation in replica-molding. Silicon masters were used to replica-mold substrates with linear nanotopographic features using both poly(dimethylsiloxane) (PDMS) and poly(xylitol sebacate) (PXS).

2.2 Synthesis and replica molding of PXS

All chemicals were purchased from Sigma-Aldrich unless otherwise stated. PXS pre-polymer was synthesized using previously established methods [12, 13]. Briefly, xylitol and sebacic acid (stoichiometric ratio 2:3) were melted in a round bottomed flask at 150°C under a blanket of inert gas, and stirred for 1 h. Vacuum (~50 mTorr) was applied for 6 h, yielding the pre-polymer. The pre-polymer was allowed to cool and stored at room temperature in a

desiccate environment until further use. 3.5 ± 0.7 g of PXS pre-polymer was melted at 100 °C and applied to the wafers for replica molding and smooth sheet formation. The polymer was then further cured at 120°C and 20 mTorr for 4 d which produced firm, elastomeric PXS layers of approximately 500 µm in thickness. The PXS substrate was statically incubated in a ddH₂O bath at 90°C for 24 h to induce delamination. The substrates were then rinsed three times with PBS, and sterilized using UV for 1 h in a laminar flow hood. The substrates were incubated with medium at 37 °C for 0.5 h prior to cell deposition. Dehydrated PXS substrates were imaged by SEM by undergoing a dehydration bake at 70°C for 15 h followed by sputter coating with gold/palladium using a Cressington 108 Auto sputter coater for 36 sec. This process deposited a 30-45 nm thick conductive film to eliminate charging of the sample (Cressington Scientific Instruments Inc, Cranberry Twp, PA USA).

2.3 Isolation, culture and imaging of primary Schwann Cells (SCs) and primary Dorsal Root Ganglia (DRG)

Cultures of primary SCs were set up as previously described [14]. Dissected nerves from postnatal day 1 Sprague-Dawley rat pups (Charles River Laboratories, Wilmington, MA) were collected in L-15 Leibovitz (Invitrogen, Carlsbad, CA). Nerves were transferred to L-15 containing 0.1% w/v collagenase (Invitrogen), incubated at 37 °C for 30 minutes, and disrupted by repetitive pipetting. The cells were washed once with L-15 containing 10% fetal calf serum (FCS) (Invitrogen), plated onto 10 cm Primaria™ dishes (Fisher Scientific) in Cb-medium [14]: DMEM (high glucose, pyruvate) media (Invitrogen), 10% FCS, 10 ng/ml 7S NGF, 100 µg/mL streptomycin (Invitrogen), and 100 U/mL penicillin (Invitrogen). The cells were incubated overnight at 37 °C and 5% CO₂. The next day, SCs were harvested using the 'cold jet' method [15] and plated into Primaria™ dishes. SCs were expanded in DMEM containing 3% FCS, 10 µM Forskolin, 5 ng/mL neuregulin-1 and 1% pen/strep, harvested using Trypsin 0.025%/ EDTA 0.01% (Invitrogen), and used between passage three and ten. Cells were seeded (at 2,000 cells/cm²) in the PXS-laden dishes at 37 °C and 5% CO₂. SCs were imaged after 4 h for the alignment and subsequently time-laps images were taken every 3 min after initial seeding for the migration assay. The transparent PXS substrates allow for the direct measurement of cell alignment angle using an optical microscope (Zeiss, Germany). Phase micrographs of cells were taken at 10x magnification and relative angle of the cell to the feature was calculated using Axiovision software (Zeiss, Germany). Each data set consists of measurements of at least 200 cells across three different experiments. Cell migration was quantified by manually tracking the spatial coordinates about the nucleus

of 100 migrating cells using AxioVision software. Average migration velocity V_{mig} was calculated by the following equation:

$$V_{mig} = \frac{\sum_{i=1}^n \sqrt{(x_i - x_{i-1})^2 + (y_i - y_{i-1})^2}}{\sum_{i=1}^n t_i} \quad (1)$$

Dorsal root ganglion (DRG) neurons were derived from postnatal day 1 Sprague-Dawley rats, similar as previously described [16]. Individual ganglia were removed from the spinal column, nerve roots stripped, and the ganglia placed in trypsin/collagenase digest solution (0.25%/0.33%) for 30 min. The tissue was triturated and the resulting cell suspension was washed in culture media, and placed in DMEM (high glucose, pyruvate) media, 10% FCS, 100 µg/mL streptomycin, and 100 U/mL penicillin (Invitrogen). When needed, DRG cultures were subjected to cycle of anti-mitotic treatment to decrease the number of fibroblasts in the culture. The anti-mitotic treatment consisted of a two day cycle of cytosine arabinoside at 10 µM supplemented in the culture media.

Two-tailed student's t-tests with unequal variances were performed to determine statistical significance (Microsoft Excel, Redmond, WA USA). Significance levels were set at $p < 0.05$.

2.4 Staining for S-100 and tubulin

Studies involving fluorescent staining procedures were performed on cells cultured collagen-coated PDMS patterned surfaces with similar periodicity to PXS patterned substrates, as PXS elastomers demonstrated an impeding autofluorescence. The cells or DRGs were fixed in 4% paraformaldehyde in PBS for 20 min, washed 3 times in PBS and then permeabilized in 0.1% Triton X in PBS. The cells were incubated with PBS/ 3% bovine serum albumin (BSA) for 10 min. The primary rabbit antineuronal class III β -tubulin (Covance) antibody was diluted in PBS (1:250) with 5% goat serum for 1 h. The cells were rinsed three times for 10 min each in PBS and then the secondary antibody, Alexafluor 488 goat anti-rabbit IgG (Molecular Probes) was added (1:500) and incubated for 1 hour. Then the cells were rinsed three times for 5 min with PBS/ 3% BSA. Then, the primary rabbit anti-S100 antibody (Dako) was added for 1 hr (1:400). Subsequent washes were done with PBS/ 1% BSA followed by TRITC-labeled swine anti-rabbit antibody (Dako) for 30 min. Two washes with PBS and one

wash with DAPI stain was done. After thorough rinsing in PBS, the samples were imaged. All washes and stains were performed at room temperature.

2.5 Scanning Electron Microscopy (SEM)

SEM images were taken after polymer films and culture substrates were washed three times in PBS and fixed with 4% (v/v) paraformaldehyde in PBS. After being rinsed with PBS buffer three times, the dishes were dehydrated in graded alcohols (50%, 70%, 80%, 90%, 95%, and 100%) and then air-dried in HMDS. The samples were then sputter-coated with platinum and examined on a JEOL JSM5910 scanning electron microscope.

2.6 In vivo contact guidance

A promising application of contact guidance is peripheral nerve reconstruction with artificial, patterned conduits. To this end, PXS implants were sutured between a 10 mm sciatic nerve gap with a patterned or smooth side facing the nerve stumps in vivo. Two female Lewis rats (Charles River Laboratories, Wilmington, MA), weighing approximately 200 g, had access to water and food *ad libitum*. Animals were cared for according to the protocols of the Committee on Animal Care of MIT in conformity with the NIH guidelines (NIH publication #85–23, revised 1985). The animals were anaesthetized using continuous 2% isoflurane/O₂ inhalation. Under sterile conditions and external body warming, the sciatic nerve on the left side was approached through a semitendinosus-biceps femoris muscle splitting approach. The sciatic nerve was exposed and a 1.0 x 1.5 x 12 mm PXS bars cut from PXS patterned films were sutured into the created sciatic nerve defect of 10 mm. The muscle layer was then closed using 4-0 Vicryl sutures (Ethicon, Somerville, NJ), and the skin was closed using staples. After 2 weeks, the rats were sacrificed and the nerve stumps and PXS bar were resected *en bloc* and fixed in formalin-free fixative (Accustain). The samples were then prepared as abovementioned for SEM imaging.

3. Results

3.1 In vitro contact guidance on nanotopographic PXS substrates

Replica-molding of PXS films produced features with high fidelity and uniformity over large surface areas as determined by SEM (**Figure 1A-C**). SCs aligned and elongated in the grating axis within 4 h (**Figure 2A and B**). Approximately 80% of the SCs had aligned themselves within 15° of the grating axis (**Figure 2C**). This is in contrast to SCs that were

seeded onto smooth surfaces ($p < 0.001$). Migration velocity was increased in SCs cultured on nanotopographic PXS (16.43 ± 9.20 micron/ hr) compared to SCs cultured on flat PXS substrates (6.18 ± 3.13 micron/ hr) ($p < 0.05$, **Figure 2D**).

When DRG explants were seeded onto the patterned surfaces, we observed that the outgrowth from the explants favored the direction of the grating axis. Representative images of FITC anti-tubulin staining of the DRG alignment are shown in **Figure 3A** and **B**, 48 hr after seeding. Approximately 73% of the neurites that extended from the disrupted DRGs fell within a 15° range from the direction of the pattern, as demonstrated in **Figure 3C**. An additional interesting observation after 7 d of culture, was that DRGs on the patterned substrates demonstrated outgrowing neurites that were organized into a network that spanned across the entire tissue culture well (1 cm diameter), which was not found to be the case for the randomly outgrowing neurites from the DRGs cultured on flat surfaces (**Figure 3D** and **F**).

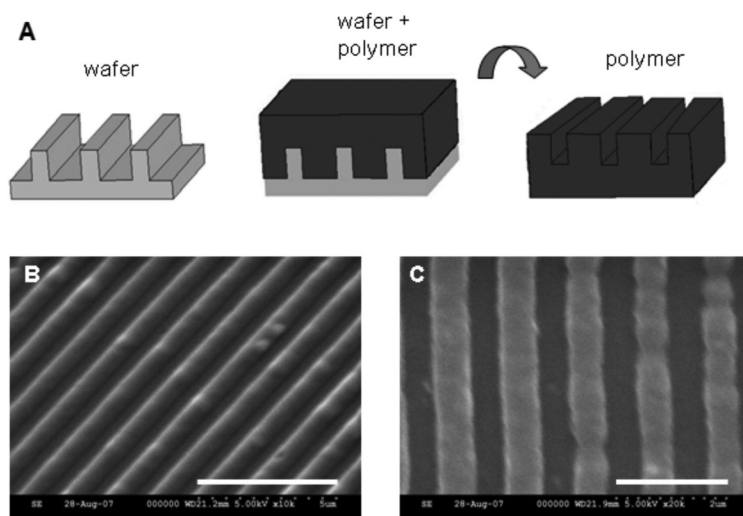


Figure 1. Fabrication of replica-molded PXS substrates. **(A)** Patterned silicone wafers were produced by deep reactive etch microfabrication processes. PXS was replica molded on this surface, cured, and delaminated by incubation in 80°C ddH₂O for 24 h. **(B)** SEM characterization of replica-molded PXS substrates showing close to uniform reproduction of micron-size features in three dimensions. Bar represents 5 μm . **(C)** Detailed SEM micrograph of the pattern studied here, revealing a period of ± 1.2 μm . Bar represents 2 μm .

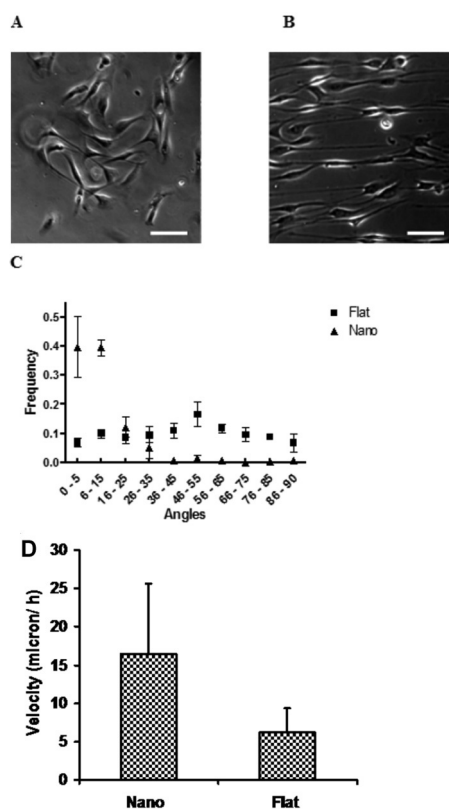


Figure 2. Representative phase contrast images (100x magnification) of the attachment and subsequent alignment of primary rat SCs on flat (A) and patterned (nano) (B) PXS substrates. Bars represent 50 μm . (C) The distribution of SC orientation on flat and patterned (nano) PXS substrates. (D) Average velocity in micron/h of SCs on flat and patterned (nano) PXS substrates ($p < 0.05$).

After 4 days of DRG culture on the flat and patterned surfaces, we found that the extending neurites from the DRGs (Figure 4A and B) and the SCs co-localized as demonstrated by the anti-S100 stain (Figure 4C and D). There was also a significant population of aligned fibroblasts in these cultures, shown by the DAPI stain (Figure 4E and F).

When the proliferation of SCs and fibroblasts was suppressed by the presence of Ara-C in the growth media, we confirmed that DRGs showed alignment on patterned PXS substrates, and not on flat PXS substrates. As demonstrated by SEM, most of the outgrowing neurites and SCs aligned along the grooves in the PXS material (Figure 5A) and random outgrowth was seen on the smooth PXS surfaces (Figure 5B). Figure 5C and D show this in more detail. In addition, these representative SEM images show that the cells on the flat surfaces seemed to spread more readily.

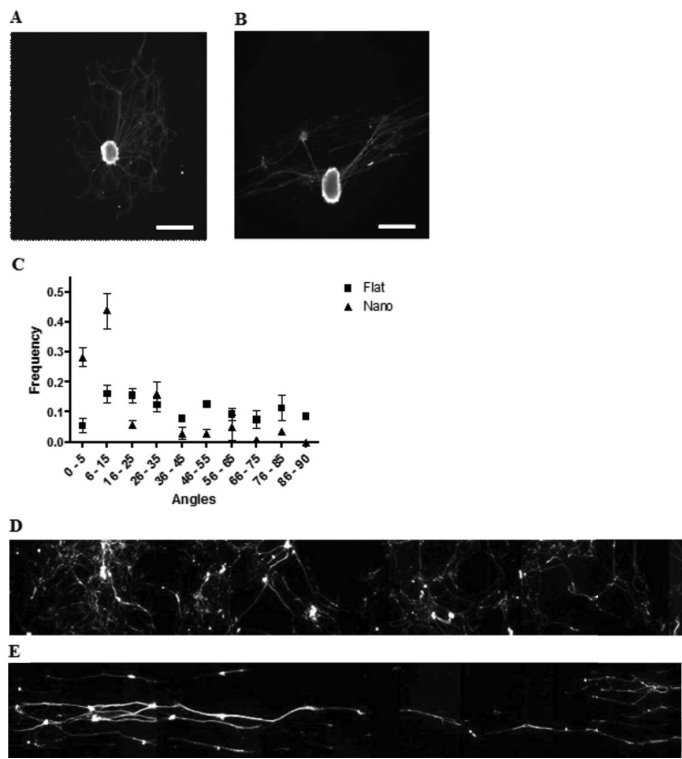


Figure 3. Representative fluorescent images (40x magnification) of DRGs stained with antitubulin antibodies on flat (A) and nano (B) collagen-coated PDMS substrates. Bars represent 125 μm . (C) The distribution of DRG neurite orientation on flat and patterned (nano) substrates. Representative fluorescent overview of anti-tubulin stained DRGs, cultured for 7 d on flat (D) and patterned (E) surfaces. Total length of image D and E represents 1 cm.

3.2 In vivo contact guidance

We investigated the potential of patterned PXS substrates in a more complex system: the site of the peripheral nerve damage. **Figure 6A** demonstrates how the patterned PXS bar was sewn in between the nerve endings, with either the flat or the patterned side facing the nerve. After two weeks, the fibrous capsule surrounding the smooth PXS bar (**Figure 6B**) did not reveal a gross tissue aspect that could contain outgrowing nerve tissue, which seemed to be the case for nanotopographic PXS implant (**Figure 6C**). The arrows point at what appeared an outgrowing nerve from the proximal stump. Higher magnification of the fibrous capsules surrounding the implants revealed a similar phenomenon: on the flat surface, the fibroblasts seemed to be randomly organized (**Figure 6D**), and on the patterned surface, they seemed to be more aligned (**Figure 6E**), although this observation could not

be quantified. Finally, the PXS elastomer had started to degrade at 2 weeks in vivo (**Figure 6F**) and did so by surface erosion, which is reported elsewhere [13]. Small excavates were visible on both the smooth as well as the patterned surfaces underneath the fibrous capsule. More importantly, PXS does not swell during degradation, potentially obscuring the patterned surface, which was still intact apart from the eroded areas (**Figure 6G**).

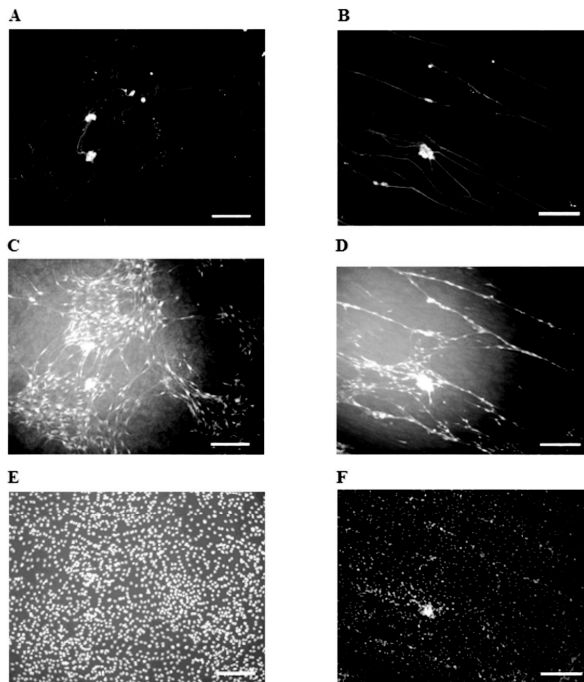


Figure 4. Representative fluore-scent photomicrographs (20x magnification) of DRGs stained with anti-tubulin, anti-S100 antibodies and Hoescht on flat ((**A**), (**C**) and (**E**) respectively) and nano ((**B**), (**D**) and (**F**) respectively) collagen-coated PDMS substrates. Bars represent 250 μm .

4. Discussion

As previously demonstrated for another thermoset elastomer, poly(glycerol sebacate) (PGS), replica-molding of PXS elastomers was straightforward [5]. Unlike PGS however, higher crosslinked PXS 2:3 elastomers delaminated more readily from the silicon wafers, and a sacrificial sucrose layer on the silicon wafer was not needed, resulting in less rounded

features on the polymer substrate (**Figure 1** and [5]). In addition, the PXS elastomer used in this study degrades at a slower rate than PGS *in vivo* [13], which we consider a more favorable rate for a nerve conduit material than PGS [17]. Also, PXS elastomers allowed for rapid and efficient Schwann cell attachment without pre-treatment of the polymer with serum or collagen. A more comprehensive study on the biocompatibility of PXS elastomers with components of the peripheral nerve is reported elsewhere [17].

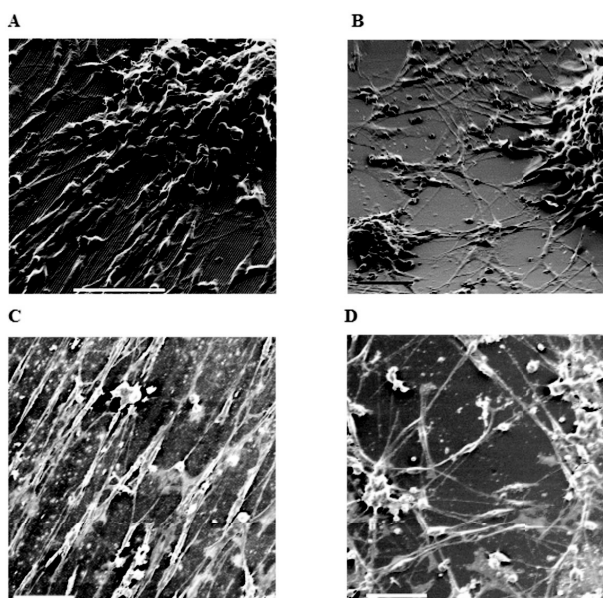


Figure 5. Representative SEM micrographs of DRGs cultured on flat and patterned PXS substrates. **(A)** DRG on patterned PXS substrate. **(B)** DRG on flat PXS substrate. Bars represent 75 μm . **(C)** Aligned neurites on patterned PXS substrates. **(D)** Randomly organized neurites on flat PXS substrates. Bars represent 50 μm .

PXS elastomers unfortunately displayed an impeding autofluorescence during staining procedures. Imaging studies presented here that required fluorescent staining were performed on collagen-coated PDMS patterned surfaces (**Figures 3** and **4**). The collagen coating may induce biological responses different from ‘naked’ PXS surfaces. However, control phase-contrast images as well as additional SEM imaging demonstrated revealed similar static observations between SCs or DRGs cultured on collagen-coated PDMS surfaces and PXS surfaces.

The in vitro alignment of SCs, and to a lesser extent DRGs, on patterned surfaces has been reported [8,10,11,18-25]. These patterns were mostly induced by coating laminin, or by induced grooves in the material's surface. Walsh *et al.* showed that, using rippled non-degradable polystyrene, the best size of features to induce alignment of DRGs was in the 600-1000 nm order [25]. Most reports in this growing body of literature have not (yet) employed topography at this resolution, but typically in the order of tens of microns. In vivo however, it remains unclear if smaller features (e.g. grooves, fibers on (sub)micron scale) are more beneficial to nerve regeneration than larger topographic cues (on the order of tens to hundreds of microns), such as conduits containing polymeric microfilaments. Using a slowly degrading poly(lactic acid) (PLA) microfilaments, coated with laminin, Wen and Tresco found that the smallest diameter (5 micron) microfilament tested, was most effective in stimulating neurite outgrowth in vitro [11]. It can be hypothesized however, that the degradation profile as well as biocompatibility will dictate the resolution of the topography on a biomaterial. We therefore anticipated that biodegradable PXS elastomers with nanotopographic features were excellent candidate materials to induce alignment of SCs and DRGs in vitro.

However, increased migration velocity of cells on nanopatterned surfaces is more dependent on the material, pattern and cell-type [4, 26]. It is well known that migratory SCs have an ability to stimulate outgrowing axons [27, 28]. More specifically, SCs migrating from the distal nerve stump are more potent in their stimulating activity than those from the proximal stump [28]. However, no reports exist on the effect of nanotopography on the migration velocity of SCs. We observed an increase in migration velocity of SCs on nanotopographic PXS substrates (**Figure 2D**), but we have not investigated the mechanism of this phenomenon. These structures could however, potentially promote the rapid migration of neurites across the nerve gap in vivo.

There are reports applying these promising in vitro data of SC alignment and enhanced migration in an in vivo model for peripheral nerve repair. The conduits investigated are based on a rolled-up micropatterned polymer sheet seeded with SCs or on PLA microfilaments within the conduit, and were compared to empty conduits showing beneficial effects of the alignment [10, 29, 30]. PXS elastomers presented here, are produced by polycondensation of xylitol and sebacic acid. During this process, PXS oligomers are a flowing substance until the gelation point is reached, setting the polymer in its given form. The fabrication of a complex 3-D structure such as a mold to obtain porous PXS conduits with a longitudinally directed nanotopographic lumen is a challenging task that still lies ahead. Therefore, a thin nanopatterned PXS film, rolled up and sewn shut may be the most straightforward way of obtaining nanopatterned PXS nerve conduits. However, in this report, we performed a

pilot study of a nanopatterned PXS bar sewn into a 1 cm rat sciatic nerve defect, showing potential in in vivo contact guidance (**Figure 6**). However, the results were not quantifiable and no conclusions in terms of benefit for peripheral nerve regeneration can be drawn from this pilot experiment.

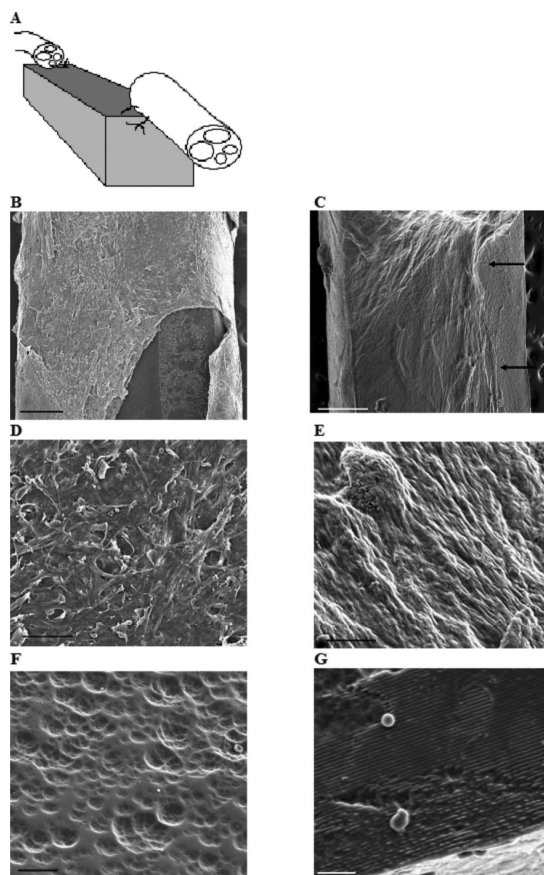


Figure 6. (A) Cartoon depicting how rat sciatic nerves were “reconstructed” with a flat or patterned PXS bar (side with substrate topography: dark grey area). After 14 d, bars with surrounding fibrous capsule and nerves were harvested and characterized by SEM. (B) Overview SEM micrograph of fibrous capsule surrounding the PXS bar with flat surface. The capsule is opened to reveal the underlying PXS surface. Bar represents 225 μm . (C) Overview SEM micrograph of fibrous capsule surrounding the PXS bar with patterned surface. Arrows indicate aligned tissue bridges between the proximal and distal nerve stump. Bar represents 275 μm . (D) Detailed SEM micrograph revealing the orientation of cells of the tissue capsule surrounding the PXS implant with flat surface topography. Bar represents 50 μm . (E) Detailed SEM micrograph revealing the orientation of cells of the tissue capsule surrounding the PXS implant with patterned surface topography. Bar represents 50 μm . (F) SEM micrograph of the degrading, flat PXS substrate. Bar represents 20 μm . (G) SEM micrograph of the degrading, flat PXS substrate. Bar represents 10 μm .

Although these are promising initial results, studies comparing PXS conduits with a longitudinally directed nanotopographic lumen compared to empty conduits as well as autologous nerve grafting are warranted and currently pursued.

5. Conclusions

We have engineered implant materials based on the flexible, biodegradable and biocompatible elastomer PXS. The implants organized and aligned cell populations of the peripheral nerve system, facilitating guidance of peripheral nerve regeneration and migration velocity of SCs in vitro. These implants also demonstrated in vivo contact guidance of surrounding fibrous capsules in vivo. This ability may be beneficial to the nerve regeneration potential of empty nerve conduits and should be further investigated.

6. References

1. Anselin AD, Fink T, Davey DF. Peripheral nerve regeneration through nerve guides seeded with adult Schwann cells. *NeuroPath Appl Neurobiol* 1997;23:387-398.
2. Dubey N, Letourneau PC, Tranquillo RT. Guided neurite elongation and Schwann cell invasion into magnetically aligned collagen in simulated peripheral nerve regeneration. *Exp Neurol* 1999;158:338-350.
3. Gerecht-Nir S, Bettinger CJ, Zhang Z, Borenstein J, Vunjak-Novakovic G, Langer R. The effect of actin disrupting agents on contact guidance of human embryonic stem cells. *Biomaterials* 2007;28(28):4068-4077.
4. Bettinger CJ, Zhang Z, Gerecht S, Borenstein J, Langer R. Enhancement of in vitro capillary tube formation by substrate nanotopography. *Adv Mater* 2008;20(1):99-103.
5. Bettinger CJ, Orrick B, Misra A, Langer R, Borenstein JT. Microfabrication of poly(glycerolsebacate) for contact guidance applications. *Biomaterials* 2006;27:2558-2565.
6. Itoh S, Fujimori KE, Uyeda A, Matsuda A, Kobayashi H, Shinomiya K, Tanaka J, Taguchi T. Long-term effects of muscle-derived protein with molecular mass of 77 kDa (MDP77) on nerve regeneration. *J Neurosci Res* 2005;81(5):730-738.
7. De Ruiter GC, Spinner RJ, Malessy MJ, Moore MJ, Sorenson EJ, Currier BL, Yaszemski MJ, Windebank AJ. Accuracy of motor axon regeneration across autograft, single-lumen, and multichannel poly(lactic-co-glycolic acid) nerve tubes. *Neurosurgery* 2008;63(1):144-153.
8. Miller C, Jeftinija S, Mallapragada S. Micropatterned Schwann cell-seeded biodegradable polymer substrates significantly enhance neurite alignment and outgrowth. *Tissue Eng* 2001;7(6):705-715.
9. Moore MJ, Friedman JA, Lewellyn EB, Mantila SM, Krych AJ, Ameenuddin S, Knight AM, Lu L, Currier BL, Spinner RJ, Marsh RW, Windebank AJ, Yaszemski MJ. Multiple-channel scaffolds to promote spinal cord axon regeneration. *Biomaterials* 2006;27(3):419-429.

10. Rutkowski GE, Miller CA, Jeftinija S, Mallapragada SK. Synergistic effects of micropatterned biodegradable conduits and Schwann cells on sciatic nerve regeneration. *J Neural Eng* 2004;1:151-157.
11. Wen X, Tresco PA. Effect of filament diameter and extracellular matrix molecule precoating on neurite outgrowth and Schwann cell behavior on multifilament entubulation bridging device in vitro. *J Biomed Mater Res*. 2006;76A:626-637.
12. Bruggeman JP, Bettinger CJ, Nijst CLE, Kohane DS, Langer R. Biodegradable xylitol-based polymers. *Adv Mater* 2008;20(10):1922-7.
13. Bruggeman JP, Bettinger CJ, Langer R. Biodegradable xylitol-based elastomers: in vivo behavior and biocompatibility. *J Biomed Mater Res A* 2010;95(1):92-104.
14. Mandemakers W, Zwart R, Jaegle M, Walbeehm E, Visser P, Grosveld F, Meijer D. A distal Schwann cell-specific enhancer mediates axonal regulation of the Oct-6 transcript factor during peripheral nerve development and regeneration. *EMBO* 2000;19(12):2992-3003.
15. Jirsova K, Sodaar P, Mandys V, Bar PR. Cold jet: a method to obtain pure Schwann cell cultures without the need for cytotoxic, apoptosis-inducing drug treatment. *J Neurosci Methods* 1997;78:133-137.
16. Sandrock AW, Matthew WD. Identification of a peripheral nerve neurite growth-promoting activity by development and use of and in vitro bioassay. *Proc Natl Acad Sci U S A* 1987;84:6934-6938.
17. Bruggeman JP, De Bruin BJ, Bettinger CJ, Alford A, George PM, Hovius SE, Langer R. Biodegradable poly(xylitol sebacate) (PXS) conduits for peripheral nerve reconstruction. In preparation.
18. Clark P, Britland S, Connolly P. Growth cone guidance and neuron morphology on micropatterned laminin surfaces. *J Cell Sci* 1993;105(1):203-212.
19. Goldner JS, Bruder JM, Li G, Gazzola D, Hoffman-Kim D. Neurite bridging across micropatterned grooves. *Biomaterials* 2006;27(3):460-472.
20. Hsu SH, Chen CY, Lu PS, Lai CS, Chen CJ. Oriented Schwann cell growth on microgrooved surfaces. *Biotechnol Bioeng* 2005;92(5):579-588.
21. Lietz M, Dreesmann L, Hoss M, Oberhoffner S, Schlosshauer B. Neuro tissue engineering of glial nerve guides and the impact of different cell types. *Biomaterials* 2006;27(8):1425-1436.
22. Schmalenberg KE, Uhrich KE. Micropatterned polymer substrates control alignment of proliferating Schwann cells to direct neuronal regeneration. *Biomaterials* 2005;26(12):1423-1430.
23. Thompson DM, Buettner HM. Schwann cell response to micropatterned laminin surfaces. *Tissue Eng* 2001;7(3):247-265.
24. Thompson DM, Buettner HM. Neurite outgrowth is directed by Schwann cell alignment in the absence of other guidance cues. *Ann Biomed Eng* 2006;34(1):161-168.
25. Walsh JF, Manwaring ME, Tresco PA. Directional neurite outgrowth is enhanced by engineered meningeal cell-coated substrates. *Tissue Eng* 2005;11(7):1085-1094.
26. Bettinger CJ, Langer R, Borenstein J. Engineering substrate topography at the micro- and nanoscale to control cell function. *Angew Chem Int Ed* 2009;48:5406-5415.
27. Taniuchi M, Clark HB, Johnson EMJ. Induction of nerve growth factor receptor in Schwann cells after axotomy. *Proc Natl Acad Sci U S A* 1986;83:4094-4098.
28. Torigoe K, Tanaka HF, Takahashi A, Awaya A, Hashimoto K. Basic behavior of migratory Schwann cells in peripheral nerve regeneration. *Exp Neurol* 1996;137:301-308.
29. Cai J, Peng X, Nelson KD, Eberhart RC, Smith GM. Permeable guidance channels containing microfilament scaffolds enhance axon growth and maturation. *J Biomed Mater Res A* 2005;75:374-386.
30. Hsu S, Lu PS, Ni HC, Su CH. Fabrication and evaluation of microgrooved polymers as peripheral nerve conduits. *Biomed Microdevices* 2007;9(5):665-674.

Chapter 9

**Fabrication of scaffolds composed of
biodegradable poly(polyol sebacate) elastomers
for tissue engineering purposes**

Joost P. Bruggeman, Berend-Jan de Bruin, Jason W. Nichol, Lisa E. Freed,
Robert Langer

Abstract

For the successful design and integration of tissue engineered constructs into living systems, it is key to engineer polymers into three-dimensional (3-D) scaffolds. Electrospinning and fused salt-leaching are two abundantly used techniques to obtain 3-D scaffolds, and were employed on a recently synthesized group of synthetic elastomeric materials, PPS polymers. PPS polymers are challenging materials to use for electrospinning. For the purpose of electrospinning as well as developing materials that can be readily polymerized under physiological conditions, PPS polymers were acrylated and subsequently photopolymerized. Electrospinning was possible using this approach and fiber diameter ranged from 2-5 microns. This technique needs to be explored more to obtain better electrospun scaffolds composed of PPS polymers. The fabrication of porous scaffolds of thermally cured PPS polymers was straightforward and allowed for tissue ingrowth throughout the whole scaffold in vivo. Compression moduli of these porous PPS scaffolds ranged from the kPa scale up to 1 MPa, and changed after 3 weeks in vivo to the compression moduli of the fibrous tissue that had grown into the scaffolds. This study showed that PPS polymer scaffolds can be engineered in scaffolds for tissue engineering purposes.

1. Introduction

The well-known tissue engineering paradigm accounts for the importance of scaffolds in combination with other important components such as cells and growth factors [1]. One of several advantages of using synthetic polymers as scaffolding material, is the ability to tailor physical and chemical properties of scaffolds as well as degradation kinetics through chemistry and processing [2-4].

Many tissues exhibit elasticity such that they can function and recover in the mechanically challenging environment of the human body. For this reason, Wang *et al.* synthesized a tough biodegradable elastomer, poly(glycerol sebacate) (PGS) that has potential for the engineering of soft tissues [5]. Although PGS displayed excellent biocompatibility and favorable degradation kinetics compared to poly(lactic-co-glycolic acid) (PLGA), PGS is completely degraded in vivo within 60 d [6]. Bruggeman *et al.* recently synthesized a platform of comparable biodegradable polymers, based on different polyols and sebacic acid, designated poly(polyol sebacate) (PPS) polymers [3,4]. The mechanical properties and degradation rates of these novel polymers could be tuned in a wider range than PGS while demonstrating similar biocompatibility and form stability during degradation [7].

For the successful design and integration of tissue engineered constructs into living systems, it is key to engineer polymers into three-dimensional (3-D) scaffolds that mimic natural cellular environments. Different approaches have been described to create scaffolds with 3-D micro- and nanoscale features, such as replica molding [8, 9], particulate leaching [10-12] and electrospinning [13-15], amongst many more. Particulate leaching is an attractive, cost-effective method to create scaffolds due to its simplicity. Electrospinning is a promising technique in which a mat of a continuous polymer fiber is created by applying a voltage to a polymer/ solvent solution. The resulting fibrous scaffolds may be advantageous for tissue engineering due to their high surface-to-mass ratio and their ability to mimic the native extra-cellular matrix in size as well as architecture [8,14]. However, a common strategy for most of these approaches is to dissolve the polymer in an organic solvent. Although these techniques are readily applicable to thermoplastic polymers such as PLGA, thermoset (or, crosslinked) PPS polymers do not dissolve in solvents. In addition, harsh curing conditions and long reaction times are typical for PPS polymers, excluding the ability to polymerize these materials instantly into a desired complex shape, or in or around living cells or tissue. To tackle this issue, Nijst *et al.* recently developed a photopolymerizable

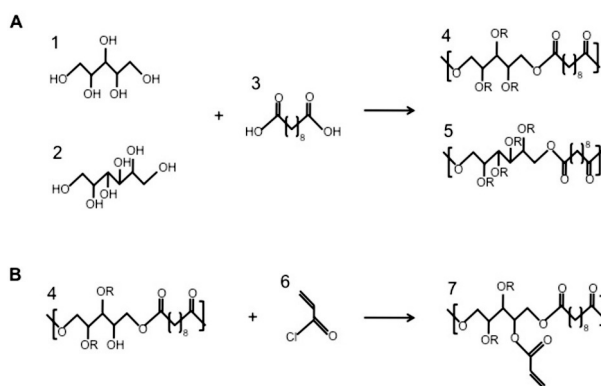
form of PGS (PGSA), allowing for the formation of a crosslinked network within minutes at ambient temperatures [16].

The overall objective of this work was to demonstrate the applicability of PPS polymers in two different approaches fabricating 3-D PPS scaffolds for tissue engineering purposes: electrospinning and particulate leaching. To accomplish this, photopolymerizable PPS polymers were developed in a similar fashion as PGSA, and electrospun into fibrous mats. These mats demonstrated *in vitro* cellular attachment. The production of thermally cured, porous PPS scaffolds is straightforward through salt-fusion, subsequent polymer curing and salt-leaching, as previously described for PGS. Porous PPS scaffolds were vascularized *in vivo* and preserved their elastomeric properties.

2. Materials and methods

2.1 Synthesis of PPS pre-polymers

All chemicals were purchased from Sigma-Aldrich (St. Louis, MO, USA) unless stated otherwise. PPS pre-polymers were synthesized as previously described [4]. In brief, appropriate molar amounts of the polyol and sebacic acid monomer were melted in a 250 mL round bottomed flask at 150°C under a blanket of inert gas, and stirred for 2 h. Vacuum (~50 mTorr) was applied for 2 – 12 h, yielding the pre-polymers poly(xylitol sebacate) (PXS) 2:3 and PXS 1:2, poly(mannitol sebacate) (PMS) 1:2 (**Scheme 1**).



Scheme 1. (A) Polycondensation of xylitol (1) or mannitol (2) with sebacic acid (3), yielding the PXS (4) or PMS (5) pre-polymer. R represents H or the polymer chain. (B) Acrylation of the PXS pre-polymer (4) with acryloyl chloride (6) into PXSA (7) (not all binding possibilities are shown). R represents H, an acrylate group or another (acrylated) polymer chain.

2.2 Synthesis of photopolymerizable PPS pre-polymers

The PXS 2:3 pre-polymer was acrylated in the following manner: a flame-dried round bottomed flask was charged with 10 g of PXS pre-polymer, 200 mL of anhydrous tetrahydrofuran (THF), and 4dimethylaminopyridine (DMAP) (20 mg, 0.18 mmol). The reaction flask was kept at room temperature under a positive pressure of N_2 . Acryloyl chloride (0.5-0.66 mol/mol to PXS pre-polymer) was slowly added parallel to an equimolar amount of triethylamine. The reaction was protected against light and kept at room temperature for an additional 24 h. The resulting PXS-acrylate (PXSA) mixture was filtered, dried at 35°C and 70-150 mTorr using a rotary evaporator, and stored at -20°C.

2.3 Pre-polymer characterization

1H nuclear magnetic resonance (1H -NMR) spectra of the PXS pre-polymer and PXSA pre-polymer were recorded (Varian Unity-300 NMR spectrometer). Chemical shifts were referenced relative to the peaks for deuterated dimethylformamide (dDMF) at 2.75, 2.95 and 8.03 ppm. The chemical composition was determined by calculating the signal integrals of $-COCH_2CH_2CH_2-$ at 1.2, 1.5, and 2.2 ppm for sebacic acid, $-OCH_2(CH(OR))_3CH_2O-$ at 3.5-5.5 ppm for xylitol and $-CH=CH_2$ from the acrylate groups at 5.9, 6.3 and 6.5 ppm for the protons on the acrylate groups. The signal intensity of the methylene groups of sebacic acid (1.2 ppm) and the acrylate groups (average signal intensities of 5.9, 6.1, and 6.5 ppm) were used to calculate the DA.

2.4 Preparation and characterization of Photocured PXSA

PXSA networks were formed by mixing PXSA with 0.1% photoinitiator (2,2-dimethoxy-2-phenylacetophenone), and the polymerization reaction was initiated by exposure to ultraviolet light (ca. 4 mW/cm², model 100AP, Black-Ray) for 10 min. Attenuated total reflectance Fourier transform infrared (ATR-FTIR) spectroscopy analysis was performed on a Nicolet Magna-IR 500 spectrophotometer to confirm the cross-link reaction. For that purpose, thermally cured PXS and photocured PXSA slabs, PXS pre-polymer, and dissolved PXSA pre-polymer were placed on top of a ZnSe crystal.

2.5 Mechanical testing

Tensile and compression tests were conducted using an Instron 5542 (according to ASTM standard D412-98a) on dog-bone shaped polymer strips (115 x 25 x 1.2 mm) or circular films (10mm x 1-3 mm) cut from photocured PXSA or thermally cured porous PXS or PMS

sheets, respectively. The strain rate was 50 mm/min, and all samples were elongated to failure or compressed to maximum compression force (50 N).

2.6 Electrospinning PXSA scaffolds

See **Figure 1** for the electrospinning setup. Components for the case, electrodes and electrical wiring were purchased from McMaster-Carr Supply Inc. The high voltage power supply (ES30p-5W) was custom built by Gamma High Voltage Research (of Ormond Beach, FL). A Harvard Apparatus syringe pump was used for injecting the polymer at a constant speed through an 18 gauge stainless steel blunt tip needle into the charged field. Voltages between 15 and 24 kV were applied to the copper electrodes, spaced at 20 cm. Electrospun pre-polymer was injected at flow rates between 1 and 1.5 ml/h, accumulated on a glass slide, placed on the grounded electrode and exposed to ultraviolet light for several minutes. Both PLGA (65/35, high M_w , Lakeshore Biomedical, Birmingham, AL, USA) and PXSA were dissolved in THF in different w/w ratios prior to injection into the electromagnetic field.

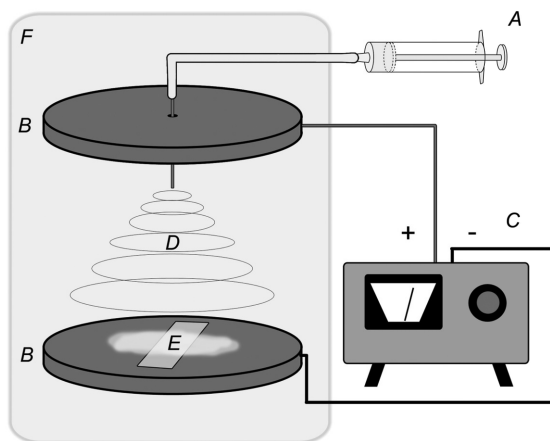


Figure 1. Schematic representation of the setup used for electrospinning. The polymer solution (A) is injected in a high potential electrical field between two copper electrodes (B), generated by a high voltage power supply (C), through a charged metal needle. The polymer solution is drawn into a thin, continuous fiber that undergoes a bending instability once it progresses further down the field (D) and finally gets deposited on the glass slide (E) and ground plate. The electrodes and needle are encased in an airtight Plexiglas cabinet (F), allowing control over temperature and humidity.

2.7 Preparation of porous PPS scaffolds

Porous PPS scaffolds were prepared by a salt fusion method, previously described for PGS [11]. In brief, ground salt particles of 100-300 micron were used as porogens for salt fusion. The salt particles were put into a mold consisting of a Teflon-coated stainless-steel dish. A glass rod was used to scrape the top of the salt-filled mold to produce uniform scaffold thickness. The molds were transferred to and kept in an incubator at 37 °C and 88% relative humidity for 4 h. The fused templates of salt particles were dried in a vacuum oven at 90°C and 100 mTorr overnight before further processing. PPS pre-polymers were heated above their melting temperatures, and added to the disk-shaped salt mold allowing to settle for 2 h. The polymer laden dishes were then cured for 48 to 72 h at 140°C. The dishes were allowed to cool to room temperature, and then soaked in ddH₂O for 48 h, regularly changing the water.

2.8 Scanning Electron Microscopy (SEM) imaging

The electrospun fiber scaffolds, the salt-leached porous PXS and PMS scaffolds and their cell seeded and in vivo vascularized versions respectively, were washed three times in PBS and fixed with Accustain (Sigma Aldrich). After being rinsed with PBS buffer three times, the dishes were dehydrated in graded alcohols (50%, 70%, 80%, 90%, 95%, and 100%) and then air-dried in HMDS. The samples were then sputter-coated with gold paladium and examined on a JEOL JSM-5910 scanning electron microscope.

2.9 In vitro cell attachment

A mouse myoblast cell-line (C2C12) and primary Human Foreskin Fibroblasts (HFFs) (ATCC, Manassas, VA) were cultured in high-glucose Dulbecco's minimal essential medium (DMEM), supplemented with 10% Fetal Bovine Serum and 100 U/ml Penicillin and 100 ug/ml streptomycin (Invitrogen), further denoted as growth medium, at 37 °C and 5% CO₂. Between passage 3 and 5 the cells were harvested using trypsin (0.025%) in EDTA (0.01%) (Invitrogen) and resuspended in growth medium. Photocured PXSA covered 5.5 cm diameter glass dishes were prepared by 2 ml 6.25% PXSA and photoinitiator in THF. The dishes were then exposed to UV-light to polymerize PXSA. The dishes were exposed on several washes in PBS on a orbital shaker. Glass slides with electrospun fibers were placed in these tissue culture dishes and both were UV sterilized for 30 minutes and presoaked with growth medium for 6 hours to wash out photoinitiator, THF and unreacted monomers, before the cells were seeded at a density of 7500 cells/cm². Cells were allowed to attach and proliferate for 4 days before imaging.

2.10 In vivo implantation of porous PPS scaffolds

Porous PPS discs ($d = 10$ mm, $h = 2$ -3 mm) were implanted. Two female Lewis rats (Charles River Laboratories, Wilmington, MA) weighing 200-250 grams had access to water and food *ad libitum*. Animals were cared for according to the protocols of the Committee on Animal Care of MIT in conformity with the NIH guidelines (NIH publication #85-23, revised 1985). The animals were anaesthetized using continuous 2% isoflurane/O₂ inhalation. The implants were introduced by small midline dorsal incisions, and the scaffolds were placed in subcutaneous pockets created by blunt lateral dissection. The skin was closed with staples. Rats were sacrificed 3 weeks post implantation. The implants for H&E and Masson's trichrome staining were resected *en bloc* with surrounding tissue and fixed in formalin-free fixative (Accustain). These specimens were embedded in paraffin after a series of dehydration steps in ethanol and xylene. Sequential sections (8-15 μ m) were stained and histology was evaluated by a medical doctor (JPB). Other implants were carefully dissected out of their subcutaneous pockets and fixed in Accustain before their preparation for SEM imaging. Throughout the study, all rats remained in good general health as assessed by their weight gain.

3. Results and discussion

3.1 Synthesis and characterization of PXSA

The introduction of the acrylate functionality in PXS pre-polymers introduces control over the crosslinking reaction, expanding the processing options for this elastomer: the vinyl entities present in the bulk of the PXSA pre-polymers can now be crosslinked through both photo-initiated free radical polymerizations [14,16] as well as by other means, e.g. using multifunctional nucleophile entities (Michael-type addition reactions with e.g. di-thiols, diamines [17]) or by redox initiation reactions [18]. Recently, there has been great interest in using photopolymerization techniques to prepare polymeric networks for tissue engineering applications: photopolymerized PGSA polymers were successful in encapsulating stem cells [19] as well as forming complex 3-D structures [20].

PXSA was prepared by the acrylation of the PXS pre-polymer, similar to previously described PGSA. The PXS 2:3 pre-polymer had a weight-average molecular weight (M_w) of 3156 g/ mol, a number-average molecular weight (M_n) of 1117 g/ mol as determined by GPC compared with linear polystyrene standards, and a polydispersity index (*PDI*) of 2.7. The molar composition of the PXS pre-polymer was approximately 1:1.63 xylitol/

sebacic acid as confirmed by ^1H NMR analyses (**Figure 2A**). The incorporation of acrylate groups was confirmed by ^1H NMR by the appearance of the peaks at δ 5.9, 6.1, and 6.4 ppm (**Figure 2A**, lower panel). This was also confirmed by ATR-FTIR by the appearance of an absorption band at $\sim 1630\text{ cm}^{-1}$, corresponding to the vinyl groups [21] of the acrylate moieties in PXSA (**Figure 2B**, **b** and **c**). The degree of acrylation (DA) can be calculated from signal intensities of ^1H NMR. PXSA with a DA of 0.28 and 0.41 were obtained for further investigation (meaning every xylitol monomer was on average equipped with 0.28 or 0.41 acrylate groups). After exposure to UV-light, polymerization occurred. The disappearance of the absorption band at $\sim 1630\text{ cm}^{-1}$ in FT-IR analysis confirmed the consumption of vinyl groups for the polymerization process (**Figure 2B**, **e** and **f**).

The mechanical properties of PXSA were as follows: PXSA with DA 0.28 revealed a Young's modulus of $1.73 \pm 0.21\text{ MPa}$, with an elongation at break of $180.3 \pm 14.4\%$. PXSA with DA 0.41 demonstrated a Young's modulus of $2.66 \pm 0.27\text{ MPa}$, and an elongation at failure of $98.9 \pm 4.3\%$.

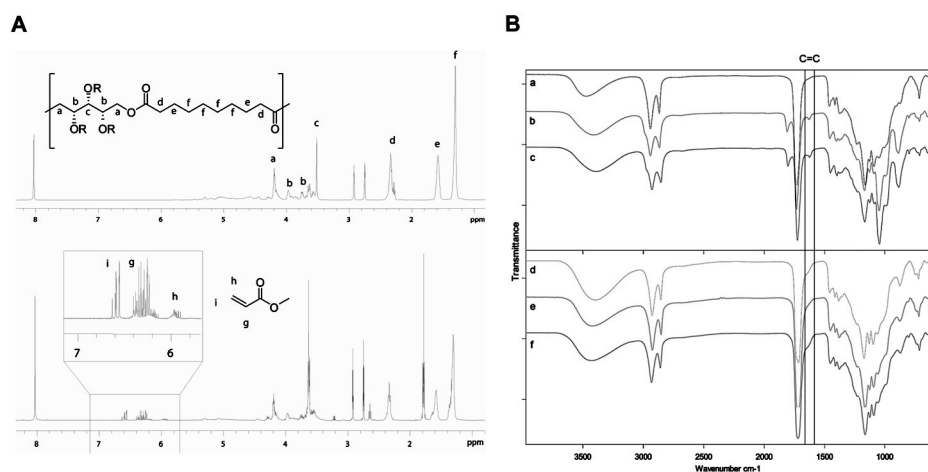


Figure 2. (A) ^1H NMR spectra of PXS pre-polymer (upper) and PXSA 2:3 (lower). Peaks a, b and c at respectively 4.2, 3.9 and 3.6 ppm correspond with the hydrogens on the xylitol molecule, peaks d, e and f at respectively 2.3, 1.6 and 1.3 with the hydrogens of sebacic acid and peaks i, h and g with the hydrogens of the acrylate group. (B) ATR FT-IR spectra of PXS pre-polymer (a), PXSA DA 0.28 and 0.41 (b and c, resp.), thermally cured PXS (d) and photocured PXSA 0.28 and 0.41 (e and f, resp.). The distinctive dent on the C=C band denotes the acrylate's double bond region at $\sim 1630\text{ cm}^{-1}$ and disappears after photocuring.

3.2 Electrospun PXSA scaffolds

PXSA/PLGA mixtures in THF were electrospun, as evaluated by SEM imaging, shown in **Figure 3**. **Figure 3A** and **3H** demonstrate scaffold morphology of electrospun PLGA 100% and PXSA 100% respectively. Decreasing the amount of carrier polymer (PLGA) below a 50/50 w/w ratio to PXSA (either DA), resulted in loss of fiber integrity and fibers started to fuse together (**Figure 3B-G**). Despite repeated efforts, it did not seem possible to directly electrospin microfibers from either crosslinked PXS or PXS pre-polymers. Crosslinked PXS is not soluble in solvents and cannot be extruded once the polycondensation reaction has passed the gelation point. PXS pre-polymers can be spun, but these materials are flowing liquids, thus the drawn fibers coalesce into a puddle of PXS pre-polymer. Yi and LaVan have solved this electrospinning problem for PGS polymers by coaxial core/shell spinning [15]. The PGS pre-polymer was first trapped during electrospinning by a shell of poly(L-lactic acid) (PLLA) polymer, then the PGS was thermally cured after which the PLLA shell was removed by dichloromethane. This technique resulted in electrospun PGS fibers with an average fiber diameter of 450 ± 180 nm. Although a very solid approach towards the problem, this approach unfortunately does not allow for the incorporation of temperature sensitive entities such as cells and growth factors.

Electrospinning of pure PXSA proved to be a challenging task still: although photopolymerization of PXSA dramatically shortens the polymerization process, fibers merged and coalesced into a polymer slab instead of maintaining the integrity of solid, independent microfibers. This very phenomenon is also reported by Ifkovits and colleagues for electrospinning PGSA fibers [14]. To bypass this problem, they used a carrier polymer (poly(ethylene oxide) (PEO), 200 kDa) which is a non-degradable, synthetic polymer. When they increased the PGSA/PEO content up to 40/60 w/w, electrospun PGSA fibers merged, losing typical electrospun scaffold morphology. In our study, we used a biodegradable PLGA as a carrier polymer and observed fibers merging at 50/50 w/w ratio of the PXSA/carrier polymer. Spinning with a higher molecular weight PXSA pre-polymer, as well as a more volatile solvent (e.g. hexafluoro-2-isopropanol) may help decrease the amount of carrier polymer in solution. Interestingly, our obtained fiber diameter seemed comparable to the diameters reported for PGSA by Ifkovits *et al.* Fiber diameter averages for different PXSA/PLGA ratios are summarized in **Figure 3I**.

Our initial in vitro biocompatibility study showed that the photocured elastomers support cell adhesion and proliferation of two different cell types. Both C2C12 and HFF cells demonstrated attachment and proliferation seeded onto the PXSA polymer (**Figure 4A** and **B**). Similar behavior and morphology was observed for these cells when they were seeded

onto 60:40 PLGA:PXSA (DA 0.41) electrospun scaffolds (**Figure 4C and D**). Before implanting these electrospun scaffold for an assessment of *in vivo* biocompatibility or an *in vivo* tissue engineering purpose, one must realize that the degradation kinetics and behavior of these electrospun polymers may be completely different from assessments based on solid implants of the same polymer. Electrospinning results in an increase in the surface to volume ratio, potentially allowing for a significant shorter *in vivo* lifetime [22]. Solid PXS 2:3 elastomeric constructs have a projected half-life time *in vivo* of more than 6 months [7], which is considerably longer than the reported *in vivo* lifetime of an elastomeric construct composed of PGS [6]. Both PGS and PXS elastomers display an enzymatic surface eroding profile *in vivo*, and therefore it is hypothesized that electrospun scaffolds composed of PXSA may be more applicable for implantation applications with a longer aimed *in vivo* lifetime than electrospun PGSA scaffolds.

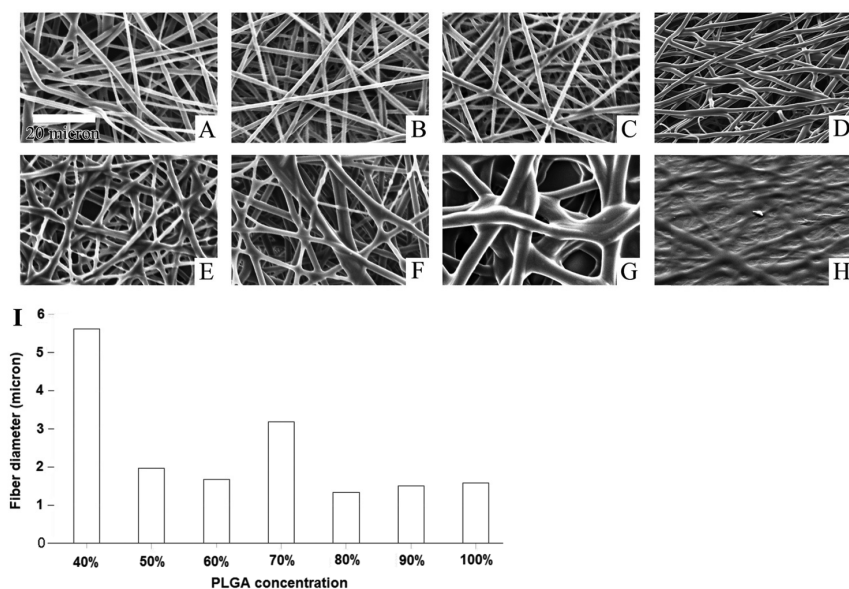


Figure 3. SEM images of electrospun PLGA (**A**), and PLGA and PXSA mixtures: (**B**) 90:10 w/w PLGA/PXSA, (**C**) 80:20, (**D**) 70:30, (**E**) 60:40, (**F**) 50:50, (**G**) 40:60 and 100% PXSA (**H**). (**I**) Average fiber diameter of the fibers in micrometers after electrospinning PLGA and PXSA 2:3 mixtures.

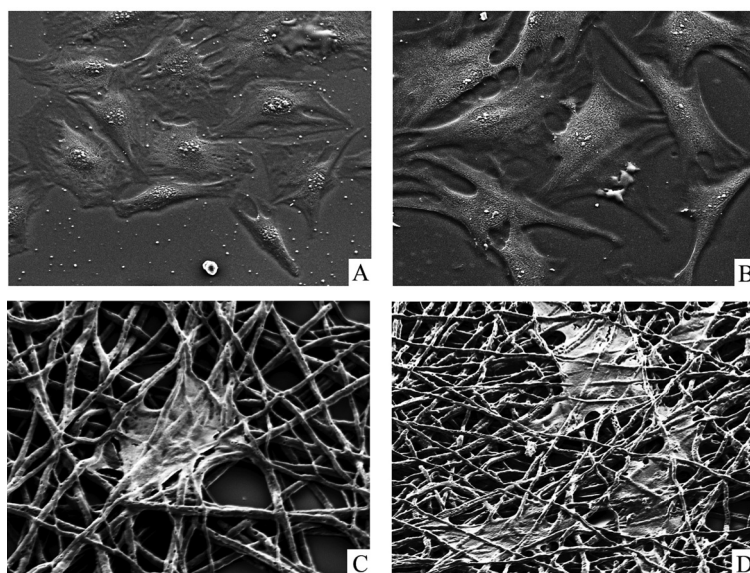


Figure 4. SEM images of C2C12 cells (**A**, and **C**) and HFFs (**B**, and **D**), 6 hr after seeding on flat photocured PXSA (DA 0.41) (**A** and **B**), and 4 d after seeding on electrospun 60:40 PLGA:PXSA substrates (**C** and **D**).

3.3 Salt-leached PPS scaffolds

Porous PPS scaffolds were created by curing PPS polymers dispersed throughout a fused salt particle template, followed by salt-leaching. This technique was previously described by Gao *et al.* for PGS scaffolds [11]. Their study on porous PGS scaffolds is extensive and relates mechanical properties of the PGS scaffolds to salt particle size, polymer curing times and in vitro cell survival. The pores in the PPS scaffolds obtained by this technique are large, and demonstrated interconnectivity (**Figure 5**). In addition, SEM examination showed no isolated salt particles within the polymer. This is an important observation as this may facilitate mass transfer within the scaffold, increasing intercellular communication and survival. Indeed, our porous PPS (PXS and PMS 1:2 in this case) scaffolds demonstrated tissue ingrowth and vascularization of the ingrown tissue in vivo, indicating a responsive milieu within the 3-D construct (**Figure 6** and **7**), as is frequently seen with biodegradable polymer foams [12].

Changing curing times was used to tailor mechanical properties of porous PPS scaffolds. Porous PXS scaffolds cured for 48 h demonstrated a compression modulus of 0.07 ± 0.02 MPa and porous PMS 1:2 scaffolds cured for 48 h had a similar compression modulus of 0.09 ± 0.02 MPa (**Figure 8A**). Porous PMS 1:2 scaffolds cured for 72 h however, revealed a compression modulus of 1.00 ± 0.17 MPa (**Figure 8B**). Mechanical testing of the

scaffolds after 3 weeks of subcutaneous implantation revealed an increase in stiffness upon implantation for PXS 1:2 scaffolds, to 0.12 ± 0.05 MPa. The modulus of PMS 1:2 scaffolds that were cured for 72 h however decreased towards the value of PXS *ex vivo* moduli, 0.28 ± 0.16 MPa (**Figure 8C**). The increase in compression modulus for porous PXS scaffolds is most likely due to tissue filling up the previously empty pores. The explants clearly remained elastomeric, whereas the decrease in modulus of porous PMS scaffolds may be due to degradation of the weakest places in the porous scaffolds, slowly declining to the modulus of the fibrous tissue that had grown into the scaffold.

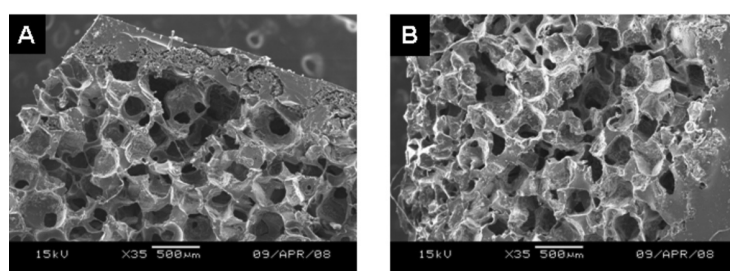


Figure 5. SEM images of salt-leached scaffolds from thermally cured PMS 1:2 (**A**) and PXS 1:2 (**B**). Bars represent 500 microns.

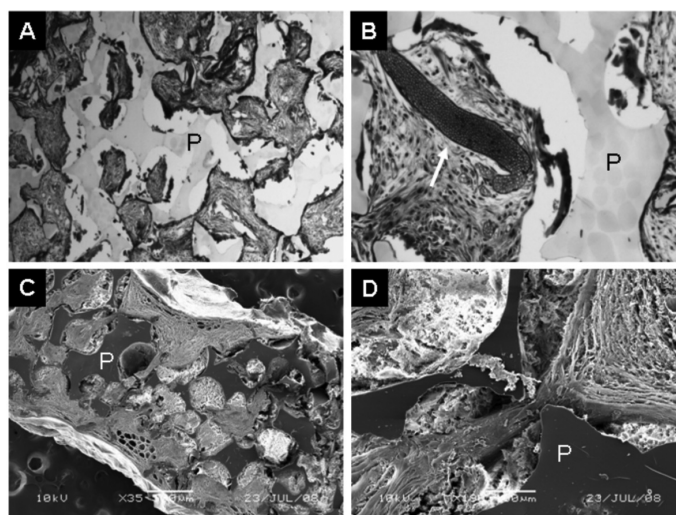


Figure 6. Representative Masson's trichrome staining images of salt-leached PXS 1:2 scaffolds, after 3 weeks of subcutaneous implantation at 2.5x (**A**) and 10x magnification (**B**). The white arrow in (**B**) points at a large blood vessel, grown into the scaffold. Representative SEM images of the same scaffolds in overview (bar represents 500 micron) (**C**), and in more detail (bar represents 100 micron) (**D**). P = polymer.

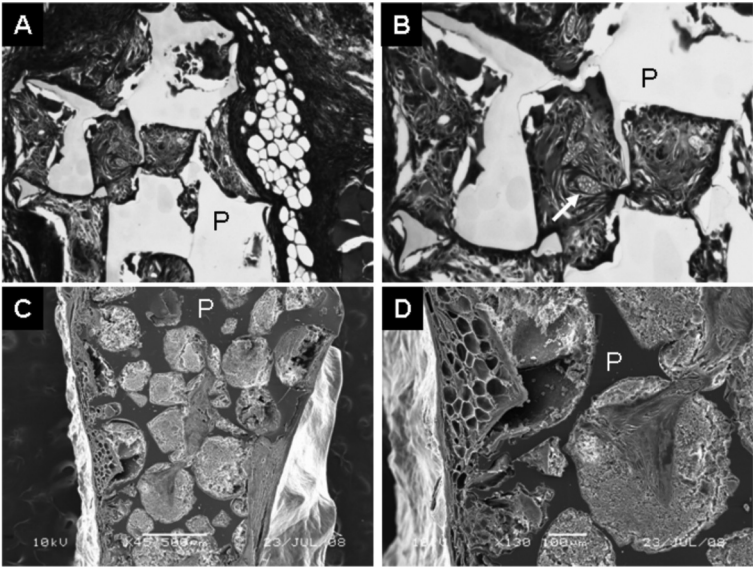


Figure 7. Representative Masson's trichrome staining images of salt-leached PMS 1:2 scaffolds, after 3 weeks of subcutaneous implantation at 2.5x (A) and 10x magnification (B). The white arrow in (B) points at a blood vessel, grown into the scaffold. Representative SEM images of the same scaffolds in overview (bar represents 500 micron) (C), and in more detail (bar represents 100 micron) (D). P = polymer.

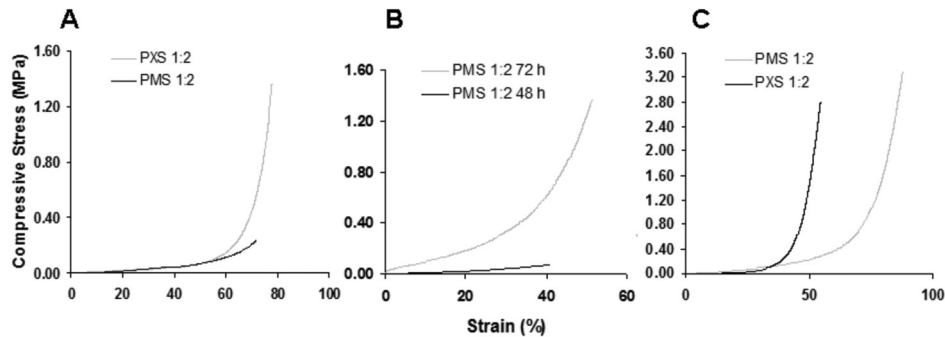


Figure 8. Representative compressive stress vs strain plots of (A) salt-leached PXS 1:2 and PMS 1:2 scaffolds (thermally cured for 48 hr), of (B) salt-leached PMS 1:2 scaffolds, cured for 48 and 72 hr, and (C) of ex vivo PMS 1:2 – and PXS 1:2 salt-leached scaffolds (both 72 hr thermally cured).

4. Conclusions

In this study, photopolymerized as well as thermally polymerized PPS polymers were successfully synthesized and characterized for the formation of biodegradable scaffolds for tissue engineering. This group of biomaterials as scaffolding materials can be further explored, modified and characterized.

5. Acknowledgements

JPB acknowledges financial support from the J.F.S. Esser Stichting and the Stichting Prof. Michaël-Van Vloten Fonds. This work was funded by NIH grant HL060435 and through a gift from Richard and Gail Siegal.

6. References

1. Langer R, Vacanti JP. Tissue engineering. *Science* 1993;260(5110):920-6.
2. Anderson DG, Tweedie CA, Hossain N, Navarro SM, Brey DM, Van Vliet KJ, Langer R, Burdick JA. A combinatorial library of photo-crosslinkable and degradable materials. *Adv Mater* 2006;18(19):2614-2617.
3. Bruggeman JP, Bettinger CJ, Nijst CLE, Kohane DS, Langer R. Biodegradable xylitol-based polymers. *Adv Mater* 2008;20(10):1922-7.
4. Bruggeman JP, De Bruin BJ, Bettinger CJ, Langer R. Biodegradable poly(polyol sebacate) polymers. *Biomaterials* 2008;29(36):4726-4735.
5. Wang Y, Ameer GA, Sheppard BJ, Langer R. A tough biodegradable elastomer. *Nat Biotechnol* 2002;20(6):602-606.
6. Wang Y, Kim YM, Langer R. In vivo degradation characteristics of poly(glycerol sebacate). *J Biomed Mater Res A* 2003;66(1):192-7.
7. Bruggeman JP, Bettinger CJ, Langer R. Biodegradable xylitol-based elastomers: in vivo behavior and biocompatibility. *J Biomed Mater Res A* 2010;95(1):92-104.
8. Bettinger CJ, Langer R, Borenstein JT. Engineering substrate topography at the micro- and nanoscale to control cell function. *Angew Chem Int Ed* 2009;48:5406-5415.
9. Bettinger CJ, Orrick B, Misra A, Langer R, Borenstein JT. Microfabrication of poly(glycerolsebacate) for contact guidance applications. *Biomaterials* 2006;27:2558-2565.
10. Chaikof EL, Matthew H, Kohn J, Mikos AG, Prestwich GD, Yip CM. Biomaterials and scaffolds in reparative medicine. *Ann N Y Acad Sci* 2002;961:96-105.
11. Gao J, Crapo PM, Wang Y. Macroporous elastomeric scaffolds with extensive micropores for soft tissue engineering. *Tissue Eng* 2006;12(4):917-925.

12. Lu L, Peter SJ, Lyman MD, Lai HL, Leite SM, Tamada JA, Uyama S, Vacanti JP, Langer R, Mikos AG. In vitro and in vivo degradation of porous poly(DL-lactic-co-glycolic acid) foams. *Biomaterials* 2000;21(18):1837-1845.
13. Fridrikh SV, Yu JH, Brenner MP, Rutledge GC. Controlling the fiber diameter during electrospinning. *Phys Rev Lett* 2003;90(14):144502.
14. Ifkovits JL, Padera RF, Burdick JA. Biodegradable and radically polymerized elastomers with enhanced processing capabilities. *Biomed Mater* 2008;3:34104.
15. Yi F, LaVan DA. Poly(glycerol sebacate) nanofiber scaffolds by core/shell electrospinning. *Macromol Biosci* 2008;8(9):803-806.
16. Nijst CLE, Bruggeman JP, Karp JM, Ferreira L, Zumbuehl A, Bettinger CJ, Langer R. Synthesis and characterization of photocurable elastomers from poly(glycerol sebacate). *Biomacromolecules* 2007;8(10):3067-3073.
17. Green JJ, Langer R, Anderson DG. A combinatorial polymer library approach yields insight into nonviral gene delivery. *Acc Chem Res* 2008, [Epub ahead of print].
18. Punyani S, Deb S, Singh H. Contact killing antimicrobial acrylic bone cements: preparation and characterization. *J Biomater Sci Polym Ed* 2007;18:131-145.
19. Gerecht S, Townsend SA, Pressler H, Zhu H, Nijst CLE, Bruggeman JP, Nichol JW, Langer R. A porous photocurable elastomer for cell encapsulation and culture. *Biomaterials* 2007;28(320):48264835.
20. Mahdavi A, Ferreira L, Sundback C, Nichol JW, Chan EP, Carter DJ, Bettinger CJ, Patanavanich S, Chignozha L, Ben-Joseph E, Galakatos A, Pryor H, Pomerantseva I, Masiakos PT, Faquin W, Zumbuehl A, Hong S, Borenstein J, Vacanti J, Langer R, Karp JM. A biodegradable and biocompatible gecko-inspired tissue adhesive. *Proc Natl Acad Sci U S A* 2008;105(7):2307-2312.
21. A. Svatos, S. B. Attygalle, Characterization of Vinyl-substituted, carbon-carbon double bonds by GC/FT-IR analysis. *Anal Chem* 1997;69(10):1827-1836.
22. Ranganath SH, Wang CH. Biodegradable microfiber implants delivering paclitaxel for postsurgical chemotherapy against malignant glioma. *Biomaterials* 2008;29(20):2996-3003.

Chapter 10

General discussion, conclusions

Joost P. Bruggeman, Steven E.R. Hovius, Robert Langer

The design of synthetic biodegradable polymers for bio-engineering purposes is challenging. The aim of this thesis was to develop a polymer platform, resulting in a family of tunable, biodegradable polymers that can meet demands on the physical properties including mechanical compliance and degradation rates, and the need for biocompatibility and low cytotoxicity. We have used straightforward polycondensation reactions between polyols and multi-functional carboxylic acids, yielding biodegradable Polyol-Based Polymers (PBPs). This thesis contains three parts: in the first part, polymer synthesis schemes of PBPs are described and polymers are characterized. In the second part, the in vivo behavior of some of the polymers that were described in the first part is investigated in more detail. The last and third part describes PBPs that are investigated for potential in vivo applications such as tissue engineering and peripheral nerve reconstruction.

Part 1 Polymer synthesis and characterization

1.1 Polyol-Based Polymers are composed of monomers endogenous to mammalian metabolism

As the current tissue engineering paradigm advocates biomimicry, scaffolds are designed to imitate the structural composition of the organ or tissue it is intended to replace or enhance. This approach resulted in novel materials over the last decades with biomimetic mechanical properties, surface chemistries, architectural structures and polymer compositions. Indeed, natural polymers such as collagen are therefore an obvious choice and successfully applied, despite the drawbacks as described in the introduction of this thesis. To bypass these drawbacks, the synthetic polymers studied in this thesis were designed to use monomers endogenous to the human metabolism with the purpose of biomimetic scaffold design.

We prepared polymers through polycondensation reactions of xylitol with sebacic or citric acid described in **Chapter 2** that are inert and composed of monomers that are endogenous to human metabolism. We focused on xylitol as an attractive biologically relevant monomer as it has an established history as a sweetener with proven anti-cariogenic activity [1]. Furthermore, it has an antimicrobial effect on upper airway infections caused by Gram positive streptococci [2,3]. Other endogenously produced polyols, such as sorbitol and mannitol, can be utilized for clinically relevant biodegradable polymers as well. Also, for its high functionality ($f = 9$), a non-endogenously produced monomer, maltitol, was included as a monomer in this platform. Maltitol is a man-made polyol of two endogenously produced alcohol monomers (sorbitol and glucose) covalently bound through an ether-bond. **Chapter 3** demonstrates that these polyol monomers, combined

with sebacic acid in different stoichiometric ratios, result in versatile elastomeric PBP platform that is biocompatible as well as degradable.

The use of molecules that are normally present in the human metabolism may offer a route to minimize toxic side effects, but does not result in superior biocompatibility per se. Additionally, the idea of incorporating metabolite monomers has been previously demonstrated in clinically applicable biodegradable α -hydroxy polyesters such as poly(lactic acid) (PLA). PLA is a perfect example of a polymer composed of a metabolite monomer with questionable biocompatibility. Therefore, with respect to biomimicry, other properties in addition to chemical composition are equally important (e.g. mechanical properties, degradation behavior, cellular attachment, and toxicity) to attain materials that are useful in biomedical applications. To achieve this, many polymer compositions using lactic acid as a starting material have therefore been engineered. Pego *et al.* described elastomers useful for tissue engineering based on co-polymerization of PLA with poly(1,3-trimethylene carbonate) (PTMC) polymers to obtain softer, elastomeric materials for the purpose of soft tissue engineering. These copolymers (PLTMC) demonstrated an impressive range of mechanical properties (Young's moduli ranging from 4–1100 MPa, T_g s from -9–33 °C), but displayed irreversible deformation upon elongation. Also, the co-polymer compositions displayed bulk hydrolysis upon degradation in vivo. Another copolymer of PLA with poly(ϵ -caprolactone) (PLCL), displayed similar disadvantageous bulk hydrolysis. Den Dunnen and co-workers developed this co-polymer for the purpose of peripheral nerve guidance and noticed the negative effect of bulk hydrolysis for small lumen polymer constructs based on this chemical composition [4]. Similar to PLTMC, PLCL polymers displayed a range of mechanical properties relevant for soft tissue engineering applications (Young's moduli 0.2 – 68 MPa). Nonetheless, ϵ -caprolactone and 1,3-trimethylene carbonate are not endogenous to the mammalian organism.

Many polymer compositions exist today with one metabolite monomer. Therefore PBPs will only be discussed with respect to other polymers composed of at least two monomers endogenous to the human metabolism that have been reported to date:

1. Poly(1,3-diamino-2-hydroxypropane-co-polyol sebacate) (APS)

Bettinger and co-workers have published the synthesis and characterization of APS elastomers, based on a similar synthesis scheme presented in this thesis [5-7]. An additional monomer with amine functionalities was included in the polycondensation reaction between glycerol and sebacic acid, resulting in thermoset polyester-amide elastomers. Including an amine functionality has several advantages, i.e. expanding the possible

chemical modification strategies for functionalization and forming poly(amide esters) that are less susceptible to biodegradation than polyesters. The mechanical properties are listed in **Table 1**.

Material	Metabolite monomers	Network type	Young's modulus (MPa)	Degradation rate (complete degradation)	Reference(s)
PGS	glycerol sebacic acid	Thermoset	0.282	In vivo: < 42d	Chapter 6, [14]
PBPs	xylitol, sorbitol, mannitol sebacic acid citric acid	Thermoset	0.006–378.0	In vivo: 10d–2yr	Chapter 5, [15, 16]
PGSA	glycerol sebacic acid	Thermoset	0.048–1.375	In vivo: 9–20wk	Chapter 6
APS	glycerol sebacic acid	Thermoset	2.45–4.24	In vivo: up to ~3yr	[5, 6]
PAOS	sorbitol sebacic acid	Thermoplastic	?	?	[8]
PGSu	glycerol succinic acid	Thermoset	?	?	[9]
PTK	glycerol ketoglutarate	Thermoset	0.1–657.4	In vitro: 2–28d	[10]
PGSG	glycerol sebacic acid	Thermoplastic	2.5–20	In vivo: 40–60d	[12]
RBP	ricinoleic acid sebacic acid	Thermoplastic	?	In vivo: ~21d	[11]

Table 1. Polymers composed of at least two monomers endogenous to the human metabolism at a glance.

2. Poly(adipic acid-co-octanediol-co-sorbitol) (PAOS)

These thermoplastic polyesters based on 1,8-octanediol and the metabolites sorbitol and adipic acid were described by Mei and co-workers [8]. In a bulk lipase-catalyzed polycondensation reaction, they investigated the effect of the molar fraction of sorbitol on the crystallinity of the linear poly(octanediol adipate) with molecular weights around 60,000-117,000 g/mol, but unfortunately do not investigate tensile properties of these polymers. They investigate contact angles and cellular biocompatibility, and demonstrated

that PAOS polymers are comparable to PCL in terms of hydrophobicity and cellular attachment as well as morphology.

3. Poly(glycerol succinate) (PGSu)

Grinstaff *et al.* developed biodendrimers based on succinic acid and glycerol by a stepwise synthesis using a protecting group, resulting in dendrimers of which the terminal functionality can be controlled (either acid or alcohol), and can be functionalized [9]. The primary goal seemed to obtain photocrosslinkable hydrogels based on these biodendrimers, for biomedical applications such as cartilage tissue engineering and repairing corneal wounds. Unfortunately, none of the publications using this material mention the mechanical properties of these photocrosslinkable hydrogels.

4. Poly(triol α -ketoglutarate) (PTK)

Thermal polycondensation reactions similar to the PBP synthesis described in this thesis has been used to achieve similar biodegradable elastomers. Using α -ketoglutaric acid as the reacting dicarboxylic acid resulted in polymers that contain ketones for functionalization (e.g. oxyamine conjugation with biologically relevant ligands) [10]. As multifunctional alcohol, glycerol, 1,2,4butanetriol and 1,2,6-hexanetriol were used. By altering the reacting alcohol monomer and varying the curing conditions, a wide range of mechanical properties was obtained (Young's moduli 0.1-657.4 MPa, ultimate strain 22-583%. See **Table 1**) In general, these elastomers degrade very rapidly (complete hydrolysis in 2 to 28 days in PBS), and were deemed biocompatible based on cellular attachment and proliferation.

5. Ricinoleic based polymers (RBP)

Several fatty acid based biodegradable polymers have been described by Domb's group [11]. These polymers constitute thermoplastic poly(anhydrides) with sebacic acid using melt condensation after the hydroxyl group in ricinoleic acid was transformed into a carboxyl group using succinic anhydride or maleic anhydride. These polymers have molecular weights ranging from 31,200 – 48,700 g/mol with acceptable polydispersity indexes and biocompatibility profiles. No mechanical testing is performed, as these polymers are developed for injectable drug delivery systems.

6. Poly(glycerol, sebacic acid, glycolic acid) (PGSG)

Sun and co-workers tried to alter the properties of PGS with the addition of glycolic acid in the thermal bulk condensation polymerization [12]. In contrast with PGS, PGSG elastomers

are thermoplastic. Adding glycolic acid in different molar ratios to glycerol and sebacic acid, elastomers were obtained that displayed different microstructures based on phase separation. Elastic moduli were calculated to be between 2.5 and 20 MPa as measured by nanoindentation. In addition, degradation rates *in vivo* were determined by intra-muscular placement of PGSG bars in rats, and ranged from 40 to 60 days *in vivo*. They further tested platelet adhesion and whole blood clotting time, and concluded that drug-eluting stents are a promising application for PGSG polymers. Some of the abovementioned polymers were produced in similar polycondensation reactions as the synthesis schemes reported in this thesis. Thus, apart from many possible (other) interesting alternatives for the reacting carboxylic acid monomers (e.g. dodecanedioic acid and traumatic acid) and polyol monomers (e.g. catechols, panthenol), as well as alcohol-acid monomers (e.g. ricinoleic acid and salicylic acid), straightforward co-polymerizing of all above mentioned polymers into new materials may be possible as well (e.g. a co-polymer of PXS and PTK). This allows for an extended PBP platform, displaying an even wider range of properties and composite materials. In 2008, Bruggeman *et al.* filed a patent application with an extensive list of possible polyols and polycarboxylic acids that can potentially yield interesting biodegradable polymers for medical applications [13].

The main conclusion is that a whole plethora of biodegradable, biomimetic biomaterials can be generated from a relatively simple synthesis scheme, based on metabolite monomers to create scaffolds for biomedical applications. These materials can be tailored to tune cell-cell or cell-biomaterial interactions, degradation rates as well as many more material properties.

1.2 Biodegradable Polyol-Based Polymers are elastomeric materials and can be engineered to meet a wide range of mechanical properties

As many tissues in the body have elastomeric properties, successful tissue engineering will require the use of compliant biodegradable scaffold materials [17]. In the last decade, synthetic biodegradable elastomers have been designed to match mechanical properties of natural tissues. The synthesis scheme described in this thesis allowed for randomly crosslinkable 3-D networks and a tunable degree of crosslinking, as well as hydrogen bond formation within the polymer backbone, ensuring elastomeric properties of the resulting polymers. The degree of crosslinking as well as extent of hydration of the polymer network proved to be important determinants for the mechanical properties of PBPs.

Hydrophilic polymers, and their crosslinked forms, known as hydrogels, are a class of biomaterials that have shown great potential for biological and medical applications

[18]. Polycondensation of xylitol with water soluble citric acid yielded biodegradable, water soluble pre-polymers, designated PXC. Methacrylation of this polymer resulted in an elastomeric photocrosslinkable hydrogel (PXCma hydrogels). The PXCma hydrogels presented in **Chapter 2** revealed elastomeric properties with compression moduli in the kPa range after equilibrium hydration, properties typically associated with hydrogels [17-19]. Although no application for the PXCma hydrogel is further investigated in this thesis, hydrogels are considered promising materials in tissue engineering and drug delivery. Hydrogels based on these monomers will be pursued in future research. Furthermore, as shown in this chapter, when xylitol reacts with a monomer that is not water soluble, such as sebacic acid, the resulting polymers are elastomers with Young's moduli in the MPa range.

The elastomeric PBPs described in **Chapter 3** revealed moduli ranging from hundreds of kPa to hundreds of MPa upon equilibrium hydration, as well as reversible compressions. Polymer properties changed by altering the stoichiometric ratio of the monomers. Sebacic acid monomer feeding ratios tuned 1) degree of crosslinking, 2) hydration of the polymer network and 3) cellular attachment. The degree of crosslinking is a determinant for thermal and mechanical properties of polymers. Altering processing conditions of thermally cured polymer networks has an effect on crosslink density and subsequently mechanical and thermal properties of thermoset elastomers such as PGS and PDC, but oddly enough, not their degradation rate [20-22]. Adjusting the stoichiometry of the polycondensation reaction (i.e. adding more sebacic acid monomers) allowed us to exceed the range of crosslink densities accessed by changing processing conditions. In addition, introducing more hydrophobic monomers in the polymer affected polymer hydration and degradation kinetics (the latter is discussed below). The PBP with the highest degree of crosslinking was obtained using maltitol and sebacic acid in a 1:4 molar ratio. This polymer displayed a high modulus (~ 0.4 GPa) and an elongation at break at approximately 10%, characterizing it as stiff and brittle under the conditions tested. However, this material is an amorphous elastomer in a glassy state at room – and physiological temperatures as the T_g was 46°C . As shown in **Chapter 3**, this PBP may be beneficial for tissue engineering applications for tissues with higher moduli (e.g. cartilage, bone). Another approach to alter crosslink density and subsequent thermal, mechanical and degradation properties is co-polymerization of different PBP pre-polymers (**Chapters 3**), or similar PBPs with different stoichiometries (**Chapter 5**). The resulting materials from this approach may result in more heterogeneous materials and can potentially decouple mechanical properties from degradation kinetics.

In conclusion, PBPs are biomimetic elastomers that can be tailored to have mechanical properties close to mechanical properties of human tissues and organs. The moduli and some ultimate strains are compared with human tissues and listed in **Table 2**.

1.3 Biodegradable Polyol-Based Polymers can be engineered to polymerize under ambient conditions

Our approach to polymerize PBPs under ambient conditions was to combine step growth polymerization (obtaining PBP pre-polymers) with radical-induced chain growth polymerization. This is demonstrated in **Chapter 2, 4 and 9** where the free hydroxyl groups within the PBP pre-polymer backbone were functionalized with acrylate groups resulting in acrylated PBPs (designated PXCma, PGSA or PXSA respectively) [23]. The acrylate groups were then polymerized in a second step, using a photoinitiator and exposure to UV-light (inducing chain growth polymerization), setting the acrylated pre-polymer into its given shape. The synthesis of acrylated PBP networks is not as straightforward as thermally cured PBPs, and requires multiple steps as well as the use of toxic solvents and reagents. Trace amounts of solvent and reagent can be found in the PGSA pre-polymers. However, in addition to the free radical induced polymerization process itself, this never appeared to be cytotoxic to stem cells that were incorporated within the polymer matrix during photopolymerization [35]. The major advantage of photopolymerization is better temporal and spatial control over the polymerization process as opposed to thermally polymerized PBPs. Thermally curing PBPs is performed in a vacuum oven for hours to days. Using photopolymerization, many more mold materials as well as shapes were readily accessible for PGSA and PXSA (**Figure 1**) [35,36]. Also, the modification of hydroxyl groups with acrylate groups introduced an additional way to control material properties: a higher degree of acrylation resulted in stiffer materials. As reported by Ifkovits *et al.* [19] but not investigated in this thesis, PGSA pre-polymer molecular weight proved to be important in the material properties of PGSA networks as well.

Part 2 Polymer in vivo degradation behavior and inflammation

Different in vivo applications may require different degradation kinetics. In tissue engineering, engineers aim to develop scaffolds that degrade at the same rate the cells within the scaffold generate their tissue specific extra-cellular matrix. Thus, the rate of degradation of the polymer should be tailored at the same rate of tissue growth within the scaffold. In addition to this challenging design criterium, another important factor is the characteristic of these polymers to co-exist with human tissues without causing an unacceptable degree of tissue damage and inflammation during degradation [37].

Material	Young's Modulus (MPa)	Ultimate Strain (%)	Reference(s)
PXCma	5.80×10^{-3} ^a	79.9 ^b	Chapter 2, [15]
PGSA	0.05 – 1.38	47.4 – 170	Chapter 4, [23]
PXS	0.82 – 5.33	205 – 33.1	Chapter 2, 3, [15], [16]
PSS	0.37 – 2.67	65.9 – 192	Chapter 3, [16]
PMS	2.21 – 12.8	50.0 – 50.5	Chapter 3, [16]
PMtS	378	10.9	Chapter 3, [16]
Bladder	0.25	0.69	[24]
Aortic valve	6.4 – 44.7	48.7 – 135	[25]
Intervertebrate disc	0.84 – 1.80 ^a	-	[26]
Knee cartilage	2.1 – 11.8	-	[27]
Cornea	2.87 – 3.40	-	[28]
Peripheral nerve	0.45 – 4.03	26.6 – 31.9	[29, 30]
Trabecular bone	50.0 – 100	-	[31]
Small artery	1.41	94.1	[32]
Malleolar ligament	1.11	48.0	[33]
Collagen fibers	100	50	[34]

Table 2. Mechanical properties of some PBPs and some human tissues. ^a Compression modulus. ^b Ultimate compression. The moduli of the human tissues listed here are accessible with the PBPs presented.

2.1 Biodegradable Polyol-Based Polymers can be tailored for a wide range of in vivo degradation rates

A few of the many possible PBPs have been studied for their degradation kinetics in this thesis: one PXCma hydrogel, four different PXS elastomers and three different PGSA formulations. As shown in **Chapters 2, 5 and 6**, PBPs can be tailored to degrade in vivo within days to years. For thermally cured PBPs, tailoring the rate of degradation is straightforward and was demonstrated by adjusting monomer ratios and by co-polymerization of different PBPs. Adding more hydrophobic crosslink entities in the polycondensation reaction of PXS elastomers yielded stiffer, but also more slowly degrading materials. This is shown in **Chapter 5** as well as **Figure 2A**. In addition, we demonstrated that introducing acrylate moieties on PGS resulted in a PGSA polymer of which the rate of degradation can be tuned (**Chapter 6**, and **Figure 2B**). This can be seen as an improvement over conventional, thermally cured PGS elastomers, which demonstrated rapid degradation in vivo, regardless of processing properties [14,22]. In addition, PGSA can be easily co-polymerized with acrylated molecules that are less susceptible to degradation, such as diacrylated PEG. Similar to the effect of increasing crosslink density by altering sebacic acid monomer feed ratio for PXS elastomers, increasing crosslink density by a higher degree of acrylation also

introduced more hydrophobic entities in the polymer backbone. Both increasing crosslink density as well as influencing contact angle and hydration are known to alter the rate of hydrolysis as well as enzymatic degradation of the polymer network *in vivo* [38,39].

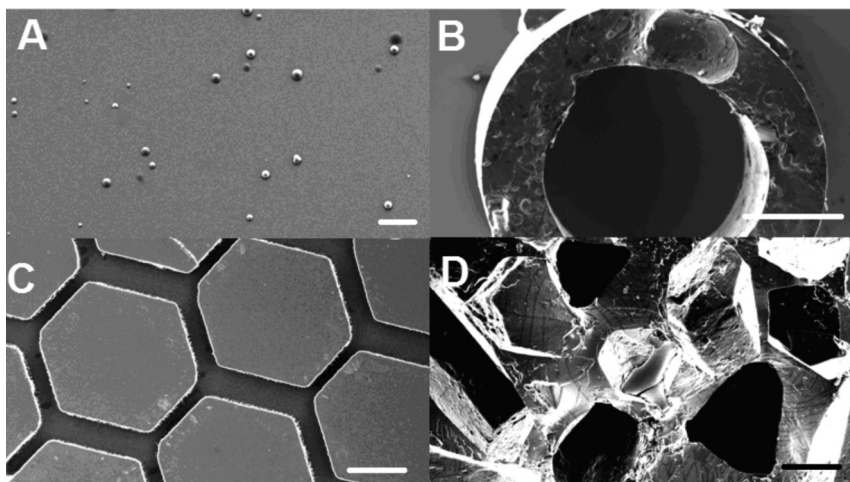


Figure 1. PGSA elastomers in different configurations: (A) microparticles (bar represents 20 μm), (B) a nerve conduit (bar represents 250 μm), (C) honeycomb network (bar represents 50 μm) and (D) a salt-leached scaffold (bar represents 150 μm).

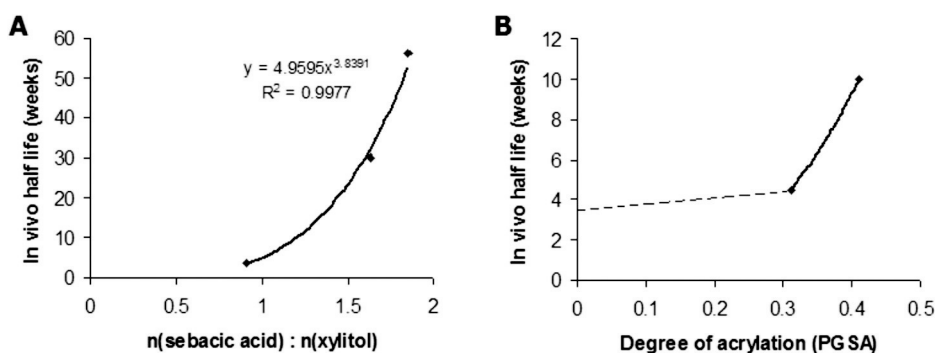


Figure 2. (A) Degradation rates for PXS 1:1, 2:3 and 1:2 depicted by plotting true polymer compositions as determined by ^1H -NMR versus *in vivo* half life. (B) The degree of acrylation increased *in vivo* half life for PGSA polymers. When there are no acrylates in the polymer backbone (thermally cured PGS), and the network is thermally cured, *in vivo* half life is approximately 3.5 weeks (dashed line).

2.2 Biodegradable Polyol-Based Polymers degrade in a biocompatible, predominantly surface eroding manner

As demonstrated in **Chapters 2, 3, 5, 6 and 7**, PBPs reveal acceptable foreign body responses in vivo, both in the acute inflammatory – as well as chronic inflammatory phase of wound healing: compared to the prevalent PLGA polymer, subcutaneous tissues in rats responded milder to PBPs (**Chapters 5 and 6**). Fibrous capsule thicknesses surrounding the implants were thinner for PBPs and, in the case of PXS elastomers, contained less activated macrophages in the acute and chronic wound healing response. Also, biodegradable PXS elastomers that were investigated for their suitability as peripheral nerve conduits, demonstrated a very mild tissue response from peripheral nerve and muscle tissues that were in contact with the PXS polymer (**Chapter 7**). This may be due to chemical composition of PXS elastomers. It is well known that utilizing short aliphatic acids as monomers for biodegradable polymers results in biocompatibility issues. This is most clearly demonstrated by inappropriate in vivo responses of clinically applied PLA devices developed for fracture fixation based on these monomers in the 1990s [40-42]. The unfavorable biocompatibility during degradation of these materials may be due to the chemical composition of the polymers (acidic byproducts of degradation harming the surrounding tissues) but may as well be related to characteristics of their degradation profile: large devices composed of bulk degrading polymers may cause a burst release of acidic by-products at end-stage degradation, causing harm to the surrounding tissues [37,43]. The degradation profile of PXS and PGSA elastomers seemed to be dominated by surface erosion, although some degree of bulk hydrolysis occurred as well. Interestingly, PBPs such as PSS and PMS demonstrated a more pronounced in vitro mass loss, indicating that these PBPs may be more susceptible to bulk hydrolysis than PGSA or PXS. However, PSS and PMS were not investigated for this behavior in vivo (**Chapter 3**). Based on morphological–, mechanical– and calorimetric studies during degradation, both degradation mechanisms seemed to occur during degradation of PXS and PGSA elastomers in vivo. We hypothesized however that the rate of bulk hydrolysis is too slow to have a dramatic effect, as compared to the rate of surface degradation (**Chapter 5, 6**). This surface degradation is most likely caused by enzymes, such as esterases (shown in [23]), proteases (shown in [5]) and lipases (demonstrated in [22]), cleaving the ester bonds in vivo. This mechanism is similar to polymeric devices composed of natural polymers such as collagen [44] that undergo enzymatic cleavage of specific sites. With their pre-dominantly surface eroding profile, PBPs demonstrated another important biomimetic property.

Part 3 In vivo applications of polyol-based polymers

3.1 Biodegradable Poly(xylitol sebacate) elastomers are promising materials for peripheral nerve reconstruction and regeneration

The PXS 1:1 elastomer was chosen as biomaterial for the development of peripheral nerve conduits. Biocompatibility analysis showed promising results for this elastomer in vitro with Schwann cells (SCs) in **chapter 7** and dorsal root ganglia cells (DRGs) in **chapter 8**), as well as in vivo (**Chapter 7**). The pilot study of PXS nerve conduits presented in chapter 7 is the first report of a PBP (including PGS) in an experimental animal model for disease to date. However, the decision of employing the 1:1 stoichiometry for the purpose of peripheral nerve reconstruction may have negatively influenced the performance of PXS nerve conduits: PXS conduits performed marginally better than commercially available PGA conduits in vivo, whereas non-degradable silicone conduits performed better than PXS conduits. We hypothesized that this was largely due to a loss of structural support by PXS 1:1 conduits to the fragile, regenerating nerve. PXS 1:1 is the fastest degrading PBP presented in this thesis, and therefore room exists to optimize PXS as a conduit material (**Table 3**).

Design criteria for peripheral nerve conduits [45-52]	PGA	PDLLC	Collagen	PXS
1. Non-toxic	☹	☹	☺	☺
2. Non-immunogenic	☺	☺	☹	☺
3. Biodegradable	☺	☺	☺	☺
4. Maintain form stability and structural integrity upon hydration and degradation	☹	☹	☺	☺
5. Readily tunable in vivo degradation rate	☺	☺	☹	☺
6. Mechanically match nerve and soft tissue surroundings	☹	☹	☹	☺
7. Soft enough for micro-sutures, strong enough to hold sutures	☹	☹	☹	☺
8. Allow for nerve growth stimulating factors such as				
a. micropatterned walls	☹	☹	☺	☺
b. (micro)porous walls	☺	☹	☺	☹
c. controlled release of growth-stimulating factors	☹	☹	☹	☹
9. Allow for direct SC attachment, migration and proliferation	☺	☹	☺	☺

Table 3. Important design criteria compared for commercially available and PXS peripheral nerve conduits. PGA (Neurotube ©), poly((D,L)-lactide-co-ε-caprolactone) (PDLLC, Neurolac ©) and collagen (NeuraGen © or NeuroMatrix ©) are currently the biodegradable polymers of choice for peripheral nerve conduits in clinical practice.

3.2 Biodegradable Polyol-Based Polymer scaffolds may be useful for tissue engineering

Extra-cellular matrices such as basement membranes and proteins such as collagen exhibit nanometer-scale structural cues for cells within a tissue to interact directly with cells within that tissue [53,54]. Tissue engineers have demonstrated that cellular behavior such as attachment, adhesion, morphology, proliferation and migration are affected by nano- and micropatterned gratings on polymer films. We therefore developed nanograted PXS elastomeric films for the purpose of nerve regeneration. PXS elastomers were readily functionalized with nanotopography using the replica-molding technique and demonstrated contact guidance during in vitro peripheral nerve regeneration, as well as in vivo contact guidance properties (**Chapter 8**). However, it remains a challenge to fabricate 3D structures relevant for an experimental model of nerve reconstruction and evaluate the importance of nanograted tubes in peripheral nerve reconstruction.

Thermoplastic polymers are more readily processed into polymer scaffolds than thermoset polymers such as PBPs. PXS and PMS were evaluated in two other 'classic' techniques for the production of scaffolds in this thesis: electrospinning and salt-leaching (**Chapter 9**). To obtain more biomimetic scaffolds, we electrospun PXS. For this purpose, acrylated PXS (PXSA) was developed, similar to PGSA. However, it was not possible to electrospin PXSA fibers without the use of a carrier polymer (PLGA in this case). Potentially, another hypothetical polyol based, linear, diacrylated polymer of poly(catechol sebacate), or PEG diacrylate could have better been used as a carrier polymer that can be incorporated within the PXSA backbone. In contrast, the production of classic salt-leached porous scaffolds of PXS and PMS polymers was effortless and resulted in classical, biocompatible, useful PBP scaffolds for their use in tissue engineering.

Drawbacks of Polyol-Based Polymers

Thermoset polymers assume a permanent shape and cannot be reshaped once cured in that specific shape. Thermoplastic polymers however, such as PLGA, can be extruded into fibers to weave polymer mats, sutures, or compression molded into different shapes, as well as (re)dissolved in organic solvents to obtain nano- or microparticles for drug delivery as well as allow for other processing techniques such as electrospinning. With thermoset PBPs this is not as straightforward and requires solid engineering as well as creativity to obtain useful devices composed of these polymers.

Another disadvantage of PBPs is the time required to thermally cure and set the polymer into a desired shape. This process takes hours to days in a vacuum oven.

Microwave-assisted polycondensation may shorten curing times dramatically without sacrificing mechanical and other material properties [55]. Also, in our synthesis scheme, only compatible and accessible melting temperatures can be used for the monomers, as they are bulk polymerized in a melt, excluding monomers such as aminoacids and monomers that caramelize at their melting temperatures (e.g. sugars). Other polymerization techniques such as interfacial polymerization may be applied to obtain interesting PBP substrates as well.

Future directions

The general conclusion of this thesis is that polyol-based polymers as displayed herein can be tuned as useful biomaterials for a whole plethora of biomedical applications. Most of the effort in this thesis focused on synthesizing and characterizing these new polymers, and included brief studies on peripheral nerve conduits as well as developing tissue engineering scaffolds. However, we propose to optimize, as well as develop these materials for the following biomedical applications:

Polymer synthesis and characterization

- In situ crosslinkable poly(polyol dicarboxylic anhydride)s may be useful as bone cement, or
- biodegradable putty for transdermal tissue augmentation, etc.
- Microwave assisted polycondensation may dramatically shorten curing times of PBPs
- Functionalize PXC pre-polymers with aldehydes and dihydrazides to obtain in situ crosslinkable hydrogels

Polymer characterization in vivo

- Degradation rates and profile for PMS and PMtS polymers, as well as other PBPs,
- Degradation rates and profiles of in situ crosslinkable hydrogels based on PBPs.

PXS as peripheral nerve conduits

- Develop PXS 2:3 and 1:2 porous nerve conduits.
- Develop PXSA nerve conduits containing longitudinal nanotopography.
- Develop PXSA drug eluding conduits (e.g. FK506, neurotrophic factors, etc).
- Determine in vitro degradation with esterases of these conduits before applying them in an in vivo nerve reconstruction model.

PBPs for other biomedical applications

- Develop porous PMS 1:2 meshes for abdominal wall reconstruction.
- Develop porous PMS 1:2 scaffolds for cartilage tissue engineering purposes.
- Further develop and investigate phase-separated microparticles from PBP pre-polymers.
- Develop similar particles from acrylated pre-polymers.
- Develop in situ crosslinkable hydrogels for intra-articulate injections.

Many more experiments and applications can be listed here. PBPs are therefore a versatile tool in the field of tissue engineering and may function as a platform to rationally design biomimetic materials for various biomedical applications.

References

1. Honkala E, Honkala S, Shyama M, Al-Mutawa SA. Field trial on caries prevention with xylitol candies among disabled school students. *Caries Res* 2006;40(6):508-513.
2. Durairaj L, Launsbach J, Watt JL, Mohamad Z, Kline J, Zabner J. Safety assessment of inhaled xylitol in subjects with cystic fibrosis. *J Cyst Fibros* 2007;6(1):31-34.
3. Uhari M, Kontiokari T, Koskela M, Niemelä M. Xylitol chewing gum in prevention of acute otitis media: double blind randomised trial. *BMJ* 1996;313(7066):1180-1184.
4. Den Dunnen WF, Van der Lei B, Robinson PH, Holwerda A, Pennings AJ, Schakenraad JM. Biological performance of a degradable poly(lactic acid-epsilon-caprolactone) nerve guide: influence of tube dimensions. *Journal of biomedical materials research* 1995;29(6):757-766.
5. Bettinger CJ, Bruggeman JP, Borenstein JT, Langer R. In vitro and *in vivo* degradation of poly(1,3-diamino-2-hydroxypropane-co-polyol sebacate) elastomers. *J Biomed Mater Res A* 2009;91(14):1077-1088.
6. Bettinger CJ, Bruggeman JP, Borenstein JT, Langer RS. Amino alcohol-based degradable poly(ester amide) elastomers. *Biomaterials* 2008 May;29(15):2315-2325.
7. Bettinger CJ, Kulig KM, Vacanti JP, Langer R, Borenstein JT. Nanofabricated collagen-inspired synthetic elastomers for primary rat hepatocyte culture. *Tissue Eng* 2009 Jun;15(6):1321-1329.
8. Mei Y, Kumar A, Gao W, Gross R, Kennedy SB, Washburn NR, *et al.* Biocompatibility of sorbitol-containing polyesters. Part I: Synthesis, surface analysis and cell response in vitro. *Biomaterials* 2004;25:4195-4201.
9. Grinstaff MW. Biodendrimers: New polymeric biomaterials for tissue engineering. *Chem Eur J* 2002;8:2839-2846.
10. Barrett DG, Yousaf MN. Poly(triol alpha-ketoglutarate) as biodegradable, chemoselective, and mechanically tunable elastomers. *Macromolecules* 2008;41:6347-6352.
11. Teonim D, Nyska A, Domb AJ. Ricinoleic acid-based biopolymers. *J Biomed Mater Res A* 1999;45:258-267.
12. Sun ZJ, Wu L, Huang W, Chen C, Chen Y, Lu XL, *et al.* Glycolic acid modulates the mechanical property and degradation of poly(glycerol, sebacate, glycolic acid). *J Biomed Mater Res A* 2009;92(1):332-9.
13. Bruggeman JP, Nijst CL, Kohane DS, Langer R, inventors. Polyol-based polymers, 2008.

14. Wang Y, Kim YM, Langer R. In vivo degradation characteristics of poly(glycerol sebacate). *Journal of biomedical materials research* 2003 Jul 1;66(1):192-197.
15. Bruggeman JP, Bettinger CJ, Nijst CL, Kohane DS, Langer R. Biodegradable xylitol-based polymers. *Adv Mater* 2008;20(10):1922-1927.
16. Bruggeman JP, J. DBB, Bettinger CJ, Langer R. Biodegradable poly(polyol sebacate) polymers. *Biomaterials* 2008;29(36):4726-4735.
17. Wang Y, Ameer GA, Sheppard BJ, Langer R. A tough biodegradable elastomer. *Nature biotechnology* 2002 Jun;20(6):602-606.
18. Peppas NA, Hilt JZ, Khademhosseini A, Langer R. Hydrogels in Biology and Medicine: From Molecular Principles to Bionanotechnology. *Adv Mater* 2006;18:1345-1360.
19. Ifkovits JL, Padera RF, Burdick JA. Biodegradable and radically polymerized elastomers with enhanced processing capabilities. *Biomedical materials (Bristol, England)* 2008 Sep;3(3):034104.
20. Yang J, Webb AR, Ameer GA. Novel Citric Acid-Based Biodegradable Elastomers for Tissue Engineering. *Adv Mater* 2004;16(6): 511-516.
21. Yang J, Webb AR, Pickerill SJ, Hageman G, Ameer GA. Synthesis and evaluation of poly(diol citrate) biodegradable elastomers. *Biomaterials* 2006 Mar;27(9):1889-1898.
22. Pomerantseva I, Krebs N, Hart A, Neville CM, Huang AY, Sundback CA. Degradation behavior of poly(glycerol sebacate). *J Biomed Mater Res A* 2008;91(4):1038-47.
23. Nijst CL, Bruggeman JP, Karp JM, Ferreira L, Zumbuehl A, Bettinger CJ, *et al.* Synthesis and characterization of photocurable elastomers from poly(glycerol-co-sebacate). *Biomacromolecules* 2007 Oct;8(10):3067-3073.
24. Dahms SE, Piechota HJ, Dahiya R, Lue TF, Tanagho EA. Composition and biomechanical properties of the bladder acellular matrix graft: Comparative analysis in rat, pig, and human. *Br J Urol* 1998;82:411-419.
25. Sung HW, Chang Y, Chiu CT, Chen CN, Liang HC. Mechanical properties of a porcine aortic valve fixed with a naturally occurring crosslinking agent. *Biomaterials* 1999;20:1759-1772.
26. Skrzypiec DM, Pollintine P, Przybyla A, Dolan P, Adams MA. The internal mechanical properties of cervical intervertebral discs as revealed by stress profilometry. *Eur Spine J* 2007;16:1701-1710.
27. Shepherd DET, Seedhom BB. The 'instantaneous' compressive modulus of human articular cartilage in joints of the lower limb. *Rheumatology* 1999;38:124-132.
28. Hjortdal JO. Regional Elastic Performance of the Human Cornea. *J Biomech* 1996;29(7):931-942.
29. Rydevik BL, Kwan MK, Myers RR, Brown RA, Triggs KJ, Woo SL, *et al.* An in vitro mechanical and histological study of acute stretching on rabbit tibial nerve. *J Orthop Res* 1990;8(5):694-701.
30. Borschel GH, Kia KF, Kuzon WM, Dennis RG. Mechanical properties of acellular peripheral nerve. *J Surg Res* 2003;114(2):133-139.
31. Anseth KS, Shastri VR, Langer R. Photopolymerizable degradable polyanhydrides with osteocompatibility. *Nature biotechnology* 1999;17:156-159.
32. Clerin V, Nichol JW, Petko M, Myung RJ, Gaynor JW, Gooch KJ. Tissue engineering of arteries by directed remodeling of intact arterial segments. *Tissue engineering* 2003;9(3):461-472.
33. Cheng T, Gan RZ. Mechanical properties of anterior malleolar ligament from experimental measurement and material modeling analysis. *Biomechan Model Mechanobiol* 2008;7(5):387-394.
34. Chandran KB. *Cardiovascular Biomechanics*. New York, NY, USA: New York University Press, 1992.
35. Gerecht S, Townsend SA, Pressler H, Zhu H, Nijst CL, Bruggeman JP, *et al.* A porous photocurable elastomer for cell encapsulation and culture. *Biomaterials* 2007 Nov;28(32):4826-4835.

36. Mahdavi A, Ferreira L, Sundback C, Nichol JW, Chan EP, Carter DJ, *et al.* A biodegradable and biocompatible gecko-inspired tissue adhesive. *Proceedings of the National Academy of Sciences of the United States of America* 2008 Feb 19;105(7):2307-2312.
37. Williams DF. On the mechanisms of biocompatibility. *Biomaterials* 2008 Jul;29(20):2941-2953.
38. Amsden B. Curable, biodegradable elastomers: emerging biomaterials for drug delivery and tissue engineering. *Soft Matter* 2007;3:1335-1348.
39. Pitt CG, Hendren RW, Schindler A, Woodward SC. The enzymatic surface erosion of aliphatic polyesters. *J Control Release* 1984;1:3-14.
40. Bergsma JE, de Bruijn WC, Rozema FR, Bos RR, Boering G. Late degradation tissue response to poly(L-lactide) bone plates and screws. *Biomaterials* 1995 Jan;16(1):25-31.
41. Bostman O, Hirvensalo E, Makinen J, Rokkanen P. Foreign-body reactions to fracture fixation implants of biodegradable synthetic polymers. *The Journal of bone and joint surgery* 1990 Jul;72(4):592-596.
42. Bostman OM. Reaction to biodegradable implants. *The Journal of bone and joint surgery* 1993 Mar;75(2):336-337.
43. Middleton JC, Tipton AJ. Synthetic biodegradable polymers as orthopedic devices. *Biomaterials* 2000;21:2335-2346.
44. Nair LS, Laurencin CT. Biodegradable polymers as biomaterials. *Prog Polym Sci* 2007;32:762-798.
45. Dahlin LB, Lundborg G. Use of tubes in peripheral nerve repair. *Neurosurg Clin N Am* 2001;12(2):341-352.
46. Den Dunnen WFA, Stokroos I, Schakernraad JM, Zondervan GJ, Pennings AJ, Van der Lei B, *et al.* A New PLLA/PCL Copolymer for Nerve Regeneration. *J Mater Sci Mater Med* 1993;4:521-525.
47. Harley BA, Spilker MH, Wu JW, Asano K, Hsu HP, Spector M, *et al.* Optimal degradation rate for collagen chambers used for regeneration of peripheral nerves over long gaps. *Cells Tissues Organs* 2004;176(1-3):153-165.
48. Hoppen HJ, Leenslag JW, Pennings AJ, Van der Lei B, Robinson PH. Two-ply biodegradable nerve guide: basic aspects of design, construction and biological performance. *Biomaterials* 1990;1990(11):286-290.
49. Mackinnon SE, Dellon AL. Clinical Nerve Reconstruction with a Bioabsorbable Poly(glycolic acid) Tube. *Plast Reconstr Surg* 1990;85:419-424.
50. Pêgo AP, Poot AA, Grijpma DW, Feijen J. Copolymers of trimethylene carbonate and ε-caprolactone for porous nerve guides: Synthesis and properties. *J Biomater Sci Polymer Edn* 2001;12(1):35-53.
51. Lundborg G, Rosén B, Dahlin L, Danielsen N, Holmberg J. Tubular versus conventional repair of median and ulnar nerves in the human forearm: early results from a prospective, randomized, clinical study. *J Hand Surg Am* 1997;22(1):99-106.
52. Meek MF, Coert JH. US Food and Drug Administration/Conformit Europe-Approved Absorbable Nerve Conduits for Clinical Repair of Peripheral and Cranial Nerves. *Ann Plast Surg* 2008;60:110-116.
53. Goodman SL, Sims PA, Albrecht RM. Three-dimensional extracellular matrix textured biomaterials. *Biomaterials* 1996;17(21):2087-2095.
54. Bettinger CJ, Langer R, Borenstein J. Engineering substrate topography at the micro- and nanoscale to control cell function. *Angew Chem Int Ed* 2009;48:5406-5415.
55. Wiesbrock F, Hoogenboom R, S. SU. Microwave-assisted polymer synthesis: State-of-the-art and future perspectives. *Macromol Rapid Commun* 2004;25:1739-1764.

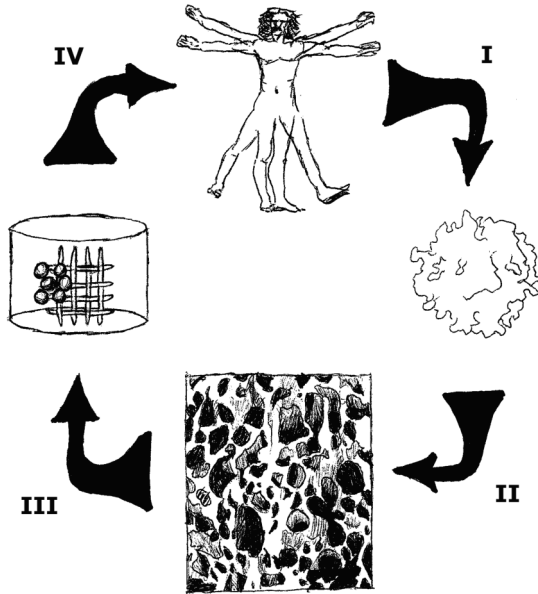
Chapter 11

Dutch Summary/ Nederlandse samenvatting

Joost P. Bruggeman, Steven E.R. Hovius

In dit proefschrift is getracht een materiaalkundige bijdrage te leveren aan het gebruik van biomaterialen. Biomaterialen worden steeds belangrijker in verschillende takken van biomedische technologie, waaronder *tissue engineering*. *Tissue engineering* is een technologie die gebruik maakt van medische, biologische en materiaalkundige principes in de (re)generatie van nieuw weefsel, ter reconstructie van weefsels of organen die door ziekte of trauma verloren zijn gegaan [Langer R, Vacanti JP. *Tissue engineering*. Science 1993;260(5110):920-6]. In het kort worden in *tissue engineering* lichaamseigen (stam)cellen gecombineerd met plastic materialen (polymeren) waarop cellen gegroeid of geïntegreerd kunnen worden. Deze cellen kunnen zich met behulp van deze polymeren organiseren in een nieuw, rudimentair weefsel of orgaan. Deze combinatie van cellen en ondersteunende plastics kunnen dan in kweek (in vitro) verder uitgerijpt worden en op het juiste moment in het lichaam teruggeplaatst worden (in vivo) voor integratie en ontwikkeling tot het gewilde weefsel of orgaan (**Figuur 1**). De materialen die hiervoor ontwikkeld worden, zijn doorgaans biodegradeerbare polymeren, dat wil zeggen dat deze plastics oplossen in het lichaam. De snelheid waarmee het polymeer degraderen moet, is afhankelijk van veel factoren. De cellen van het beoogde weefsel of orgaan moeten bijvoorbeeld het polymeer op tijd kunnen vervangen met polymeren die de cellen zelf produceren en de cellen structuur en steun geven. Idealiter degradeert het polymeer met dezelfde snelheid als de cellen zelf materialen produceren. De natuurlijke polymeren die de cellen zelf kunnen aanmaken om steun te geven aan hun omgeving zijn onder andere eiwitten zoals collagenen en polymeren op basis van suikers zoals hyaluronzuur.

Logischerwijs worden natuurlijke polymeren zoals collagenen of hyaluronzuren zeer vaak toegepast voor *tissue engineering* en andere biomedische applicaties, alleen worden deze materialen geoogst uit dieren of geproduceerd door bacteriën. Dit leidt helaas tot moeilijk controleerbare materiaaleigenschappen en kunnen deze materialen zelfs ongewilde afweerreacties tot gevolg hebben. Om deze redenen zijn sinds hun introductie in de jaren 1970 synthetische afbreekbare polymeren als afbreekbare hechtmaterialen erg in trek geraakt. Het grote voordeel van synthetische polymeren is de mate van controle op materiaaleigenschappen zoals mechanische eigenschappen, de snelheid waarmee het afbreekt in het lichaam, de mate waarin cellen er zich op of in kunnen huisvesten, etc. Echter, aan synthetische materialen kleven ook nadelen: een essentiële vereiste voor biomaterialen is gunstige biocompatibiliteit. *Biocompatibiliteit* verwijst naar de capaciteit van een biologisch materiaal om zijn gewenste functie met betrekking tot een medische therapie uit te oefenen, zonder het onthullen van enige ongewenste lokale of systemische gevolgen in de ontvanger of de begunstigde van die therapie, maar het produceren van



Figuur 1. De kern principes van *tissue engineering*. In de eerste stap (I), worden (stam)cellen geoogst uit de patiënt. Na de in vitro expansie en/ of differentiatie worden de cellen in de tweede stap (II) op een bioafbreekbare polymeren construct gezaaid. Dit wordt vaak gevolgd door een incubatie in een bioreactor (stap III). Dit staat het met cellen bezaaide construct toe in vitro te rijpen voor de implantatie in de patiënt (stap IV), waarbij het in vitro gekweekte weefsel het beschadigde weefsel vervangt.

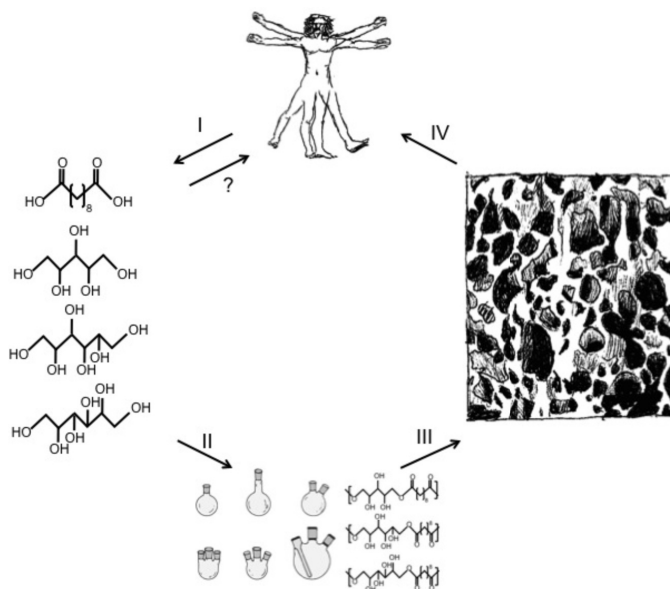
de meest aangewezen voordelige cellulaire of weefselreactie in die specifieke situatie, en de klinisch relevante prestaties van die therapie te optimaliseren [David F. Williams. On the mechanisms of biocompatibility. *Biomaterials*, 29(20):294153]. Dit kan dus helaas in ongunstige gevallen gepaard gaan met veel lokale of systemische schade aan het lichaam. Bijvoorbeeld, synthetische polymeren gemaakt van melkzuur (*poly(lactic acid)* (PLA)) zijn harde materialen die uit elkaar vallen in zure afvalproducten die de omringende weefsels en cellen kunnen beschadigen. Hoewel dit materiaal tegenwoordig veel gebruikt wordt in de geneeskunde, is PLA niet ideaal voor *tissue engineering* van (zachte) weefsels of organen waarbij een aanzienlijk volume van dit materiaal gebruikt moet worden. Veel *tissue engineers* proberen daarom synthetische polymeren te ontwikkelen die zoveel mogelijk op het beoogde weefsel of orgaan moet lijken, m.a.w. de eigenschappen van natuurlijke weefsels zoveel mogelijk te imiteren. Dit heeft er toe geleid dat in de laatste decennia veel elastische materialen ontwikkeld zijn met verschillende degradatie snelheden. Hoewel deze materialen veelbelovend zijn, zijn ze vaak gebaseerd op moleculen die lichaamsvreemd

zijn, en kunnen een voor synthetisch materiaal typerend degradatiegedrag vertonen: door het gehele plastic heen vallen de verbindingen tussen de afzonderlijke moleculen (de monomeren) uit elkaar, op basis van hydrolyse. Kort gezegd leidt dit ertoe dat gedurende de degradatie het synthetische polymeer steeds slapper wordt, en kan gaan deformeren onder druk van de omliggende weefsels. Polymeren zoals collagenen worden op een andere manier afgebroken in het lichaam: door het werk van enzymen worden constructen van collagenen langzaam dunner, en blijven deze vorm-stabiel gedurende de degradatie in vergelijking met de polymeren die op basis van hydrolyse afbreken. Kortom, er kleven zowel voordelen als nadelen aan natuurlijke polymeren zoals collageen, en dit geldt ook voor synthetische polymeren zoals PLA. Idealiter zouden voordelen van natuurlijke en synthetische polymeren gecombineerd moeten worden, terwijl de nadelen vermeden worden.

Dit is getracht in dit proefschrift, waarbij we, in plaats van complete polymeren zoals collagenen uit bijvoorbeeld koeien te isoleren, individuele monomeren hebben gekozen uit het menselijk metabolisme (**Figuur 2**). Suikers en vetzuren, of zuren uit de citroenzuurcyclus, zijn in dit proefschrift als *proof of principle* gebruikt. Het was bedoeling om hiermee materialen te ontwikkelen die:

1. compleet gemaakt zijn van monomeren die reeds in het lichaam aanwezig zijn en dus weer gemetaboliseerd kunnen worden wanneer het polymeer afbreekt
2. in principe elastisch zijn
3. wel of niet water oplosbaar kunnen zijn
4. gemaakt kunnen worden onder fysiologische omstandigheden
5. een controleerbare variatie hebben t.a.v. mechanische eigenschappen
6. een controleerbare variatie hebben t.a.v. degradatie snelheden
7. een gunstig degradatiegedrag vertonen zoals collageen
8. bruikbaar kunnen zijn als materiaal voor *tissue engineering* en perifere zenuwreconstructie als een bioafbreekbare plastic buis?

In het eerste deel van dit proefschrift, worden polyol-gebaseerde polymeren, ofwel 'PBP' (*Polyol-Based Polymers*) genaamd, beschreven en gekarakteriseerd. Deze polymeren worden verkregen door een polycondensatie reactie (een combinatie van een hoge temperatuur en vacuüm op een gesmolten mengsel van suikers en zuren) verkregen.



Figuur 2. De kern principes van *biodegradable polyol-based polymers*. De mens produceert dagelijks grote hoeveelheden van de monomeren welke gebruikt zijn in dit proefschrift (I). Daarvan kunnen in het laboratorium polymeren van gemaakt worden, door gebruik te maken van eenvoudige chemische reacties (II). Deze polymeren kunnen dan in verschillende configuraties gemaakt worden (III) om zo een bepaalde, tijdelijke functie in het menselijk lichaam te vervullen na implantatie (IV). Vervolgens degradeert het polymeer in het menselijk lichaam en geeft wederom dezelfde monomeren die het lichaam reeds dagelijks aanmaakt, af (I). Het is de vraag of deze metabolieten ook daadwerkelijk in het menselijk metabolisme wordt opgenomen (?).

Hoofdstuk 2 beschrijft een polymeren platform op basis van xylitol als suiker, waarmee bioafbreekbare hydrogels (elastische, hydrofiele polymeren) en elastomeren (elastische, niet water oplosbare polymeren) verkregen kan worden wanneer je het polymeriseert met citroenzuur of kurkzuur, respectievelijk. De mechanische eigenschappen en degradatie snelheid van de poly(xylitol sebacinezuur), of kortweg PXS, elastomeren kan simpelweg worden gereguleerd op basis van de molaire ratios van xylitol en sebacinezuur (of kurkzuur) in de polycondensatie reactie. Dit idee wordt verder uitgewerkt in **Hoofdstuk 3**, waarbij we andere suikers, zoals sorbitol, mannitol en ook maltitol laten reageren met sebacinezuur in verschillende molaire ratios. Dit resulteerde in materialen met mechanische eigenschappen die overeenkomen met veel weefsels van het menselijk lichaam: bijvoorbeeld zachte en elastische weefsels zoals kleine bloedvaten, spier- en zenuwweefsel, maar ook weefsels die veel harder edoch elastisch zijn, zoals kraakbeen en bot. Deze nieuwe polymeren zijn afbreekbaar en blijken een gunstige biocompatibiliteit te hebben wanneer deze subcutaan

(onder de huid) in ratten worden geplaatst en histologisch geëvalueerd na 10 dagen en 12 weken. Tevens kunnen op sommige van deze plastics cellen specifiek voor vaten, spier-, kraakbeen- en botweefsel worden opgegroeid. Dat betekent dat deze polymeren interessant zijn voor het *tissue engineer*-en van deze weefsels. Om te demonstreren dat deze polymeren ook gevormd kunnen worden onder fysiologische omstandigheden (en niet alleen maar door middel van hoge temperaturen en vacuüm), veranderen we met een chemische reactie de alcohol groepen van de suikers aanwezig in deze polymeren. In **Hoofdstuk 4** laten we zien dat het reeds in 2002 beschreven poly(glycerol sebacinezuur) (PGS), gemaakt van de polyol glycerol en sebacinezuur, dat met behulp van acryloyl chloride uitgerust wordt met vinylgroepen, kan polymeriseren onder invloed van ultraviolet licht. Door in meer- of mindere mate vinylgroepen te hebben in het polymeer, bestaat er een mogelijkheid de mechanische eigenschappen van dit door licht te polymeriseren materiaal, genaamd PGSA, te bepalen. We laten verder zien dat dit materiaal een gunstige in vitro biocompatibiliteit heeft.

Het tweede deel van het proefschrift beschrijft het in vivo gedrag van PXS en PGSA elastomeren. Deze polymeren lijken bij voorkeur door (waarschijnlijk) enzymen afgebroken te worden, en in veel mindere mate door hydrolyse. Vier PXS elastomeren zijn onderzocht in **Hoofdstuk 5**, waarbij het duidelijk werd dat de snelst afbreekbare PXS elastomeer (molaire ratio xylitol:sebacinezuur 1:1) een halfwaardetijd had van ongeveer 3-4 weken, en de minst snel afbreekbare elastomeer een halfwaardetijd van 52 weken had (molaire ratio xylitol:sebacinezuur 1:2). Vergeleken met een in de kliniek zeer gangbaar polymeer, *poly(lactic-co-glycolic acid)*, of PLGA, toonden de PXS elastomeren een gunstigere biocompatibiliteit ten aanzien van de dikte van het fibrotische kapsel om het polymeer, alsook de hoeveelheid geactiveerde macrofagen (bepaalt type afweercel) in dit kapsel. **Hoofdstuk 6** laat zien dat de PGSA elastomeren ook een variabele degradatiesnelheid hebben op basis van de hoeveelheid vinylgroepen die er zijn toegevoegd. Zonder vinylgroepen, dus 'gewoon' PGS, heeft een halfwaardetijd van ongeveer 3 weken. Echter, door de andere manier van polymeriseren (middels de vinyl-groepen) en de hoeveelheid vinylgroepen, kon de degradatie snelheid van PGSA worden bepaald: de halfwaardetijd liep op tot ongeveer 10 weken wanneer 41% van alle glycerol moleculen in PGS uitgerust werden met een vinylgroep. De biocompatibiliteit van de PGSA elastomeren is vergelijkbaar met PGS, welke al reeds in de literatuur was beschreven als gunstiger dan het PLGA polymeer.

In het laatste deel van dit proefschrift worden verschillende *tissue engineering* applicaties onderzocht voor PBPs. Letsel van perifere zenuwen kunnen grote gevolgen hebben voor de patiënt en zijn/haar omgeving. De gouden standaard in de behandeling van

grotere zenuwdefecten is het inhechten van een zenuw interpronaat in het defect. Hiervoor wordt een gezonde zenuw elders uit het lichaam opgeofferd, en dit brengt nadelen met zich mee, zoals extra zenuwuitval, wondgenezing problemen van de donorplaats, langere operatieduur, en een dimensionale *mismatch* van de donorzenuw met de acceptorzenuw. Een alternatief is het gebruik van zenuwbuisen. Dit zijn plastic buizen waarin de uiteinden van de beschadigde zenuw gehecht kunnen worden. Deze techniek heeft vele voordelen maar het klinische resultaat is vaak nog teleurstellend. Veel onderzoek is inmiddels gedaan naar verscheidene biodegradeerbare polymeren als buismateriaal, en uit deze literatuur is een aantal belangrijke criteria voor geschikte polymeren gekomen. In **Hoofdstuk 7** wordt PXS (1:1) geëvalueerd als biomateriaal voor de kunststofbuis in zenuwreconstructies. De biocompatibiliteit van dit polymeer werd uitgebreid getest in vitro alswel in vivo met (onderdelen van) ratten zenuwweefsel. Vervolgens bestudeerden we 'buisen' gemaakt van PXS 1:1 in een nervus ischiadicus rattenmodel, waarbij we een zenuwdefect van 1 cm reconstrueerden met PXS buizen en vergeleken hebben met commercieel verkrijgbare PGA buizen en siliconen buizen. Van deze drie buizen, bleken siliconen buizen het beste te zijn na 3 maanden, zichtbaar in de minste mate van spieratrofie als gevolg van denervatie en reïnnervatie van de spieren. PXS en PGA buizen waren vergelijkbaar, waarbij PXS een trend richting siliconen buizen laat zien, hoewel er geen significant verschil bestond met PGA buizen. We verklaren deze resultaten van PXS buizen aan de te snelle degradatie van het PXS 1:1 polymeer, waarbij de wanden van de vierkante buizen te snel geopend werden tijdens degradatie, en daardoor waarschijnlijk geen voldoende steun meer konden bieden aan de regenererende zenuwen. Een langzamer degraderende PXS buis zal in de toekomst geëvalueerd worden en vergeleken met siliconen of PGA buizen en autologe interpronaten. In **Hoofdstuk 8** en **9** bestudeerden we of PBPs gemakkelijk in verschillende voor *tissue engineering* interessante configuraties gemaakt kunnen worden. Dat materialen op basis van micro- en nano-topografische aanwijzingen cellen kunnen sturen en gedrag van cellen kunnen beïnvloeden is reeds langer duidelijk. In onderzoek naar perifere zenuwregeneratie weten we dat microstructuren in biomaterialen regenererende zenuwen in vitro kunnen sturen. In **Hoofdstuk 8** hebben we op nanometerschaal groeven aangebracht in PXS polymeren door middel van *replica molding*. Cellen uit perifere zenuwen en ganglia lieten zien dat ze zich keurig langs de groeven lieten uitgroeien. Tevens gaven de groeven in PXS elastomeren Schwann cellen uit rattenzenuwen in vitro een grotere migratie snelheid. Deze cellen spelen namelijk een belangrijke rol in zenuwregeneratie en moeten daarbij migreren tussen beide zenuwuiteinden. In vivo bleken repen van PXS uitgerust met nanotopografie ook over sturende eigenschappen te beschikken ondanks dat dit materiaal degradeerde.

Een echt effect op zenuwregeneratie en reconstructie in vivo zal pas kunnen geëvalueerd worden als er 3D constructs gemaakt kunnen worden waarbij nanotopografie geïncorporeerd wordt in PXS buizen. In **Hoofdstuk 9** hebben we PXS zoals eerder voor PGSA beschreven, veranderd en uitgerust met vinylgroepen om het materiaal te kunnen electrospinnen en direct erna te foto-polymeriseren. Electrospinnen is een techniek waarbij er uiterst dunne vezels (met diameters van micrometers tot nanometers) getrokken kunnen worden. Hoewel de eerste stappen hiertoe belovend zijn, is er nog veel ruimte voor optimalisering en verbetering van de techniek voor PBPs. Verder is in hoofdstuk 9 een klassieke manier van polymeren constructs te fabriceren voor *tissue engineering* gepresenteerd: de *particulate leaching* techniek. Dit bleek gemakkelijk te zijn voor PBPs. Macroporeuze PBP constructs lieten uitgebreide ingroei en vascularisatie te zien in vivo.

De belangrijkste conclusies van dit proefschrift worden in **Hoofdstuk 10** uiteengezet. Tevens worden de nadelen van PBPs beschreven en toekomstige onderzoekslijnen besproken waarbij geconcludeerd wordt dat er een eindeloze reeks aan applicaties vervuld kan worden, gebruikmakend van dit PBP platform.

Appendix 1: Gratitude

Good times gone, and you miss them
What's gone wrong in your system
Things they bounce like a Spaulding
What'd you think: did you miss your calling?
It's so free, this kind of deal and
It's like life; it's so appealing

When you got so much to say
It's called gratitude
And that's right

Good times gone, but you feed it
Hate's grown strong; you feel you need it
Just one thing: do you know you?
What'd you think: that the world owes you?
What's gonna set you free
Look inside and you'll see

When you got so much to say
It's called gratitude
And that's right!

Beastie Boys (Check your head)

Dr. Cox Terhorst, PhD. Beste Cox, natuurlijk begint deze lijst bij jou: ondanks mijn eerste *rocky ride* in je lab steunde je me in mijn keuze voor het ambachtelijk vak en de toegepaste wetenschap. Dank voor alle mogelijkheden die je gunde op MIT.

Dr. Robert Langer, ScD. Dear Bob, I cannot believe how fast these three years in the Langer Lab have flown by. Without a doubt this has been the most inspiring time of my life. I was fortunate to be a member of the Langer Lab as a post-doc as well as special graduate student in the Department of Chemical Engineering. The collaborative and positive environment of the laboratory as a whole is truly indicative of your way of passing on your principles to (1) feel good, and (2) then solve problems. Your absurdly swift Blackberry responses using three word sentences have always been extremely supportive as well as humorous from time to time. But most of all: thanks for accepting me into the Langer Lab family. I am extremely proud of this. Ms. **Constance Beal**. Dear Connie, how many times have I not bothered you with annoying problems? I thank you for letting me squad in the office when I was illegal, and I sincerely thank you for all your patience with me.

Prof. dr. **Steven Hovius**. Beste Prof! Dit is m dan: het resultaat van dat geklooi overzees. Ik bladerde onlangs nog even door de vele vage e-mails over wel 10 verschillende materialen, vage plannen over zenuwreconstructies, vage beursaanvragen over dit alles, en uw vragen over zogenaamde navragen van Amerikaanse collegae. Het mooiste vind ik dat ik nooit mooi weer hoeft te spelen als ik bakzijl moet halen met sommige plannen. Tijdens mijn 3 jaar buiten het ziekenhuis kwam ik telkens geïnspireerd voor het vak uit uw kantoor vandaan. Bedankt voor dit alles. Mw. **Carin Oostdijk**. *Mrs C!* Dank je wel voor alle gehonoreerde *last minute* verzoeken betreffende mijn eeuwige chaos in de papierwinkel, en het fijne email contact al die jaren.

Geleerde leden van de commissie, ik wil u hartelijk bedanken voor uw bereidheid zitting te nemen in de promotiecommissie.

Lieve **Richard**, dank je wel dat je me ooit, lang geleden, toch enthousiast wist te maken voor geneeskunde, ondanks je goede bedoelingen. Ik hoop dat we ooit nog over die colletjes gaan rochelen in België en Frankrijk. Dear **Dr. Maria Simarro-Grande**: Mamita bonnita, thanks so much for sharing frustrations and giving me some confidence doing basic science. That memory means a whole lot to me.

Langer Lab:

I am grateful for the efforts and assistance of *all* members of the Langer Laboratory with extended gratitude to the *nerve minds* Drs. **Paul George**, **Micheal Moore**, **Rajiv Saigal**, and **Will Neeley**. Thanks to **Sarah Hudson**, **Grace Kim**, Pipe-club members/ office-nuts **Jason Fuller**, **David Nguyen**, and of course **Manny Simmons**, **Ben Teply** and **Matteo Morretti**, thanks for the dinners, coffees and conversations. Also **Jason Nichol** and **Lisa Freed** thanks for some collaborative action in the end: I wish I had another year. Also thanks to **Dan Kohane** for the challenges, MGH trauma rounds and your wisdom (on karma, a.k.a. The Test and “Homesick abortion”). I would also like to recognize the contributions of **Alex Alford**, my cool UROP who always seemed to know how to enjoy life as an MIT undergraduate. I have to explicitly and specifically thank **Leah Bellas** (Belly!) for always being there to share labstuff, frustrations, the South End, amongst much more. Hopefully we'll stay in touch every now and then.

My Boston 2001/ 2005 Friends:

Julie weten wat de opofferingen en opgaves zijn van meer dan een jaartje leven in de VS. Deze gemeenschappelijke ervaring bindt ons en voelt soms als een broederschap. **Jacobus Bosch**, beste Co: we zaten altijd ‘n beetje in hetzelfde schuitje. Ik kijk uit naar jouw promotie. Nürnbergring is dichterbij dan Montreal, toch? **Jochem Fockema Andreae**, beste Manny: *Manny-being-Manny* is op jouw lijf geschreven dus ik houd ‘t kort. Bleachers! **Hinne Rakhorst**: plastische en tissue engineering – jij deed ‘t al in 2000. Je geeft me vaak waardevolle adviezen en als collega en vriend word ik blij dat ik nog even bij je in Rotterdam ben. **Sebastiaan Souer**: samen op Union Park 38. Gepruts met vrouwen, slechte teksten (“*No. She’s special...*”), catabool slenterend Boston skylines vanaf de Longfellow, de competitie, gefukte squashpartijtjes, Texas en dromen over snijden. Dank dat we dat moois gedeeld hebben. **Herman Tolboom**: jouw prettig pervasief gestoorde manier van je obsessies “delen” werkt soms aanstekelijk. *Trapelo Rd* en *Ti* hebben dus naast jou ook een plaats in mijn hart. Cheers *bru*. **Svend Rietdijk**. Beste Svendster, jij natuurlijk ook bedankt voor onze geschiedenis en vriendschap in en buiten Boston. **Christiaan Nijst**: samen met jou begon het wetenschappelijk allemaal te lopen. Daarnaast waren de standaard *doppios*, *cookie-times* en ‘*howyadoin*’ een noodzakelijke tegenhanger van de slangenkuil waar we ons soms in bevonden. Om maar te zwijgen over de telefoon en *nanosamples* die tijdens de vele uren *office soccer* geleden hebben. **Trevor Squire**: we found out that an Afro-American female welder who worked in the Boston harbor during the 80s (Mary!) can kick our ass in a blink and that setting clothes on fire is relatively easy. That *Flamboyant* frame will

someday be ridden by us, together, on a mountain in the US, Africa or Europe. **Berend-Jan de Bruin**: dank je wel voor al het plezier, je inzet, je enthousiasme en je talent ongevraagd en moeiteloos triviale wikipedia *stubs* op te dreunen. Ik ben blij dat je ook zoveel plezier gemaakt hebt in jouw tijd in Boston, en hoop dat we later mogen samenwerken.

Mijn vrienden en vriendinnen in NL:

Sjak, Belle, Enya, Janneke, As, Eef, Huug: dank voor jullie inzet voor de leuke momenten en mijn geijkte gehobbel achter jullie aan. **Jelle**: we hadden altijd op tijd contact ook al was het niet vaak. Je hip-hop CD'tjes kwamen altijd op tijd. **Hein**: als een van de weinigen heb jij mijn mindere tijden in de The Big Fruit gedeeld. Thanks dude. **Arvind**: samen dromen doen we al vanaf de 5^e klas. De wereld ligt nog steeds aan onze voeten. **Menno**: vanaf onze 14^e zijn we beste vrienden en ik hoop echt dat dat nooit verandert.

Het *paranymfenduo*:

Kerry Mahon. Dear Kerry: That dude in Fenway Pah'k was right. It sometimes really feels like you are my American brother. However, apart from the curly hair and nerdy humor we can't possibly be related as you have such an incredibly friendly personality (*"Is that... is that bad?"*). Shannon and the Cozzos: I am so happy to have met you too. Mahonkey – I am proud to be your friend and have you by my side during my thesis defense. **Gijs van Acker**, beste Gijs: natuurlijk ben jij mijn paranymf. Hoe anders was mijn eerste en tweede Boston avontuur geweest zonder jou. Ik heb altijd als 'n soort jongere broer bewondering voor je gehad, en je voorbeeld, steun en humor waren zo cruciaal in beide jaren (*"Wij zijn gewoon gaaf"*). Dank voor deze waardevolle vriendschap.

Chris Bettinger. Dear Betty: I have never met a person with such a different character who was so compatible with my fuzzy personality. Mocking situations and personalities, especially our own, and then 'developing' the jokes by endless repetition in solid but inappropriate situations had to be the social glue between us. I don't think the Langer Lab has *ever* seen nutcases like us before. Concerning this thesis: your endless patience in explaining material science and chemistry basics to me whenever I was intuitively yabbing on about subjects I knew nothing of, in conversation as well as writing, was fundamentally important. I am proud to boldly state that I am your first graduate student. Furthermore: thank you so much for all the cool things and times and just being my friend. *Animay-serrees!*

Mijn familie:

Lieve **mam**. Dank je wel voor het leren kritisch naar mezelf te zijn en goed naar mijn gevoel te luisteren. Het geluk zit in jezelf – het kon zich niet beter verstoppen, leerde je me. Je hebt me met je woorden en liefde zo onwijs gesteund over die grote afstand. Ik heb bewondering voor hoe jij het leven leeft en wie je bent. Hopelijk lijkt ik ook daarin op jou.

Lieve **dad**. Als het niet zo goed met me ging, had jij een excuus om op Union Park langs te komen en samen te sleutelen aan m'n Fleetwood. Natuurlijk delen we de liefde voor technologie, het prutsen, *de MIT*, maar er is veel meer. Je bent er altijd als vader voor me zonder dat jij dat voorbeeld ooit had. Dank je wel voor je liefde en steun die je me geeft.

Lieve **zus** – je bent één van de mooiste vrouwen die ik ken en ik ben zo verschrikkelijk dol op jou.

Lieve **Marjan**, wat fijn dat ik je heb leren kennen in mijn laatste maanden in Amsterdam. Henny Huisman zong het al zo voortreffelijk over onze 010-020 afstand (“Riets out en tuts!”).

Hermien Schreurs en de rest van de maatschap heelkunde van het Medisch Centrum Alkmaar: bedankt voor de inspirerende tijd in de heelkunde en voor het maken van een echte dokter van me. Dat geldt overigens net zo hard voor mijn mede-assistenten **Nike Hanneman** en **Michiel Teijgeler** *et al.* Alle collegae en verpleegkundigen op de SEH, 270/330/331: dank voor het werkplezier in de afgelopen 2 jaar.

Lastly – *thanks* to all laboratory rats that never had a say in their destiny. With all the terrible things I have done to you as well as the boring lives you must have lived you have never held a grudge against me, so it seemed.

Appendix 2: Curriculum vitae

Joost P. Bruggeman was born on February 8th, 1978 in Amsterdam, the Netherlands. He graduated from high school (*Sint Nicolaas Lyceum*, Amsterdam) in 1996, considering a career as an aeronautical engineer. However, owing to his mother's wisdom, he enrolled into Medical School of the *University of Amsterdam* that same year. After obtaining his MSc he left for Boston the first time in Y2K to study SLAM/SAP physiology in T cells under direct supervision of Dr. Cox Terhorst, PhD (Beth Israel Deaconess Medical Center, *Harvard Medical School*) until December 2001. The author returned to Boston in July 2005 after graduating Medical School (2004) and working in the Department of Plastic and Reconstructive Surgery of the Erasmus MC (Head: Prof. Dr. S. Hovius, MD PhD) of the *Erasmus University Rotterdam*, The Netherlands. He was fortunate to work and play with brilliant minds at the Langer Lab (Department of Chemical Engineering, *Massachusetts Institute of Technology*) under the direct supervision of Institute Professor Robert Langer, ScD until September 2008. Upon returning to the Netherlands, the author was trained at the Department of General Surgery of the *Medisch Centrum Alkmaar* (Supervisor: Dr. W.H. Schreurs, MD PhD). As of September 2010, the author participates in the Plastic and Reconstructive Surgery residency program of the Erasmus MC (Supervisor: Prof. Dr. S. Hovius, MD PhD).

Appendix 3: Scientific publications

1. **Bruggeman JP**, Bettinger CJ, Langer R. Biodegradable xylitol-based elastomers: in vivo behavior and biocompatibility. *J Biomed Mater Res A*. 2010;95(1):92-104.
2. Bettinger CJ, **Bruggeman JP**, Borenstein JT, Langer R. In vitro and in vivo degradation of poly(1,3-diamino-2-hydroxypropane-co-polyol sebacate) elastomers. *J Biomed Mater Res A*. 2009;91(4):1077-88.
3. Bettinger CJ, **Bruggeman JP**, Misra A, Borenstein JT, Langer R. Biocompatibility of biodegradable semiconducting melanin films for nerve tissue engineering. *Biomaterials*. 2009;30(17):3050-7.
4. **Bruggeman JP**, de Bruin BJ, Bettinger CJ, Langer R. Biodegradable poly(polyol sebacate) polymers. *Biomaterials*. 2008;29(36):4726-35.
5. Bettinger CJ, **Bruggeman JP**, Borenstein JT, Langer RS. Amino alcohol-based degradable poly(ester amide) elastomers. *Biomaterials*. 2008;29(15):2315-25.
6. **Bruggeman JP**, Nijst CL, Bettinger CJ, Kohane DS, Langer R. Biodegradable xylitol-based polymers. *Advanced Materials*. 2008;20(10):1922-7.
7. Gerecht S, Townsend SA, Pressler H, Zhu H, Nijst CL, **Bruggeman JP**, Nichol JW, Langer R. A porous photocurable elastomer for cell encapsulation and culture. *Biomaterials*. 2007;28(32):4826-35,
8. Nijst CL, **Bruggeman JP**, Karp JM, Ferreira L, Zumbuehl A, Bettinger CJ, Langer R. Synthesis and characterization of photocurable elastomers from poly(glycerol-co-sebacate). *Biomacromolecules*. 2007;8(10):3067-73.
9. Ten Hove T, The Olle F, Berkhout M, **Bruggeman JP**, Vyth-Dreese FA, Slors JF, Van Deventer SJ, Te Velde AA. Expression of CD45RB functionally distinguishes intestinal T lymphocytes in inflammatory bowel disease. *J Leukoc Biol*. 2004;75(6):1010-5.
10. Simarro M, Lanyi A, Howie D, Poy F, **Bruggeman J**, Choi M, Sumegi J, Eck MJ, Terhorst C. SAP increases FynT kinase activity and is required for phosphorylation of SLAM and Ly9. *Int Immunol*. 2004;16(5):727-36.
11. Howie D, Okamoto S, Rietdijk S, Clarke K, Wang N, Gullo C, **Bruggeman JP**, Manning S, Coyle AJ, Greenfield E, Kuchroo V, Terhorst C. The role of SAP in murine CD150 (SLAM)-mediated T-cell proliferation and interferon gamma production. *Blood*. 2002;100(8):2899-907.

Patents

1. Langer R, Zumbuehl A, Bettinger CJ, **Bruggeman JP**, Ferreira L, Karp J, Nijst CLE, Burdick J, Kim S. Biodegradable Elastomers. WO/2007/082304.
2. **Bruggeman JP**, Nijst CLE, Kohane DS, Langer R. Polyol-based Polymers. WO/2008/144514.

